THE DEVELOPMENT AND USE OF A TROCHOIDAL BETA-RAY SPECTROMETER

by

Colin Allan
Department of Physics
University of Manitoba.

A Thesis

Submitted to the

Faculty of Graduate Studies

University of Manitoba

in partial fulfillment of the

requirements of the degree of

Doctor of Philosophy

Winnipeg, Manitoba

June, 1970

To My Wife

Lynn

ACKNOWLEDGEMENTS

I wish to thank my supervisor Dr. K. G. Standing for his kind interest and assistance in this work and for his many helpful comments concerning this thesis. Thanks are also extended to Professors R. D. Connor and S. K. Sen for the use of their equipment and for their helpful comments and to Doctors R. M. Craig and M. J. Canty for much useful discussion.

In addition the author would like to thank the members of the machine shop and of the electronics shop, particularly Mr. R. H. Batten and Mr. R. Shabaga. As well I wish to thank Mr. P. O'Connor and Mr. J. Ramrath who were responsible for developing the orbit dynamics computer programme and Miss Karen McFadden who translated my written hieroglyphics into legible type.

The financial assistance of the Atomic Energy Control Board of Canada and the award of studentships by the National Research Council of Canada are gratefully acknowledged.

ABSTRACT

A trochoidal β-ray spectrometer has been constructed at the University of Manitoba. The spectrometer unambiguously separates positrons and electrons. Energy determination is made using solid state detectors and the resolution is that of the detectors plus associated electronics. Numerous difficulties were encountered in the development of the instrument but these were eventually overcome. The instrument was used as a pair spectrometer to study internal pair formation in ^{205}Pb, ^{206}Pb, ^{207}Pb and ^{88}Sr and it was also used to measure the internal conversion coefficients of various transitions in these nuclides.

TABLE OF CONTENTS

Title Page i

Dedication ii

Acknowledgements iii

Abstract iv

List of Figures v

List of Tables x

CHAPTER 1. Introduction ---------- 1

CHAPTER 2. Magnetic Field Measurements ---------- 5

Introduction ---------- 5

Description of the Apparatus Used in the Field Measurements ---------- 8

Calibration of the Hall Plate ---------- 12

Field Measurements ---------- 15

CHAPTER 3. Theoretical Analysis of the Spectrometer ---- 25

Field Fitting ---------- 25

Study of the Spectrometer's Performance ---------- 34

CHAPTER 4. Experimental Properties of the Spectrometer - 51

Introduction ---------- 51

Apparatus and Experimental Arrangement ---------- 51

Some Problems Related to the Line Shape ---------- 58

Calibrating the Spectrometer ---------- 63

CHAPTER 5. On Pair Production ---------- 73

Some Theoretical Considerations ---------- 73

Use of the Present Spectrometer to Study Pair Production ---------- 83

.....2

con't.

CHAPTER 6. Study of ^{206}Pb Following Decay of ^{206}Bi ----- 93

Introduction ---------- 93

Electron and Gamma-Ray Singles Study ---------- 95

Gamma-Gamma Coincidence Study ----------114

(a) Introduction ----------11
(b) On the Coincidence Resolving Time --------116
(c) The 1878 keV transition ----------118
(d) The 1903 keV transition ----------121
(e) The 1844 keV transition ----------123
(f) Summary of the γ-γ Coincidence Study -----126

New Transitions ----------126

Internal Pair Production in ^{206}Pb ----------131

Summary ----------147

CHAPTER 7. Internal Pair Production and Internal Conversion in ^{88}Sr Following the Decay of ^{88}Y --148

Introduction ----------148

Internal Conversion Measurements ----------148

Internal Pair Production Measurements ----------155

CHAPTER 8. Study of ^{205}Pb Following Decay of ^{205}Bi -----165

Introduction ----------165

Gamma and Electron Work ----------167

Internal Pair Production ----------180

Summary ----------193

CHAPTER 9. Discussion of the Spectrometer ----------194

List of References ----------204

LIST OF FIGURES

Fig.	Title	Page
1-1	The nature of the trochoidal orbits.	2
2-1	Magnet cross-section.	6
2-2	Plane view of magnet.	7
2-3	Apparatus used in positioning the Hall Plate.	9
2-4	Hall plate mounts for the measurement of the vertical and radial field components.	10
2-5	Hall plate control current power supply.	11
2-6	Alignment of the rotating-coil gaussmeter used in calibrating the Hall plate.	13
2-7	Median Plane magnetic field.	18
2-8	Vertical field component for a magnet current of 300A.	19
2-9	Radial field component for a magnet current of 300A.	20
3-1	The vertical field component as a function of Z in the region of the pole-tip edge.	27
3-2	The radial field component as a function of Z in the region of the pole-tip edge.	28
3-3	Comparison of the predicted vertical field component with measurement.	32
3-4	Comparison of the predicted radial field component with measurement.	33
3-5	The trochoidal motion of the electrons.	36
3-6	The vertical motion of the electrons.	37
3-7	Assumed detector cross-section.	38

.....2

Fig.	Title	Page
3-8	Nature of the motion for electrons which do not strike the detector as they cross the $\theta=15^{o}$ plane for the first time.	40
3-9	Computed transmission of the spectrometer and the computed detection efficiency for a $100mm^2$ circular detector.	42
3-10	The computed dependence of the detection efficiency on detector area for various electron energies.	43
3-11	The computed distribution of 100 keV electrons across the $\theta=15^{o}$ plane.	44
3-12	The computed distribution of 195 keV electrons across the $\theta=15^{o}$ plane.	45
3-13	The computed distribution of 500 keV electrons across the $\theta=15^{o}$ plane.	46
3-14	The computed distribution of 1000 keV electrons across the $\theta=15^{o}$ plane.	47
3-15	The computed time of flight for an electron to drift 135^{o} around the pole tips from the source.	49
4-1	Portion of ^{207}Bi electron spectrum.	52
4-2	Plane view of magnet showing the location of the detectors and source.	53
4-3	Details of the detector assembly.	55
4-4	Details of the source interlock.	56
4-5	Details of the baffle and liquid nitrogen cold trap used to reduce oil backstreaming.	57
4-6	Portion of ^{139}Ce electron spectrum.	60
4-7	Details of the source frame.	61
4-8	Calibration curve for the Ge(Li) detector used in calibrating the spectrometer.	65

.....3

Fig.	Title	Page
4-9	Calibration curves for the spectrometer.	67
4-10	Details of the lead shielding used in acquiring γ-spectrum of sources prepared by sublimation.	69
4-11	^{207}Bi 1064-K plus 570-K sum peak.	72
5-1	The shape of the positron spectrum, in Born approximation, for Eℓ transitions.	79
5-2	The shape of the positron spectrum, in Born approximation, for Mℓ transitions.	80
5-3	Comparison of the shape of the Z=0 and Z=82 positron spectra.	81
5-4	Comparison of the shape of the Z=0 and Z=38 positron spectra.	82
5-5	Definition of the angle of pair emission.	86
6-1	^{206}Bi decay scheme.	94
6-2	Typical ^{206}Bi electron spectrum.	96
6-3	The 497-K, 516-K and 538-K triplet of ^{206}Bi.	98
6-4	Typical ^{206}Bi γ-spectrum.	101
6-5	Ortec and P.γ.T. Calibration curves.	102
6-6	Mixed source energy calibration spectrum.	105
6-7	Details of the γ-spectrum in the vicinity of the 107, 124 and 203 keV γ-peaks.	111
6-8	Details of the γ-spectrum in the vicinity of the 816 keV γ-peak.	112
6-9	Block diagram of the electronics used for the γ-γ coincidence work.	115
6-10	Block diagram of the electronics set-up used for setting the ΔT S.C.A. window.	117
6-11	γ-spectrum in coincidence with the 1878 keV transition of ^{206}Pb.	119

.....4

Fig.	Title	Page
6-12	γ-spectrum in coincidence with the 1903 keV transition of ^{206}Pb.	122
6-13	γ-spectrum in coincidence with the 1844 keV transition of ^{206}Pb.	124
6-14	Decay scheme of ^{206}Pb showing the tentative assignment of the new transitions.	130
6-15	Typical ^{206}Bi pair sum spectrum	132
6-16	Positron continuum obtained by gating on the 1719 pair sum peak.	134
6-17	Positron singles spectrum.	135
6-18	Comparison of the positron spectrum from pairs with theory.	136
6-19	Block diagram of the electronics used in operating the spectrometer as a pair spectrometer.	137
6-20	The dependence of the pair detection efficiency on positron energy for E_γ=1719 keV.	143
7-1	Decay scheme of ^{88}Y.	149
7-2	Typical ^{88}Y electron spectrum.	151
7-3	Details of the 898-K, L+M and 1836-K,L+M conversion peaks.	152
7-4	Typical peak fitting to extract the contribution of the L+M conversion peak.	153
7-5	Typical ^{88}Y pair sum spectrum.	155
7-6	Details of the pair sum peaks from the 1836 keV and 2734 keV transitions of ^{88}Sr.	156
7-7	Comparison of the electron and positron continua of internal pairs from the 1836 keV transition of ^{88}Sr.	158
7-8	Comparison of the theoretical and experimental positron continua for the 1836 keV transition of ^{88}Sr.	159

.....5

Fig.	Title	Page
7-9	Variation of the pair detection efficiency with positron energy for E_γ=1836 keV.	160
7-10	Variation of the pair detection efficiency with positron energy for E_γ=2734 keV.	161
8-1	Decay scheme of ^{205}Bi.	166
8-2	Typical ^{205}Bi γ-spectrum.	168
8-3	Typical ^{205}Bi electron spectrum.	173
8-4	Typical ^{205}Bi pair sum spectrum.	181
8-5	Comparison of the electron and positron continua of internal pairs from the 1764 keV transition of ^{205}Pb.	182
8-6	The extraction of the 1776 pair sum peak.	186
8-7	The pair sum peak of the 1770 keV transition of ^{207}Bi.	188
9-1	Suggested field shaping to introduce focusing at the detector location.	197

LIST OF TABLES

Table	Title	Page
2-1	Alignment of the top and bottom pole tips.	15
2-2	Some typical values of the vertical field component showing the reproducibility of the measurements from port to port.	22
2-3	Some typical values of the radial field component showing the reproducibility of the measurements from port to port.	23
3-1	Comparison of the predicted radial field component with experimental values.	30
3-2	Comparison of the predicted vertical field component with experimental values.	31
4-1	Summary of the sources used in calibrating the spectrometer.	64
6-1	Relative electron line intensities for ^{206}Bi.	97
6-2	Comparison of the relative ^{206}Bi γ-ray intensities obtained using two different Ge(Li) detectors.	103
6-3	Summary of the ^{206}Bi plus mixed sources energy calibration.	106
6-4	Summary of the ^{206}Bi γ-ray singles work.	108
6-5	Summary of the ^{206}Bi conversion coefficients.	109
6-6	Summary of new transitions identified in the decay of ^{206}Bi.	127
6-7	Possible sum peaks in the ^{206}Bi γ-spectrum.	129
6-8	Summary of the ^{206}Bi pair formation study.	146
7-1	Summary of the ^{88}Y conversion electron study.	154
7-2	Summary of the ^{88}Y pair formation study.	163
8-1	Summary of the ^{205}Bi transition energies.	169

.....2

Table	Title.	Page
8-2	Relative γ-ray intensities for ^{205}Bi.	170
8-3	Relative electron line intensities for ^{205}Bi.	174
8-4	Summary of the ^{205}Bi conversion coefficients.	175
8-5	Summary of the pair formation study of ^{207}Bi.	190
8-6	Summary of the pair formation study of ^{205}Bi.	191
8-7	Summary of the ^{205}Pb transition multipolarities.	192
9-1	Comparison of the performance of the trochoidal β-ray spectrometer with that of a high transmission magnetic spectrometer.	199

CHAPTER 1

INTRODUCTION

"But screw your courage to the sticking-place,
And we'll not fail." .....Lady Macbeth

In 1933 Thibaud[1] used a trochoidal β-ray spectrometer to separate the positrons and electrons produced by γ-rays of a few MeV. Such a spectrometer consists essentially of a cylindrically symmetric magnetic field produced by a pair of circular pole tips. If an electron source is placed in the fringing field beyond the edge of the pole tips the emitted electrons will follow trochoidal orbits such as that shown in Fig. 1-1, and will drift around the pole tips. The direction of drift is independent of the original direction of emission and all electrons drift in the same direction. Positrons, on the other hand, drift in the opposite direction, since they are oppositely charged, so the spectrometer unambiguously separates positrons and electrons.

The radial field component produces strong vertical focussing. Thus particles emitted out of the median plane are subject to strong focussing forces towards the median plane, so that superimposed on the trochoidal motion is a vertical oscillation about the median plane. The percentage of emitted electrons which are captured into stable vertical oscillations and drift around the pole tips without colliding with the poles or walls of the magnet may be used as a convenient definition of the instrument's transmission . Because of the vertical focussing

FIG. 1-1

The nature of the trochoidal orbits.

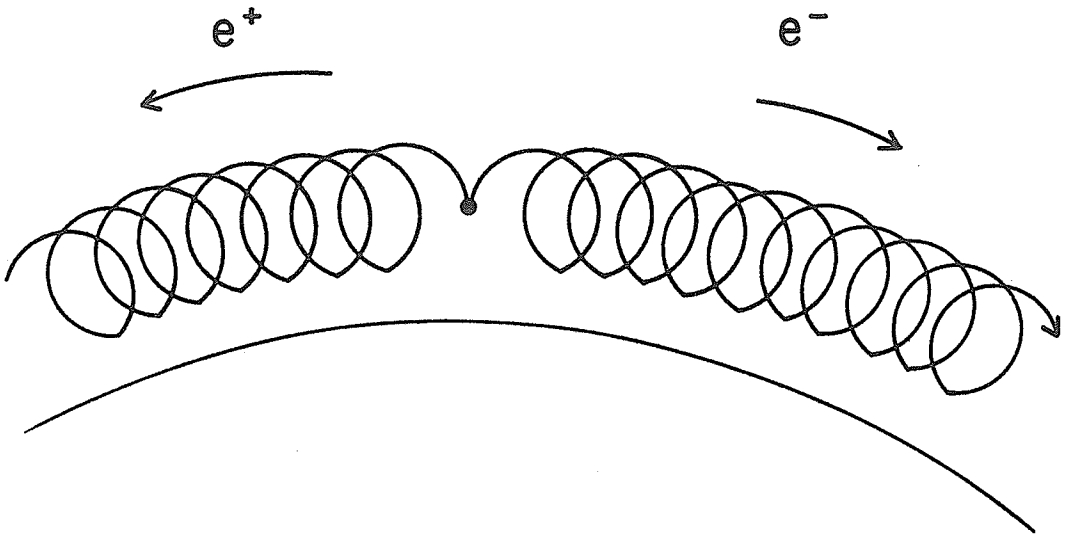
e+
e−

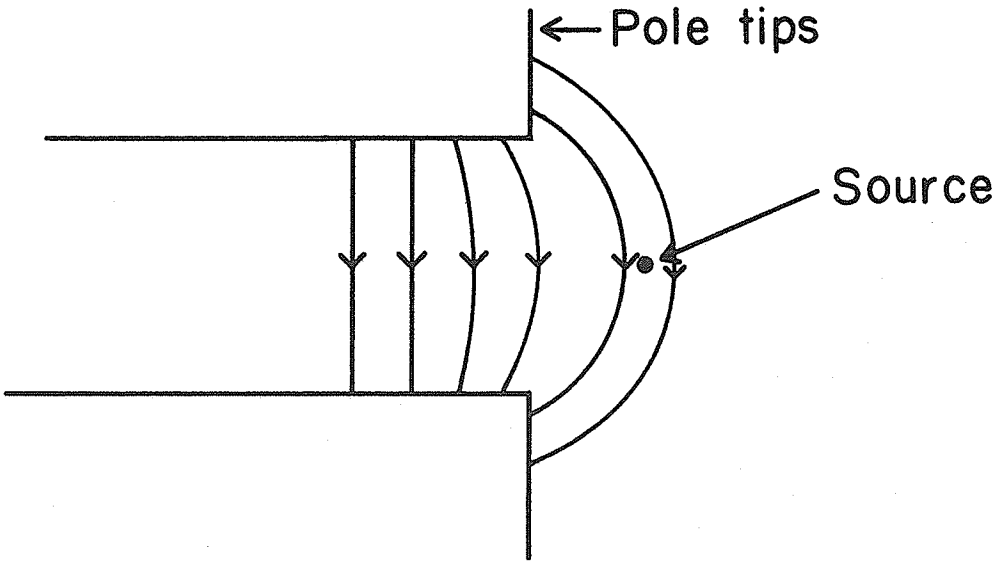
Pole tips
Source

the transmission, thus defined, is expected to be large, ~50%, and it is insensitive to the energy of the particle, aside from an expected gradual decrease with increasing energy.

Since the spectrometer transmits electrons of all energies the magnetic resolution of the instrument is essentially non-existent. Malmfors[2] has suggested using time of flight as a method of energy determination in such a spectrometer. Because of the trochoidal orbits which the particles follow the distance through which they travel in drifting a given azimuthal distance around the pole tips is many times larger than the actual arc-length. Then, because of the long flight path, the time taken to drift through some fixed angular displacement, such as 180°, is relatively long and can be measured electronically. The flight time is energy dependent and therefore provides a suitable measure of the particle's energy. Malmfors[2], using a field which, in the median plane, satisfied the equation $B=B_o(\frac{r_o}{r})^{\frac{1}{2}}$, was able to obtain an energy resolution of about 2% for the K-conversion electrons from the 570 keV transition of ^{207}Pb. This line width was a reflection of the variation in flight time with direction of particle emission. The actual time of flight was ~1μs.

An alternative method of energy determination is to measure the electrons' energy in a counter by intercepting the particles at some azimuthal distance around the pole tips from the source. The resolution is then determined by the detector and with the development of solid state detectors it became possible to achieve good resolution. (A resolution ~5keV FWHM in the region 100-1000 keV is not unreasonable). The magnetic field then acts as a guide to convey the electrons from the source

to the detector and because of the high transmission the electron detection efficiency is expected to be high. Thus a trochoidal β-ray spectrometer employing solid state detectors for energy determination has the dual advantage of high efficiency and good resolution.

Although the electron efficiency, in such a spectrometer, is high the γ-ray detection efficiency is small, because of the small solid angle which the detector subtends, and because of the inherently smaller γ-ray efficiency of the detector. The γ-ray detection efficiency can be further reduced by placing lead shielding between the source and detector, (between the pole tips). This shielding does not interfere with the electrons' motion since they drift around the pole tips.

Because of the unambiguous separation of positive and negative charge, combined with the high efficiency and good resolution, such an instrument is particularly well suited for use as a pair spectrometer. In this application a pair of solid state detectors are used, one for positrons and one for electrons. A spectrometer of this type has been constructed at the University of Manitoba and in the following chapters the development and use of this instrument are discussed.

CHAPTER 2

MAGNETIC FIELD MEASUREMENTS

"If it were done when 'tis done, then 'twere well
It were done quickly:" .....Macbeth

INTRODUCTION

The spectrometer magnet assembly is shown in Figs. 2-1 and 2-2. The flat circular pole tips are 10.625" in diameter, 0.75" thick and are separated by a gap of 2". The height of the vacuum chamber beyond the edge of the pole tips is 3.5". The magnet structure forms part of the vacuum chamber. Access to the vacuum chamber is provided through four ports as shown in Fig. 2-2. The field is generated by six sets of water-cooled coil pancakes, three around each pole piece, wired in series and located outside the vacuum chamber.

A programme of magnetic field measurements was undertaken with the intention of using the results in a computer study of the spectrometer. The vertical and radial field components were measured independently as a function of radial displacement from the pole tip edge and as a function of vertical displacement from the median plane using a Hall Plate†. The field components were measured over a radial range of approximately 3",from 1.5" beyond the pole tip edge to 1.5" inside the pole tip edge at various vertical displacements from the median plane. Independent measurements were carried out above and below the median plane, at current settings of 250, 300 and 350 A.

---

† - F. W. Bell, model BH207.

FIG. 2-1

Magnet cross section showing the location of the coils and the vacuum chamber.

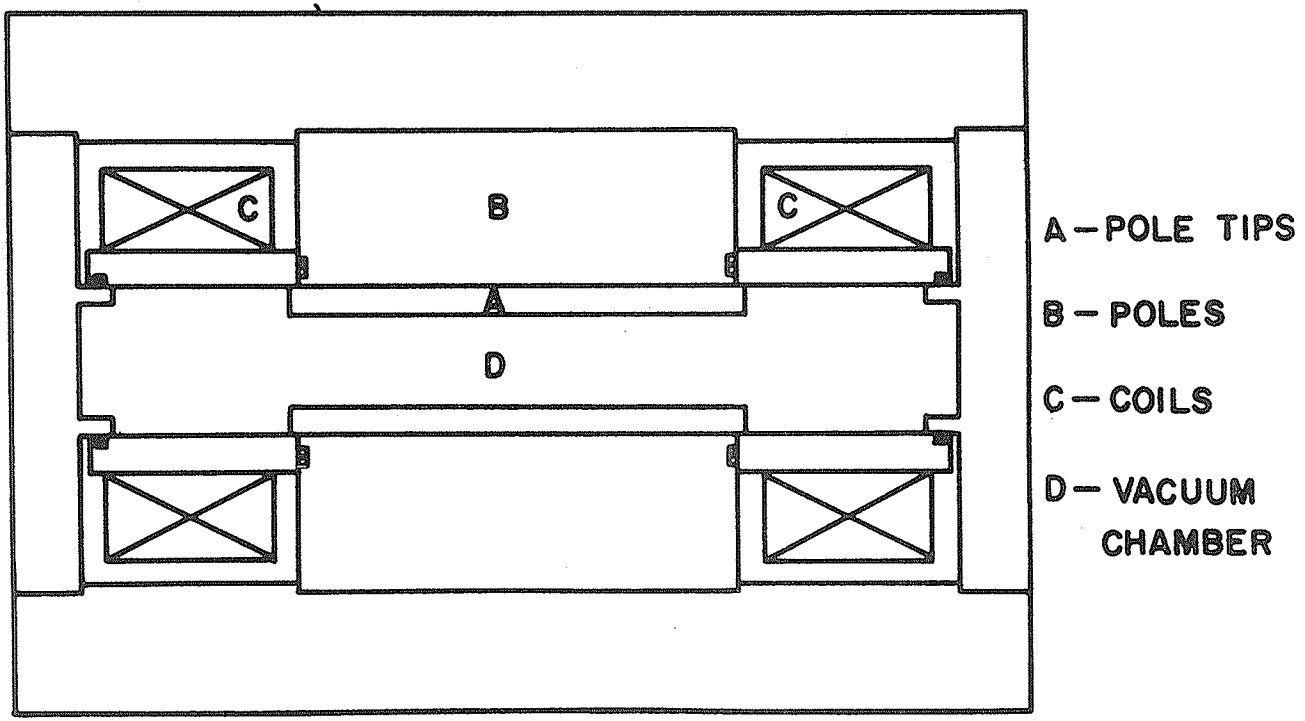
C
B
C
A
D
A – POLE TIPS
B – POLES
C – COILS
D – VACUUM CHAMBER

FIG. 2-2

Plane view of magnet showing the location of the access ports.

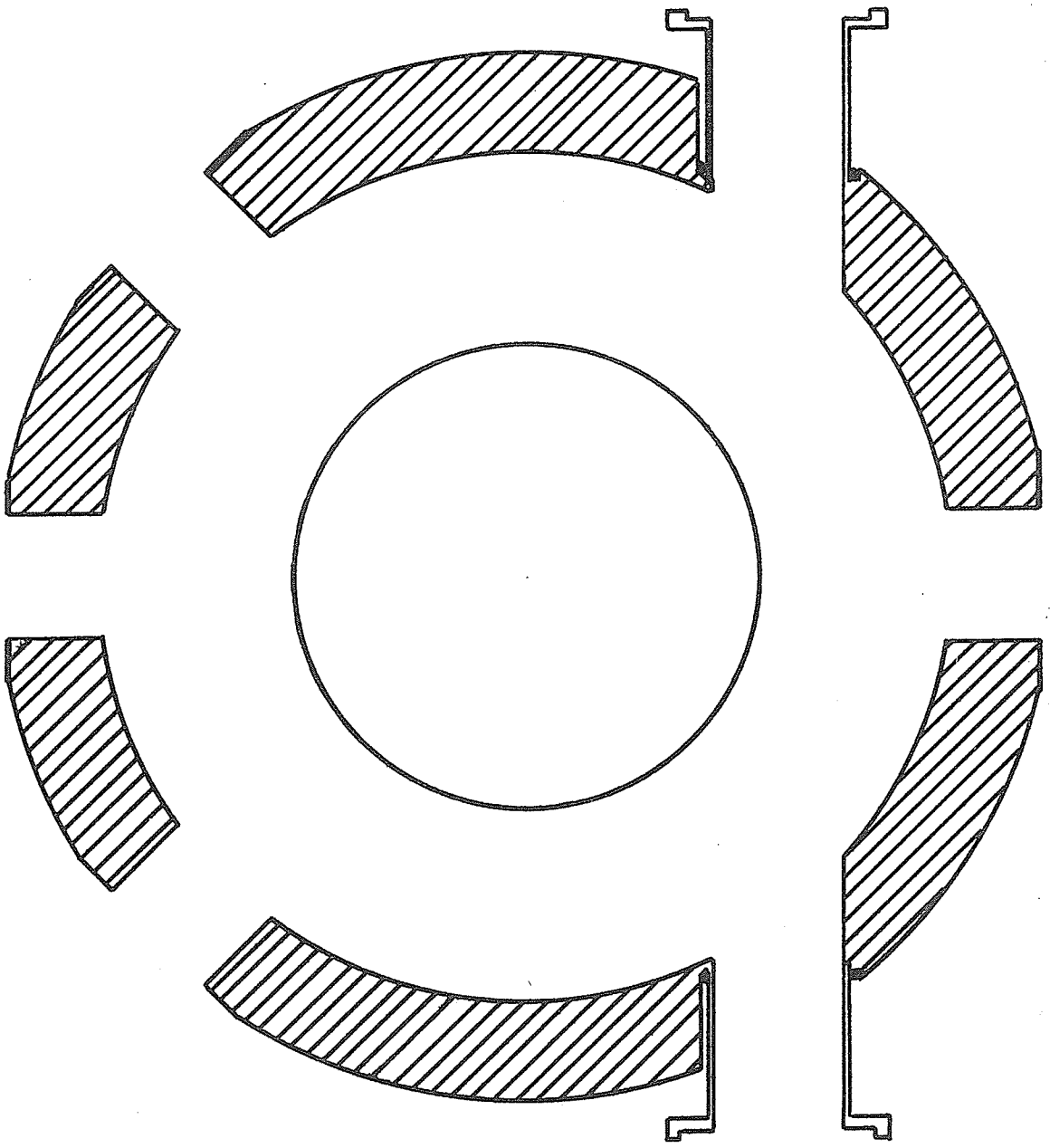

DESCRIPTION OF THE APPARATUS USED IN THE FIELD MEASUREMENTS

Since the intention of the field measurements was to obtain an accurate plot of the magnetic field it was necessary to be able to position the Hall plate accurately and reproducibly as a function of radial distance from the pole tips and vertical displacement from the median plane. This was done using the drive mechanism shown in Fig. 2-3. The aluminum drive shaft is driven by a threaded star wheel, 20 turns to the inch, and can be positioned radially with an accuracy of ±.001". The Hall plate itself was mounted on aluminum supports shown in Fig. 2-4 which in turn were fastened to the brass support base shown in Fig. 2-3. The brass base serves a dual purpose. The series of tapped holes enables the Hall plate to be positioned accurately at various vertical displacements from the median plane and the base is water-cooled to serve as a heat sink for the Hall plate. (Mean temperature coefficient ~.1%/^{o}C). The Hall plate was held in position on the aluminum support using a thin layer of vacuum grease.

A Hall plate measures the field perpendicular to its sensitive area and therefore the radial and vertical field components were measured independently by aligning the sensitive area perpendicular to and parallel to the median plane respectively, using the supports shown in Fig. 2-4. Care was taken to ensure that the Hall plate was properly aligned and that the drive shaft moved parallel to the pole tips. The reliability of this alignment was confirmed by a null reading for the radial field component in the median plane.

FIG. 2-3

The apparatus used for positioning the Hall plate for the magnetic field measurements.

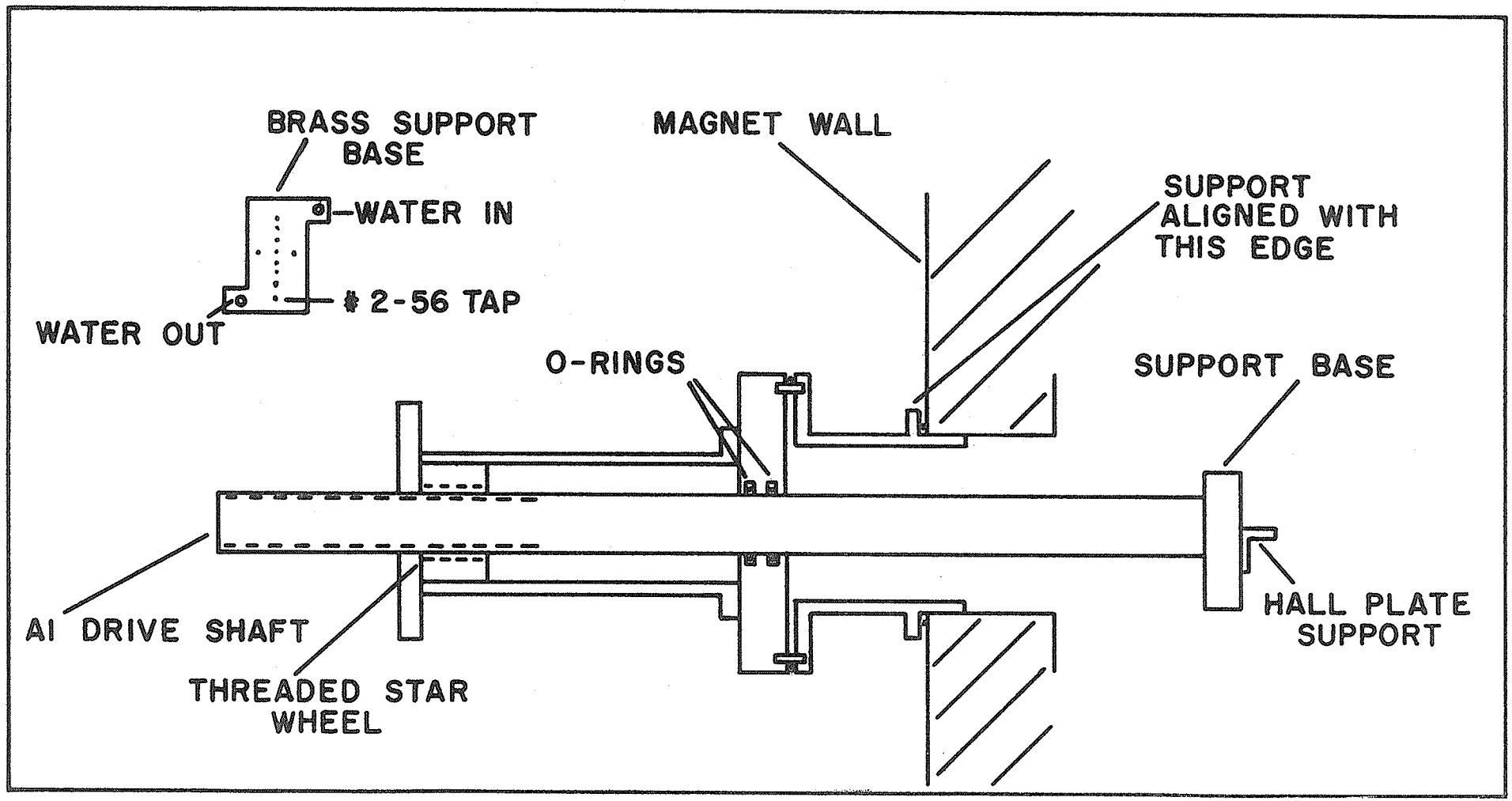
BRASS SUPPORT BASE
MAGNET WALL
WATER IN
SUPPORT ALIGNED WITH THIS EDGE
2-56 TAP
WATER OUT
O-RINGS
SUPPORT BASE
Al DRIVE SHAFT
HALL PLATE SUPPORT
THREADED STAR WHEEL

FIG. 2-4

Hall plate supports.

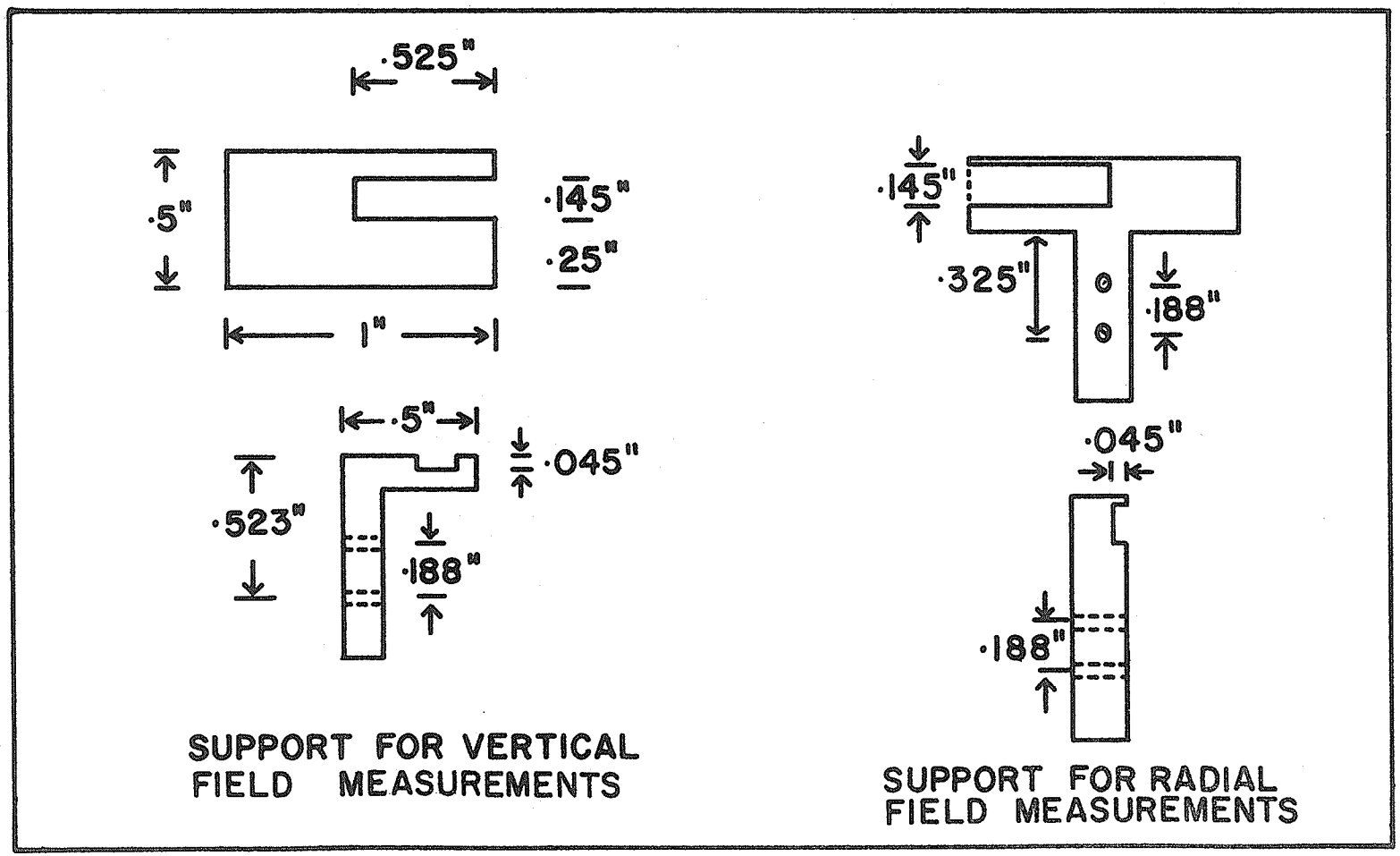
.525"
.5"
.145"
.25"
1"
.5"
.045"
.523"
.188"
SUPPORT FOR VERTICAL
FIELD MEASUREMENTS
.145"
.325"
.188"
.045"
.188"
SUPPORT FOR RADIAL
FIELD MEASUREMENTS

FIG. 2-5

Power supply for the Hall plate control current.

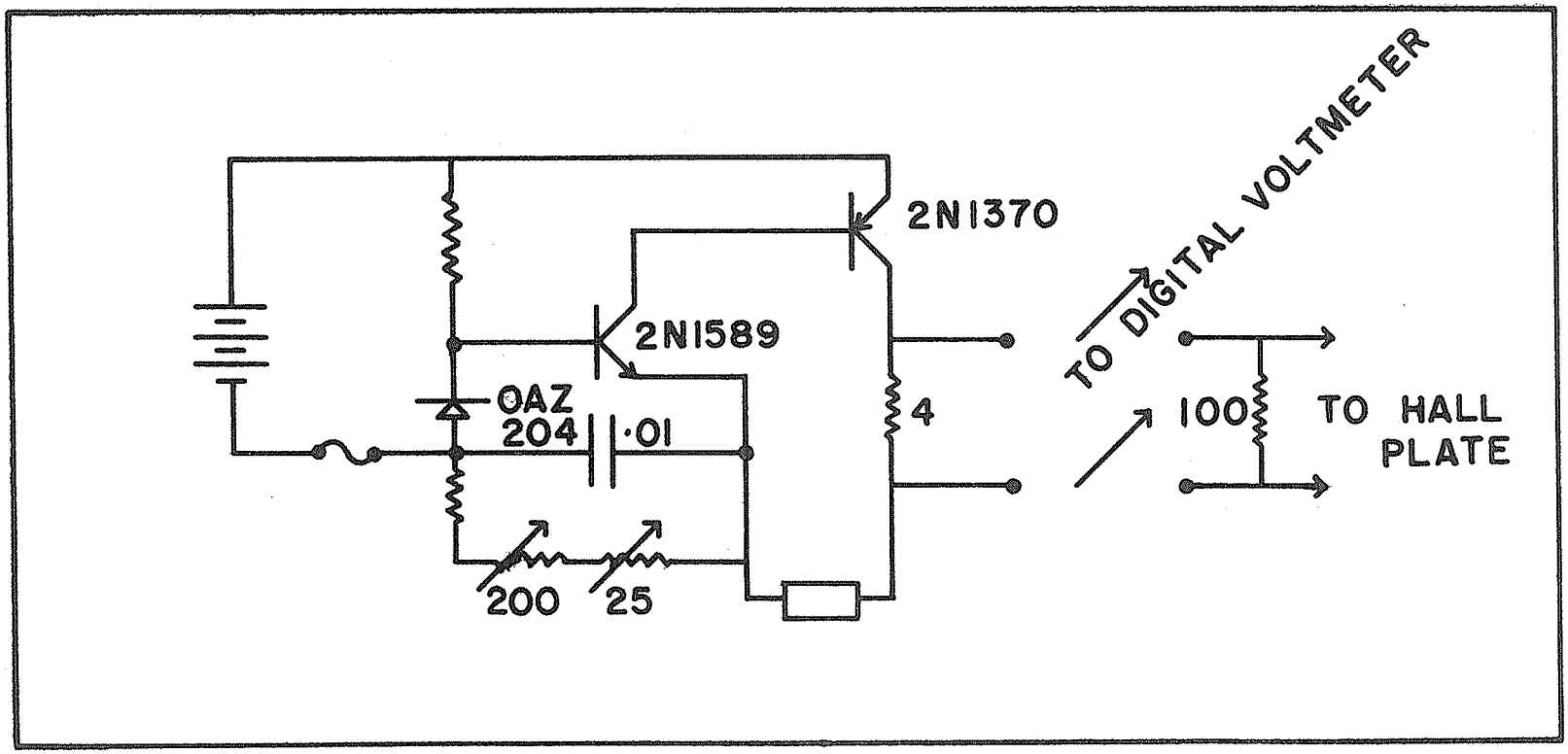
2N1370
2N1589
OAZ
204
·01
4
200
25
TO DIGITAL VOLTMETER
100
TO HALL
PLATE

The Hall plate control current was supplied by the current generator shown in Fig. 2-5. A stable 8 volt supply was used for the current generator and a coarse gain and fine gain potentiometer were used to keep the Hall current at a constant value. The control current was monitored by measuring the voltage drop across the 4Ω resister and was kept at a constant value of 90.15mv. The Hall voltage was measured using a Non-Linear Systems digital milli-voltmeter,model V60, with a range of 0.01 mv to 99.99 mv.

CALIBRATION OF THE HALL PLATE

The Hall plate was calibrated over the field range 0 to 12 kilogauss using a Rawson-Lush, type 820, rotating coil gaussmeter having a quoted accuracy of 0.1% or 2 gauss,(whichever is larger), and a coil diameter of 0.125". The coil was housed near the end of a long (~19") probe tube, and the Hall plate was calibrated by placing it beside the coil in the median plane of the magnet (as shown in Fig. 2-6). Since the Hall plate and coil were not in exactly the same position, the uniformity of the field, in the area of interest, was checked with the gaussmeter and no deviations larger than 0.1% were found. With the plane of the Hall plate horizontal, the plate was calibrated independently for field directions "up" and "down".

Care was taken to obtain the correct mechanical alignment of the rotating-coil gaussmeter. The meter reads the component of field perpendicular to the axis of the probe tube and therefore the probe tube

FIG. 2-6

The alignment of the rotating-coil gaussmeter and the Hall plate for Hall plate calibration.

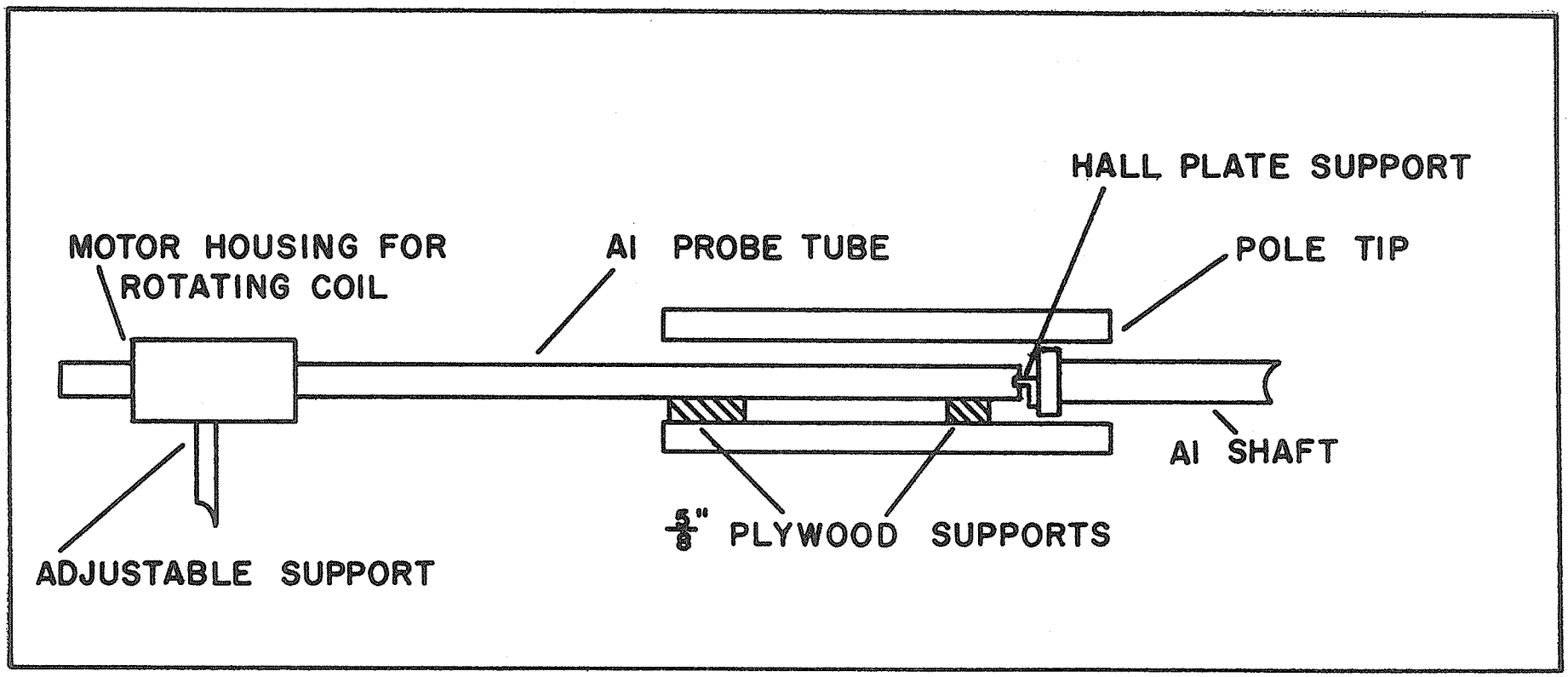
HALL PLATE SUPPORT
MOTOR HOUSING FOR ROTATING COIL
Al PROBE TUBE
POLE TIP
Al SHAFT
5/8" PLYWOOD SUPPORTS
ADJUSTABLE SUPPORT

must be parallel to the pole tips. The gaussmeter was supported as shown in Fig. 2-6. Parallel alignment was obtained by varying the height of the rear support so that no light was transmitted between the probe tube and the plywood blocks. To check this procedure the rear support was purposely "mis-adjusted" slightly and a decreased field reading was obtained. A second alignment was necessary since the tube has to be rotated to align a preferred direction of the probe parallel to the magnetic field. This alignment was accomplished by rotating the gaussmeter until a maximum field reading was obtained. Since the output of the gaussmeter falls off as the cosine of the angle between the field and the preferred direction this method of alignment was considered adequate.

Several calibrations were made and for each run the probe was independently aligned. Above 1kG. readings were taken approximately every 300 gauss, while below 1kG. readings were taken at fields of 35, 155, 370 and 710 gauss. The mean deviation in the calibration points was the greater of 0.15% and 3 gauss. The data obtained were used to generate a table relating Hall voltage to magnetic field by using a straight line interpolation between adjacent calibration points. Based on the variation in slope of these straight lines the estimated accuracy of the resulting conversion table is 0.2% or 4 gauss, whichever is larger.

FIELD MEASUREMENTS

Because of the construction of the magnet it was convenient to measure the field at each of the four access ports shown in Fig. 2-2. Before beginning the measurements it was necessary to shift the top and bottom pole tips so that they were exactly over one another. This adjusting of the pole tips was checked using the Hall plate positioning apparatus shown in Fig. 2-3. The Hall plate support was mounted so that it did not clear the pole tips and the distance from the outermost position of the drive shaft to the point of contact of the pole tip and the aluminum support was measured on each of the four ports. The pole tips were aligned so that for a given port the distance to the top and bottom pole tips was the same. Table 2-1 below shows the results of this alignment.

TABLE 2-1.

Port	Distance to Top	Distance to Bottom	Mean
1	1.313"	1.316	1.315
2	1.321	1.323	1.322
3	1.317	1.319	1.318
4	1.304	1.306	1.305

It will be noted that the mean distance to the pole tip edge (from the outermost position of the drive shaft), varies from port to port. This variation was adjusted for in measuring the magnetic field by defining the radial distance with respect to the edge of the pole tip.

The sensitive area of the Hall plate is approximately .030" by .060". For measuring the vertical field component the longer edge was orientated parallel to the radial line along which the Hall plate moved. This corresponded to the sensitive area subtending an angle ~0^{o} 10', (measured from the centre of the pole tip), when the Hall plate is at the edge of the pole tips. For measuring the radial field component the sensitive area was orientated with the longer edge perpendicular to the median plane.

The following general procedure was followed in taking the data:

(1) The Hall plate support was mounted on the brass support base (See Fig. 2-3), to measure the field at a given vertical displacement from the median plane.

(2) The positioning apparatus was mounted on a given port with the Hall plate above the median plane and the magnet current was run up to 250A from zero.

(3) The field was measured at intervals of 0.500",with the Hall plate advancing towards the centre of the magnet, over a radial distance of 3", starting from approximately 1.5" outside the pole tip edge.

(4) When the measurement was completed for the magnet current of 250A the Hall plate was withdrawn to the outermost position, the current was raised to 300A and the field measurements were repeated for the new current setting.

(5) The same procedure was repeated for a magnet current of 350A and the magnet current was then returned to zero. The positioning apparatus was de-mounted and the Hall plate was examined to see if it had moved out of position in the aluminum support. The assembly was then rotated through 180^{o} and

re-mounted on the same port to measure the field below the median plane.

(6) Following this set of measurements the assembly was removed and the Hall plate support was re-positioned on the support base to measure the field at a different vertical displacement.

Field measurements were made with the positioning apparatus mounted on all four ports and all measurements were done with the Hall plate advancing towards the magnet centre to compensate for any back-lash in the drive shaft. The magnet current was monitored by measuring the voltage drop across a 1mΩ shunt and could be controlled to ±0.3 amp. For the vertical field component measurements were made at vertical displacements from the median plane ranging from +1.471" to -1.479" in vertical steps of .1875" and for the radial field component measurements were made at vertical displacements ranging from +1.467"to -1.475" in steps of .1875". In addition the vertical field component was also measured at displacements of +.808" and -.816". The gap space, between the pole tips, is only 2". Therefore,for vertical displacements >1" the field was measured only outside the edge of the pole tips.

The results of the field measurements are summarized in Figs. 2-7, 2-8 and 2-9. The curves represent the average of the fields obtained from measurements on the four ports. The pronounced "bump" in the vertical field component,(Fig. 2-8), in the neighbourhood of the pole tip edge, is attributed to the "sharp" edge of the pole tip. Tables 2-2 and 2-3 show a representative set of Hall plate voltages indicating the reproducibility of the measurements from port to port.

FIG. 2-7

The median plane magnetic field for magnet currents of 250, curve A, 300, curve B, and 350A, curve C. The origin is taken to be the edge of the pole tip.

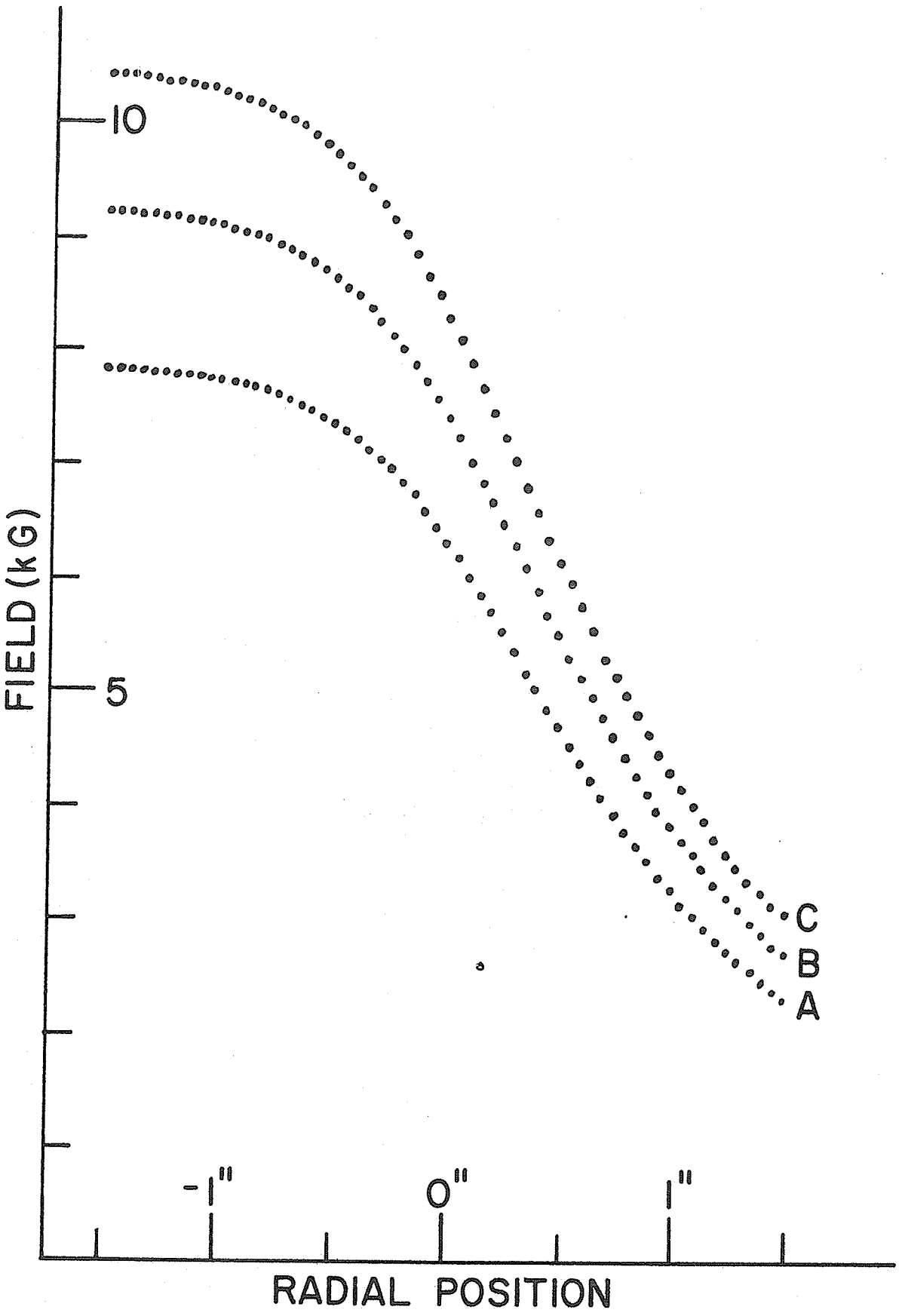
10
5
FIELD (kG)
C
B
A
-1"
0"
1"
RADIAL POSITION

FIG. 2-8

The vertical field component for a current of 300A at displacements from the median plane of 0", A, .559", B, .746", C, .808", D, .934", E, 1.121", F, 1.321", G and 1.471", H. The origin is taken to be the edge of the pole tips.

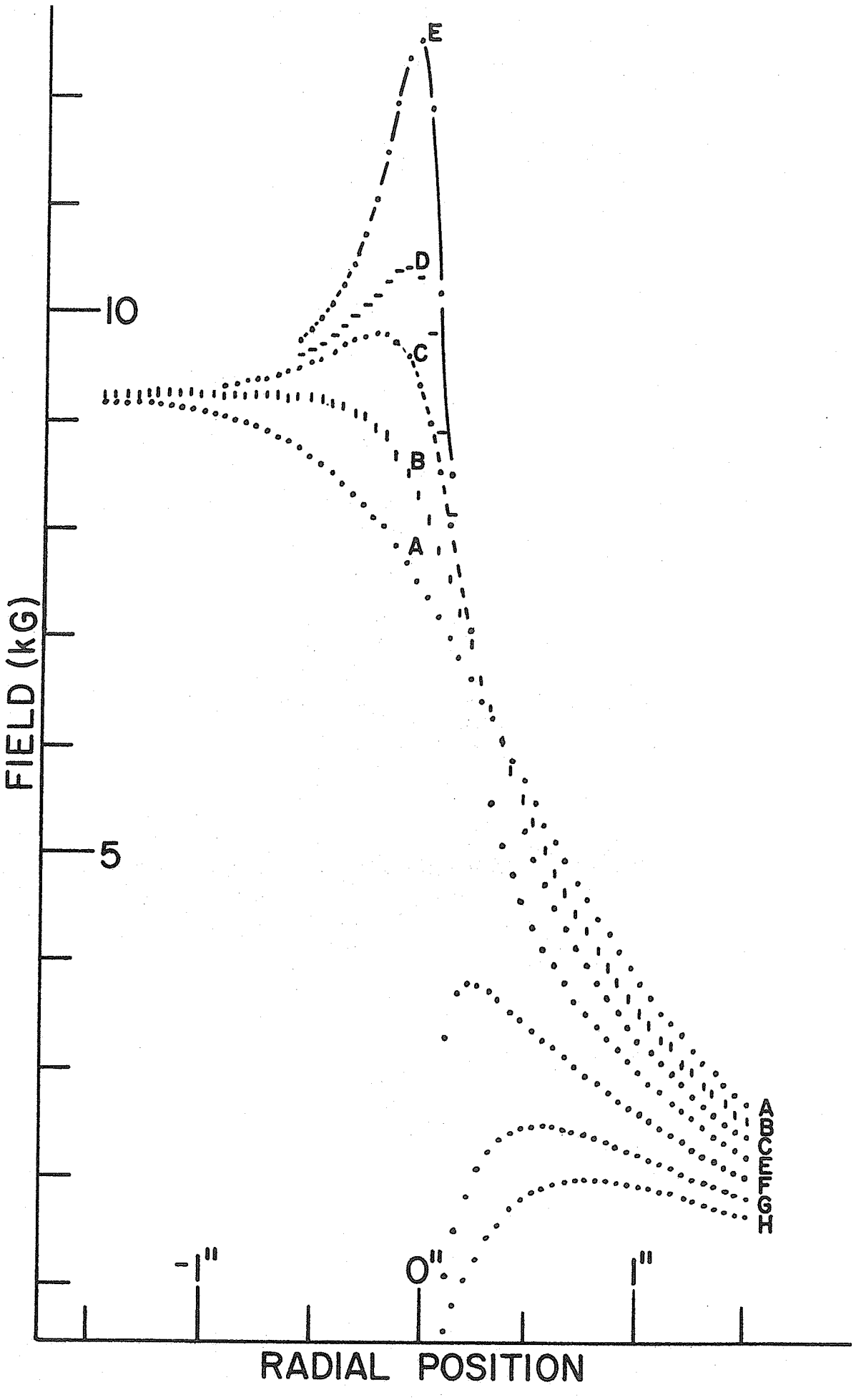
E
D
C
B
A
10
5
FIELD (kG)
ABCDEFGH
-1"
0"
1"
RADIAL POSITION

FIG. 2-9

The radial field component for a current of 300A at displacements from the median plane .180", A, .375", B, .555", C, .742", D, .930", E, 1.117", F, 1.317", G and 1.475", H. The origin is taken to be the edge of the pole tips.

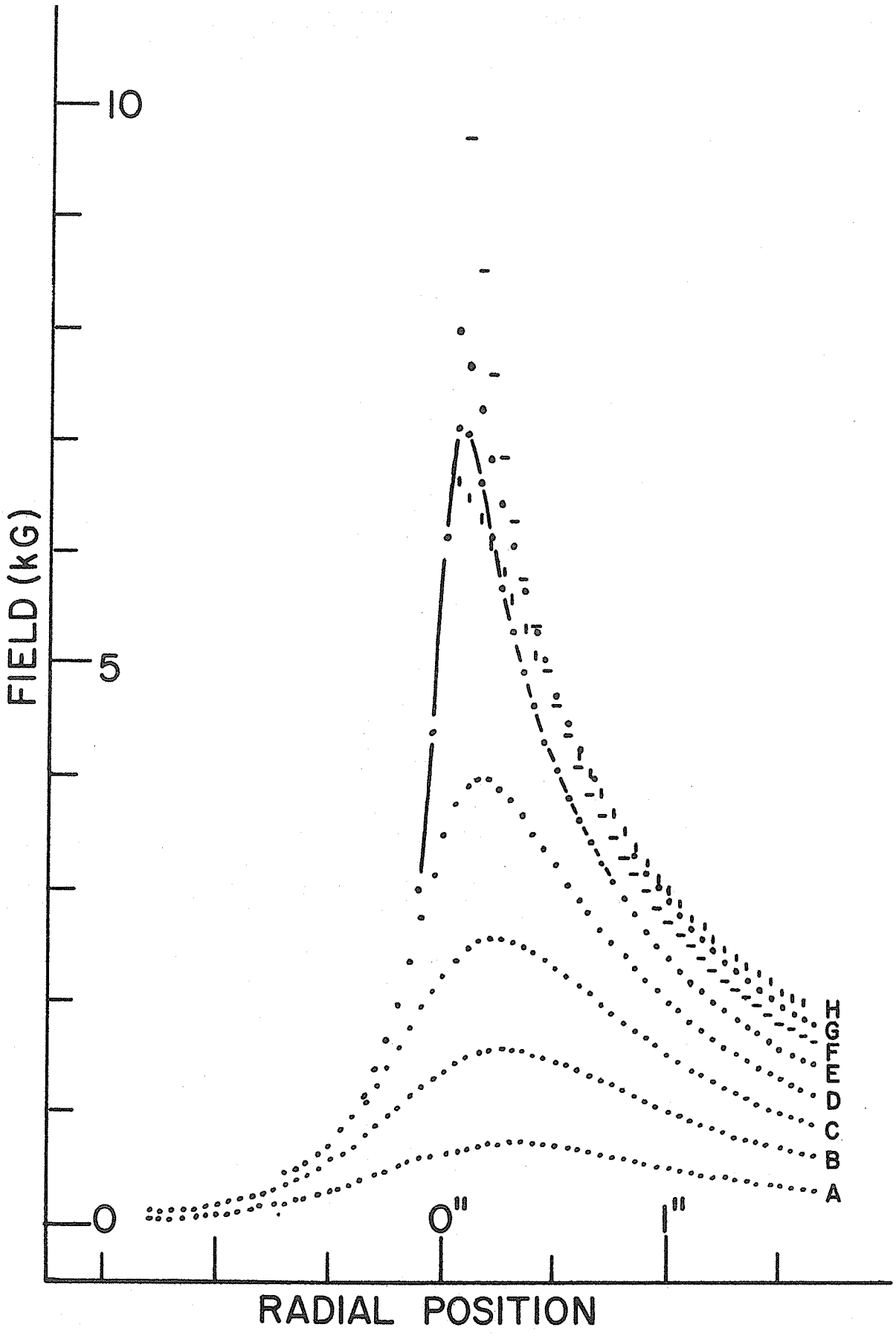
10
5
0
FIELD (kG)
0"
1"
RADIAL POSITION
H
G
F
E
D
C
B
A

For the vertical field measurements the greatest deviation from the mean is ~1% and this occurs only in a limited region close to the edge of the pole tip. The radial field component is generally not as reproducible as the vertical field but the largest deviation of a measurement on a given port from the mean is ~1%.

The reproducibility of the measurements from port to port, coupled with the accuracy of the Hall plate calibration, limits the accuracy of the field measurements. Thus the vertical field is estimated to have an absolute accuracy of 0.5%, except in the immediate vicinity of the pole tip edge. This error is composed of a contribution, from the reproducibility of the Hall plate voltages from port to port, of .2% and a contribution from the calibration of .3%. It is worthwhile pointing out that the median plane field was remeasured one year after the initial measurements and the Hall voltages were reproduced to within the stated accuracy of ±.2%.

How does the finite area of the Hall plate affect the accuracy of the measurements? The Hall voltage represents some sort of "average field", averaged over the area of the Hall Plate. (Recall that the dimensions of the Hall plate used here are .030" x .060"). For the vertical field component the Hall plate was mounted so that the output represented the average field over a radial distance of .060". If the field, over this length, varies linearly with the radius this "average" field is then the same as the field at the midpoint, which we have used to define the location of the Hall plate. The results of the field measurements indi-

TABLE 2-2

Some representative results of the magnetic field measurements indicating the reproducibility of the vertical field component from port to port.

HALL PLATE VOLTAGE (mV)

Radial Position	Port #1	Port #2	Port #3	Port #4	Mean
		(a) Median Plane			
+1.50"	6.08	6.08	6.09	6.09	6.09
+1.00"	8.72	8.72	8.74	8.70	8.72
+0.50"	12.67	12.68	12.69	12.65	12.67
0.00"	17.28	17.29	17.30	17.26	17.28
-0.50"	20.31	20.32	20.33	20.30	20.32
-1.00"	21.40	21.39	21.40	21.38	21.39
-1.50"	21.68	21.66	21.68	21.66	21.67
		(b) 9/16" above Median Plane			
+1.50"	5.69	5.67	5.69	5.67	5.68
+1.00"	8.09	8.05	8.09	8.05	8.07
+0.50"	12.21	12.19	12.21	12.19	12.20
0.00"	19.01	19.02	18.99	18.93	18.99
-0.50"	21.72	21.72	21.70	21.66	21.70
-1.00"	21.81	21.80	21.79	21.78	21.79
-1.50"	21.80	21.79	21.77	21.77	21.78
		(c) 15/16" above Median Plane			
+1.50"	5.02	5.00	5.01	4.98	5.00
+1.00"	6.81	6.78	6.80	6.78	6.79
+0.50"	10.00	9.97	10.04	9.99	10.00
0.00"	28.73	28.52	28.26	28.32	28.40
-0.50	23.70	23.54	23.58	23.52	23.58
-1.00"	22.15	22.16	22.11	22.13	22.14
-1.50"	22.02	21.94	21.90	21.89	21.94

TABLE 2-3

Some representative results of the magnetic field measurements indicating the reproducibility of the radial field component from port to port.

HALL PLATE VOLTAGE (mV)

Radial Position	Port #1	Port #2	Port #3	Port #4	Mean
	(a) 3/16" above Median Plane				
+1.50"	0.75	0.74	0.73	0.73	0.74
+1.00"	1.11	1.10	1.09	1.08	1.10
+0.50"	1.55	1.54	1.53	1.51	1.53
0.00"	1.43	1.40	1.40	1.41	1.41
-0.50"	0.64	0.63	0.60	0.62	0.62
-1.00"	0.19	0.17	0.18	0.16	0.18
	(b) 9/16" above Median Plane				
+1.50"	2.21	2.23	2.19	2.21	2.21
+1.00"	3.37	3.39	3.34	3.36	3.37
+0.50"	5.13	5.17	5.09	5.11	5.13
0.00"	4.97	5.00	4.91	4.94	4.96
-0.50"	1.53	1.54	1.52	1.52	1.53
-1.00"	0.34	0.35	0.35	0.35	0.35
	(c) 12/16" above Median Plane				
+1.50"	2.88	2.90	2.88	2.91	2.89
+1.00"	4.42	4.45	4.43	4.45	4.44
+0.50"	7.22	7.26	7.20	7.24	7.23
0.00"	7.80	7.81	7.74	7.80	7.79
-0.50"	1.43	1.44	1.41	1.45	1.43
-1.00"	0.30	0.31	0.27	0.31	0.30
	(d) 15/16" above Median Plane				
+1.50"	3.48	3.50	3.45	3.45	3.47
+1.00"	5.34	5.37	5.30	5.30	5.33
+0.50"	9.23	9.29	9.19	9.19	9.23
0.00"	14.20	14.44	13.83	13.96	14.11
-0.50"	0.55	0.60	0.55	0.55	0.56
-1.00"	0.08	0.14	0.05	0.06	0.08

cate that, for a limited radial distance, the field can be considered to vary linearly with radius, so for the vertical field component the finite area of the Hall plate does not introduce any significant error, except for those points around the top of the "bump" in the vertical field. (See Fig. 2-8). For vertical displacements ~13/16" and 15/16" from the median plane, the vertical field, near the top of the "bump" is not as accurate as the reproducibility of the Hall plate readings indicates. It is estimated that in this region the vertical field is only accurate to ~±5%. For the radial field component the Hall plate was mounted so that the output represented the "average" radial field over a vertical displacement of .060". Over this limited range the radial field can be considered to vary linearly with heighth so the effect of the finite area is small. Thus the accuracy of the radial field component is ~±1% as indicated by the reproducibility of the measurements from port to port.

CHAPTER 3.

THEORETICAL ANALYSIS OF THE SPECTROMETER

"Everything's got a moral, if you can only find it."

..... Lewis Carroll

FIELD FITTING:

The experimental data for the vertical and radial field components was used in a computer study of the spectrometer's performance. For this study it was desirable to fit the magnetic field to an analytic expression and an attempt was made to find a function, $F(r,z)$, for each field component, which would adequately reproduce the experimental data throughout the entire region. Initially a least squares fit to a polynomial $B = \sum_{n,m} A_{n,m} r^n z^m$ was tried but the results were not adequate. A second attempt was made using the standard expansion [3] in Legendre polynomials. Up to 9th order polynomials were included in the expansion but again an adequate fit was not obtained, presumably because not enough terms were included in the expansion. Following this, the search for a single fitting function was abandoned.

It was finally decided to fit the field components to appropriate functions, $B_r(z)$ and $B_z(z)$, at each of the radial positions at which the fields had been measured, and to generate the fields at an arbitrary position, (r,z), in the following manner: The two nearest radial positions, R and $R + \Delta R$, at which the fields had been

measured, are determined. The fields at (R,z) and (R + ΔR,z) are calculated using the functions $B_r(z)$, and $B_z(z)$. The fields at (r,z) are then calculated using a straight line interpolation in r. Because the field components above and below the median plane differed slightly, they were fitted independently in the two regions $z \geq 0$ and $z \leq 0$. It was possible to obtain good fits to both the radial and vertical field components at most radial positions using simple polynomials. However, for radii close to the radius of the pole tips, r_o, the polynomial fits were far from satisfactory. To gain some feeling for the functional forms which might be used the measured values of B_z and B_r were plotted as functions of z for $r \sim r_o$. See Figs. 3-1 and 3-2. The shape of the curves suggested using exponential terms and satisfactory fits were eventually obtained using the equations

$$B_z = A_1+A_2|z|+A_3|z|^2+A_4/[1+\mathrm{Exp}\{A_6(|Z|-z_1)\}]$$

$$+ A_5\ \mathrm{Exp}\{A_7(|Z|-z_2)^2\}\ ,$$

where z_1 = 2.90 cm., z_2 = 2.30 cm., and

$$Br = \pm(C_1+C_2|z|+C_3|z|^2+C_4|z|^3+C_5\ \mathrm{Exp}[C_6(|z|-z_o)^2]$$

where z_o = 2.8375 cm.

Except for 7 radial positions in the immediate vicinity of the pole tip edge the coefficient A_5, (vertical field), was set = 0.

FIG. 3-1

The vertical field component versus Z for radial displacements of .23cm., A, .48cm., B, .73cm., C, and .99cm., D, from the pole tip edge.

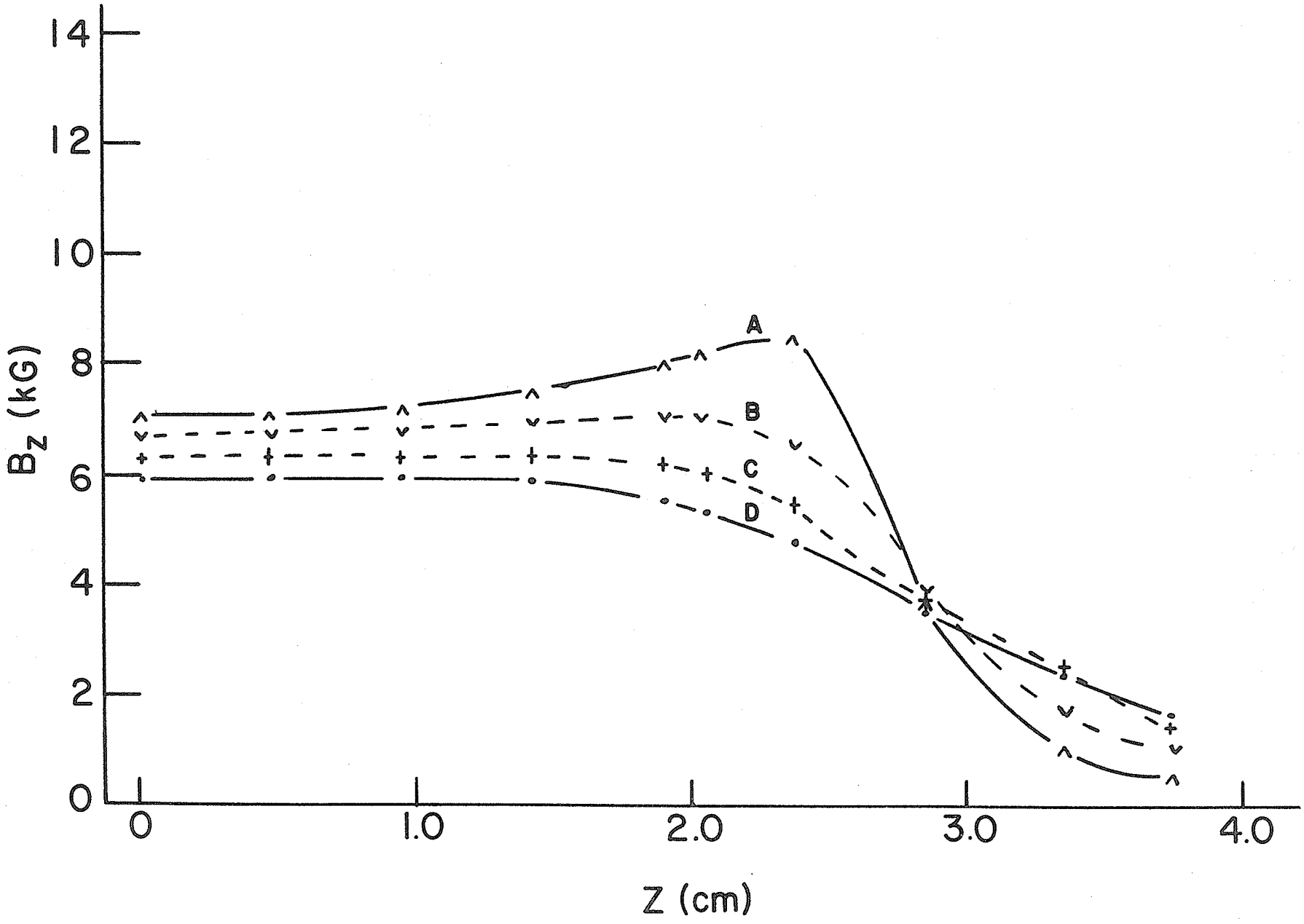
14
12
10
8
6
4
2
0
B_z (kG)
A
B
C
D
0
1.0
2.0
3.0
4.0
Z (cm)

FIG. 3-2

The radial field component versus Z for radial displacements of .28cm., A, .53cm., B, .79cm., C, and 1.29cm., D, from the pole tip edge.

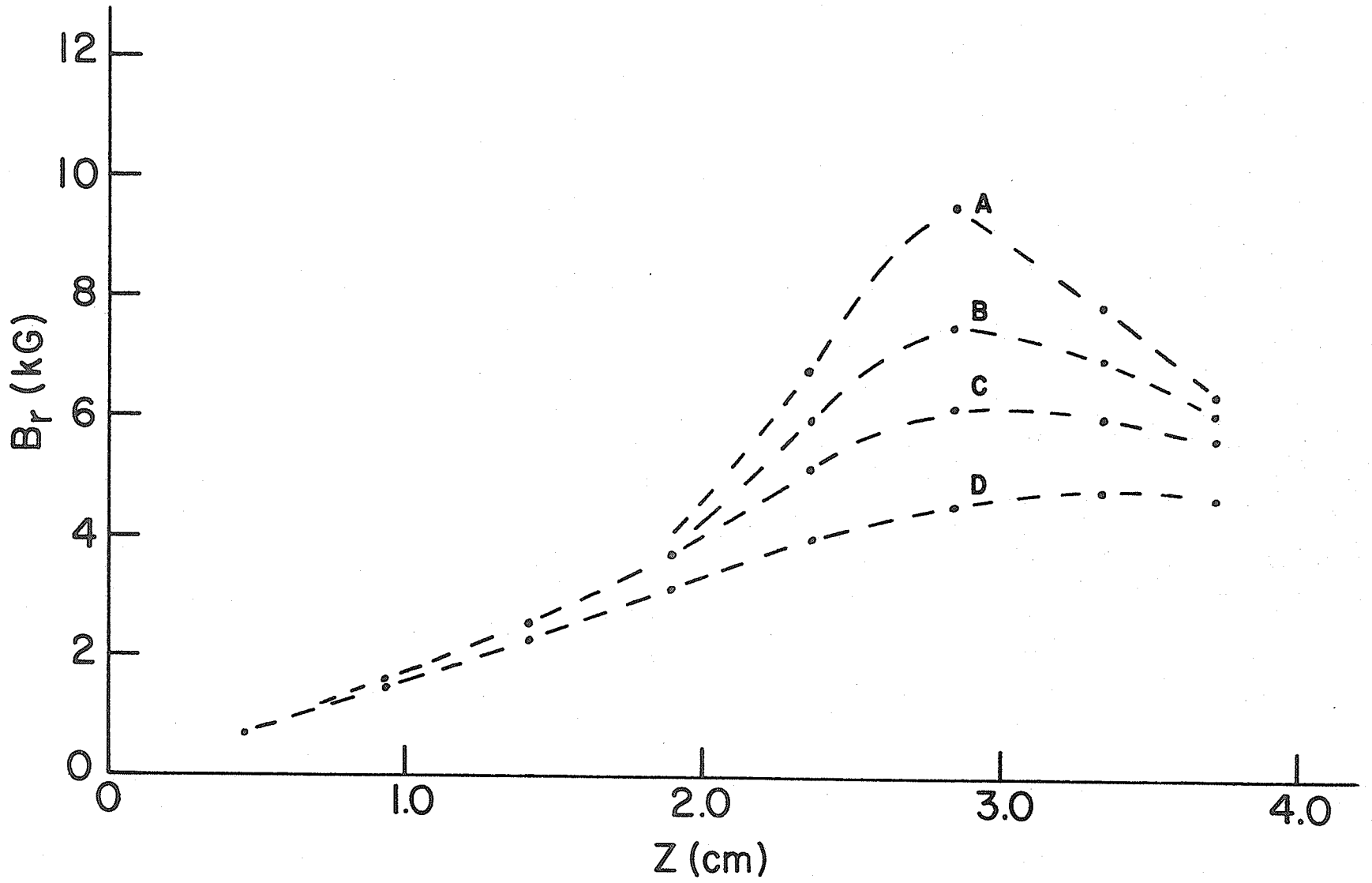
12
10
8
6
4
2
0
B_r (kG)
A
B
C
D
0
1.0
2.0
3.0
4.0
Z (cm)

The method of obtaining the "best" fit to the experimental data, using the above equations, was similar for both components. For the radial field several reasonable values of C_6 were chosen and for each value the coefficients C_1 to C_5 were generated by a least squares fit to the data using a polynomial regression technique. The results were then compared to obtain the "best" value of C_6. The judgement, as to which, of two values of C_6, gave the better fit, was somewhat subjective and involved a comparison between the overall shape of the curve, the maximum deviation of the calculated field from the measured field, and the value of Z at which this maximum occurs, the average algebraic error between the calculated fields and the measured fields, and the average absolute error. For the vertical field A_6 and A_7 were determined in a similar fashion.

An example of the fits obtained for the radial and vertical field components are shown in tables 3-1 and 3-2 respectively. In these tables the radial position is measured with respect to the centre of the pole tips, radius 13.5cm. and the vertical position with respect to the median plane. A check on the validity of the fitting procedure was obtained by predicting the vertical and radial field components at vertical displacements different from those at which measurements were made. Figs. 3-3 and 3-4 compare the predicted fields at such displacements from the median plane, with the measured fields obtained at neighbouring values of z. These curves confirm that the fitting functions generate a field pattern consistent with the measurements.

TABLE 3-1

Comparison of the predicted radial field component with the experimental value.

Vertical Position (cm)	Measured Field (kG)	Estimated Field (kG)	Percent Error
	(a) r = 17.2cm.		
0.00"	0.0	0	0
.456	0.347	0.345	-.54
.933	0.696	0.696	+.06
1.409	1.030	1.029	-.09
1.885	1.347	1.334	-.98
2.361	1.614	1.602	-.74
2.838	1.845	1.830	-.84
3.346	2.012	2.022	+.50
3.727	2.214	2.124	-4.1
	Algebraic Average Error =		-.75%
	(b) r = 16.2cm.		
0.00	0.0	0.0	0
0.456	0.477	0.477	+0.03
0.933	0.968	0.969	+ .08
1.409	1.445	1.437	- .58
1.885	1.893	1.867	-1.40
2.361	2.262	2.244	- .78
2.838	2.562	2.545	- .65
3.346	2.744	2.754	+ .35
3.727	2.967	2.828	-4.7
	Algebraic Average Error =		.85%
	(c) r = 15.2cm.		
0.00	0.0	0.0	0
0.456	0.638	0.642	+ .61
0.933	1.329	1.318	- .81
1.409	2.043	2.025	- .83
1.885	2.766	2.741	- .92
2.361	3.391	3.370	- .63
2.838	3.831	3.798	- .87
3.346	3.997	3.977	- .49
3.727	4.182	3.966	-5.15
	Algebraic Average Error =		-1.01%

Vertical Position (cm)	Measured Field (kG)	Estimated Field (kG)	Percent Error
	(d) r = 14.2cm.		
0	0	0	0
.456	.718	.726	+1.10
.933	1.547	1.553	+ .40
1.409	2.532	2.517	- .58
1.885	3.883	3.869	- .36
2.361	5.678	5.595	-1.46
2.838	6.820	6.741	-1.16
3.346	6.414	6.454	+ .62
3.727	6.047	5.726	-5.31
	Algebraic Average Error =		- .75%
	(e) r = 13.8cm.		
0	0	0	0
.456	.678	.693	+2.2
.933	1.467	1.524	+3.9
1.409	2.428	2.435	+ .3
1.885	3.887	3.872	- .4
2.361	7.016	6.881	-1.9
2.838	9.676	9.400	-2.8
3.346	7.622	7.896	+3.6
3.727	6.630	6.298	-5.0
	Algebraic Average Error =		-.01%
	(f) r = 13.2cm.		
0	0	0	0
.456	.571	.573	+ .36
.933	1.204	1.198	- .67
1.409	1.893	1.874	- .99
1.885	2.688	2.662	- .97
2.361	2.949	2.885	-2.17
3.838			
3.346		Undefined.	
3.727			
	Algebraic Average Error =		- .74%

TABLE 3-2

Comparison of the predicted vertical field component with the experimental value.

Vertical Position (cm)	Measured Field (kG)	Estimated Field (kG)	Percent Error
	(a) r = 17.3cm.		
-0.01	2.701	2.685	- .61
.47	2.679	2.678	- .03
.94	2.618	2.619	+ .04
1.42	2.523	2.521	- .07
1.90	2.389	2.385	- .15
2.05	2.323	2.333	+ .41
2.37	2.227	2.217	- .45
2.85	2.016	2.027	+ .56
3.36	1.827	1.818	- .52
3.74	1.663	1.666	+ .20
	Algebraic Average Error =		- .06%
	(b) r = 16.3cm.		
-0.01	3.566	3.552	- .39
.47	3.537	3.535	- .05
.94	3.447	3.450	+ .10
1.42	3.302	3.302	- .0
1.90	3.092	3.087	-0.17
2.05	2.997	3.001	+ .14
2.37	2.818	2.812	- .22
2.85	2.484	2.497	+ .52
3.36	2.161	2.150	- .49
3.74	1.902	1.900	+ .19
	Algebraic Average Error =		- .04%
	(c) r = 15.2cm.		
-0.01	4.765	4.746	- .39
.47	4.739	4.737	- .04
.94	4.651	4.649	- .05
1.42	4.469	4.468	- .02
1.90	4.157	4.154	- .06
2.05	4.014	4.015	+ .02
2.37	3.686	3.683	- .09
2.85	3.062	3.086	+ .80
3.36	2.454	2.432	- .92
3.74	2.003	2.009	+ .32
	Algebraic Average Error =		- .04%

Vertical Position (cm)	Measured Field (kG)	Estimated Field (kG)	Percent Error
	(d) r = 14.2cm.		
- .01	6.269	6.244	- .39
.47	6.282	6.290	+ .13
.94	6.311	6.321	+ .15
1.42	6.340	6.330	- .15
1.90	3.212	6.213	+ .01
2.05	6.067	6.063	- .06
2.37	5.490	5.452	- .69
2.85	3.750	3.843	+2.48
3.36	2.253	2.174	-3.49
3.74	1.453	1.480	+1.83
	Algebraic Average Error =		- .01%
	(e) r = 13.7cm.		
-0.01	7.037	7.114	+1.10
.47	7.082	7.052	- .43
.94	7.234	7.254	+ .28
1.42	7.540	7.435	-1.39
1.90	8.067	7.944	-1.53
2.05	8.281	8.559	+3.35
2.37	8.543	8.376	-1.95
2.85	3.379	3.596	+6.43
3.36	1.102	1.014	-8.00
3.74	0.575	0.607	+5.63
	Algebraic Average Error =		+ .32%
	(f) r = 13.2cm.		
-0.01	7.721	7.697	- .32
.47	7.783	7.778	- .06
.94	8.023	8.029	+ .08
1.42	8.535	8.535	0
1.90	9.596	9.584	- .13
2.05	10.198	10.210	+ .12
2.37	12.379	12.377	- .02
2.85			
3.36		Undefined	
3.74			
	Algebraic Average Error =		- .05%

FIG. 3-3

Comparison of the predicted vertical field component with measurement. Curve A, Z=2.371cm. measured; α, Z=2.21cm., predicted; B, Z=2.05cm., measured; C, Z= 1.90cm., measured; γ, Z=1.56cm.,predicted; D, Z=1.42, measured.

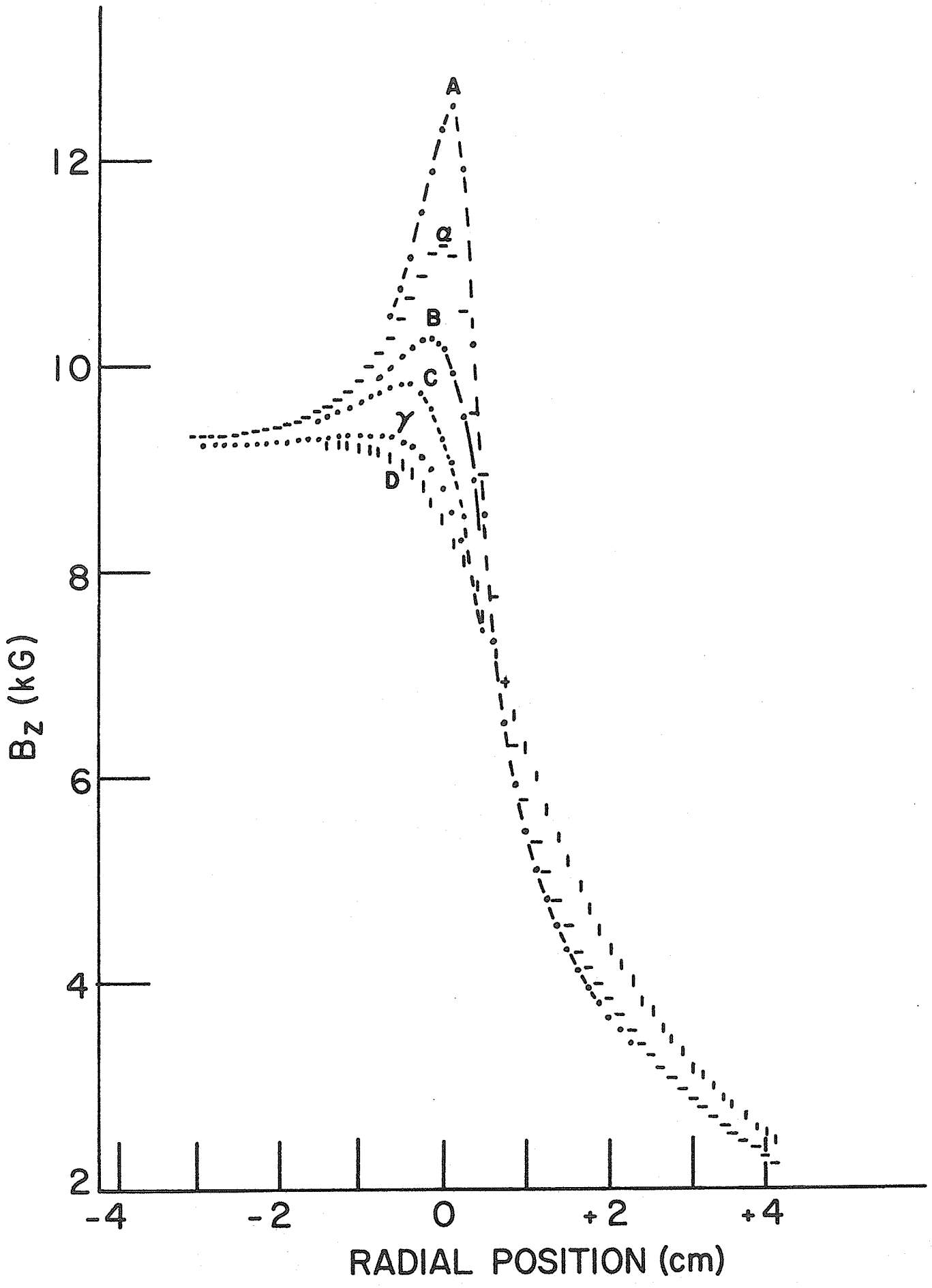
A
α
B
C
γ
D
12
10
8
6
4
2
Bz (kG)
-4
-2
0
+2
+4
RADIAL POSITION (cm)

FIG. 3-4

Comparison of the predicted radial field component with measurement. Curve A, Z=2.36cm., measured; α, Z=2.06cm., predicted;
B, Z=1.89cm., measured; β, Z=1.57cm., predicted
C, Z=1.41cm., measured; γ, Z=1.09cm., predicted
D, Z=0.93cm., measured; δ, Z= .77cm., predicted
E, Z= .47cm., measured; ϵ, Z= .21cm., predicted

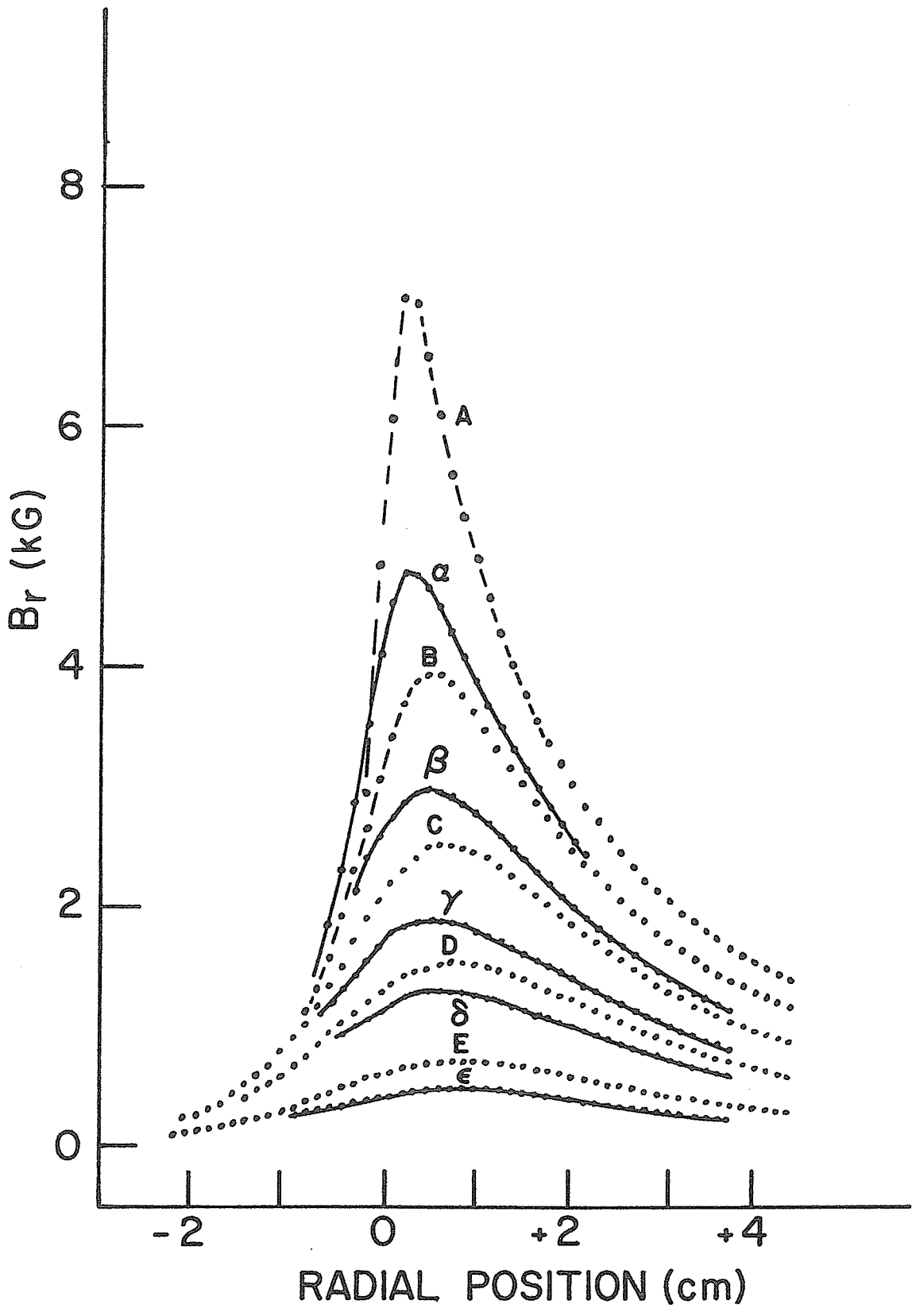
8
6
4
2
0
Br (kG)
A
α
B
β
C
γ
D
δ
E
ϵ
-2
0
+2
+4
RADIAL POSITION (cm)

THE STUDY OF THE SPECTROMETER'S PERFORMANCE

A detailed study of the spectrometer has been carried out using the magnetic field corresponding to a magnet current of 300A. Since electrons emitted from the source are subject only to magnetic interaction the equation of motion may be written $\vec{F} = m\frac{d\vec{v}}{dt} = q\,\vec{v} \times \vec{B}$ (rationalized MKS units), where $m = mo/(1-\beta^2)^{\frac{1}{2}}$ is the relativistic mass. Because of the cylindrical symmetry it is convenient to work in cylindrical polar co-ordinates. Then

$$\vec{B} = B_r\hat{r} + B_z\hat{k}$$

and the equations of motion, in component form, become

$$m(\ddot{r} - r\dot{\theta}^2) = qr\dot{\theta}B_z$$

$$m(r\ddot{\theta}+2\dot{r}\dot{\theta}) = q(\dot{Z}B_r-\dot{r}B_z)$$

$$m\ddot{Z} = -qr\dot{\theta}B_r.$$

Using the Runge-Kutta technique [4] the computer programme integrates the equations of motion numerically, in consecutive and equal increments of time, for electrons emitted in random directions from a point source located on the median plane, 7.6mm. beyond the edge of the pole tips, (the normal position of the source in the experimental work). The electrons are tracked through an angular distance of 15° around the pole tips. At the end of each iteration the position of the electron is checked to determine if it has collided with the pole tips or the walls

of the vacuum chamber. The transmission of the instrument is then defined to be the percentage of emitted electrons which are captured into stable orbits and drift to 15^{o} without suffering such collisions. Since the electrons will have gone through several periods of their vertical motion by 15^{o} no appreciable number of electrons are lost after this point.

Although no comprehensive study of the detailed motion of the electrons has been carried out, we have, for a few cases, computed the individual orbits which the particles follow. Figs. 3-5 and 3-6 show the computed motion of a 500 keV electron emitted tangentially to the pole tips and at an angle of 15^{o} to the median plane, from a source located 7.6mm. beyond the edge of the pole tips. These figures demonstrate the general nature of the motion. In these figures the points indicated by x's correspond in time. It will be noted that the period of the vertical oscillation is several times larger than the period of the trochoids.

To study the effect of finite detector area the geometrical parameters of the detectors used in the experimental work were included in the programme. (The detectors are circular with the Si wafer mounted on a brass cylinder 21mm. in diameter and 12.7mm. deep. See Fig. 3-7.) Electrons were assumed to be detected only if they struck the front of the active area of the detector and calculations were carried out for circular active areas ranging from $100mm.^{2}$ to $350mm.^{2}$. For purposes of calculation the detector was supposedly centred on the median plane at the same radius as the source and located 15^{o} from the

FIG. 3-5

Computed motion of a 500 keV electron emitted 15^{o} out of the median plane showing the trochoidal nature of the motion. The points labelled "X" in Fig. 3-5 and Fig. 3-6 correspond in time.

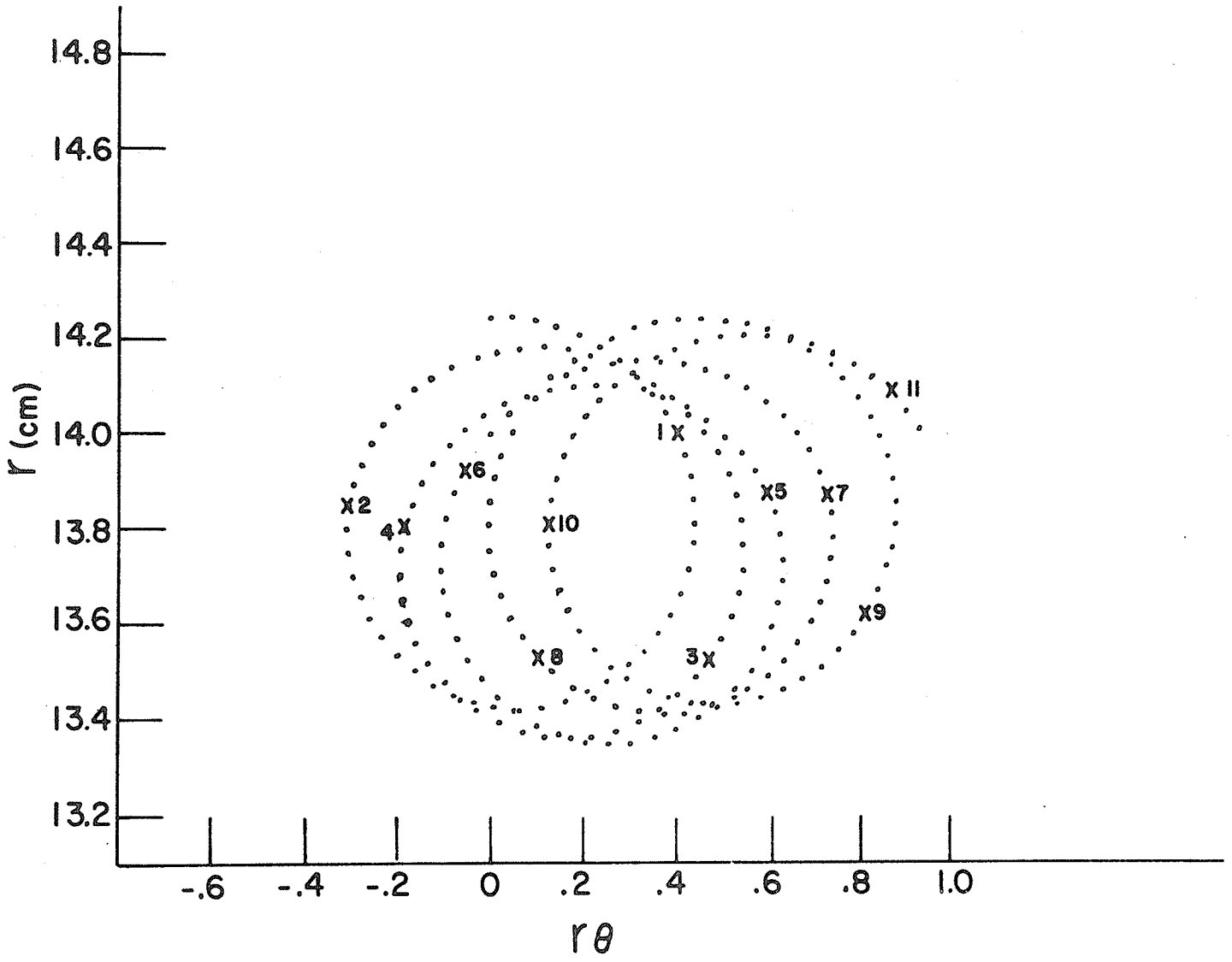
14.8
14.6
14.4
14.2
14.0
13.8
13.6
13.4
13.2
r (cm)
-.6
-.4
-.2
0
.2
.4
.6
.8
1.0
rθ
X 11
1 X
X6
X5
X7
X2
4X
X10
X9
X8
3X

FIG. 3-6

Computed motion of a 500 keV electron emitted 15^{o} out of the median plane showing the nature of the vertical motion. The points labelled "X" in Fig. 3-5 and Fig. 3-6 correspond in time.

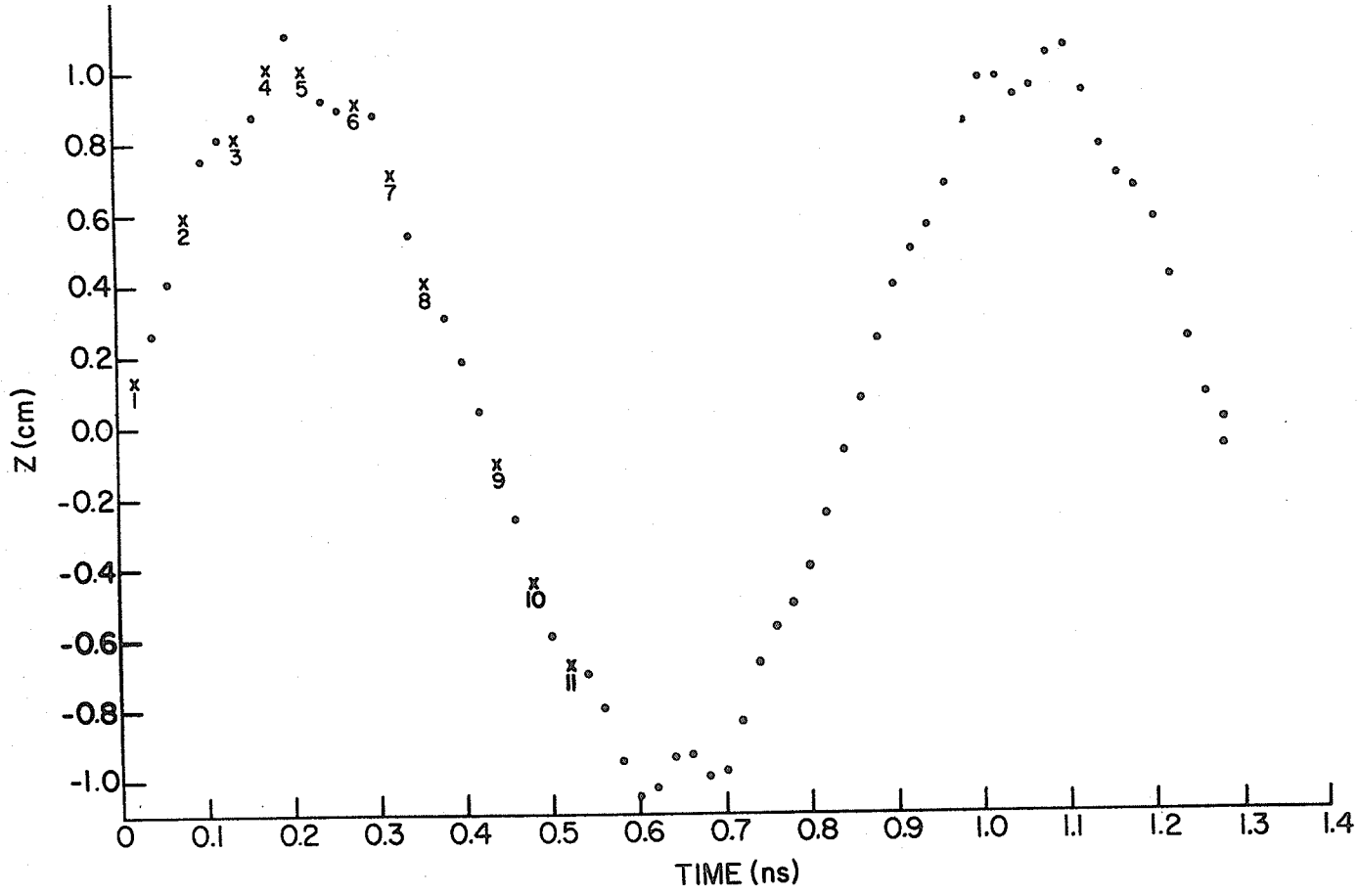
Z (cm)
1.0
0.8
0.6
0.4
0.2
0.0
-0.2
-0.4
-0.6
-0.8
-1.0
0
0.1
0.2
0.3
0.4
0.5
0.6
0.7
0.8
0.9
1.0
1.1
1.2
1.3
1.4
TIME (ns)
1
2
3
4
5
6
7
8
9
10
11

FIG. 3-7

Detector Cross-section.

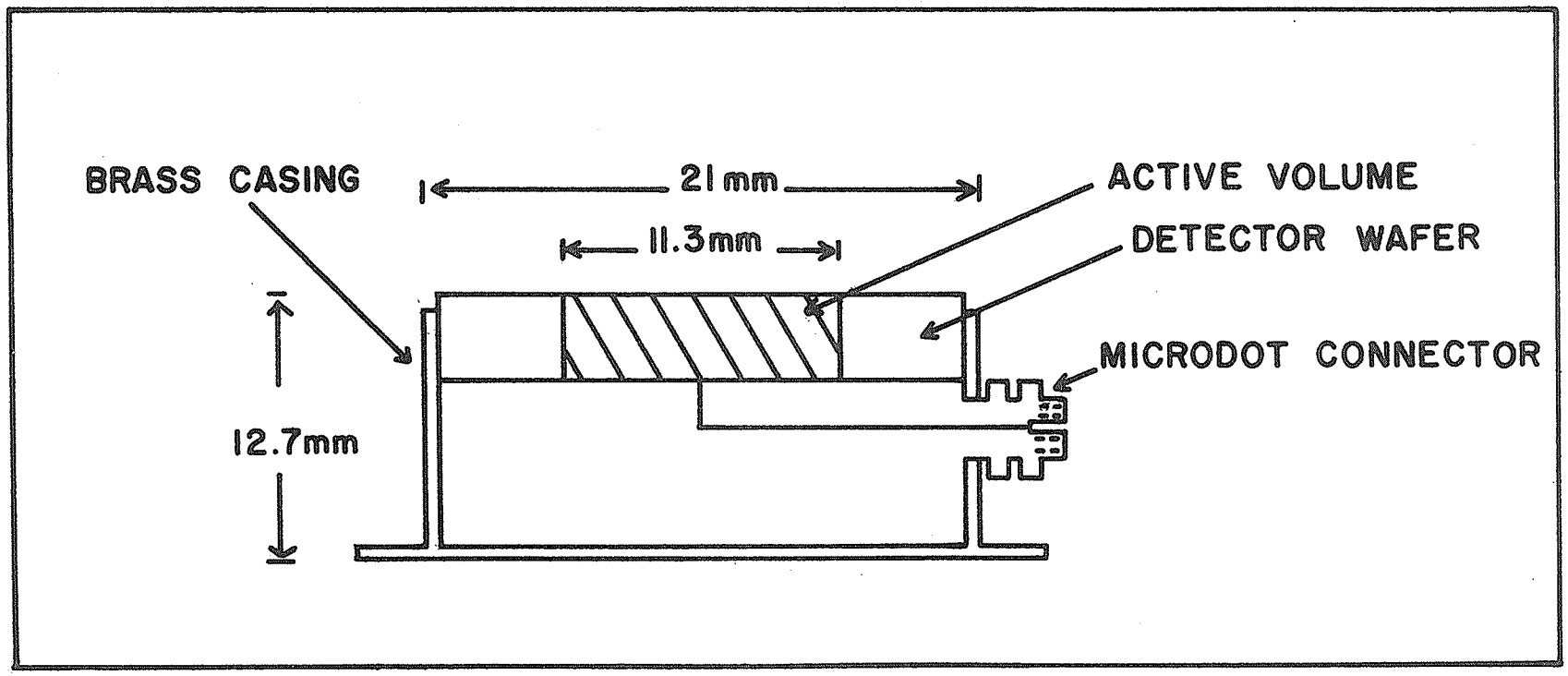
BRASS CASING
21 mm
11.3mm
ACTIVE VOLUME
DETECTOR WAFER
MICRODOT CONNECTOR
12.7mm

source. (ie. The face of the detector is assumed to lie along a radial plane $\theta=15^{o}$, where the source is at $\theta=0$.) Electrons which strike the active area of the detector may do so in two ways -

(1) They may strike the face of the detector as they cross the $\theta=15^{o}$ plane for the first time.

(2) They may cross the $\theta=15^{o}$ plane without striking the detector and, because of the trochoidal paths which they follow, the electrons may then reverse direction and recross the $\theta=15^{o}$ plane without striking the side of the detector. Having done this such an electron may then subsequently strike the active area as it again crosses the $\theta=15^{o}$ plane. This process is indicated in Fig. 3-8. Of course electrons which strike the side of the detector after having crossed the $\theta=15^{o}$ plane, (without having struck the face of the detector), are considered to be "lost".

Computer runs were made at various electron energies ranging from 100 keV to 1700 keV and for each energy three different runs were made using different sets of random directions of emission. For this work, a minimum of 500 electrons were emitted for each run. The iteration time was varied from energy to energy, decreasing with increasing energy, so that the minimum number of iterations for the electron to drift 15^{o} was $\gtrsim$ 2000. At the end of each iteration the "speed" of the electron was calculated from the velocity components which provided an internal check on the iteration procedure since the electron's speed is a constant of the motion. It was found that the calculated speed remained constant throughout the motion to within $\pm 0.1\%$.

For each electron tracked the programme listed the following:

FIG. 3-8

An example of one way in which an electron might be incident on the detector.

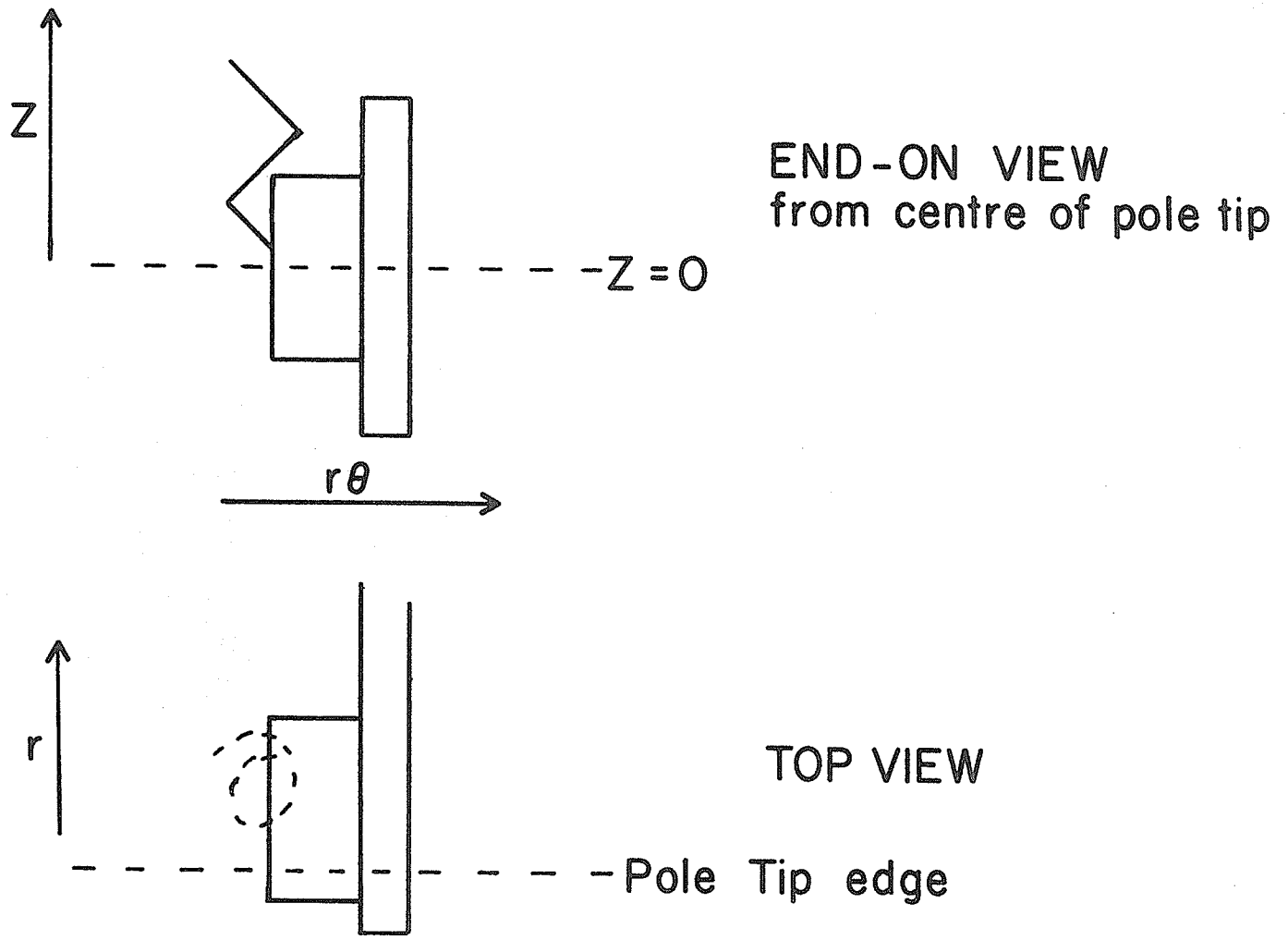
Z
Z = 0
rθ
END-ON VIEW
from centre of pole tip
r
TOP VIEW
Pole Tip edge

(1) the initial conditions such as direction of emission, total velocity and the velocity components;

(2) the final conditions, (including the reason for stopping), such as time of flight, radial and vertical positions at time of stopping, whether or not the electron has struck the detector face or side and for electrons which strike the detector face whether it struck the face on the first pass across the $\theta=15^{o}$ plane or on a subsequent pass;

(3) the minimum and maximum radial distance from the centre of the magnet; and

(4) the maximum displacement from the median plane.

For each set of electrons run the programme also computed the transmission and the percentage number of electrons striking the active area.

The results of this analysis are summarized in Figs. 3-9 and 3-10. The two solid lines, A and B, shown in Fig. 3-9 are the calculated transmission, and the calculated percentage number of electrons striking an active area of $100mm^2$ as functions of energy. The points joined by the dashed line, C, are the measured full energy peak detection efficiencies of the spectrometer using a circular detector with a nominal active area of $100mm^2$. It should be noted that the computed number of electrons striking an active area is inherently larger than the full energy detection efficiency since, experimentally, not all electrons which hit the detector's active area will result in a full energy output pulse. The open circles, on curve B, are the measured efficiencies of the spectrometer, using the same detector as for curve C, when all output pulses from zero to full energy are in-

FIG. 3-9

The energy dependence of the calculated transmission, curve A, and the calculated percentage of electrons detected by a 100mm^2 active area detector, curve B. The open circles on curve B are the measured detection efficiencies counting all pulses from zero to full energy using a Simtec detector with a nominal area of 100mm^2. Curve C is the measured full energy peak detection efficiency of the same detector.

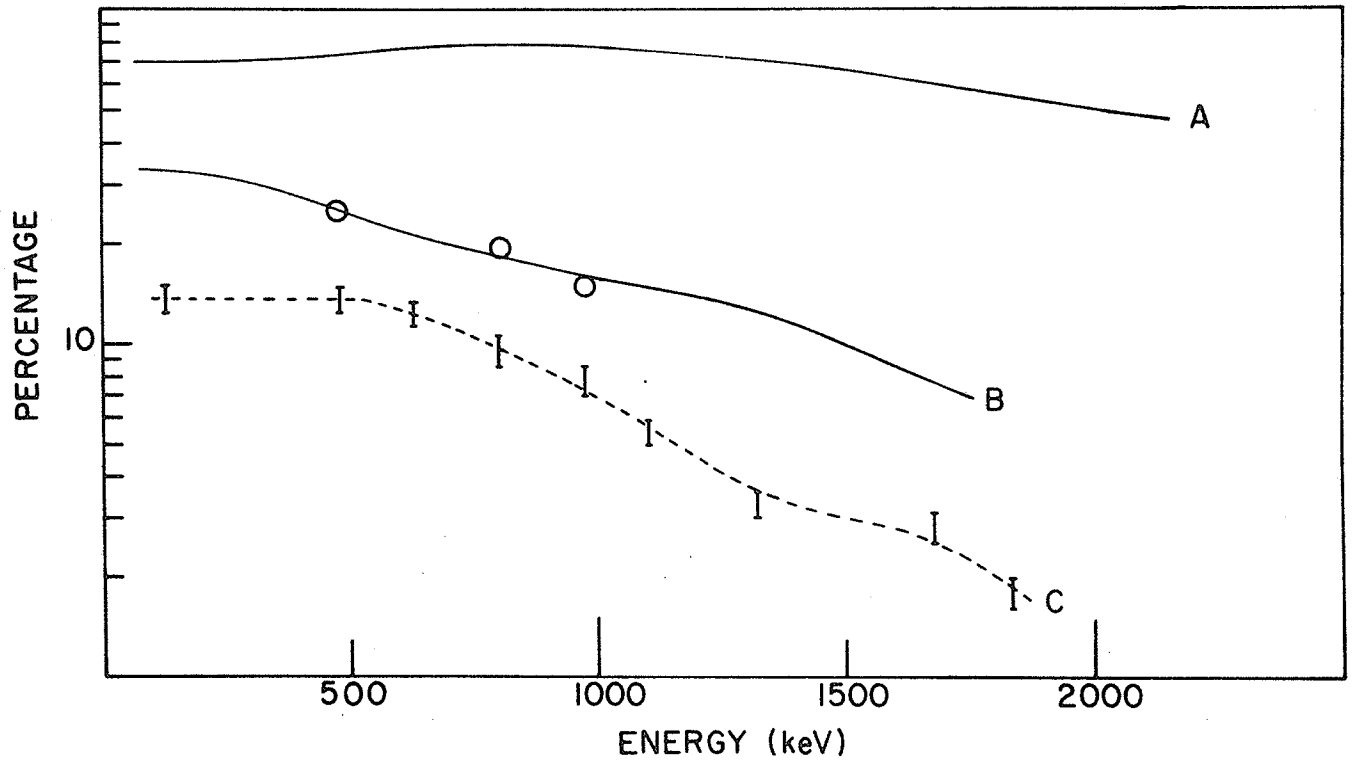
PERCENTAGE
10
A
B
C
500
1000
1500
2000
ENERGY (keV)

FIG. 3-10

Calculated percentage of electrons striking the active area, for various electron energies. Calculations were carried out using three sets of 500 electrons, emitted in random directions. The points are the mean value and the bars are the mean deviation. The solid lines are visual fits to the points and indicate an approximately linear relation.

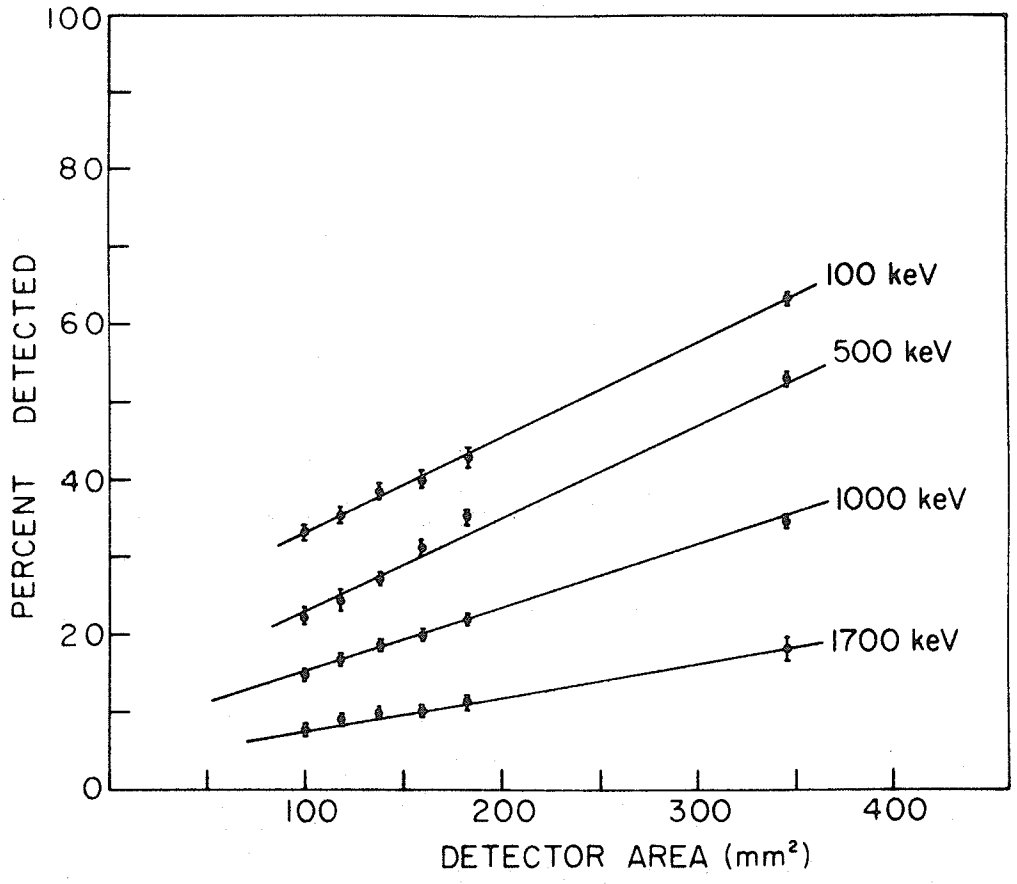
100
80
60
40
20
0
PERCENT DETECTED
100 keV
500 keV
1000 keV
1700 keV
100
200
300
400
DETECTOR AREA (mm²)

FIG. 3-11

The calculated distribution of electrons across a radial plane θ=constant for a set of 500 electrons with a kinetic energy of 100 keV emitted in random directions.

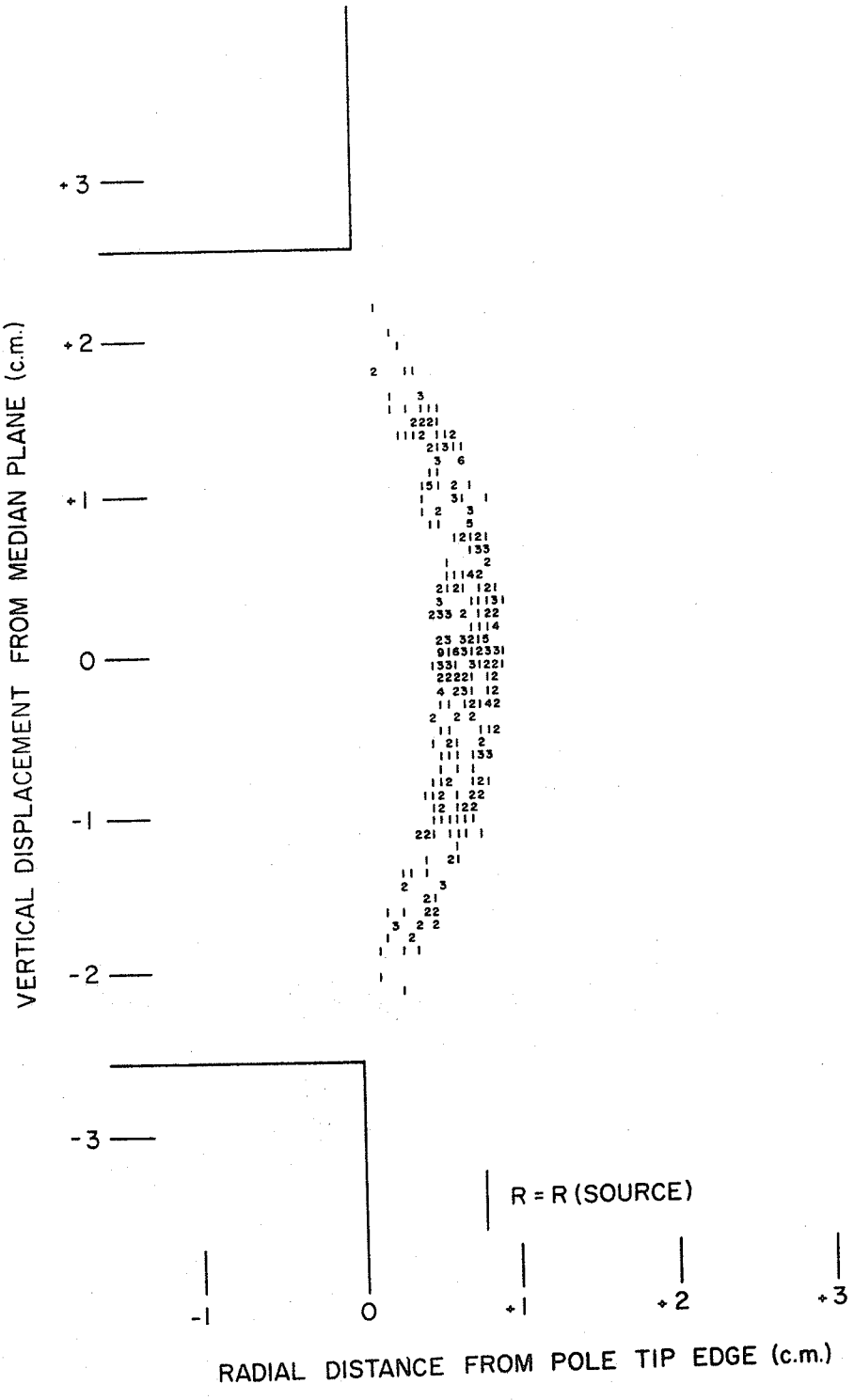
VERTICAL DISPLACEMENT FROM MEDIAN PLANE (c.m.)
+3
+2
+1
0
-1
-2
-3
R = R (SOURCE)
-1
0
+1
+2
+3
RADIAL DISTANCE FROM POLE TIP EDGE (c.m.)

FIG. 3-12
The calculated distribution of electrons across a radial plane θ=constant for a set of 500 electrons with a kinetic energy of 195 keV emitted in random directions.

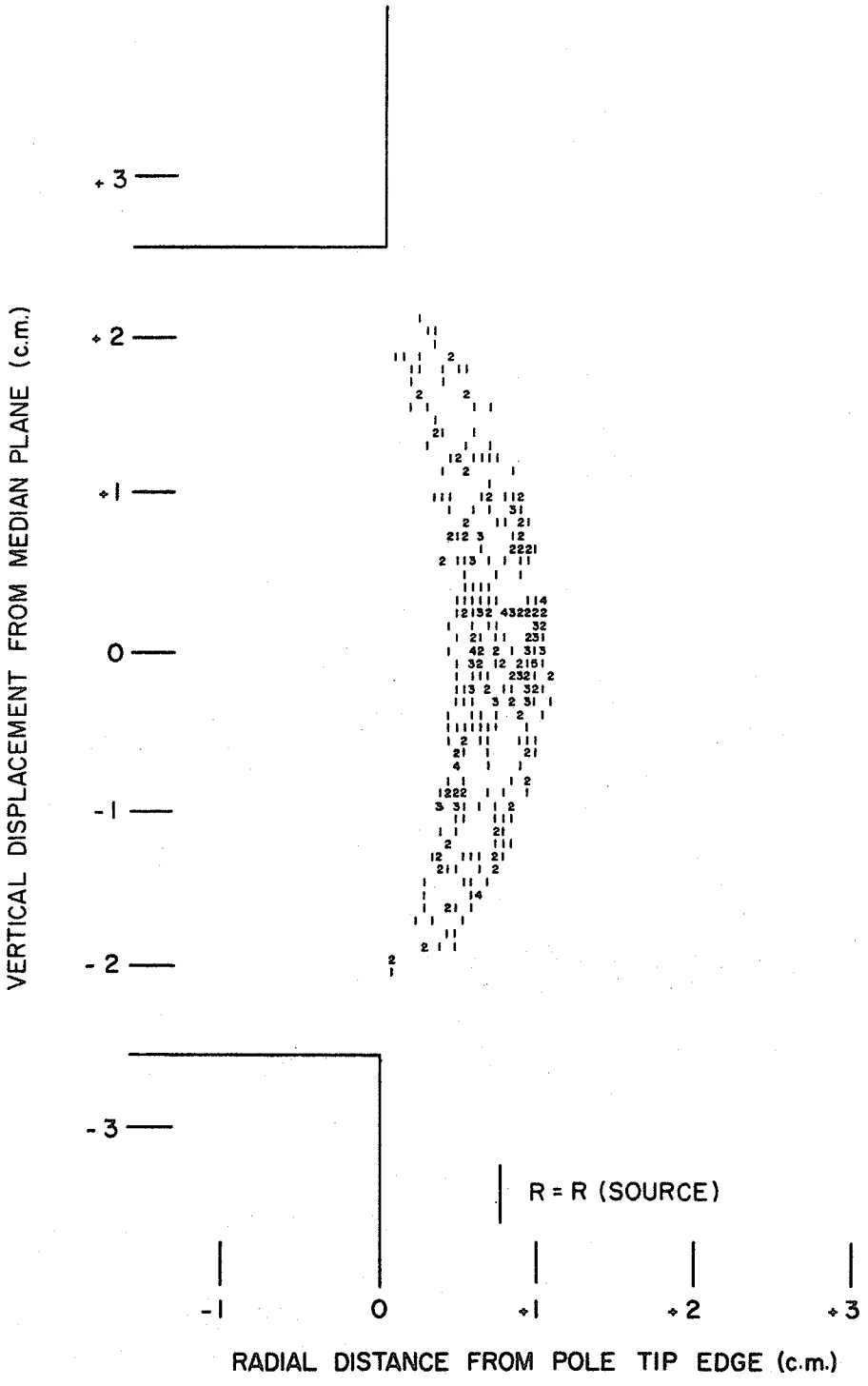
VERTICAL DISPLACEMENT FROM MEDIAN PLANE (c.m.)
+3
+2
+1
0
-1
-2
-3
R = R (SOURCE)
-1
0
+1
+2
+3
RADIAL DISTANCE FROM POLE TIP EDGE (c.m.)

FIG. 3-13

The calculated distribution of electrons across a radial plane θ=constant for a set of 500 electrons with a kinetic energy of 500 keV emitted in random directions.

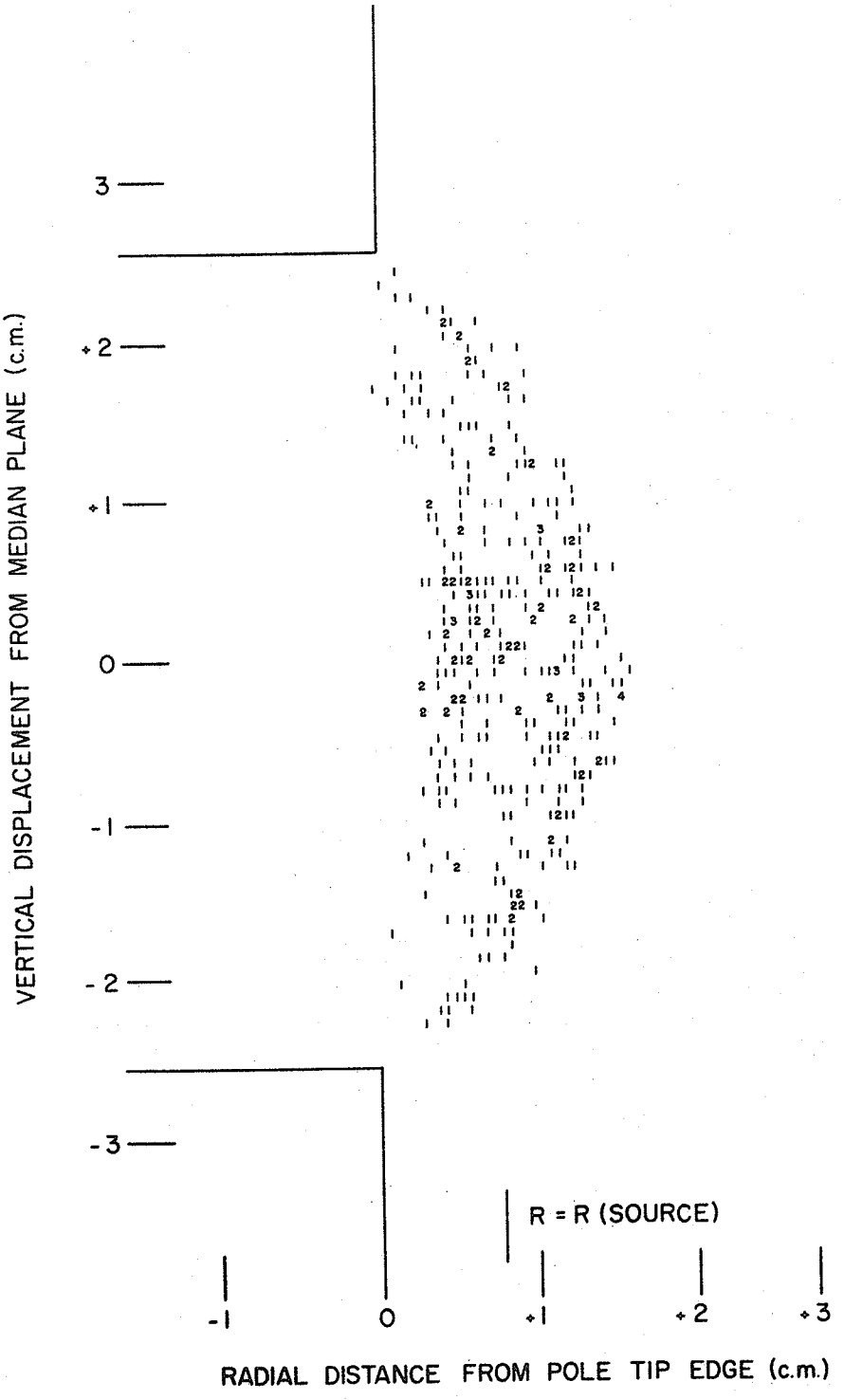
VERTICAL DISPLACEMENT FROM MEDIAN PLANE (c.m.)
3
+2
+1
0
-1
-2
-3
R = R (SOURCE)
-1
0
+1
+2
+3
RADIAL DISTANCE FROM POLE TIP EDGE (c.m.)

FIG. 3-14

The calculated distribution of electrons across a radial plane θ=constant for a set of 500 electrons with a kinetic energy of 1000 keV emitted in random directions.

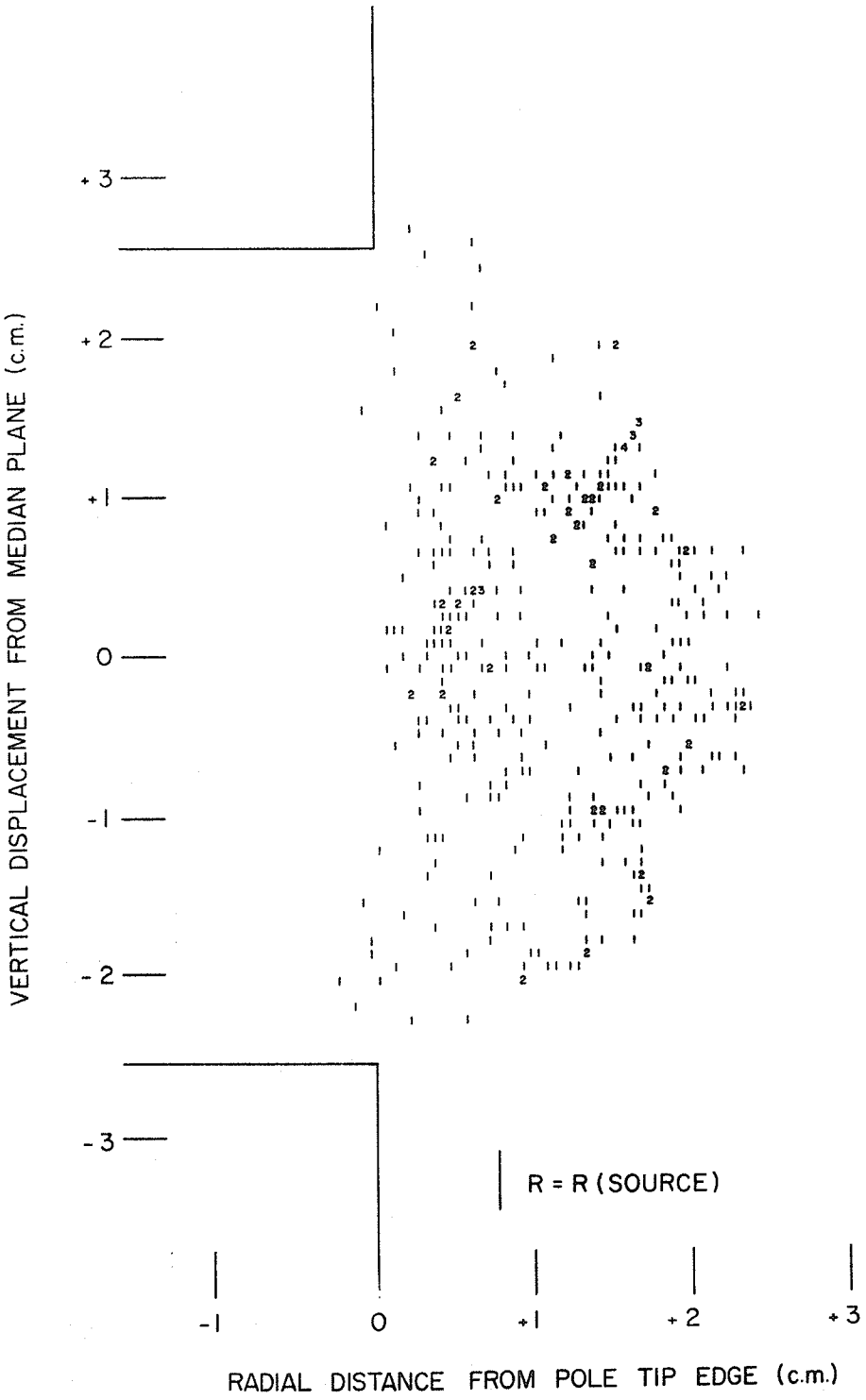
VERTICAL DISPLACEMENT FROM MEDIAN PLANE (c.m.)
+3
+2
+1
0
-1
-2
-3
R = R (SOURCE)
-1
0
+1
+2
+3
RADIAL DISTANCE FROM POLE TIP EDGE (c.m.)

cluded. It was found that the contribution to the computed detection efficiency from electrons which miss the detector on the first pass, was small ($\lesssim$15%).

Fig. 3-10 shows the relation between the active area and the computed number of electrons striking it for various electron energies. For a given energy, the number of electrons striking the active area within the range considered, is approximately linearly related to the area. These lines do not pass through the origin because the electron density across a vertical section of the annular chamber is non-uniform. (It is largest in the median plane at the same radial distance as the source.) The computed distribution of electrons across the $\theta=15^{o}$, for random directions of emission, is indicated for a few energies by Figs. 3-11 - 3-14.

In addition to the above calculations the time of flight for randomly emitted electrons to drift 135^{o} around the pole tips was calculated for various energies. (In the experimental work the source and detectors were separated by 135^{o}). The results of these calculations are shown in Fig. 3-15. Each point represents the average time for 20 electrons. The bars are the R.M.S. deviations. Malmfors[2] has derived the following expression for the time of flight:

$$T(\theta) = \frac{\theta r_o}{v_{drift}} = \frac{\theta e}{mc^2} \cdot \frac{B_o r_o^2}{n} \cdot \frac{E+1}{E(\frac{1+E}{2})} \cdot (\frac{1+n(n-2)}{4} \cdot \frac{z_1^2}{r_o^2} + \text{---}) \qquad (1)$$

FIG. 3-15

Calculated time for electrons to drift 135° around the pole tips from the source versus the electron energy. The points are the mean time for 20 electrons of a given energy emitted in random directions and the bars are the R.M.S. deviation. The solid line is the theoretical prediction.

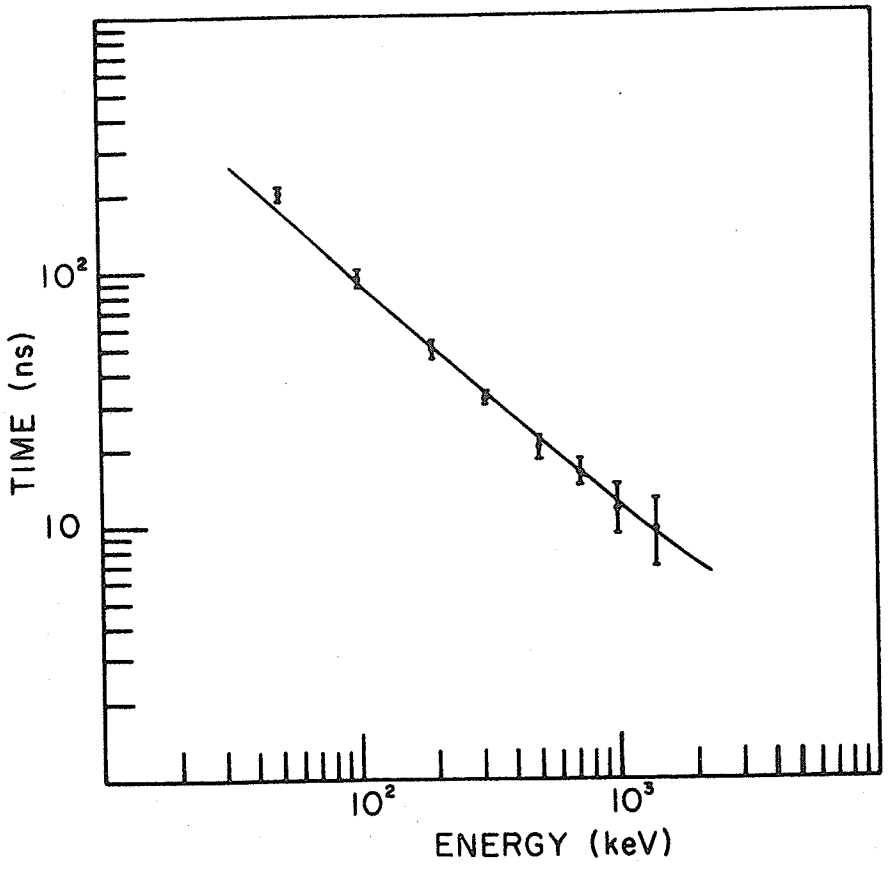
TIME (ns)
10^2
10
10^2
10^3
ENERGY (keV)

where r_o is the source position in cm., E the electron energy in units of mc^2, z, the amplitude of vertical oscillation and where the median plane field is given by $B = B_o(\frac{r_o}{r})^n$. The solid line in Fig. 3-15 is the prediction of equation (1) for electrons emitted in the median plane, (z_1=0), using the parameters n=3.59, B_o=6.27 kG and r_o=14.3 cm., which parameters correspond to the median plane of the present instrument for a current of 300A. The agreement of the present calculations with the predictions of equation (1) is gratifying since Malmfors [2] has experimentally verified (1) for the case n=½.

CHAPTER 4

EXPERIMENTAL PROPERTIES OF THE SPECTROMETER

"No! No! Sentence first - verdict afterwards."

....Lewis Carroll

INTRODUCTION

Figure 4-1 shows an electron spectrum for the 570 keV transition in ^{207}Pb obtained with the spectrometer. Here the peak detection efficiency is 23% at a resolution of 5 keV FWHM; ie: the percentage of K-conversion electrons emitted from the source which appear in the full energy peak in the detector is 23%. A limit to the resolution is of course set by the intrinsic resolution of the detector, which, according to the manufacturer, is 4 keV. The remainder is due to electronics. A number of difficulties had to be overcome to obtain results of this quality. In this chapter these problems are discussed together with the calibration of the spectrometer and the general operating procedures.

APPARATUS AND EXPERIMENTAL ARRANGEMENT

The standard arrangement of the source and detectors is shown in Fig. 4-2. The detectors are circular Simtec detectors with a nominal active area of $100mm^2$ and are located 135^o around the pole tips from the source as shown in Fig. 4-2. The detectors are mounted on liquid nitrogen cooled copper heat sinks and can be precisely posi-

FIG. 4-1

Electron spectrum of ^{207}Bi obtained using the spectrometer. The source was prepared by subliming onto gold plated V.Y.N.S. resin.

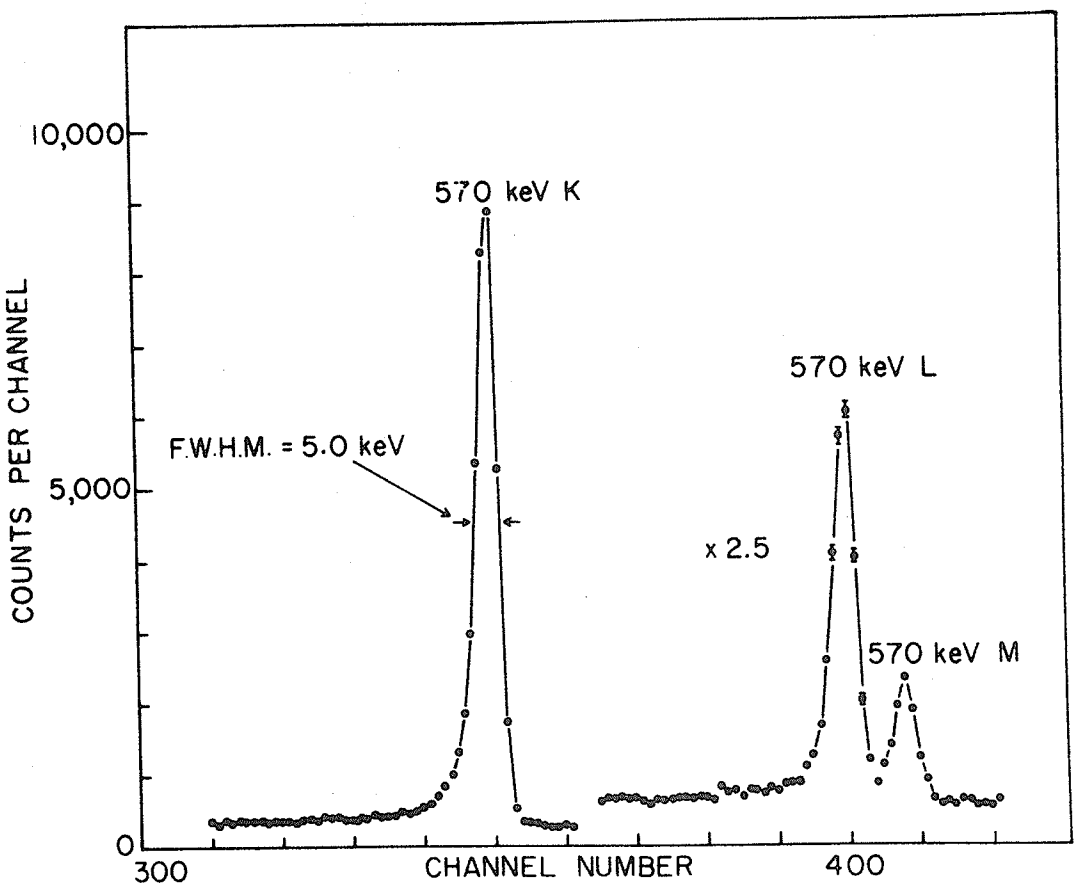
10,000
5,000
0
COUNTS PER CHANNEL
570 keV K
570 keV L
570 keV M
F.W.H.M. = 5.0 keV
x 2.5
300
CHANNEL NUMBER
400

FIG. 4-2

Plane view of magnet showing the location of the detectors and source.

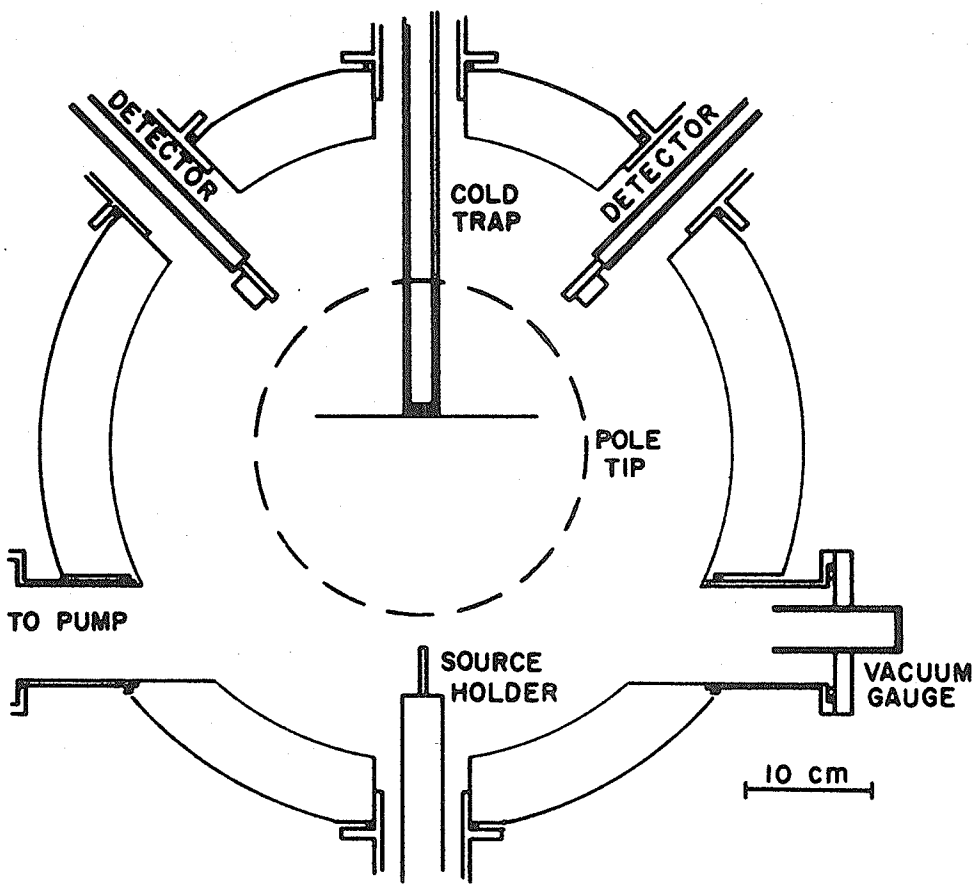
DETECTOR
DETECTOR
COLD
TRAP
POLE
TIP
TO PUMP
SOURCE
HOLDER
VACUUM
GAUGE
10 cm

tioned radially by means of a threaded star wheel. The details of the detector mount are shown in Fig. 4-3. The detector outputs are fed to Canberra 1408C pre-amps located outside the vacuum chamber. The detectors and pre-amps are separated by approximately 18" of co-axial cable which together with connectors results in an input capacitance of approximately 25pF.

Sources are placed into the main vacuum through an interlock shown in Fig. 4-4. The interlock is fitted with an auxillary 2" oil diffusion pump which is trapped by liquid nitrogen to reduce contamination of the main vacuum. The source frame is mounted on the end of a 1.5" O.D. aluminum rod which passes into the vacuum through a double "o-ring" sliding seal. The aluminum rod is driven by a threaded star wheel, 20 turns to the inch, and can be positioned radially with an accuracy of ±.001". The cold finger shown in Fig. 4-2, besides increasing the pumping speed, helps to reduce contamination of the main vacuum by vapours introduced through the source interlock.

The main vacuum is pumped by a 4" C.V.C. oil diffusion pump (type MCF-300) with an unbaffled pumping speed of 300 ℓ/sec. To reduce the amount of oil backstreaming the diffusion pump is fitted with an optically dense baffle and a liquid nitrogen cold trap as shown in Fig. 4-5. The diffusion pump is backed by a Balzer's Duo5 mechanical pump.

FIG. 4-3

The detector assembly.

DETECTOR MOUNT ASSEMBLY

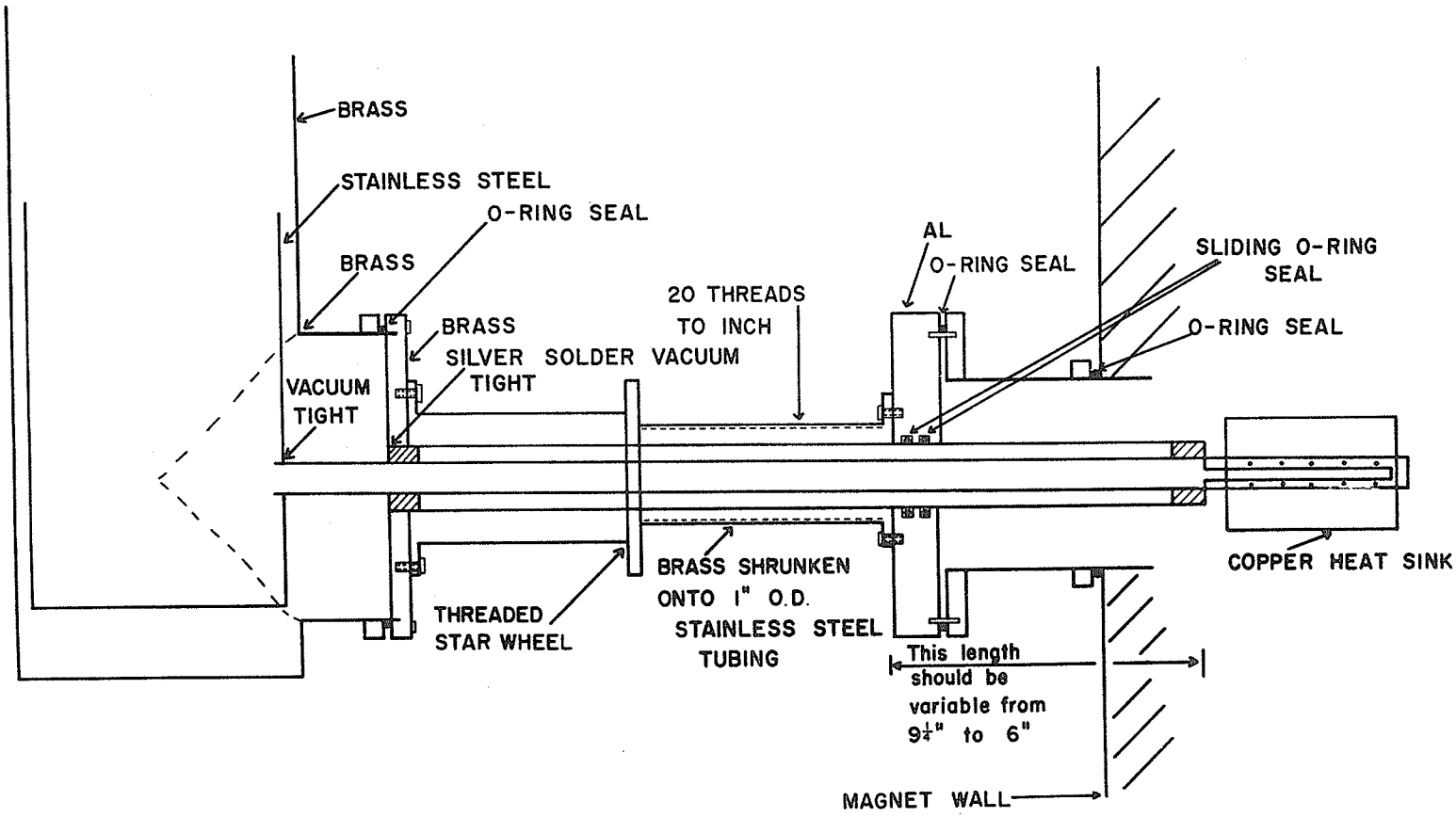

FIG. 4-4

The source interlock.

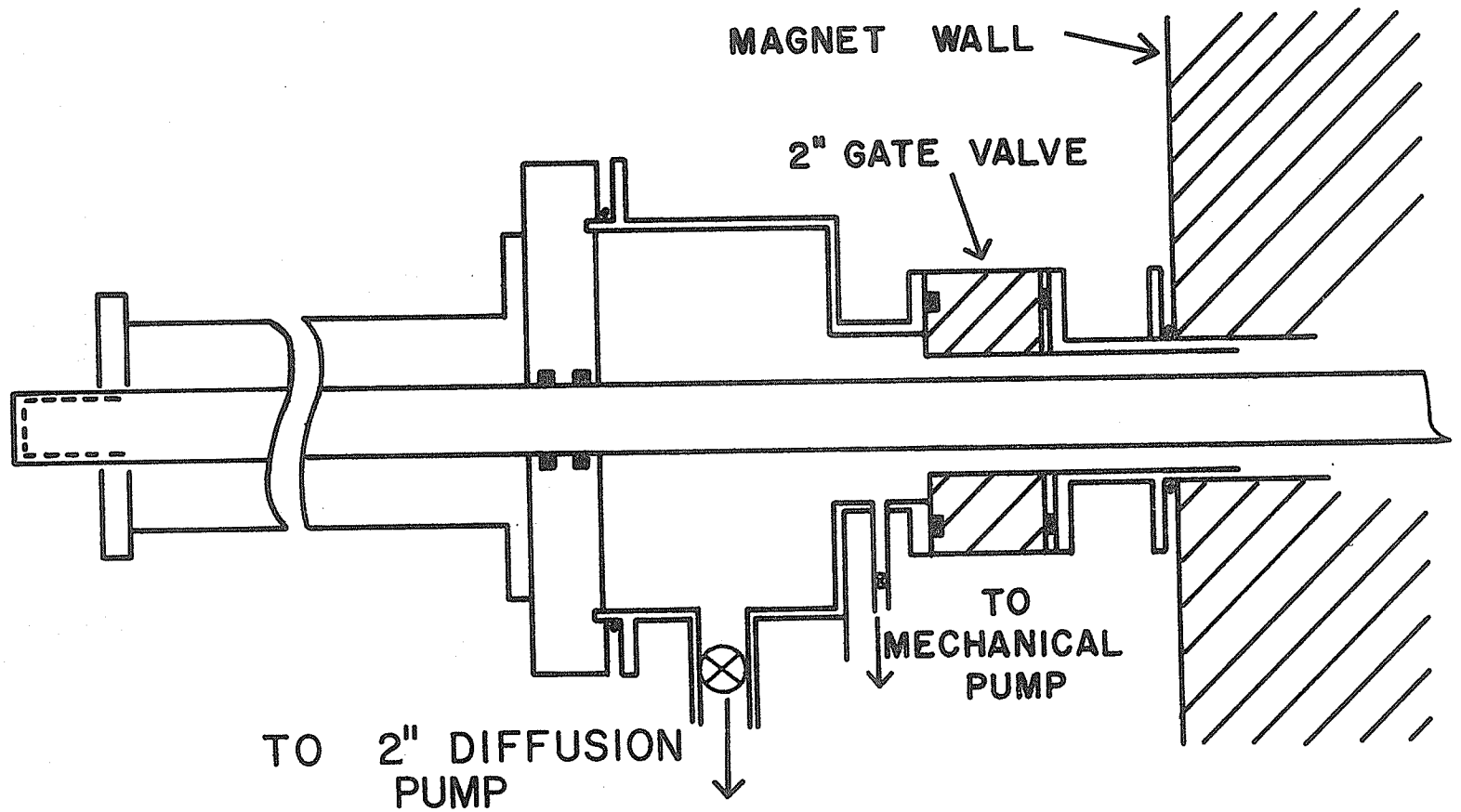
MAGNET WALL
2" GATE VALVE
TO MECHANICAL PUMP
TO 2" DIFFUSION PUMP

FIG. 4-5

The arrangement of the baffle and liquid nitrogen cold trap used to reduce oil back-streaming from the diffusion pump.

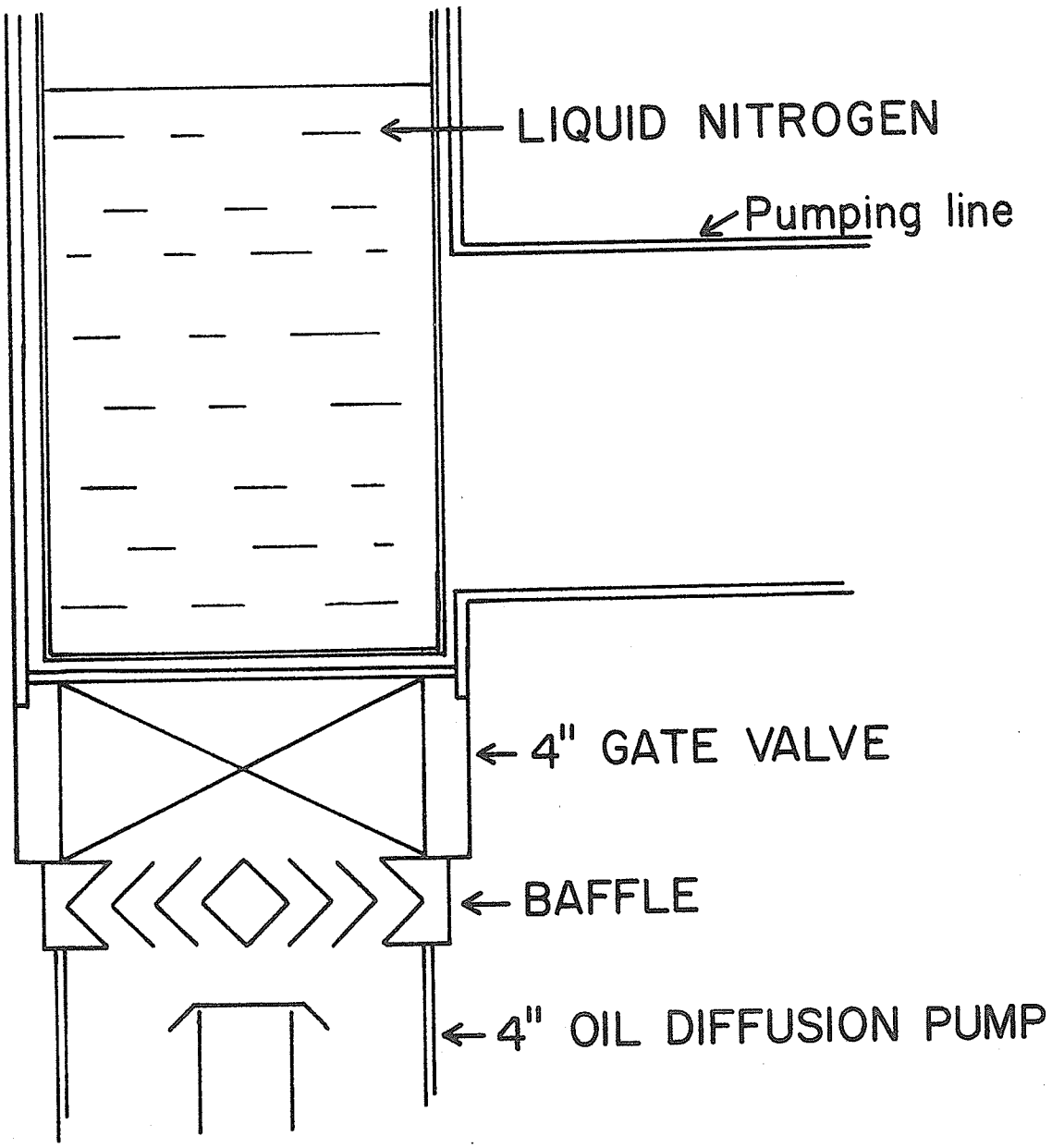
LIQUID NITROGEN
Pumping line
4" GATE VALVE
BAFFLE
4" OIL DIFFUSION PUMP

SOME PROBLEMS RELATED TO LINE SHAPE

In this spectrometer energy degradation of the electrons may occur both at the source and at the detector. Because the electrons are following curved paths the effective thickness of any material through which they pass is magnified many times and the problem of energy degradation tends to be more serious than in conventional spectroscopy.

Energy degradation at the detector is caused by the intrinsic dead layer, which according to the manufacturer is <0.2 micron, and by any layer of vapour which has condensed on the face of the detector. Increased broadening of electron lines has been observed following repeated use of the source interlock and this broadening has been attributed to just such condensation. Therefore, the detectors, which have a washable entry window were periodically removed and cleaned with alcohol.

The following pump-down procedure has been found to be satisfactory in reducing the amount of vapour condensation:

(1) With a given source in position the system is pumped on for several hours, without cooling the cold trap or the cold finger, reducing the pressure to approximately 5×10^{-6} mm Hg.

(2) The cold trap in the pumping line is cooled and the system is pumped for a further period of approximately 6 hours.

(3) The cold finger over the pole tips is then cooled and after an additional period of 8-12 hours the pressure is reduced to approximately 10^{-7} mm Hg.

(4) The detectors are then cooled.

Following this process the spectrometer could be operated for several weeks, with a given source in position, without appreciable deterioration of the line shape.

The trochoidal orbits which the electrons follow present certain problems, related to source mounting, which are peculiar to this type of instrument. In conventional β-spectroscopy only those electrons emitted in the "forward direction" are detected and one is concerned only with back-scattering. In a trochoidal spectrometer electrons which are emitted in the "backward direction" and pass through the source and source mounting may also reach the detector. In addition, many electrons, in their first few turns, pass through the source backings several times. Besides these problems, related to source thickness, the source frame which supports the backing must have a sufficiently large "open area" to prevent loss of electrons through collisions with the frame.

Three combinations of source material and backing have given good electron line shapes over the energy range 100-1800 keV. These were:

(1) Active material sublimed onto gold plated V.Y.N.S. resin, (backing thickness ~20 $\mu g/cm^2$),

(2) Active material sublimed onto a narrow strip (~.125" wide), of 180$\mu g/cm^2$ aluminum foil, and

(3) A drop of active material evaporated onto gold plated V.Y.N.S. resin.

An example of the line shape obtained using this latter combination is shown in Fig. 4-6. This spectrum shows the K and the L+M conversion peaks of the 166 keV transition of ^{139}La. By comparison, the spectrum of Fig. 4-1 was acquired using a sublimed source.

FIG. 4-6

Electron spectrum of ^{139}Ce obtained using the spectrometer. The source was prepared by evaporating a drop of active material onto V.Y.N.S. resin. The K-conversion electron energy is 127 keV.

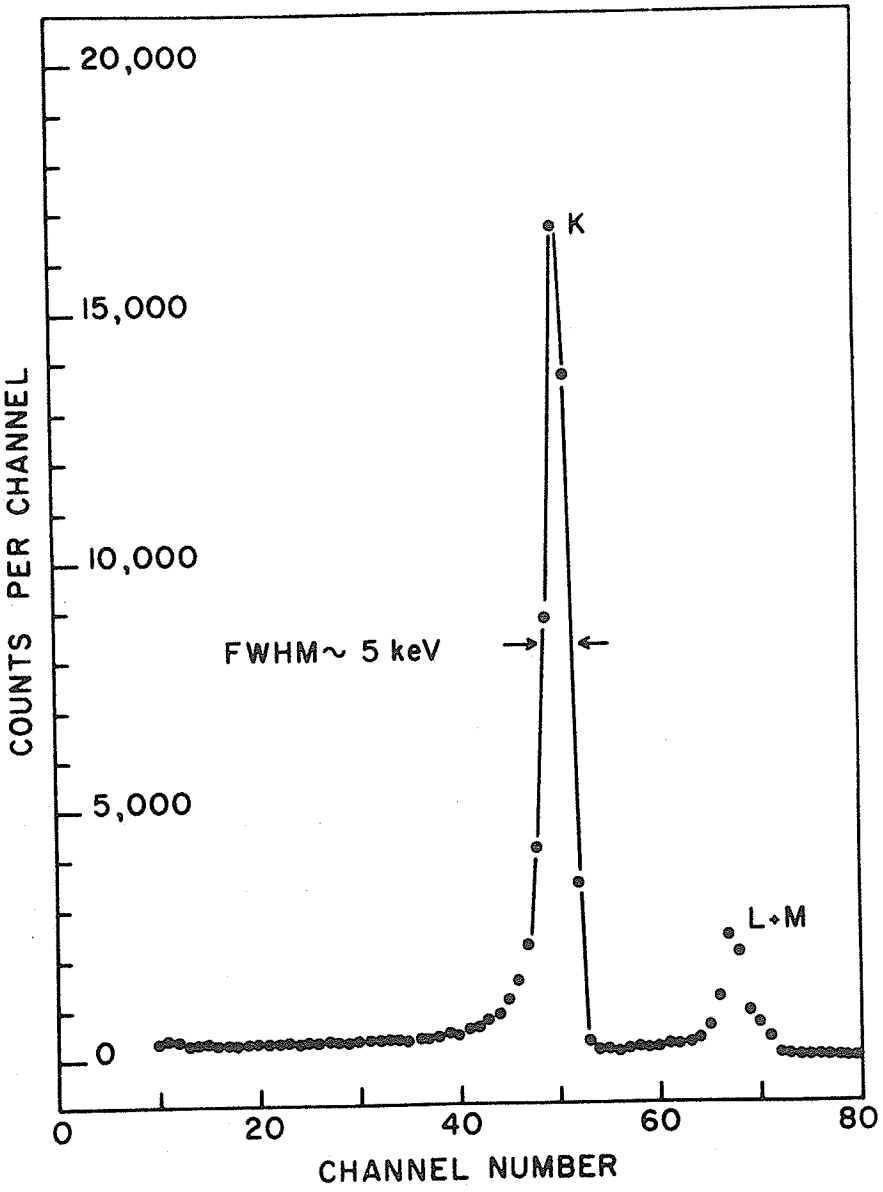
20,000
15,000
10,000
5,000
0
COUNTS PER CHANNEL
K
FWHM~ 5 keV
L+M
0
20
40
60
80
CHANNEL NUMBER

FIG. 4-7

The source frame used in the spectrometer. Also shown is the aluminum mask used to define the location of the source.

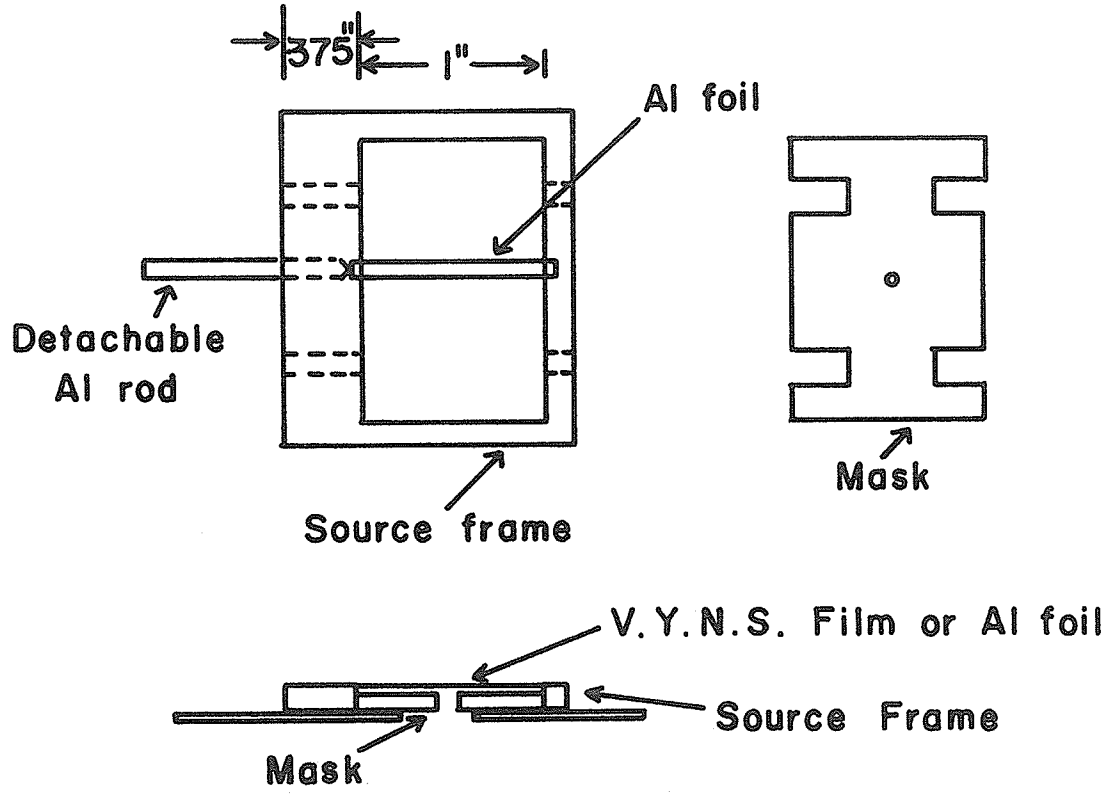
.375"
1"
Al foil
Detachable
Al rod
Source frame
Mask
V.Y.N.S. Film or Al foil
Source Frame
Mask

The sources were all mounted on the type of source frame which is shown in Fig. 4-7 together with the sublimation mask used to define the source location during source preparation. This mask was .100" thick with a central hole .079" in diameter. The mask was machined to fit inside the source frame leaving a clearance of .025" between the backing and mask. When subliming onto V.Y.N.S. resin there is a tendency for the film to be pulled down onto the mask during the initial roughing down of the sublimation chamber. To prevent this, holes were drilled through the side of the source frame to align with channels cut into the mask so that the volume between the mask and film was not pumped on solely through the central hole. (See Fig. 4-7). The drop sources were made using a glass needle having a bore of approximately 0.5mm diameter. The drop was centrally located on the V.Y.N.S. backing by placing the source frame over a sublimation mask and using the mask's central hole for alignment. It was impossible to precisely control the size of drop sources but generally they were ~2-3mm. in diameter.

The drop sources are easiest to prepare and can be used when the source material is carrier free or of high specific activity but when the source material is of low specific activity it is necessary to prepare the sources by subliming. Of course, the electron line shape is the true test whether a given source is good or not.

CALIBRATING THE SPECTROMETER

The full energy peak detection efficiency of the spectrometer has been measured over the energy range 100 - 1800 keV using conversion electrons from known sources. Table 4-1 is a summary of the sources used in this work.[5,6] The electron counts in the full energy peak were determined using a straight line background subtraction. The absolute strength of these sources was found by counting the γ-rays on an external Ge(Li) detector which had been independently calibrated using standardized I.A.E.A. sources. (See Fig. 4-8). The electron emission rate was then determined from the known conversion coefficients.

The highest detection efficiency was obtained with the source and detector centered on the median plane .300" (7.6mm) beyond the pole tip edge and all measurements were carried out using this configuration. The strength of the magnetic field also affects the peak detection efficiency. It was found that the efficiency did not increase for currents greater than 300A but that the peak shape gradually degenerated as the current was increased. Below 300A the efficiency slowly decreased with the decreasing field without significant improvement in the peak shape. It was decided, therefore, to calibrate and operate the spectrometer at a current setting of 300A.

As it was found, experimentally, that the efficiency was dependent on the detector used, the spectrometer was calibrated for both detectors. This is easily done by positioning both detectors as shown

TABLE 4-1

The calibration sources used in determining the efficiency of the spectrometer.

TABLE 4-1

Source	E_γ	Electron Energy	Conversion Coefficient
^{141}Ce	145keV	103 keV	$\alpha_K = 3.79 \times 10^{-1}$
^{139}Ce	166keV	127 keV	$\alpha_K = 2.14 \times 10^{-1}$
^{203}Hg	279keV	194 keV	$\alpha_K = 1.63 \times 10^{-1}$
^{198}Au	412keV	329 keV	$\alpha_K = 3.02 \times 10^{-2}$
^{113}Sn	392keV	364 keV	$\alpha_K = 4.38 \times 10^{-1}$
^{207}Bi	570keV	482 keV	$\alpha_K = 1.55 \times 10^{-2}$
^{205}Bi	703keV	615 keV	$\alpha_K = 1.05 \times 10^{-2}$
^{137}Cs	662keV	624 keV	$\alpha_K = 8.94 \times 10^{-2}$
^{58}Co	811keV	803 keV	$\alpha_T = 3.32 \times 10^{-4}$
^{207}Bi	1064keV	976 keV	$\alpha_K = 9.60 \times 10^{-2}$
^{65}Zn	1115keV	1106 keV	$\alpha_T = 1.85 \times 10^{-4}$
^{60}Co	1173keV	1165 keV	$\alpha_T = 1.65 \times 10^{-4}$
^{60}Co	1333keV	1325 keV	$\alpha_T = 1.26 \times 10^{-4}$
^{207}Bi	1770keV	1682 keV	570-K/1770-K=95.2/1
^{205}Bi	1903keV	1815 keV	$\alpha_K = 6.65 \times 10^{-4}$

FIG. 4-8

Efficiency calibration of the Ge(Li) detector used in calibrating the present spectrometer.

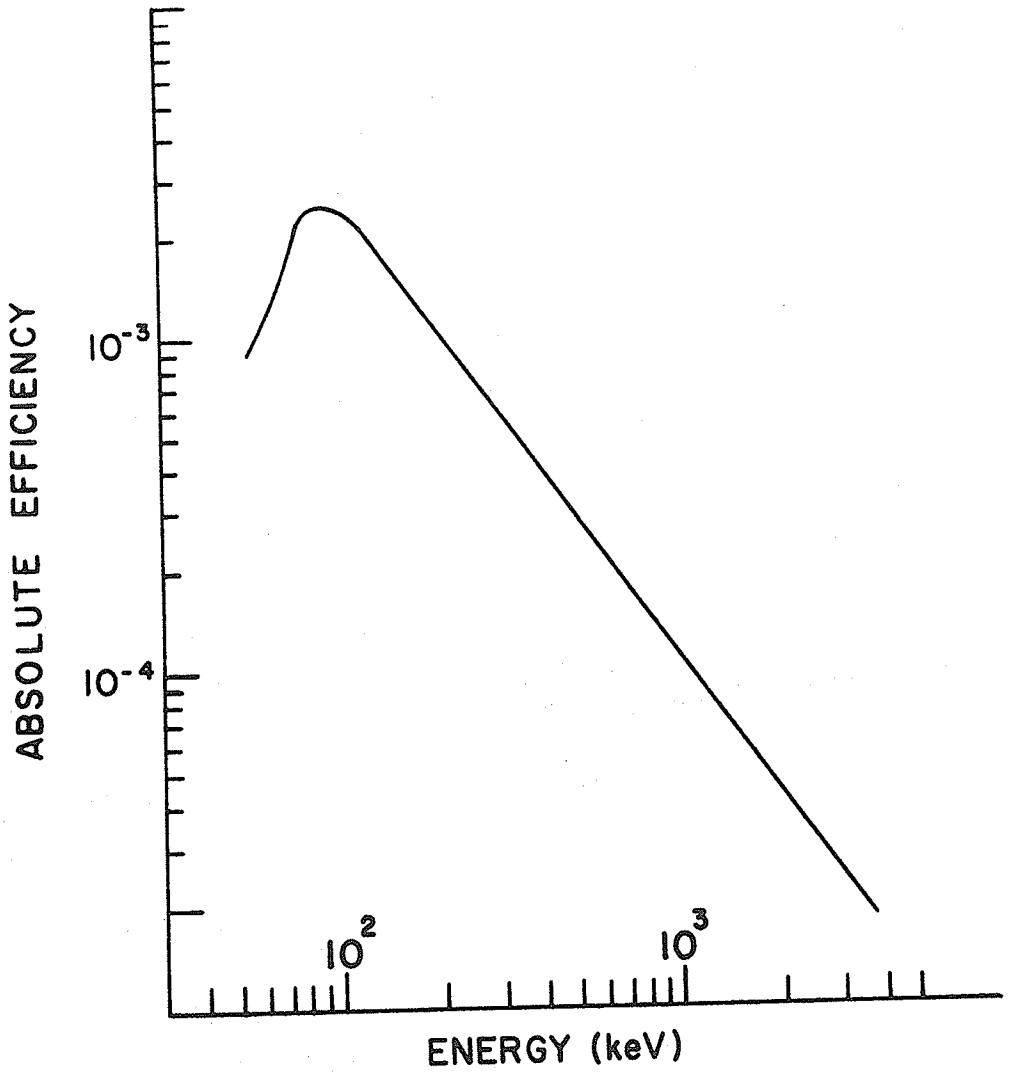
ABSOLUTE EFFICIENCY
10^{-3}
10^{-4}
10^{2}
10^{3}
ENERGY (keV)

in Fig. 4-2. Reversing the field polarity reverses the direction of electron drift so that both sides of the spectrometer may be calibrated, in succession, at a given energy, with the same source of conversion electrons. The fact that the source was on one side of the backing for one detector and on the other side for the second made no difference to the line shape.

For each nuclide used in calibration, at least two independently prepared sources were used to check the reproducibility of the measurements. The calibration curves for the two detectors are shown in Fig. 4-9. The upper curve, for detector A, is the average of efficiencies obtained using 4 sources, 2 sublimed and 2 dropped, while the lower curve has been obtained using drop sources only. The error in the measurements has been estimated at 10%. Both curves were obtained with the detectors 135° around the pole tips from the source. It will be noted that the two detectors have considerably different efficiencies, and this effect is believed caused by different active areas. The efficiency of the spectrometer, using detector B, has been compared to the theoretical calculations in Fig. 3-9. For this comparison all pulses from zero to full energy were included. Also shown is the corresponding full energy peak detection efficiencies.

The counting rates for the 570 keV and 1064 K electrons from ^{207}Bi were found to be the same with the detector at 45°, 135° and 180° from the source, indicating that the efficiency is independent of the angular separation between the source and detector as expected.

FIG. 4-9

Measured full energy peak detection efficiency of the spectrometer versus electron energy for two Simtec detectors both with a nominal area of 100mm^2. The solid lines joining the points are visual fits to the data.

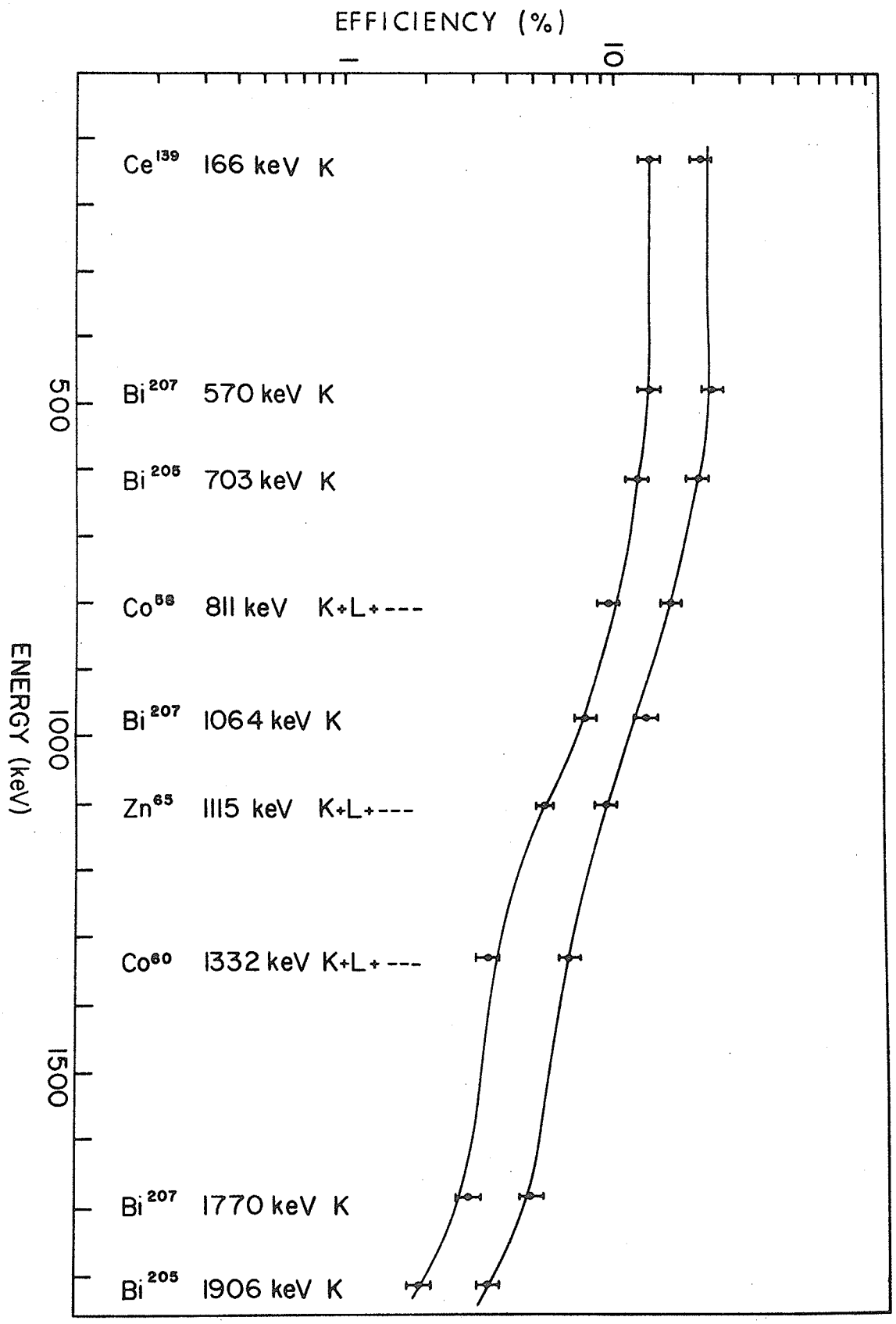
EFFICIENCY (%)
10
ENERGY (keV)
500
1000
1500
Ce139 166 keV K
Bi207 570 keV K
Bi205 703 keV K
Co58 811 keV K+L+---
Bi207 1064 keV K
Zn65 1115 keV K+L+---
Co60 1332 keV K+L+---
Bi207 1770 keV K
Bi205 1906 keV K

Several problems arose in calibrating the instrument and it is instructive to consider these since similar problems may be encountered in many experimental situations. Early work with sublimed sources yielded inconsistent results which were eventually traced to difficulties in subliming. At the sublimation temperature the pressure within the sublimation chamber rises as the material leaves the boat causing diffusion of the radioactive material throughout the chamber. Some of the activity subsequently settles on the source frame and backing resulting in a uniform layer of background activity as well as the central source spot. When one measures the γ-ray counting rate, (from which the electron emission rate is calculated), the Ge(Li) detector responds to this background activity whereas the spectrometer only responds to electrons emitted from the central region. Thus the apparent efficiency is smaller than its true value. To correct this problem, the γ-spectra of sublimed sources were subsequently acquired using a lead shield, as shown in Fig. 4-10, to eliminate contributions from the background activity. The use of the lead shield reduced the γ-counting by approximately a factor of 2. Since the surface area of the source frame is more than a factor of 1000 greater than the area of the central spot it can be inferred that the density of the diffused background activity is $< 0.1\%$ of the density of the central source spot.

Another type of problem was encountered with Hg and Sn sources. In the high vacuum the active material sublimed into the vapour state and

FIG. 4-10

Arrangement of the lead shielding used in measuring the γ-ray counting rate of the calibration sources.

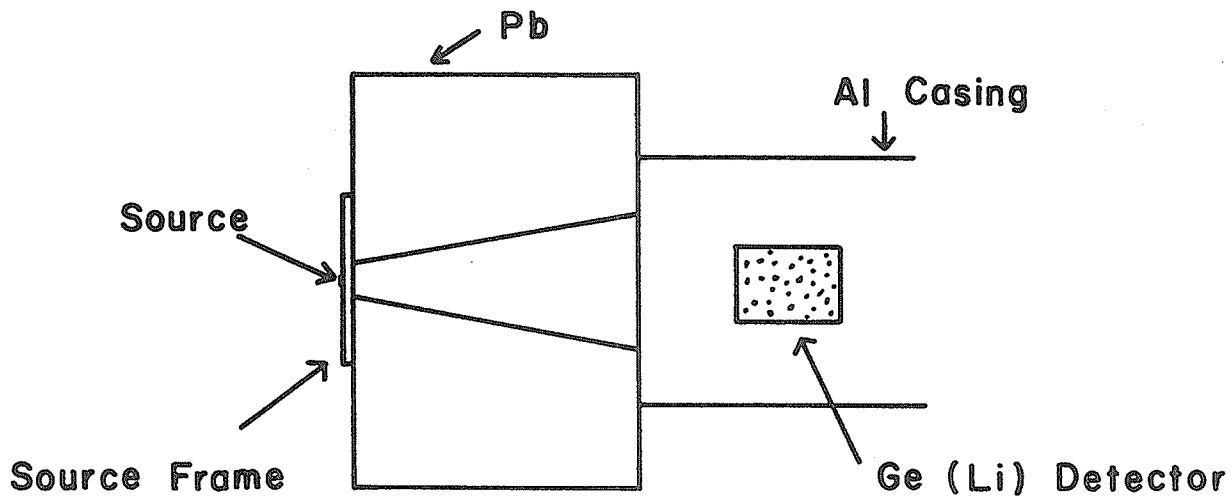
Pb
Al Casing
Source
Source Frame
Ge (Li) Detector

left the backing. Thus these sources were useless as calibration standards. M. J. Canty[7] has also observed this phenomena and he successfully eliminated the problem by encasing the source in V.Y.N.S. resin but this was not attempted in the present work.

The most interesting problem met in generating the calibration curves arose with ^{141}Ce, ^{198}Au, and ^{60}Co. Let us consider ^{60}Co. The original full energy peak detection efficiencies, at electron energies of 1166 and 1323 keV, obtained using ^{60}Co, were in marked disagreement with the curves shown in Fig. 4-9. For example, with detector A, ^{60}Co yielded an efficiency ~6% at 1166 keV whereas ^{65}Zn gave an efficiency ~9% for the conversion line at 1106 keV. This discrepancy was caused by the fact that ^{60}Co is a β^- emitter. (E_{max} = 315 keV) The decay scheme gives a β^- feed to the 2505 keV level of ^{60}Ni which de-excites by two transitions of 1173 and 1332 keV in cascade. If the conversion electron of the 1173 keV transition is detected then there is a high probability, (~30% for detector A), that the associated β^- will also be detected, because of the high efficiency of the spectrometer. Since the amplifier time constants are long, (4μs), the system will apparently see a single particle with an energy 1166 keV+E_{β^-}. Such conversion electrons will not be included in the full energy peak and the apparent efficiency will be lower than its true value. For the 1173 keV transition of ^{60}Co an empirical correction factor for this effect was determined by comparing the apparent efficiency with the value obtained by extrapolating the efficiency curve from 1106 keV (^{65}Zn). For detector A this

factor corresponds to a loss of 32% of the conversion electrons. This correction also applies to the 1333 keV transition in ^{60}Co which gives another point on the efficiency curve. It was found that the ratio of the correction factors for the two detectors was just the ratio of the detection efficiencies (in the energy region 100-300 keV). Since Ce^{141}, and Au^{198} are also β^- emitters these sources will also give apparent efficiencies which are low, but no direct method of obtaining a correction factor for these sources was available and therefore they were not used in determining the calibration curves.

It should be noted that this effect is distinct from random summing of pulses in the amplifier and will be present in many experimental measurements when transitions yield two "simultaneous electrons". Two conversion electrons from transitions in cascade can appear "simultaneously" in the detector and give a false peak and reduced intensity of the true peak. Such a false peak, obtained by the summing of the 570-K and 1064-K electrons of ^{207}Pb, is shown in Fig. 4-11. The reduction in the true peak intensity is unimportant in case of Bi^{207} (and ^{60}Co) since $\alpha \leq .01$ but it could be very important for transitions which are highly converted.

FIG. 4-11

Portion of a ^{207}Bi electron spectrum showing the 570-K plus 1064-K sum peak.

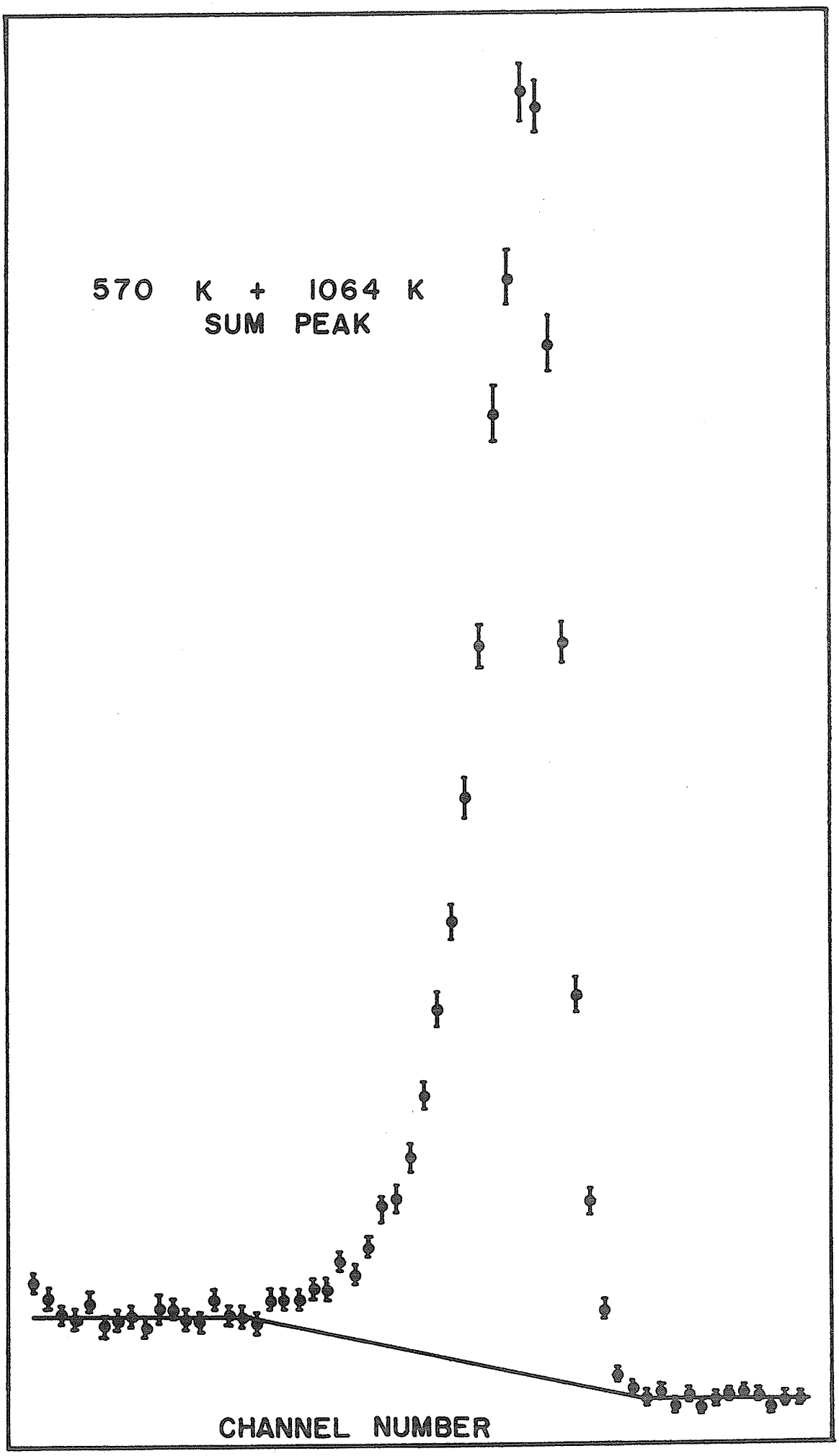
570 K + 1064 K
SUM PEAK
COUNTS (ARB. UNITS)
CHANNEL NUMBER

CHAPTER 5

ON PAIR PRODUCTION

"It is quite a three-pipe problem."

..... Sherlock Holmes

SOME THEORETICAL CONSIDERATIONS

For a nuclear transition with $E_\gamma > 2m_oc^2$ one method of de-excitation is the direct creation of an electron-positron pair. This method of de-excitation competes with both γ-emission and the ejection of a conversion electron. The pair is emitted with a total kinetic energy $T=E_\gamma-2m_oc^2$. The energy spectrum of both particles is a continuum ranging from 0 to T but such that for any given pair event $T_+ + T_- = T$, where T_+ is the kinetic energy of the positron and T_- is the kinetic energy of the electron. The electron and positron directions of emission are correlated, with both particles tending to come off in the same direction. The correlation is dependent on both the multipolarity and energy of the transition.

Numerous workers [8,9,10] have studied this problem theoretically for E1 and E2 transitions. Rose [11,12] has considered the problem of arbitrary multipole order of the electric and magnetic radiation field in the Born approximation. Using first order time dependent perturbation theory he finds that for electric 2^ℓ multipoles

$$\gamma_\ell(\theta) = \{2\alpha/\pi(\ell+1)\}(p+p_-/q)(q/k)^{2\ell-1}(k^2-q^2)^{-2} \times$$

$$\left[(2\ell+1)(w+w_-+1-\frac{1}{3}p+p_-\cos\theta)+\ell(q^2/k^2-2)(w+w_--1+p_+p_-\cos\theta)\right.$$

$$\left.+\frac{1}{3}(\ell-1)p+p_-\{(3lq^2)(p_-+p_+\cos\theta)(p_++p_-\cos\theta)-\cos\theta\}\right] \quad \ldots(1a)$$

and for magnetic 2^{ℓ} multipoles

$$\gamma_{\ell}(\theta) = (2\alpha/\pi)(p_+p_-/q)(q/k)^{2\ell+2}(k^2-q^2)^{-2} \quad x$$

$$\{1+w+w_--(p_+p_-/q^2)(p_++p_-\mathrm{Cos}\theta)(p_++p_-\mathrm{Cos}\theta)\} \qquad .....(2a)$$

where $\gamma_{\ell}(\theta)$ is the number of pairs per quantum per unit positron energy, per /dCosθ/, with positron energy w_+ and positron and electron emitted at an angle θ with respect to one another. Here W± is the total particle energy, including rest mass energy, p± is the particle momentum, α is the fine structure constant, k = transition energy and $\overline{q}=\overline{p}_+ + \overline{p}_-$. The system of units is such that $\hbar = 1 = m = c$.

Since the present instrument cannot be used to measure the angular correlation let us, for the time being, ignore this aspect of the problem. Then, to obtain the total number of pairs emitted with a positron energy w_+, per quantum, per unit energy, we integrate with respect to θ. Then

$$\Gamma_{\ell}(w_+) = \int_0^{2\pi} \gamma_{\ell}(\theta)\sin\theta d\theta$$

which gives

$$\Gamma_{\ell}(w_+) = \{\alpha/\pi(\ell+1)k^3 \; x \; \{(\ell/2)k^2 J_{\ell+1}$$

$$+ (2\ell w_+w_- - (7\ell+1)/4)J_{\ell} + (3/2\ell(w_+^2+w_-^2)+\ell+1+w_+w_-)J_{\ell-1}$$

$$- \tfrac{1}{4}(\ell-1)(w_+-w_-)^2 J_{\ell-2}\} \qquad .....(1)$$

for electric multipoles and

$$\Gamma_\ell(w_+)=(\alpha/\pi k^3)\{(1+w_+w_-)J_\ell-(k^2/4)(J_{\ell+1}-x_1x_2J_{\ell-1})\} \qquad .....(2)$$

for magnetic multipoles, where

$$J_\ell=\int_{x_1}^{x_2} x^\ell(1-x)^{-2}dx \quad , \quad x_1= (p_+-p_-)^2/k^2, \text{ and}$$

$x_2 =(p_++p_-)^2/k^2$. J_ℓ can be readily evaluated using the recurrence relation

$$J_{\ell+2}-2J_{\ell+1}+J_\ell = (x_2^{\ell+1}-x_1^{\ell+1})/(\ell+1)$$

and the results $J_0=p_+p_-$, $J_1=p_+p_-2\ln\{(1+w_+w_-+p_+p_-)/k\}$

It should be noted that equation (1), for electric multipoles, differs from the original result given by Rose [11]. The above result was obtained by integrating equation (1a). The correction had, however, already been pointed out by Rose [12].

The Born approximation ignores the effect of the nuclear charge and is therefore correct only for Z=0. For Z>0, Rose has argued that, although it gives the wrong energy distribution, the Born approximation should give a good estimate of the total pair formation coefficient, since the effect of the nuclear charge is to suppress the number of low energy positrons and enhance the number of high energy ones and on integrating over the energy distribution these two effects largely cancel. An idea of the error involved is given by comparing the Born approximation results with the results of "exact" calculations carried out using Coulomb wave functions. Jaeger and Hulme [8] have carried

out such calculations for E1 and E2 transitions, for Z=84, and the difference between the two calculations, for k ~3-5, is ~20%. Recently Lombard et al [10] have carried out similar calculations for E1, E2 and M1 transitions for various values of Z ranging from Z=34 to Z=82. Their results indicate that for E1 and E2 transitions the Born approximation results are correct to ~20% but for M1 transitions the results of the two calculations are considerably different. For example, for Z=82 and k=3.45 (1765 keV) the Born approximation calculations give a pair formation coefficient, $\alpha_\pi = 1.5 \times 10^{-4}$ whereas the "exact" calculation gives $\alpha_\pi = 2.7 \times 10^{-4}$, for an M1 transition. Thus the Born approximation seems to be reasonably accurate for E1 and E2 transitions but for M1 transitions it is not satisfactory.

Since the Born approximation is generalized to arbitrary multipole order it is desirable to be able to take into account nuclear charge effects using a correction term so that

$$\Gamma_\ell(w_+) = C_\ell(E_+,E_-,Z)\ \Gamma_{\ell,\mathrm{Born}}(w_+).$$

Horton and Phibbs [13] have argued that for all electric and magnetic multipoles the energy distribution may be approximated by

$$\Gamma_\ell(w_+) = \{(2\pi\nu_+)(2\pi\nu_-)/[\ell^{2\pi\nu_+}-1][1-\ell^{-2\pi\nu_-}]\}\ \Gamma_{\ell,\mathrm{Born}}(w_+)$$

where $\nu\pm = \alpha Z/\beta\pm$, $\beta = v/c$. Wilson [35], in his review article on internal pair production states that the above expression gives the correct shape for the energy distribution but is incorrectly normalized. This was also found to be the case in the present study. For example for Z=82, k=3.45 the above expression gives an E1 pair production

coefficient, $\alpha_\pi = 1.1 \times 10^{-4}$ whereas the "exact" calculation of Lombard et al [10] gives $\alpha_\pi = 3.3 \times 10^{-4}$. Thus the correction factor derived by Horton and Phibbs can only be used to correct the shape of Born approximation energy distribution.

Since the correction factor $2\pi\nu/(1-\ell^{\pm\nu})$ is just the non-relativistic Fermi function, which arises in β-decay, we also performed calculations using the relativistic Fermi functions. In all cases which we examined the calculated shape of the positron spectrum was essentially the same.

No systematic theoretical study of pair production has been performed in the present work since the Born approximation calculations of Rose [11] and the calculations of Lombard [10] reveal the general nature of the pair formation coefficient on the energy and multipolarity of the transition involved. Rather we have calculated, in the Born approximation, the total pair formation coefficients and the charge-corrected energy distributions for particular cases to compare with experiment. For completeness it may be noted that the probability of pair formation increases with increasing energy, as expected, but decreases with multipole order. This latter effect contrasts with the behaviour of the internal conversion coefficient which increases with multipole order. As well, the pair formation coefficient for the 2^ℓ electric multipole is generally larger than for the 2^ℓ magnetic transition.

The shape dependence of the energy distribution on multipole order, in the Born approximation, and the effect of the nuclear charge

correction term is demonstrated in Figs. 5-1 to 5-4. The shape of the energy distribution is insensitive to the multipolarity of the transition and is therefore a poor method of determining the nature of the transition. The effect of the nuclear charge on the energy distribution has been calculated using the correction term of Horton and Phibbs [13].

A comparison between the theoretical results and experiment will be delayed until a discussion of the particular experiment involved.

FIG. 5-1

Sample positron energy distribution calculated in the Born approximation for E1, E2 and E3 transitions.

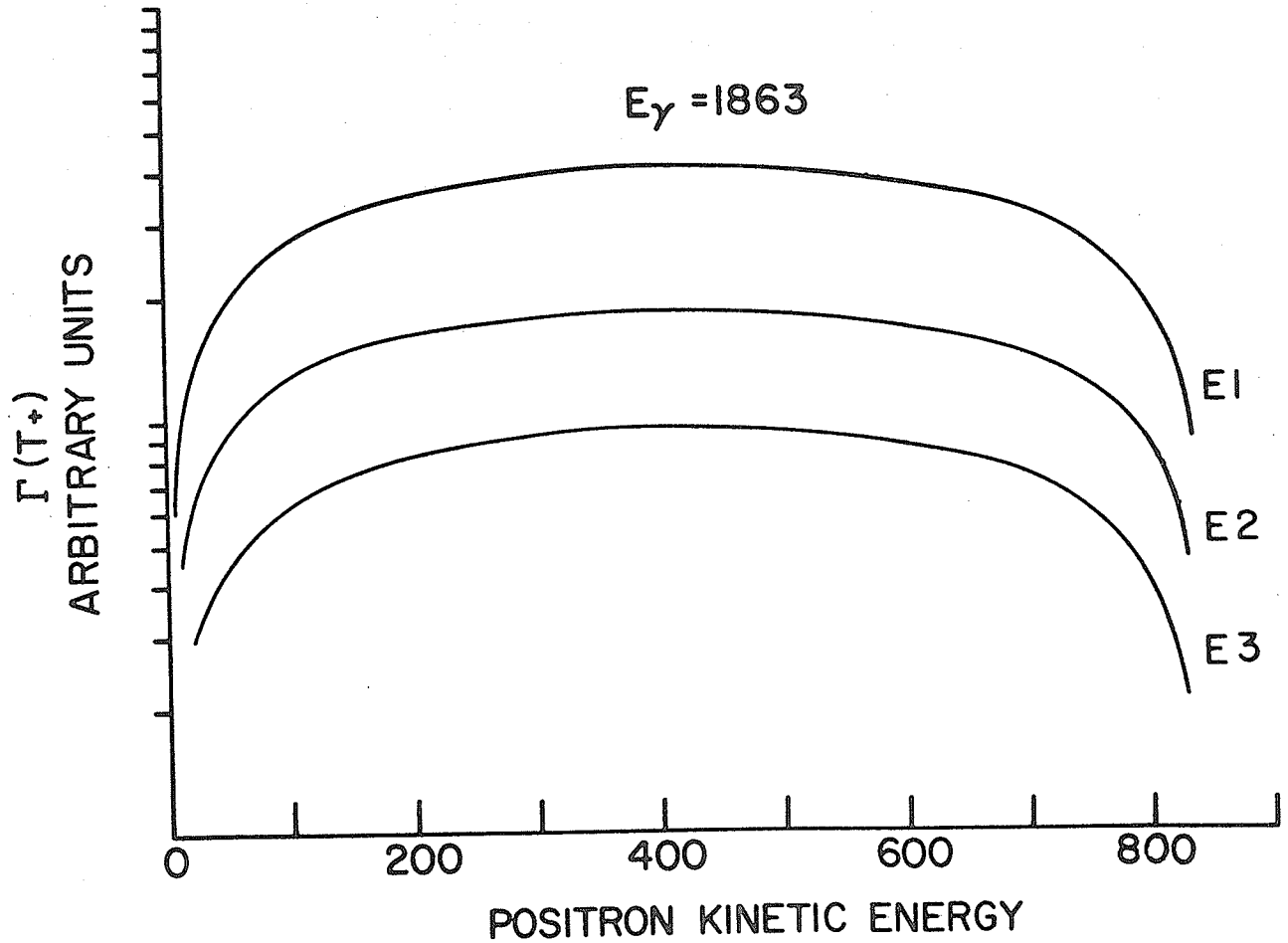
E_γ =1863
E1
E2
E3
$\Gamma(T_+)$
ARBITRARY UNITS
0
200
400
600
800
POSITRON KINETIC ENERGY

FIG. 5-2

Sample positron energy distribution calculated in the Born approximation for M1, M2 and M3 transitions.

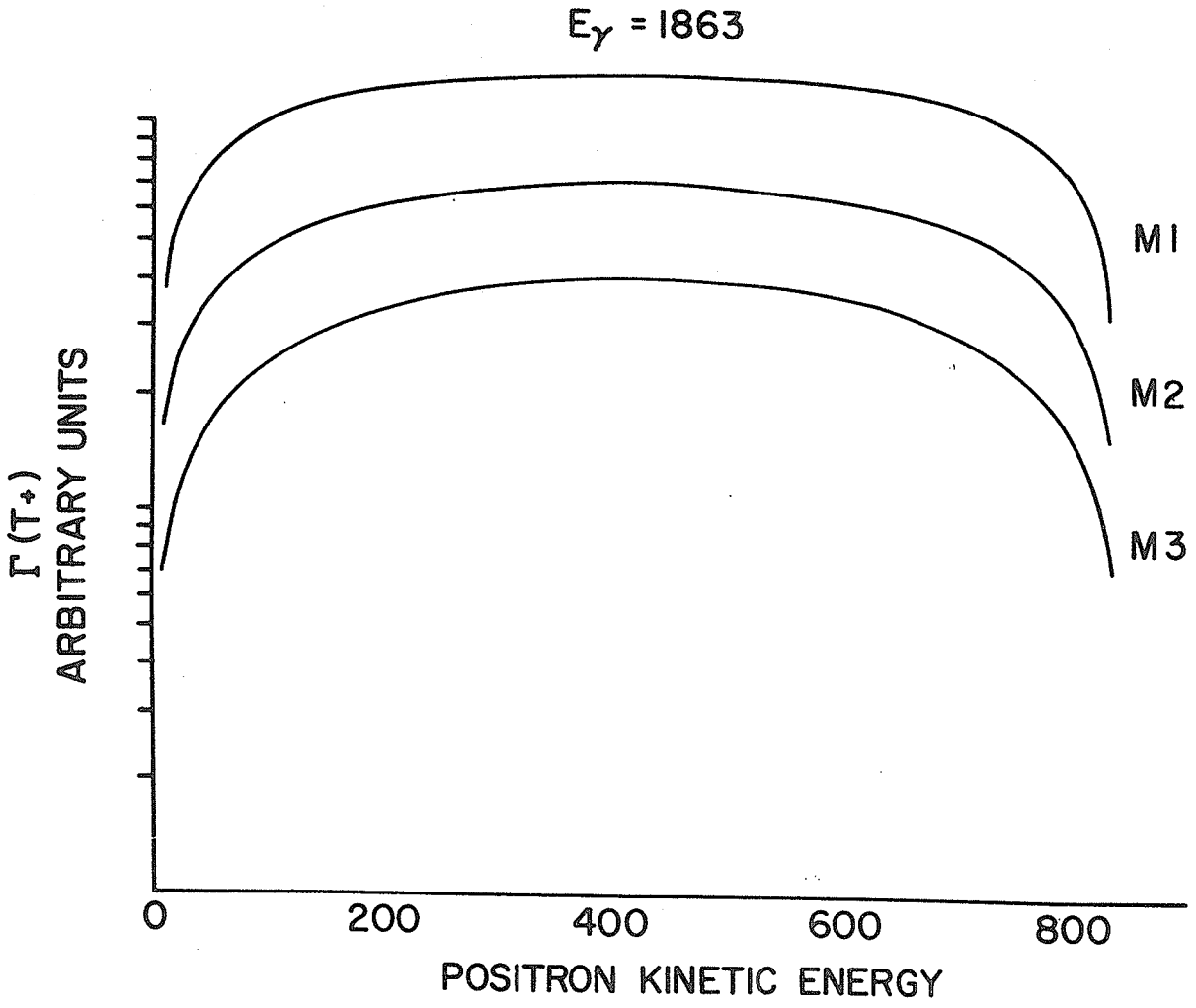
E_γ = 1863
M1
M2
M3
$\Gamma(T_+)$
ARBITRARY UNITS
0
200
400
600
800
POSITRON KINETIC ENERGY

FIG. 5-3

Comparison of the shape of the positron spectrum for Z=0 and Z=38.

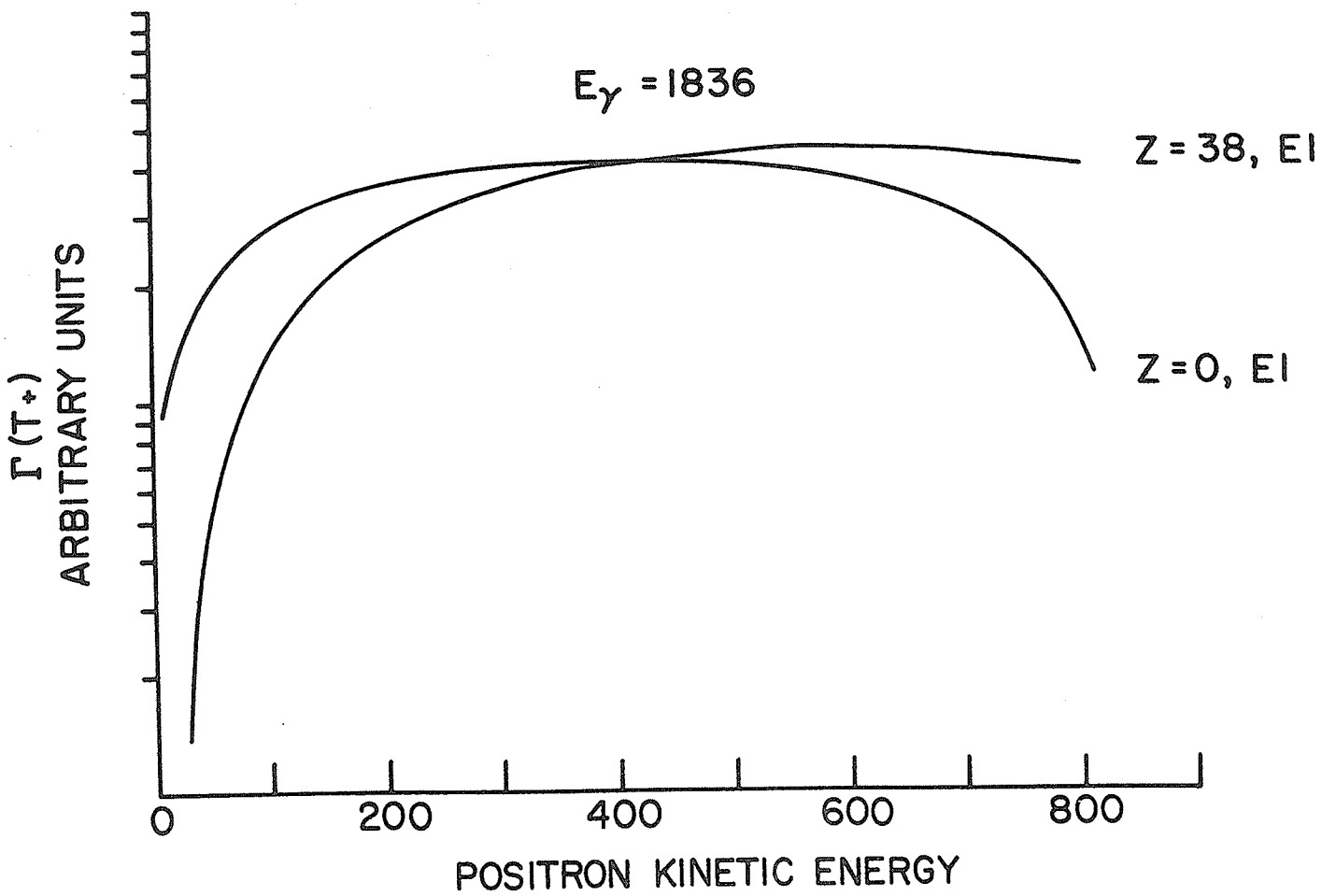
E_γ = 1836
Z = 38, EI
Z = 0, EI
Γ(T+)
ARBITRARY UNITS
0
200
400
600
800
POSITRON KINETIC ENERGY

FIG. 5-4

Comparison of the shape of the positron spectrum for Z=0 and Z=82.

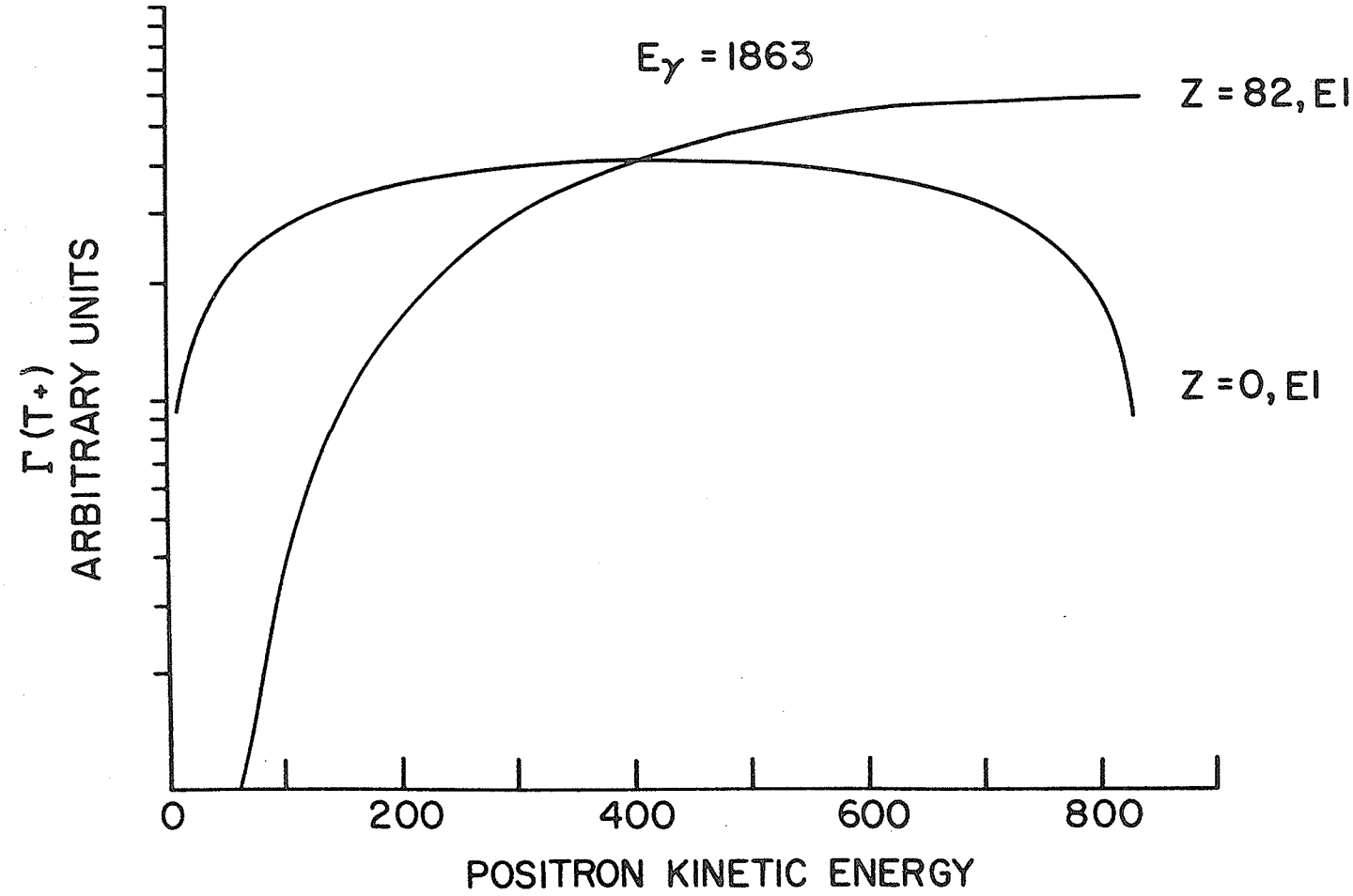
E_γ = 1863
Z = 82, El
Z = 0, El
$\Gamma(T_+)$
ARBITRARY UNITS
0
200
400
600
800
POSITRON KINETIC ENERGY

USE OF THE PRESENT SPECTROMETER TO STUDY PAIR PRODUCTION

The trochoidal β-ray spectrometer is well suited to studying the problem of internal pair production for two reasons. (1) It will be recalled that one side of the spectrometer responds only to positrons and the other only to electrons. Although the positron and electron energy distributions are continuous, for any given pair event the energies of the two particles add to a constant. Therefore, if both particles result in full energy pulses in their respective detectors the summed output of the two detectors will be a mono-energetic peak. This can be used to gate either the positron side or the electron side to study the individual continua in the presence of background radiation such as positrons from β^+ decay or other transitions producing internal pairs, or electrons from β^- decay or internal conversion processes. (2) The efficiencies of both sides is high, $\sim 10^{-1}$, and therefore the pair detection efficiency is high, $\sim 10^{-2}$.

Let us consider the pair detection efficiency of the spectrometer, ϵ_π, which we define to be the percentage of emitted pairs which contribute to the full energy "sum" peak; ie. Both the positron and electron are detected and deliver their full energy to the two detectors so the summed output of the two sides contributes to the full energy pair peak. The pair detection efficiency depends on the detection efficiencies for the positron and electron, the energy distribution of the positron continuum, the angular correlation between the directions of emission of the positron and electron, and the time of flight for the positron and electron to drift from the source to the

detectors. Let us, for the moment, neglect this last property. Then

$$\epsilon_\pi = \frac{\int_{T_+=0}^{T} \epsilon_1(T_+)\epsilon_2(T-T_+)C(T_+)N(T_+)dT_+}{N}$$

where $\epsilon_{12}(T)$ = the full energy peak detection efficiency of sides 1 and 2 at an electron energy T.

$N(T_+)dT_+$ = the number of pairs for which the positron kinetic energy is T_+

N = the total number of pairs emitted, $= \int_0^T N(T_+)dT_+$

and $C(T_+)$ is some function which reflects the angular correlation.

$C(T_+)$ depends, in general, on two things, (1) The strength of the angular correlation and (2) the effect of the trochoidal motion on the angular correlation. If the angular correlation between the two particles is isotropic then both particles can be considered to be emitted in random directions and C(T) = 1. ie. The pair detection efficiency is just the product of the efficiencies of the two sides of the spectrometer. In fact, as we shall now discuss, the trochoidal orbits which the particles follow "mask" any angular correlation so we can consider the positron and electron to be emitted in random directions with respect to one another and $C(T) \approx 1$.

Since the nature of the angular correlation is such that the positron and electron tend to come off in the same direction let us consider a case for which the angular correlation is "complete",

ie. the two particles are always emitted in the same direction and let $T_+=T_-$. Further let us assume that the two detectors are identical. Let the pair's direction of emission be defined by (θ,ϕ) where ϕ defines the vertical angle which the pair makes with the median plane and θ defines the angle which the pair makes with the radial line on which the source is located. See Fig. 5-5. Thus $\phi=0^{\circ}$ for pairs emitted in the median plane and $\phi=+90^{\circ}$ for pairs emitted straight up towards the pole tips; $\theta=0^{\circ}$ for pairs emitted straight out from the magnet centre and $\theta=90^{\circ}$ for pairs emitted tangential to the pole tips. If $\theta=0^{\circ}$, or $\theta=180^{\circ}$, independent of ϕ, then the motion of the positron is the mirror image of the motion of the electron and therefore if the electron is detected the positron must be detected and if the electron is not detected the positron is not detected. If, however, $\theta\neq 0^{\circ}$ or 180° this is not the case. For a positron emitted on an angle (θ,ϕ) the "equivalent" direction of emission for an electron is $(-\theta,\phi)$ ie. for a pair emitted on an angle (θ,ϕ) the electron's motion is the mirror image of the motion of a positron emitted at $(-\theta,\phi)$. Thus if the electron is detected the positron may not be detected and vice-versa.

To demonstrate the implications of this a computer study, for the case $T_+=T_-=500$ keV; was carried out, using the programme described in Chapter 3. If the angular correlation is "masked" by the subsequent motion of the two particles the pair efficiency will be the same as if the angular correlation was isotropic i.e. The pair detection efficiency will just be the product of the detection efficiencies of the two sides. Five hundred electron-positron pairs were emitted, in

FIG. 5-5

Illustration of the angle used to define the direction of pair emission.

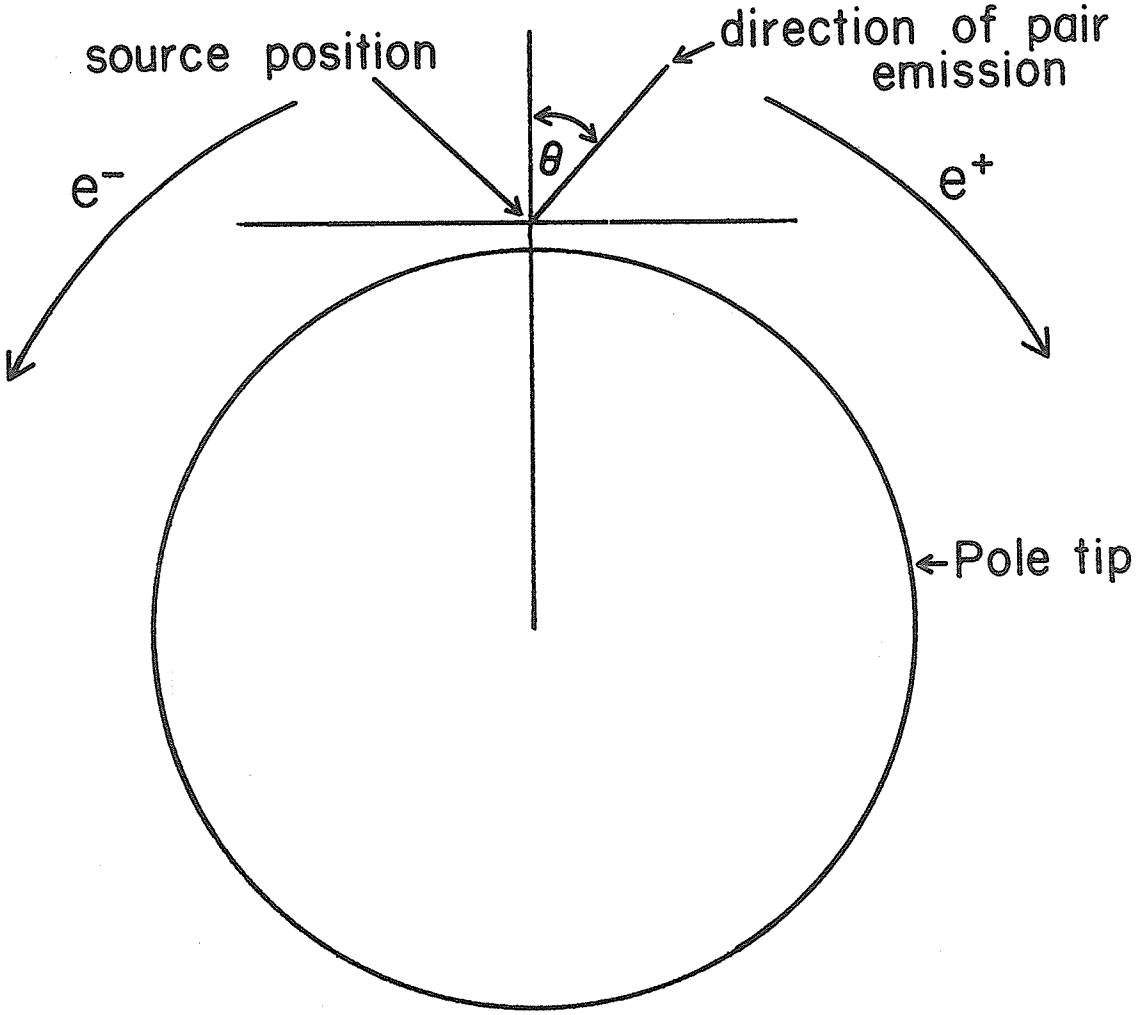
source position
direction of pair emission
θ
e⁻
e⁺
Pole tip

random directions but with the electron and positron coming off in the same direction, from a point source centred on the median plane .300" (7.6mm) beyond the edge of the pole tips. The electron and positron were tracked 15° around the pole tips and if both particles struck the active area of their respective detectors a pair was assumed to be detected. The calculations were carried out for active areas of $100mm^2$. From Chapter 3 the calculated percentage of electrons striking an active area of $100mm^2$ is 22.5% at 500 keV. It was found that the calculated pair detection efficiency was 5.0%, which is just the product of the efficiencies of the two sides of the spectrometer, assuming identical detectors. Thus the angular correlation is completely masked and C(T)=1.

The above calculation was carried out assuming that the positron and electron had the same energy, that they were emitted in the same direction and that the two detectors were identical. Of course none of these conditions hold in practice. The positrons and electrons usually have different energies, the angular correlation is never 100% and of course the two detectors are considerably different as evidenced by their calibration curves. (See Fig. 4-9). All of these effects however, only tend to further mask the effect of the angular correlation so that in fact we have been considering the worst possible case and even for this situation C(T)=1. Thus the full energy sum peak pair detection efficiency becomes -

$$\epsilon_\pi = \frac{\int_0^T \epsilon_1(T_+)\epsilon_2(T-T_+)N(T_+)dT_+}{N}$$

To evaluate ϵ_π one must know the shape of the positron continuum, a fact we do not wish to assume a priori. One can, in principle, circumvent this problem. By gating on the sum peak, the positron spectrum, for a particular transition, can be accumulated in a multi-channel analyzer. Let us assume we do this. Let $C(T_+)$ be the number of counts observed in Channel X, corresponding to a positron kinetic energy T_+. Let $N(T_+)$ be the number of positrons emitted with an energy T_+. Then

$C(T_+) = \epsilon_1(T_+)\epsilon_2(T-T_+)N(T_+)$ where $\epsilon_{1,2}$ are the full energy peak detection efficiencies of sides 1 and 2. (See Fig.4-9.) Note that the electron efficiency is for an energy $T_-=T-T_+$ where T is the total kinetic energy available to the pair. The positron spectrum is acquired by gating on the full energy sum peak so that necessarily the outputs of both the positron and electron detectors corresponded to the particle's full energy. The integral is then replaced by a sum and

$$\epsilon_\pi = \frac{\sum C(T_+)}{N} \quad \text{where } N = \sum C(T_+)/\epsilon_1(T_+)\epsilon_2(T_-)$$

and the summation is over all channel number. Thus to use the instrument as a pair spectrometer involves a measurement, in the above sense, of the pair detection efficiency. In general ϵ_π depends on E_γ and on the atomic numbers, Z. This latter dependence arises because

of the distortion of the positron energy spectrum by Coulomb repulsion.

As mentioned at the beginning of this section the pair efficiency depends on the time of flight of the particles, an effect which has been ignored until now. To see how this dependence arises one must consider the manner in which the spectrometer is being operated. The outputs of the two sides are being added to obtain a mono-energetic peak corresponding to the total pair kinetic energy. To ensure that the signals being added correspond to an electron and positron from a given pair event one must, of course, require a coincidence between the two sides. The time of flight of the particles is energy dependent, (See Fig. 3-15) and therefore if, in a given event, the positron acquires most of the energy it will be detected considerably before the electron. If the difference in time between the detection of the two particles is longer than the coincidence resolving time there will be no coincidence signal and therefore no summing. Such pairs will not contribute to the sum peak and the apparent number of pair events will be suppressed. Therefore to accept contribution to the sum peak from a wide region of the positron energy continuum one must use a relatively long coincidence resolving time. In the present instrument the resolving time has been set at 400 ns, which is the calculated time of flight for a 25 keV electron to drift 135° around the pole tips. (See Fig. 3-15.)

It is easiest to understand what this resolving time means by considering a specific example. Consider a transition for which E_{γ} = 1522 keV. Then the total kinetic energy available to an internally

produced pair is 500 keV and, as previously stated, this energy is shared between the positron and electron. If, for a given pair event, T_+ = 480 keV and T_- = 20 keV then the electron is detected approximately 480 ns after the positron, and there is no coincidence output; similarily if T_+ = 20 keV and T_- = 480 keV there is no coincidence output. The coincidence resolving time results, therefore, in a low energy "cut-off" at approximately 25 keV and a high energy "cut-off" at approximately 475 keV. ie. the full energy pair sum peak contains no contributions from pair events for which $T_+ \leq 25$ keV or $T_+ \geq 475$ keV. Since the maximum energy available to the positron is 500 keV, this means that the sum peak contains no contributions from approximately 10% of the energy region available to the positron and the pair detection efficiency is reduced by roughly the same amount.

One other point which should be considered in discussing the use of the present instrument as a pair spectrometer is the effect of a β^+ or β^- continuum. Again let us consider a specific example of say a β^- feed to an excited state for which one mode of de-excitation is internal pair production. Then associated in time with every internally produced pair is a β^- from the continuum. Thus it is possible for the positron, from the pair, to be detected in "true" coincidence with the β^- particle from the continuum. The number of events of this nature will be roughly the same as the number of coincidences between the positrons and electrons from pair events. Since, however, the β^- particles form a continuum, as do the positrons from pair production,

for events of this nature the summed output will be a continuum and will not contribute to the monoenergetic pair sum peak except as a general background of counts on which the sum peak lies. However, it is possible for a β^- from the continuum to be detected "simultaneously" with the positron and electron from a given pair event. Then the summed output of the two sides of the spectrometer will not lie in the pair sum peak and the apparent number of pair events will be smaller than the true value. This problem is analogous to that discussed in Chapter 4 where the apparent number of conversion electrons was low because the conversion electron and a β^-, from the continuum, were detected "simultaneously" so that the output of the detector did not contribute to the conversion peak.

These effects arise because the β^- particle is in true coincidence with the pair event. Such effects may also occur because of random coincidences. What ratio of true to random counting rates can be expected? The ratio is given by

$$\frac{\text{True}}{\text{Random}} = \frac{N_p \epsilon_1 \epsilon_2}{2\tau N_+ N_- \epsilon_1 \epsilon_2}$$

where ϵ_1, ϵ_2 are some sort of average detection efficiencies, N_p = internal pair production rate, N_+ = positron production rate, N_- = electron production rate and τ = coincidence resolving time. If we assume that the number of conversion electrons is small compared to the number of electrons from the β^- decay and that the positron production rate = the pair production rate and using τ=400 ns we obtain

$$R = \frac{1}{2 \times 400 \times 10^{-9}} \times \frac{N_-}{} = \frac{10^7}{8N_-} .$$

If we take 1×10^{-4} as a typical pair formation coefficient then for a source strength of 1μC the pair production rate is ~4/sec and the true to random coincidence rate is ~30/1. Again it should be pointed out that for random coincidence events the summed output of the spectrometer is a continuum.

In summary, the present instrument is applicable as a pair spectrometer to measure the total pair formation coefficient and to study the shape of the individual positron and electron continua. The angular correlation between the directions of emission of the positron and electron is masked by the motion of the particles so that on one hand the present instrument cannot be used to measure this correlation but on the other hand the correlation does not affect the pair detection efficiency.

CHAPTER 6

STUDY OF ^{206}Pb FOLLOWING THE DECAY OF ^{206}Bi

"Nature and Nature's laws lay hid in night:
God said, 'Let Newton be!' and all was light.

..... Alexander Pope

INTRODUCTION

^{206}Bi decays to ^{206}Pb essentially by 100% electron capture with a half-life of 6.24 days. The subsequent transitions in ^{206}Pb, although numerous, have been well studied by numerous workers,[14,15,16] and the decay scheme is reasonably well established. In Fig. 6-1 the decay scheme of Lederer, Hollander and Perlman [14] is presented.

There were three reasons for undertaking the present study of ^{206}Bi. (1) The relative intensities of several wall spaced K-conversion lines are known and a measurement of the intensity of these lines is a suitable test of the spectrometer's calibration. (2) Wiener et al [17] and Perdrisat et al [18] had established the existence of three high energy transitions with energies of 1845, 1879 and 1903 keV, by observing the conversion electrons. A second reason, then, for studying ^{206}Bi was to determine the location of these transitions in the decay scheme. (3) A measurement of the internal pair formation coefficient, α_π, was undertaken for the strong 1719 keV transition as a first attempt at using the instrument as a pair spectrometer. For completeness the energies and relative intensities of the various γ-rays were determined using external Ge(Li) detectors.

FIG. 6-1

^{206}Bi decay scheme taken from Lederer et al.

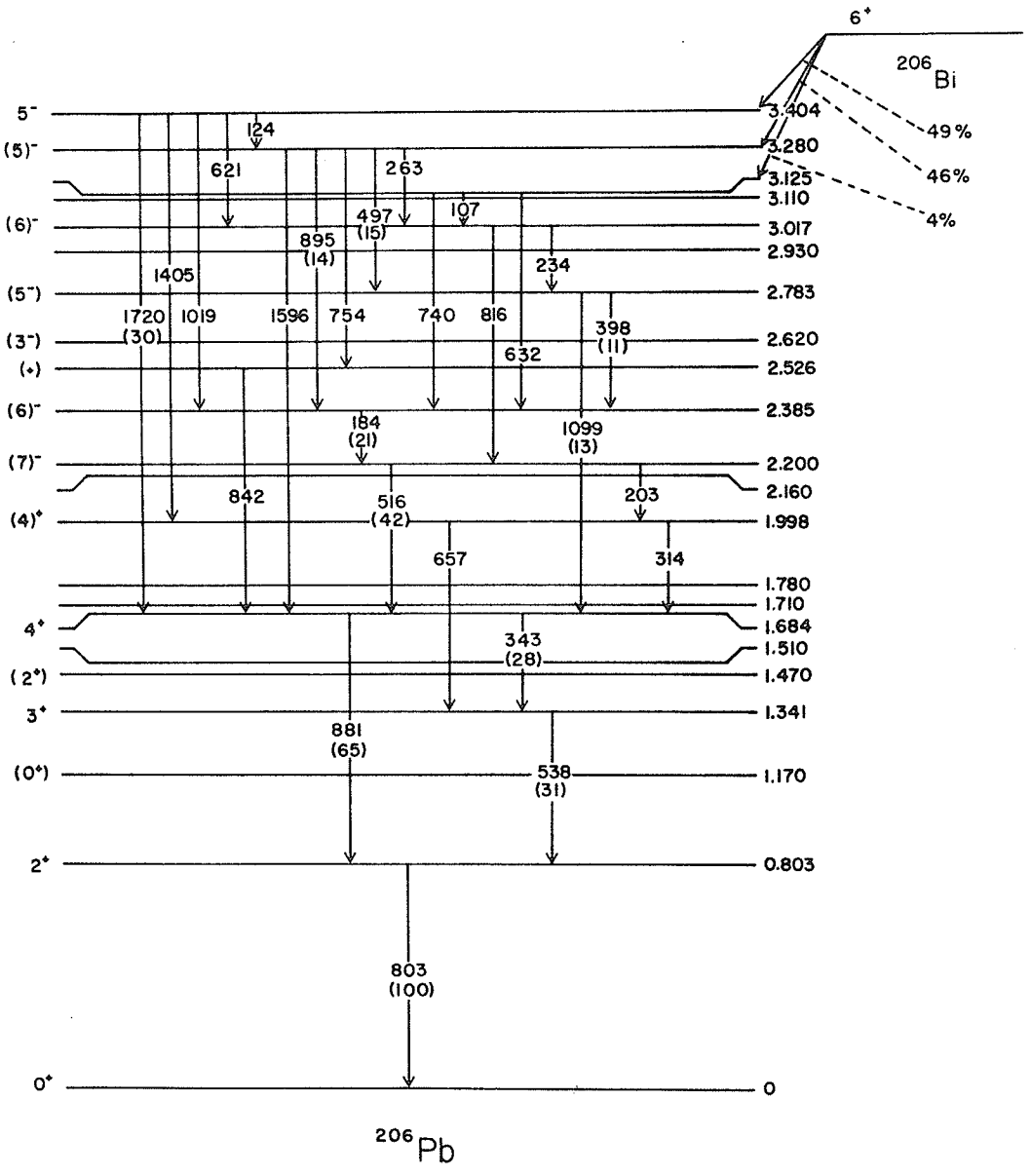
6+
206 Bi
49 %
46%
4%
5-
(5)-
(6)-
(5-)
(3-)
(+)
(6)-
(7)-
(4)+
4+
(2+)
3+
(0+)
2+
0+
3.404
3.280
3.125
3.110
3.017
2.930
2.783
2.620
2.526
2.385
2.200
2.160
1.998
1.780
1.710
1.684
1.510
1.470
1.341
1.170
0.803
0
124
621
263
497 (15)
107
895 (14)
1405
234
1720 (30)
1019
1596
754
740
816
398 (11)
632
184 (21)
1099 (13)
842
516 (42)
203
657
314
343 (28)
881 (65)
538 (31)
803 (100)
206 Pb

ELECTRON AND GAMMA-RAY SINGLES STUDIES.

A typical electron spectrum of ^{206}Bi obtained using the spectrometer is shown in Fig. 6-2. Only those peaks which have been analysed are labelled. No detailed analysis of this electron spectrum was undertaken, since the electron work was used only to verify the calibration curves previously obtained. (See Fig. 4-9). The results of this work are summarized and compared with the results of Alburger and Pryce [15], Stockendal and Hultberg [16], Weiner et al [17], and Predrisat et al [18] in table 6-1. The agreement is excellent. The reader should note, in particular that the efficiency curves are verified for the higher energies.

As can be seen from Fig. 6-2 the 497-K, 516-K and 538-K lines are not completely resolved, nor is the 398-K peak completely separated from the 343-L line. To extract the counts in these peaks it was necessary to do some simple peak fitting, which was done graphically. By way of example, the fits to the 497-K, 516-K and 538-K peaks are shown in Fig. 6-3. In Fig. 6-3 the points represent the counts per channel after a straight line background subtraction, and the solid curves, all of which have the same shape, represent the estimated contributions from each line. The shape of the fitting curve was obtained from the shape of the 538-K peak. Fitting the high-energy side of the curve to the 497-K line we were able to obtain the "exact" shape of the low energy side of the 538-K peak from 10% of full peak height to full heighth. This shape was then extrapolated down to 1% of full peak height. Since this extrapolation involves only roughly 10% of the area of the whole

FIG. 6-2

Typical ^{206}Bi electron spectrum. Only the peaks which have been analysed are labelled.

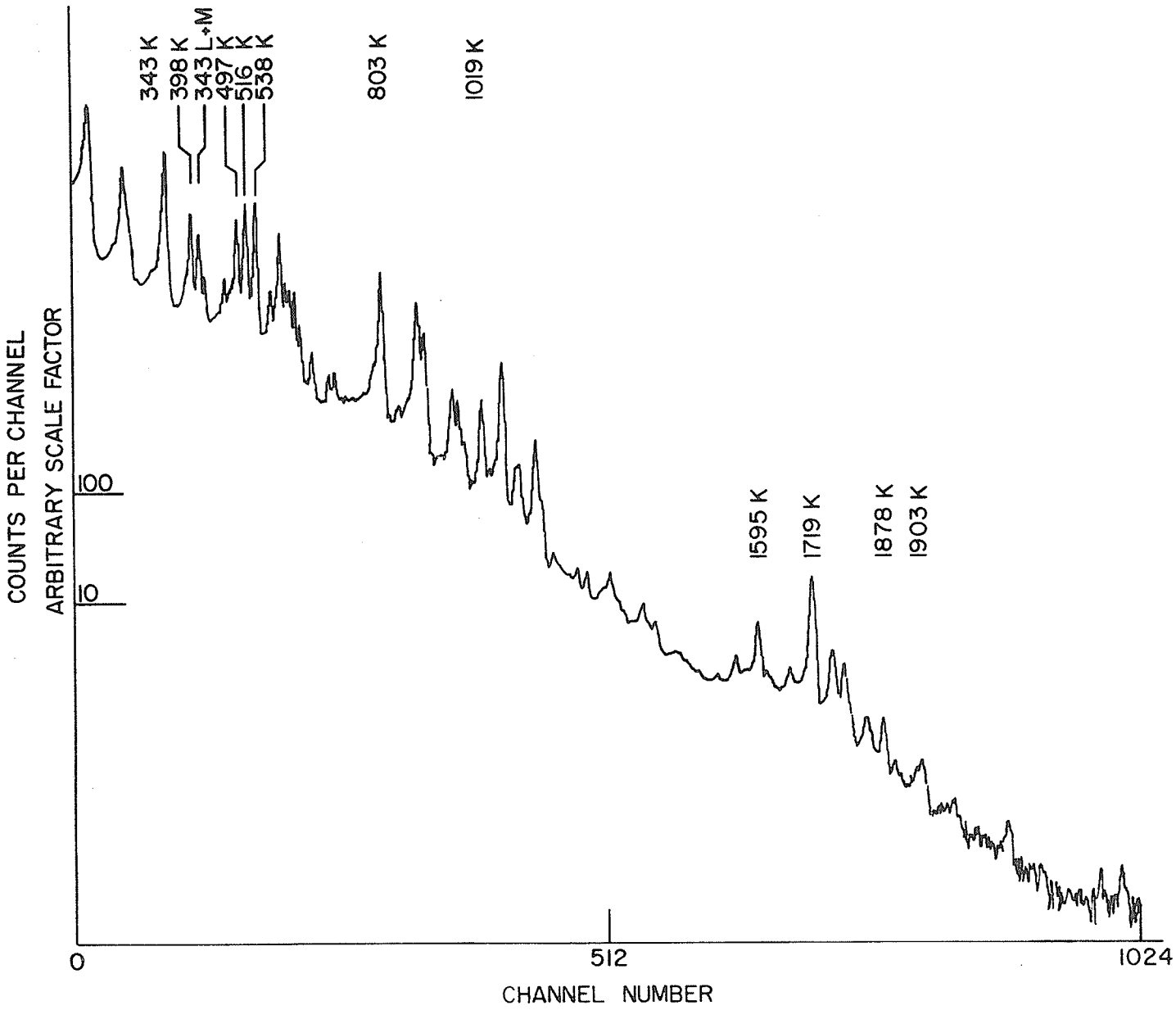
343 K
398 K
343 L+M
497 K
516 K
538 K
803 K
1019 K
1595 K
1719 K
1878 K
1903 K
COUNTS PER CHANNEL
ARBITRARY SCALE FACTOR
100
10
0
512
1024
CHANNEL NUMBER

TABLE 6-1

Comparison between the relative intensity of several electron lines of ^{206}Bi as measured in the present work and as measured by Alburger and Pryce (15), a, Stockendal and Hultberg (16), b, Wiener et al (17), c, and Perdrisat et al (18) d.

TABLE 6-1

Electron Peak	Relative Intensity			
	Detector A	Detector B	Previous Workers.	
343-K	811	823	776[a]	760[b]
398-K	188	198	207[a]	210[b]
497-K	150	174	161[a]	170[b]
516-K	233	240	229[a]	250[b]
537-K	231	241	245[a]	280[b]
803-K	100	100	100[a]	100[b]
1019-K	12.6	10.9	13[a]	15[b]
1596-K	.56		.64[a]	- [b]
1719-K	3.26		3.4[a]	3.4[b]
1880-K	.155±.02		.18[c]	.16[d]
1903-K	.021±.006		.027[c]	.020[d]

FIG. 6-3

The peak fitting for the 497-K, 516-K, and 538-K conversion lines.

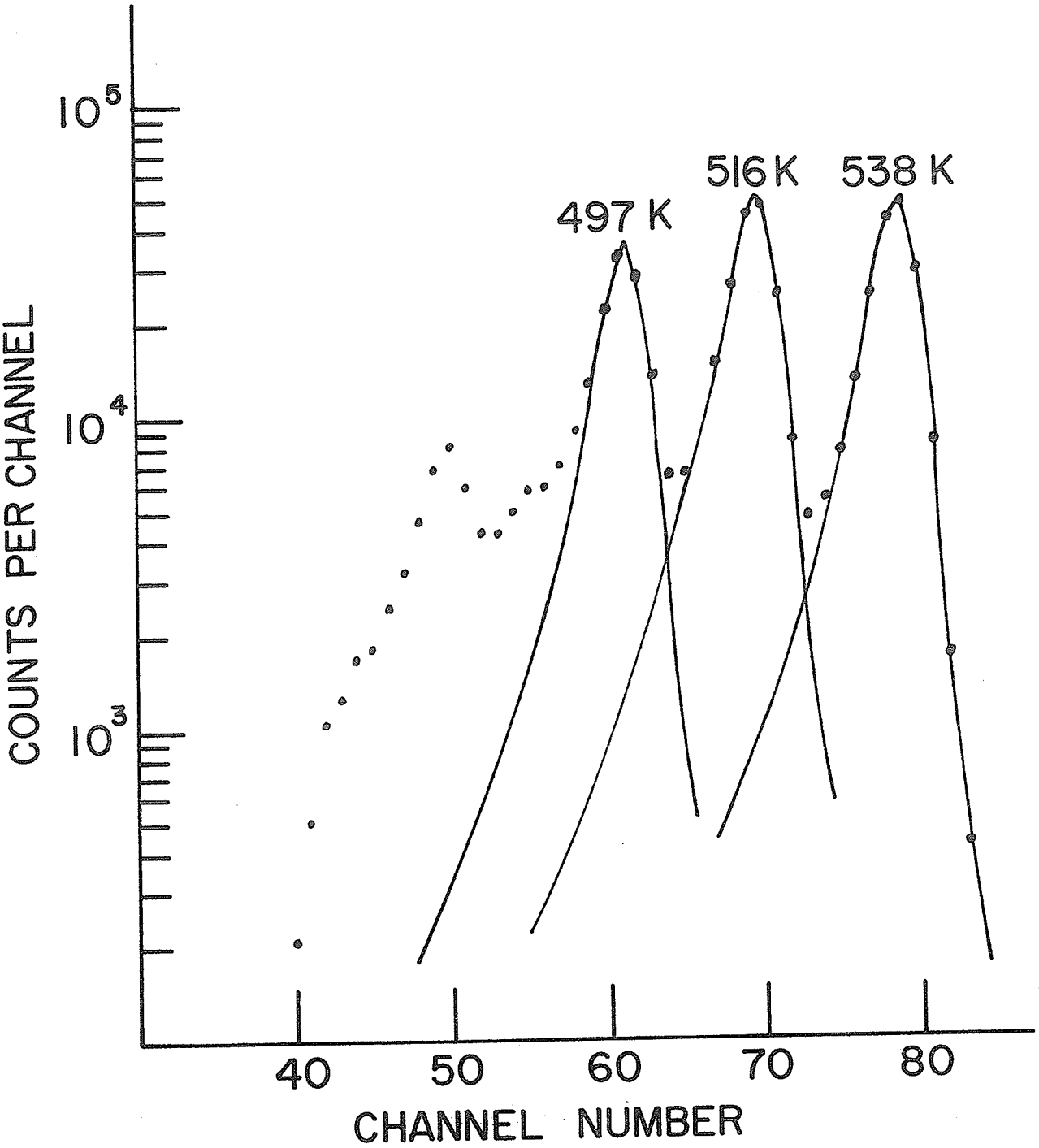
497 K
516 K
538 K
10^5
10^4
10^3
COUNTS PER CHANNEL
40
50
60
70
80
CHANNEL NUMBER

peak no significant error is thus introduced. The lack of peak separation was caused, in part, by the condensation of vapours on the face of the detectors. At the time this work was done the cold finger, shown in Fig. 4-2, was not in use.

As well as determining the relative intensities of the electron lines the K-conversion coefficient for the 803 keV, $2^+ \rightarrow 0^+$ transition was measured. The 803 keV γ-ray counting rate was determined using the same external Ge(Li) detector which was used in calibrating the spectrometer. The value obtained was $\alpha_k = 8.3 \times 10^{-3}$ which agrees well with the theoretical value of 8.1×10^{-3} calculated by Hager and Seltzer.[22] Thus the absolute normalization of the calibration curves was also verified.

As discussed in chapter 4 two conversion electrons, from transistions in cascade, may be detected simultaneously and give rise to a false peak. Such a situation was encountered in the present study. The apparent intensity of the 1595-K line was too high. This anomaly was caused by contributions to the peak from the "simultaneous" detection of 803-K and 881-K conversion electrons. The effect was corrected for using the relative intensity of the 881-K electron line as measured by Stockendal and Hultberg [16], and the K-conversion coefficient for the 803 keV transition as determined in the present work. The ratio of 803-K and 881-K sum counts observed, to 803-K counts observed is given by:

$$S = .6 \times \frac{\epsilon(881\text{-K})}{\epsilon(803\text{-K})} \times \alpha_K\,(803) \times \epsilon(803\text{-K}) \text{ where}$$

the ratio of the 881-K intensity to the 803-K intensity is .6[16]. Substituting the appropriate values we obtain X = .60 x .165 x 8.3 x 10^{-3} = 8.2 x 10^{-4}. But the observed counts in the 1507 keV peak, (1596-88), relative to 803-K counts, was 5.2 x 10^{-3}. Subtracting the contribution from the sum counts and correcting for efficiency gives the relative intensity for the 1595-K line.

Gamma-ray singles spectra were acquired using two different Ge(Li) detectors. These were (1) a 35cm^3. Ortec co-axial detector and (2) a 20cm^3. Princeton-Gamma-Tech, P.γ.T., co-axial detector. A typical γ-spectrum obtained with the Ortec detector is shown in Fig. 6-4. The detectors were calibrated for full energy peak detection efficiency, for fixed geometry, using standardized I.A.E.A. sources. See Fig. 6-5. Because of its better resolution and higher efficiency most of the singles runs were made using the Ortec detector. However, the relative intensities of several strong transitions were also measured using the P.γ.T. detector and the results were found to be consistent. See table 6-2. It should be noted that these two measurements are not completely independent since the two detectors were calibrated for efficiency using the same set of sources.

As previously mentioned, the γ-ray singles experiments were used to determine the energies of the various transitions as well as the relative γ-ray intensities. The energy determination was done in two steps. (1) The energies of the strong γ-rays were measured first as follows: (a) A γ-spectrum from mixed ^{206}Bi plus I.A.E.A. standard sources was accumulated into a 2048 multi-channel analyzer. This spec-

FIG. 6-4

Typical ^{206}Bi γ-ray spectrum obtained using the Ortec 35cm^3. Ge(Li) detector.

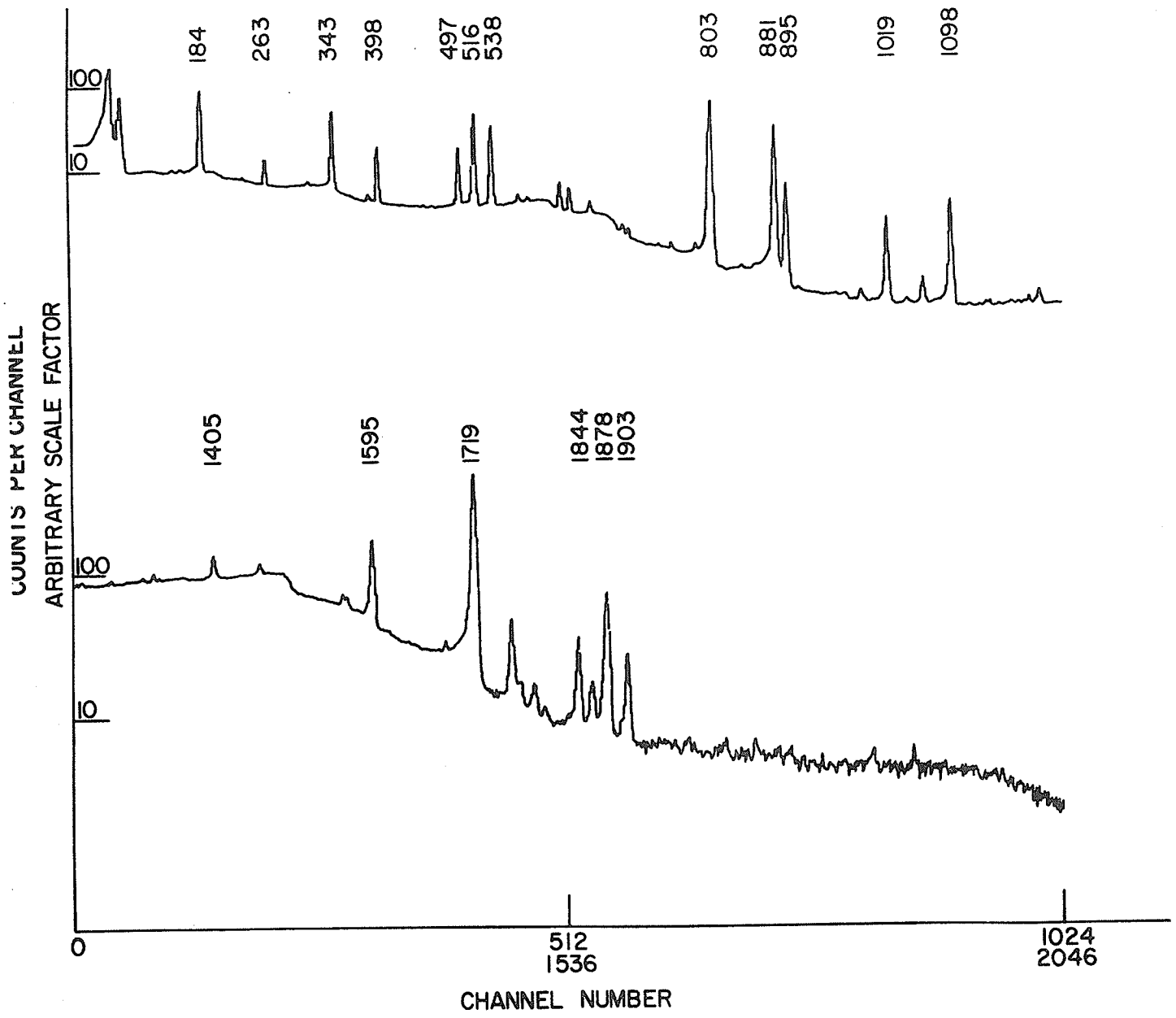
184
263
343
398
497
516
538
803
881
895
1019
1098
100
10
1405
1595
1719
1844
1878
1903
100
10
COUNTS PER CHANNEL
ARBITRARY SCALE FACTOR
0
512
1536
1024
2046
CHANNEL NUMBER

FIG. 6-5

Efficiency calibration of the Ortec and P.γ.T. Ge(Li) detectors.

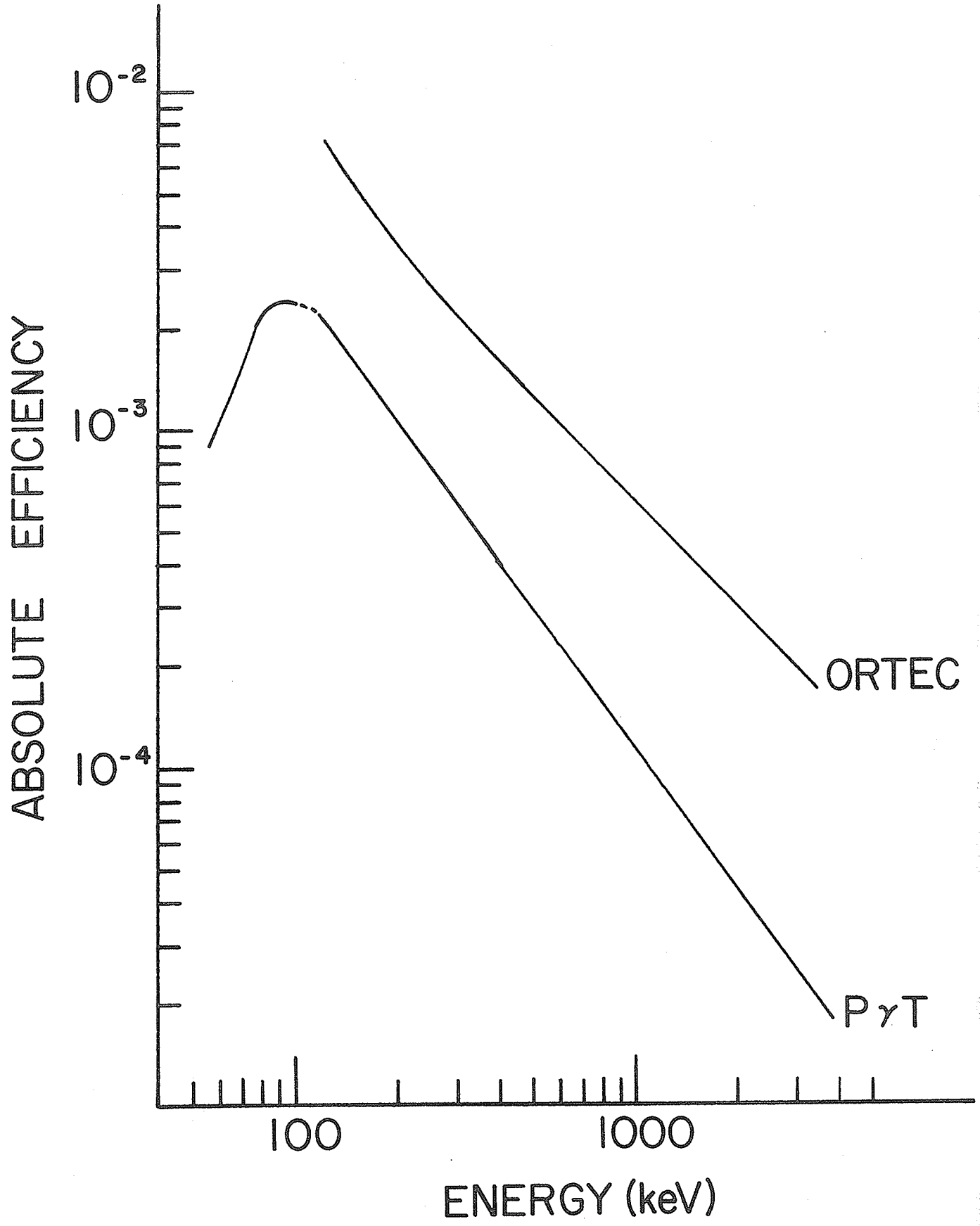
ABSOLUTE EFFICIENCY
10^{-2}
10^{-3}
10^{-4}
ORTEC
PγT
100
1000
ENERGY (keV)

TABLE 6-2

Comparison of the relative γ-ray intensities of several lines in ^{206}Bi as measured using the Ortec Ge(Li) detector and the P.γ.T. Ge(Li) detector.

TABLE 6-2

RELATIVE GAMMA RAY INTENSITIES OF STRONG LINES.

E_γ	RELATIVE INTENSITY	
	Ortec Detector	P.γ.T.
184	213	229
343	279	273
398	113	115
497	152	150
516	416	413
538	307	303
803	1000	1000
1019	72.8	74.0
1099	128	133
1596	47.4	52.0
1719	303	342

trum is shown in Fig. 6-6. (b) The analyzer was calibrated with respect to energy assuming a linear relation $E(x) = E_o + k(x-x_o)$ where $E(x)$ is the energy of the γ-ray whose peak is centred at channel x. The slope, k, was calculated using the 279.2 keV transitions of ^{203}Hg and the 1173.2 keV transition of ^{60}Co and E_o was taken to be 279.2 keV. The energies of the other standardized I.A.E.A. transitions were then predicted using the above equation and an empirical correction to the equation was obtained, at these energies, by comparing the predicted values with the "true" energies. (d) The correction was then plotted as a function of predicted energy and the resulting correction curve was used in conjunction with the linear calibration to determine the energies of the intense ^{206}Pb lines. (2) The energies of the other transitions in ^{206}Pb were then determined in a similar manner but, using the "known" ^{206}Pb transitions as energy standards.

The energy calibration of the strong ^{206}Pb transitions is summarized in table 6-3. The accuracy of this method of energy calibration is limited by the accuracy with which the peak position can be determined and by the accuracy of the correction which must be applied to the linear calibration of the multi-channel analyzer. For the strong ^{206}Pb transitions it is estimated that the peak location is accurate to ±.2 channel. Since the slope of the straight line calibration is ~1 keV per channel the resulting inaccuracy is ~±.2 keV. The empirical correction curve is estimated to contribute a further inaccuracy of ±.1 keV, for the strong lines, so that the energies of the strong transitions are accurate to ±.3 keV. The energies of the other transitions are not as

FIG. 6-6

Gamma-spectrum obtained with mixed ^{206}Bi plus I.A.E.A. calibration sources used for energy calibration of ^{206}Bi.

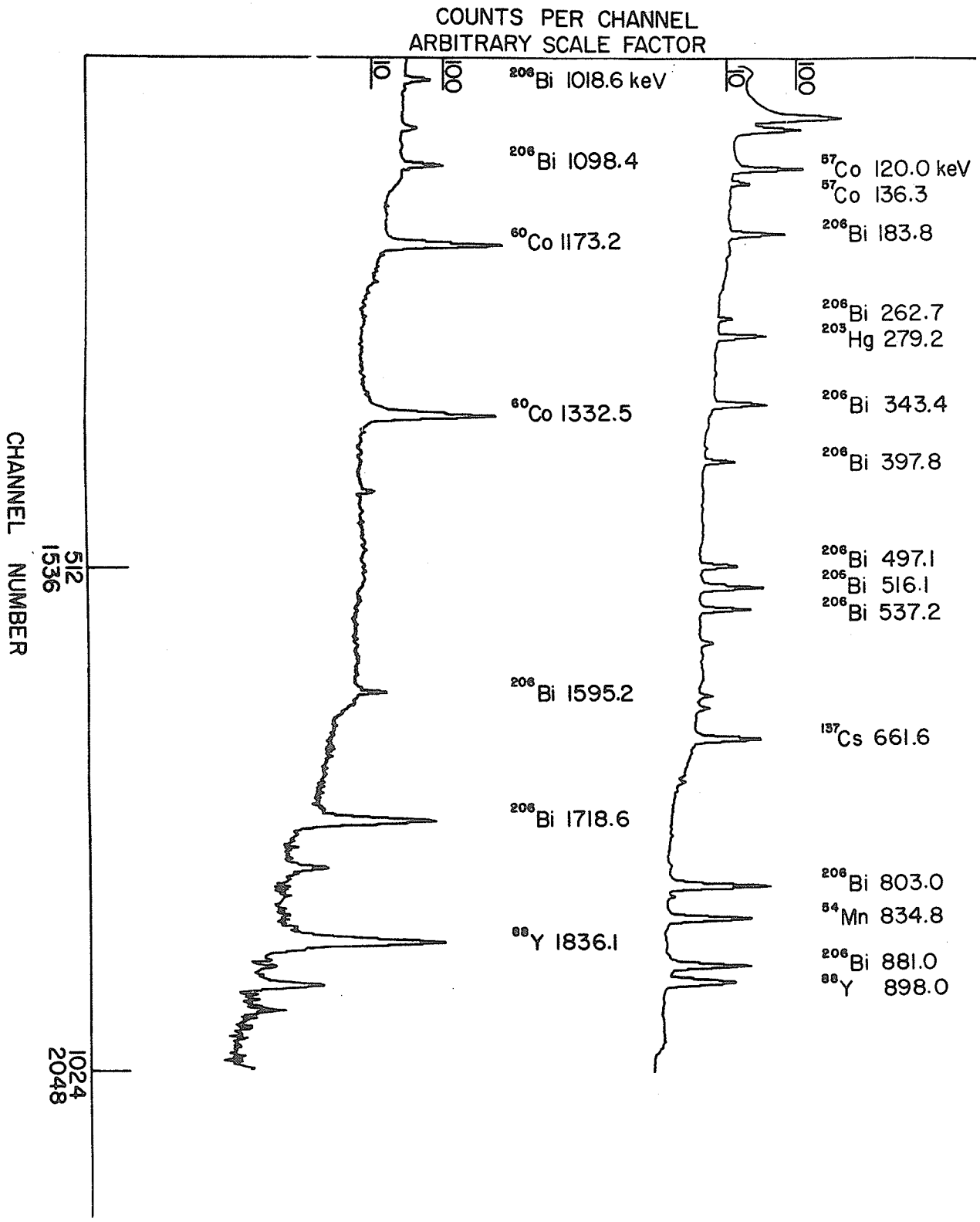
COUNTS PER CHANNEL
ARBITRARY SCALE FACTOR
10
100
10
100
^{206}Bi 1018.6 keV
^{206}Bi 1098.4
^{60}Co 1173.2
^{60}Co 1332.5
^{206}Bi 1595.2
^{206}Bi 1718.6
^{88}Y 1836.1
^{57}Co 120.0 keV
^{57}Co 136.3
^{206}Bi 183.8
^{206}Bi 262.7
^{203}Hg 279.2
^{206}Bi 343.4
^{206}Bi 397.8
^{206}Bi 497.1
^{206}Bi 516.1
^{206}Bi 537.2
^{137}Cs 661.6
^{206}Bi 803.0
^{54}Mn 834.8
^{206}Bi 881.0
^{88}Y 898.0
CHANNEL NUMBER
512
1536
1024
2048

TABLE 6-3

Summary of the energy calibration of the strong ^{206}Bi lines. Also shown are the values given by Lederer et al (14), a, and Alburger and Pryce (15), b.

TABLE 6-3

I.A.E.A. Calibration Standards

Peak Location	Predicted Energy*	True Energy	Correction
118.3 channel	122.2 keV	122.0	- .2
133.6 channel	136.8 keV	136.3	- .5
283.0 channel	279.2 keV	279.2	0
683.8 channel	661.3 keV	661.6	+ .3
865.4 channel	834.5 keV	834.8	+ .3
931.6 channel	897.6 keV	898.0	+ .4
1220.7 channel	1173.2 keV	1173.2	0
1387.8 channel	1332.5 keV	1332.5	0
1916.3 channel	1836.4 keV	1836.1	- .3

* E_γ = 279.2 keV + (0.9534 keV/channel) $\cdot \Delta X$

Peak Location	Predicted Energy*	True Energy	Previous Workers
183.3 channel	184.1	183.8	184.0[a]
265.7 channel	262.7	262.7	262.8[a]
350.3 channel	343.4	343.4	343.5[a]
407.4 channel	397.7	397.8	398.1[a]
511.3 channel	496.9	497.1	497.1[a]
531.3 channel	515.9	516.1	516.3[a]
553.4 channel	537.0	537.2	537.6[a]
832.1 channel	802.7	803.0	803.1[a]
913.8 channel	880.6	881.0	880.8[a]
1058.3 channel	1018.4	1018.6	1018.8[b]
1142.1 channel	1098.3	1098.4	1098.6[b]
1663.5 channel	1595.4	1595.2	1596.3[b]
1793.1 channel	1718.9	1718.6	1719.7[b]

well known since their determination depends on the accuracy with which the energies of the strong lines are known. For the majority of these other transitions, then, the energies are estimated to be accurate to ±.5 keV.

The results of the γ-ray singles work are summarized in table 6-4, where the relative γ-ray intensities are compared to those of Lederer, Hollander and Perlman [14] and the transition energies are compared to those of Lederer, Hollander and Perlman and to those of Alburger and Pryce [15]. The lines labelled with asterisks have been identified as new transitions. We shall postpone a discussion of these transitions until later. Unless otherwise indicated the energy is estimated to be accurate to ±.5 keV. The relative γ-ray intensity is estimated to be accurate to ±5% for those transitions listed with 3 figures, to ±10% for the other transitions, unless otherwise specified. From the present measurement of the relative γ-ray intensities the K-conversion coefficients have been calculated for a number of transitions. The results are shown in table 6-5. These calculations were done using the relative K-shell electron intensities obtained in the present study, a, and the results obtained by Alburger and Pryce [15], b, and were based on the present measurement of the 803 keV K-conversion coefficient, $\alpha_K(803) = 8.3 \times 10^{-3}$. Table 6-5 also shows the nature of the transition according to the decay scheme of Lederer et al [14] (Fig. 6-1), and the multipolarity of the transition obtained by comparing the conversion coefficient to the theoretical calculations of Hager & Seltzer [22].

TABLE 6-4

Summary of the ^{206}Bi γ-ray singles work.

TABLE 6-4

Energy			Relative Intensity	
esent Work	Lederer et al[14]	Alburger & Pryce[15]	Present Work	Lederer et al[14]
-	107.2	107.2	-	-
-	123.6	123.6	-	-
7.5±1.0*	-	-	2.5±.5	-
7.8±1.0*	-	-	3.4±.7	-
3.8± .3	184.0	184.1	213	210
-	202.7	202.5	-	-
4.2	234.4	234.3	3.8	-
2.8±.3	262.8	262.8	36.9	29
3.8	313.7	313.6	4.2	30
3.4±.3	343.5	343.4	279	260
6.1	386.1	386.0	5.2	-
7.8±.3	398.1	398.1	113	100
7.1±.3	497.1	497.1	152	180
6.1±.3	516.3	516.1	416	460
7.2±.3	537.6	537.5	307	340
2.0*	-	-	4.3	-
0.4	620.7	620.6	54.6	40
2.2	632.4	632.2	44.1	45
7.0	657.3	657.3	19.8	53
6.5*	-	-	6.3	-
9.1	740	739.9	1.9	36
4.9	754	753.9	5.4	27
4.6*	-	-	5.0	-
3.0	803.1	803.3	1000	1000
-	816	816.3	-	-
1.3	842	841.7	1.9	-
8.0±1.0*	-	-	.80±.3	-
1.0± .3	880.8	880.5	654	730
5.0	895.0	895.1	139	190
5.5±1*	-	-	1.9	-
6.6±1*	-	-	2.2	-
8.7± .3	1018.9	1018.8	72.8	80
8.4± .3	1099	1098.6	128	130
1.4±1*	-	-	.43±.2	-
5.5±1*	-	-	2.5	-
8.5±1*	-	-	6.3	-
9.0±1*	-	-	1.0	-
6.0±1*	-	-	.9	-
3.7*	-	-	2.5	-
5.3	1405	1405.2	13.2	-
0.4*	-	-	2.8	-
5.4*	-	-	2.8	-
5.2± .3	1596	1596.3	47.4	80
8.6	1720	1719.7	303	360
1.2*	-	-	1.4	-
4.1	1845	-	5.42	-
8.1	1880	-	19.6	-
2.8	1903	-	3.88	-

TABLE 6-5

K-conversion coefficients obtained from the relative γ-ray intensities of the present work and the relative electron intensities of the present work, a, of Alburger and Pryce (15), b, of Wiener et al (17), c, and Perdrisat et al (18), d. Also shown are the theoretical values of Hager and Seltzer (22) and the nature of the transition based on the decay scheme of Lederer et al (14).

TABLE 6-5

E_γ	Gamma-Ray Intensity	K-Electron Intensity	α_K Measured	α_K Theoretical	Type of Transition from Lederer et al (14)	Agreement
107.2		27[b]				
123.6		8.1[b]			$5^- \rightarrow 5^-$	
183.8	213	3290[b]	1.3	1.35(M1)	$6^- \rightarrow 7^-$	yes
202.7		2.4[b]			$7^- \rightarrow 4^+$	
234.2	3.8	28[b]	6.1×10^{-1}	7.1×10^{-1}(M1)	$6^- \rightarrow 5^-$	yes
262.8	36.9	247[b]	5.6×10^{-1}	5.3×10^{-1}(M1)	$5^- \rightarrow 6^-$	yes
313.8	4.2	16.5[b]	3.3×10^{-1}	3.25×10^{-1}(M1)	$4^+ \rightarrow 4^+$	yes
343.4	279	817[a]	2.4×10^{-1}	2.5×10^{-1}(M1)	$4^+ \rightarrow 3^+$	yes
386.1	5.2	15[b]	2.4×10^{-1}	1.85×10^{-1}(M1)	$5^- \rightarrow 6^-$	yes
397.8	113	193[a]	1.4×10^{-1}	1.65×10^{-1}(M1)	$5^- \rightarrow 6^-$	yes
497.1	152	162[a]	8.9×10^{-2}	9.2×10^{-2}(M1)	$5^- \rightarrow 6^-$	yes
516.1	416	237[a]	4.7×10^{-2}	5.0×10^{-2}(E3)	$7^- \rightarrow 4^+$	yes
537.6	307	236[a]	6.4×10^{-2}	7.6×10^{-2}(M1)	$3^+ \rightarrow 2^+$	yes
620.4	54.6	31.8[b]	4.8×10^{-2}	5.1×10^{-2}(M1)	$5^- \rightarrow 5^-$	yes
632.2	44.1	24.7[b]	4.7×10^{-2}	4.9×10^{-2}(M1)	$6^- \rightarrow 6^-$	yes
657.0	19.8	9.9[b]	4.2×10^{-2}	4.5×10^{-2}(M1)	$4^+ \rightarrow 3^+$	yes

....con't.

con't.

TABLE 6-5

E_γ	Gamma-Ray Intensity	K-Electron Intensity	α_K Measured	α_K Theoretical	Type of Transition from Lederer et al (14)	Agreement
739.1	1.9	1.3[b]	5.7×10^{-2}	3.4×10^{-2}(M1)	? $\rightarrow 6^-$	
754.9	5.4	.87[b]	1.3×10^{-2}	$.92\times10^{-2}$(E2)	$5^- \rightarrow (+)$	no
803.0	1000	100[a]	8.3×10^{-3}	8.2×10^{-3}(E2)	$2^+ \rightarrow 0^+$	yes
816.0		.29[b]			$6^- \rightarrow 7^-$	
841.3	1.9	.59[b]	2.6×10^{-2}	2.3×10^{-2}(M1)	? $\rightarrow 4^+$	
881.0	654	56.5[b]	7.2×10^{-3}	6.8×10^{-3}(E2)	$4^+ \rightarrow 2^+$	yes
895.0	139	37.6[b]	2.2×10^{-2}	2.1×10^{-2}(M1)	$5^- \rightarrow 6^-$	yes
1018.7	72.8	12.6[a]	1.4×10^{-2}	1.5×10^{-2}(M1)	$5^- \rightarrow 6^-$	yes
1098.4	128	3.4[b]	2.2×10^{-3}	1.75×10^{-3}(E1)	$5^- \rightarrow 4^+$	yes
1405.3	13.2	.24[b]	1.5×10^{-3}	1.15×10^{-3}(E1)	$5^- \rightarrow 4^+$	yes
1595.2	47.4	.56[a]	9.8×10^{-4}	9.5×10^{-4}(E1)	$5^- \rightarrow 4^+$	yes
1718.6	303	3.26[a]	8.9×10^{-4}	8.5×10^{-4}(E1)	$5^- \rightarrow 4^+$	yes
1844.1	5.42	.062[c], .042[d]	9.5×10^{-4}, 6.4×10^{-4}	7.6×10^{-4}(E1)		
1878.1	19.6	.155[a]	6.6×10^{-4}	7.4×10^{-4}(E1)		
1902.8	3.88	0.021[a], .027[c]	4.5×10^{-4}, 5.8×10^{-4}	7.0×10^{-4}(E1)=		

From tables 6-4 and 6-5 it is evident that the present work is in general agreement with the decay scheme and transition intensities of Lederer et al [14]. The reader will note that the present work has not assigned any intensity values to the 107, 124, 203 and 816 keV transitions which were observed by Alburger and Pryce [15]. Figs. 6-7 and 6-8 show the shape of the γ-spectrum, for the run with the best statistics, in the regions of these peaks. In these figures the location of the peaks has been predicted using the position of the 183.8 and 803.0 keV peaks assuming a linear calibration of the analyzer. There would appear to be a peak at 816 keV but the best we can do is give a rough estimate of its intensity.

Also there appear to be weak peaks at about 111 keV and 198 keV. It is not clear whether or not there are genuine peaks but it is believed that they do not correspond to the 107 and 203 keV transitions. The 123.6 keV γ-ray is definitely absent. Alburger and Pryce [15] have suggested multipolarities of E1, M1, E3 and M1 respectively for the 107, 124, 203 and 816 keV transitions. Based on this assignment and the relative intensity of the K-conversion electron lines, as measured by Alburger and Pryce, the calculated intensities of the 107, 124, 203 and 816 γ-peaks, relative to the 803 keV γ-ray, are 6.2×10^{-3}, 1.6×10^{-4}, 4.5×10^{-4} and 8.2×10^{-4} respectively. By comparison the relative intensities of the 147.5 and 157.5 keV transitions, which are clearly visible in Fig. 6-7, are 2.5×10^{-3} and 3.4×10^{-3}. The absence of the 124 and 203 keV γ-ray peaks is consistent with the above intensities and hence with the multipole assignments of E3 and M1. However, the absence of the 107 keV

FIG. 6-7

Details of the γ-ray spectrum in the energy region of the 107, 124, and 203 keV γ-ray peak.

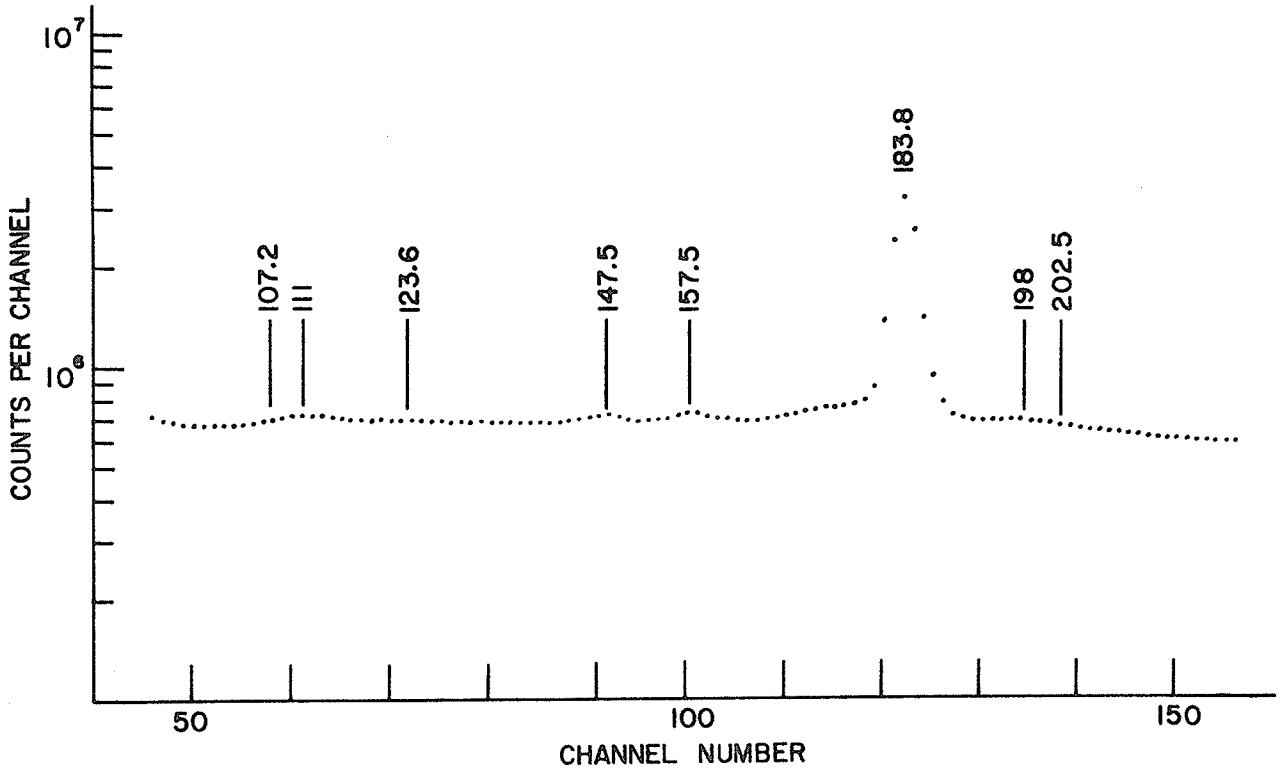
10^7
10^6
COUNTS PER CHANNEL
107.2
111
123.6
147.5
157.5
183.8
198
202.5
50
100
150
CHANNEL NUMBER

FIG. 6-8

Details of the γ-ray spectrum in the energy region of the 816 keV γ-ray peak.

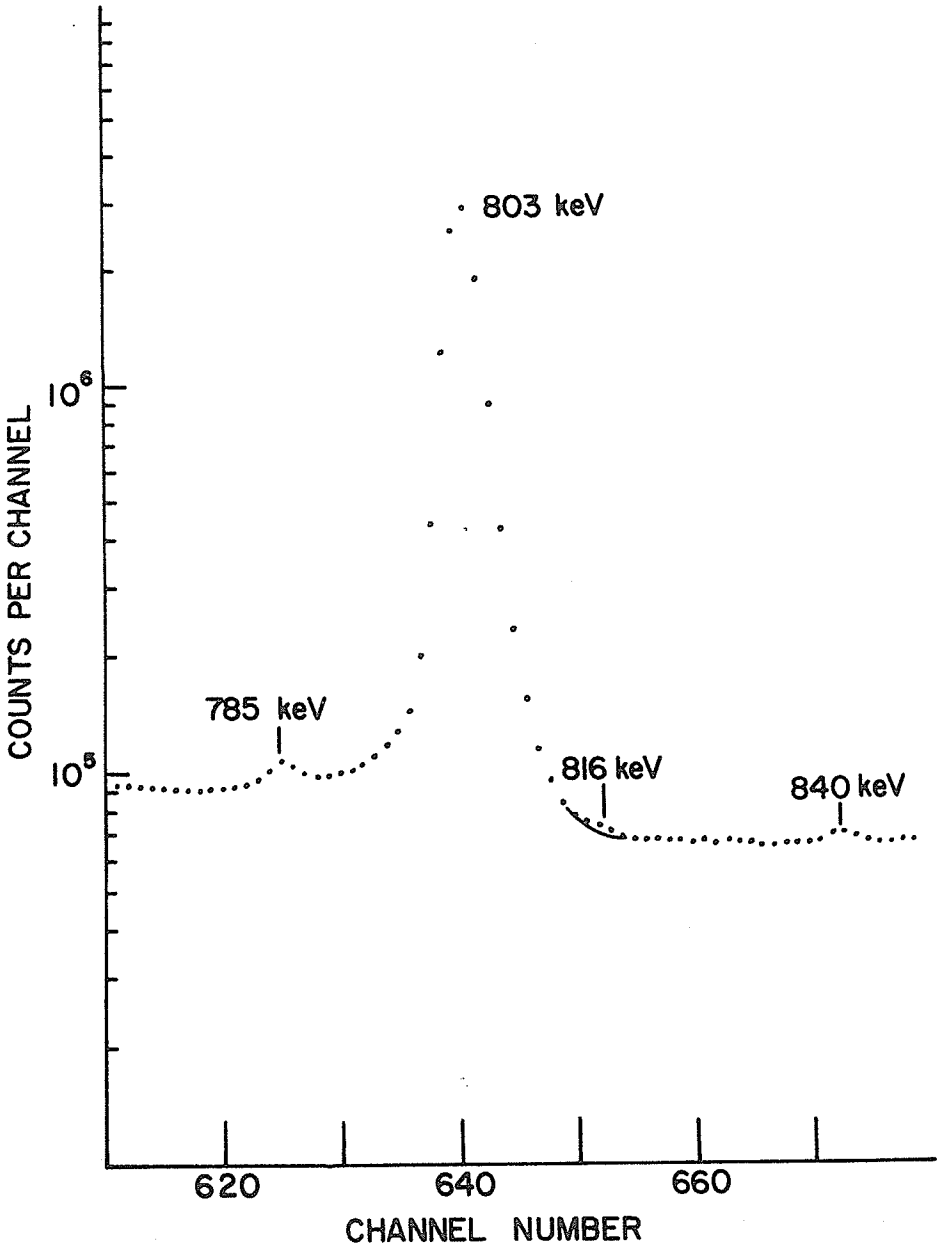
803 keV
785 keV
816 keV
840 keV
10^6
10^5
COUNTS PER CHANNEL
620
640
660
CHANNEL NUMBER

γ-peak is not consistent with an E1 multipole assignment. According to Lederer et al [14] the 107 keV transition takes place from the 3125 keV level, (spin and parity not assigned), to the 3017 keV level. (See Fig. 6-1) The 740 keV transition also originates from the 3125 keV level. Based on the conversion coefficient shown in table 6-5 the suggested multipolarity for this transition is M1. Since it terminates on the 6^- level at 2385 keV the spin and parity of the 3125 keV level is then 5^-, 6^-, or 7^-. This spin and parity assignment suggests the 107 keV transition is M1 rather than E1. (See Fig. 6-1). If we assume it to be M1 then the calculated γ-ray intensity, relative to the 803 keV γ-ray is $\sim 3 \times 10^{-4}$ which is consistent with the absence of this peak in the spectrum. In Fig. 6-8 the 842 keV γ-peak can be readily seen. The relative intensity of this line is 1.9×10^{-3}. Assuming the background indicated in Fig. 6-8 we estimate that the relative intensity of the 816 keV peak is $\sim 1 \times 10^{-3}$ which is consistent with an M1 multipolarity.

In table 6-4 there are three noticeable discrepancies between the values of the γ-ray intensities tabulated by Lederer et al [14] and those obtained in the present work. These occur for the 657, 739 and 755 keV transitions. The values of the K-conversion coefficients, calculated using the relative γ-ray intensities measured here and the relative electron intensities of Alburger and Pryce [15], suggests that these transitions are M1, M1, and E2 respectively. (See table 6-5). The M1 assignment for the 657 keV transition agrees with the decay scheme of Lederer et al [14] while the M1 assignment for the 739 keV transitions suggests a spin and parity assignment of 5^-, 6^-, or 7^- for the 3125 keV level of

^{206}Pb, as previously mentioned. However, the E2 assignment for the 755 keV transition disagrees with the decay scheme of Lederer et al [14]. There is good evidence, to be presented in the next section, that the 755 keV transition occurs between the 5^- level at 3403 keV and a 3^- level at 2647 keV, which agrees with the E2 assignment.

GAMMA-GAMMA COINCIDENCE STUDY

(a) Introduction

As mentioned in the introduction to this chapter one of the reasons for investigating the decay of ^{206}Bi was to place the 1845, 1880 and 1903 keV transitions in the decay scheme. The K-conversion coefficients for these transitions indicate that all three are E1, in agreement with the assignment of Wiener et al[17]. To determine the position of these lines γ-γ coincidence experiments were made using the Ortec and P.γ.T. Ge(Li) detectors and the electronics shown in Fig. 6-9. If a pair of γ-rays were detected in "coincidence", one in each detector, and if the γ-ray detected in the Ortec detector had the appropriate energy, as determined by the ΔE window setting of the single channel analyser, S.C.A., the output of the P.γ.T. detector was fed into a 1024 multi-channel analyser. By setting the ΔE S.C.A. window on a particular full energy peak, such as the 1844 keV line, we could collect the γ-spectrum in coincidence with this transition.

To develop a familiarity with the apparatus relatively short coincidence runs were made gating on the 184, 343, 516, 538, 803, 881 and 1719 keV transitions. Since the positions of these transitions are firmly established we shall not present a detailed discussion of these results other than to note that the results agreed with the decay scheme of Lederer et al [14] shown in Fig. 6-1. It should be pointed out that

FIG. 6-9

Block diagram of the electronics used in the γ-γ coincidence study.

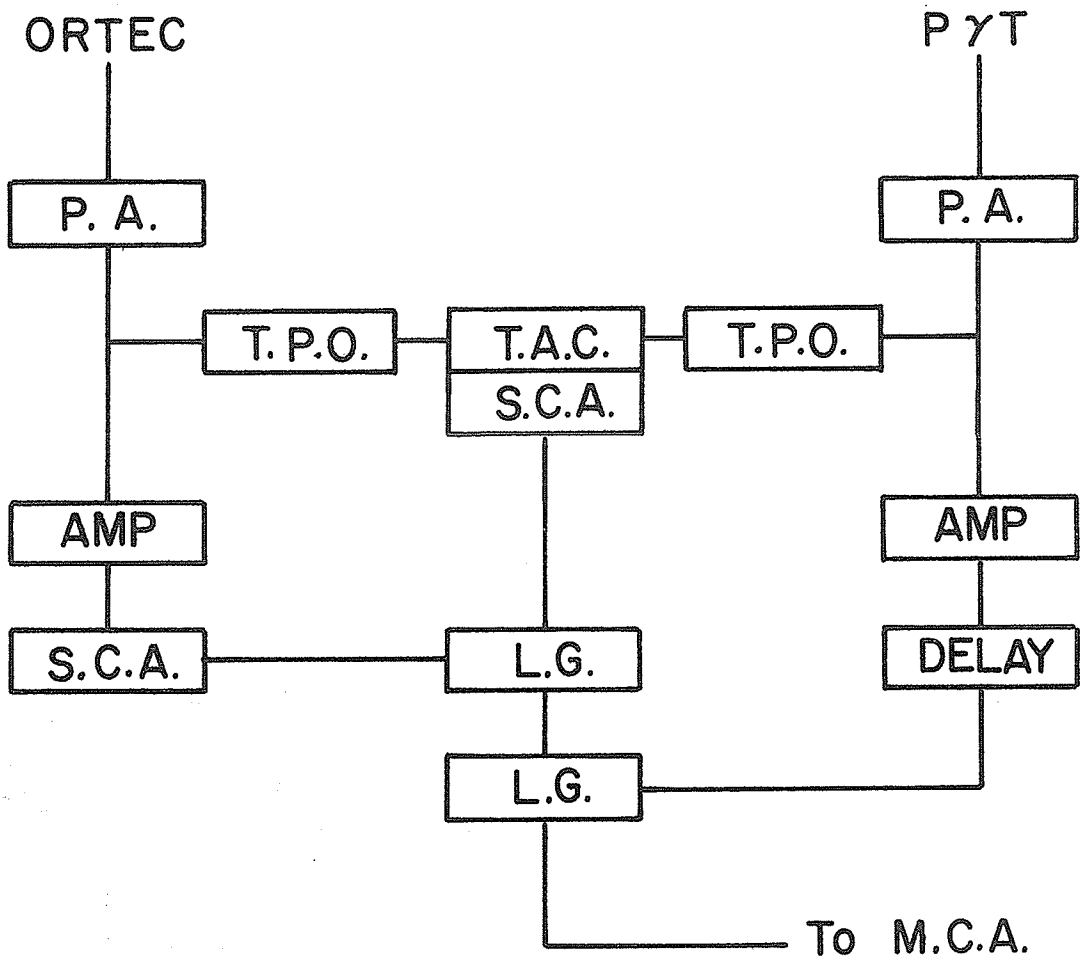
ORTEC
PγT
P. A.
P. A.
T.P.O.
T.A.C.
S.C.A.
T.P.O.
AMP
AMP
S.C.A.
L.G.
DELAY
L.G.
To M.C.A.

these runs were too short to establish the position of any but the strongest transitions.

(b) On the Coincidence Resolving Time

Although the coincidence system is relatively straightforward it is perhaps worthwhile making a few comments on the coincidence timing. The coincidence resolving time of the system is determined by the output of the time to amplitude converter, TAC. This output is a voltage pulse whose heighth is proportional to the time difference between the detection of a pair of γ-rays by the two detectors. The output of the TAC is fed into an S.C.A. which is used to select those pulses corresponding to a "true" coincidence. To determine the window settings of the ΔT S.C.A. an auxiliary experiment must be performed. Let us consider a specific example to illustrate. Suppose we are interested in obtaining the γ-spectrum in coincidence with the 184 keV transition. Then we set the window of the ΔE S.C.A. on the 184 keV line. Next, we feed the output of the TAC into a multi-channel analyser through a linear gate which is triggered by the output of the ΔE S.C.A. See Fig. 6-10. The resulting time spectrum, therefore, represents coincidences involving the 184 keV transition. This spectrum, in general, shows a "coincidence peak", F.W.H.M. ~30-50ns, lying on a broad continuum of random coincidence pulses. The ΔT S.C.A. window is then set on the coincidence peak thereby defining the coincidence resolving time.

It should be noted that, in general, the position of the coincidence peak varies somewhat depending on which γ-ray we gate. This

FIG. 6-10

The arrangement of the electronics used to set up the ΔT S.C.A. window.

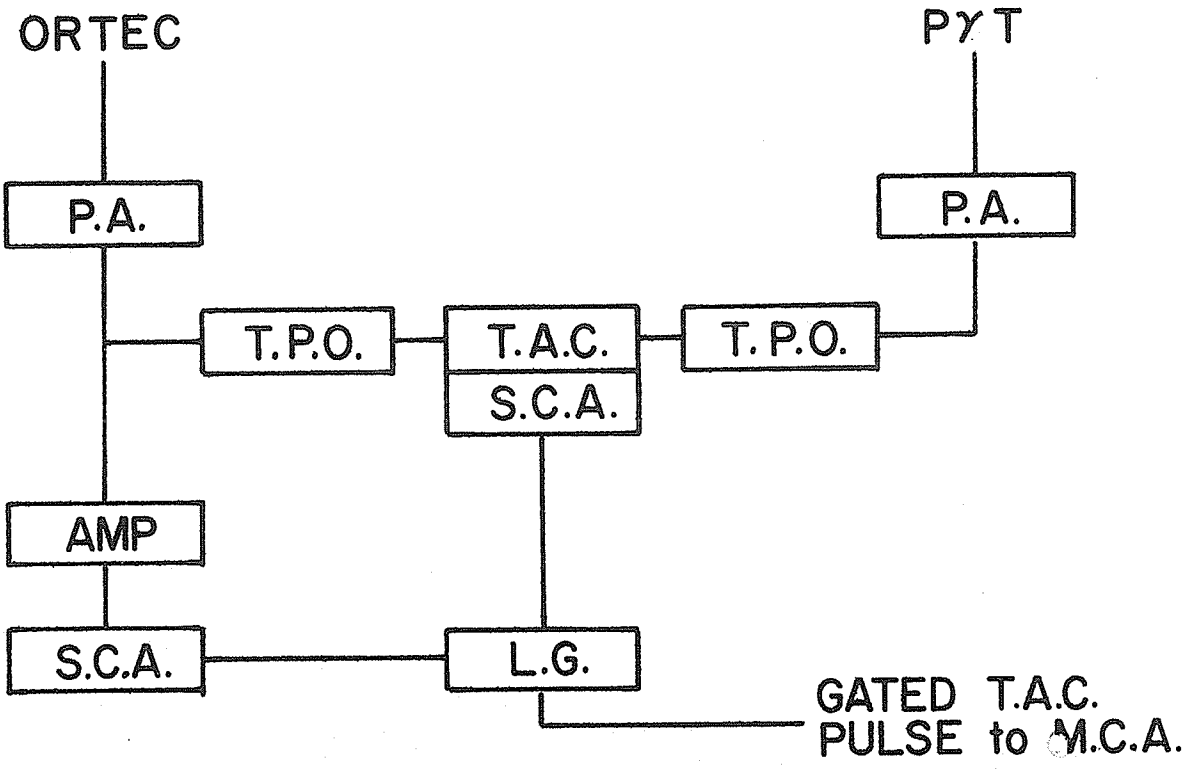
ORTEC
PγT
P.A.
P.A.
T.P.O.
T.A.C.
S.C.A.
T.P.O.
AMP
S.C.A.
L.G.
GATED T.A.C.
PULSE to M.C.A.

variation is a reflection of the detectors' variation in timing distribution with the different γ-ray energies involved.

(c) The 1878 keV Transition

To determine the position of 1844, 1878, 1903 keV transitions relatively long coincidence runs, ~2-3 days duration, were made gating on these lines. Because these transitions are relatively weak the ΔT S.C.A. window settings were not obtained by gating on the transitions themselves but by gating on the 1719 keV transition in the manner described in the preceding section. This procedure is not justified a priori but as we shall see the results of the coincidence work indicate that it was satisfactory.

The coincidence spectrum obtained by gating on the 1878 keV γ-ray, as well as the ungated singles spectrum, is shown in Fig. 6-11. The peak labelled "P", which can be seen in the ungated singles spectrum is generated by a pulser which was fed into the test input of the P.γ.T. pre-amp to obtain an estimate of the random coincidence counting rate. We observe that the 343, 538, 803 and 881 keV γ-rays are in apparent coincidence with the 1878 keV transition. Since the ΔT S.C.A. window was set using the 1719 keVtransition the question arises, are these γ-rays in true coincidence?

To try to answer this question the ΔE S.C.A. window was set on the background above the 1903 keV peak, (see Fig. 6-4), and another

FIG. 6-11

The coincidence spectrum obtained by gating on the 1878 keV γ-ray. Also shown is an ungated singles spectrum. The peak labelled P is from a pulser.

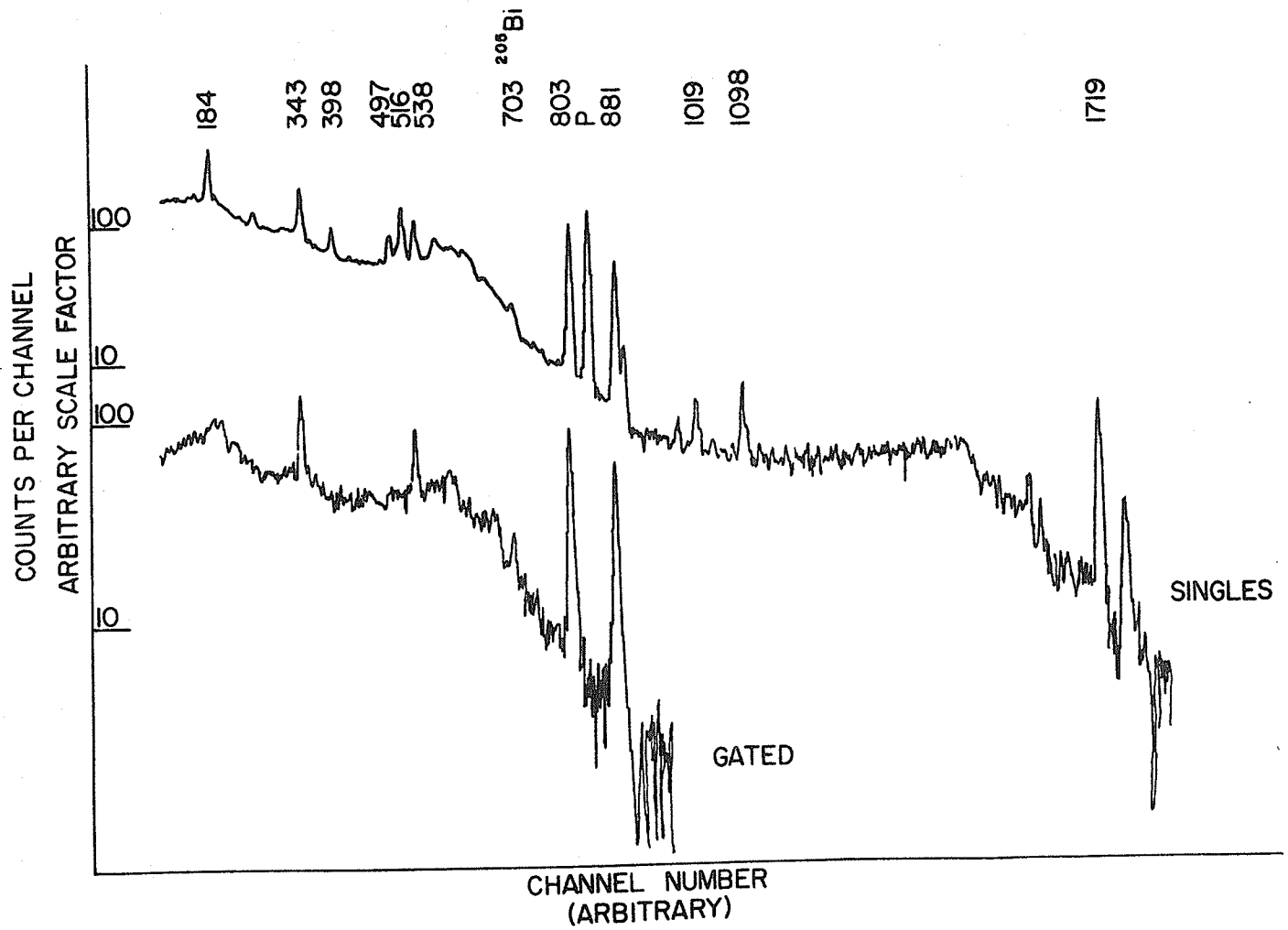
184
343
398
497
516
538
703 ^{205}Bi
803
P
881
1019
1098
1719
100
10
100
10
COUNTS PER CHANNEL
ARBITRARY SCALE FACTOR
SINGLES
GATED
CHANNEL NUMBER
(ARBITRARY)

coincidence spectrum was accumulated. It turned out that the same peaks occurred in this spectrum but the coincidence counting rate obtained when gating on the 1878 keV line was much higher. If the appearance of the 343, 538, 803 and 881 keV peaks was solely a result of the background on which the 1878 keV peak lies no increase in the coincidence counting rate would have been observed. Alternately, gating on the 1878 keV line leads to an increase in the number of gating pulses from the ΔE S.C.A. and one wonders if, as a result of this, the increased coincidence counting rate might not be attributable to increased randoms. This possibility can be ruled out since an increased random coincidence rate would lead to the appearance of other strong γ-rays. Since no other lines appear in the coincidence spectrum we can conclude that the 343, 538, 803 and 881 keV peaks do represent true coincidences.

The appearance of the 343, 538, 803 and 881 keV γ-rays in the coincidence spectrum implies a feed to the 1684 keV level of ^{206}Pb which then de-excites by the above transitions. See Fig. 6-1. From the present experiment it is not possible to ascertain whether or not the feed is a direct feed. The highest energy level of ^{206}Pb which can be fed by ^{206}Bi is at 3.65 MeV.[14] Thus if the 1878 line feeds the 1684 keV level of ^{206}Pb indirectly the intermediate level must be within 88 keV of the 1684 keV level. In the present experiment any γ-ray with $E_\gamma \leq 88$ keV would not be detected in the coincidence spectrum, as it would be masked by the Pb x-ray peaks.

If we assume that the 1878 keV transition takes place directly to the 1864 keV level of ^{206}Pb then the transition takes place from a level at E = 803.0 + 881.0 + 1878.1 = 3562.1 ± .7 keV. Vallois et al[19] has observed a level at 3562 keV in ^{206}Pb by inelastic proton scattering and has suggested a spin and parity assignment of 5^- to this level. On the basis of the K-conversion coefficient, the 1878 keV transition is E1 which agrees well with the suggestion that it takes place between the 3562 keV level and the 1684, (4^+), keV level.

(d) The 1903 keV Transition

The coincidence spectrum obtained by gating on the 1903 keV γ-ray is shown in Fig. 6-12, as well as an ungated singles spectrum. Again we observe the 343, 538, 803 and 881 keV lines in coincidence and, by the arguments outlined in the preceding section, these lines represent genuine coincidence events. Thus we can conclude that the 1903 keV transition feeds the 1684 keV level. Again we cannot determine if the feed is indirect, since, if an intermediate level is involved, it must be within 63 keV of the 1684 keV level. (1684 + 1903 + $\Delta X \leq 3650$).

If we assume that the 1903 keV transition takes place directly to the 1684 keV level then ^{206}Pb has an excited state at E = 1684.0 + 1902.8 = 3586.8 ± .7 keV. As far as is known there is no good confirming evidence for the existence of such a level but Jolly, Lin and Cohen [20] have observed a level at 3.58 MeV, by inelastic deuteron scattering, which might be the level suggested here. Since the multipolarity of the 1903 keV transition is E1 the spin and parity of the

FIG. 6-12

The coincidence spectrum obtained by gating on the 1903 keV γ-ray. Also shown is an ungated singles spectrum. The peak labelled P is from a pulser.

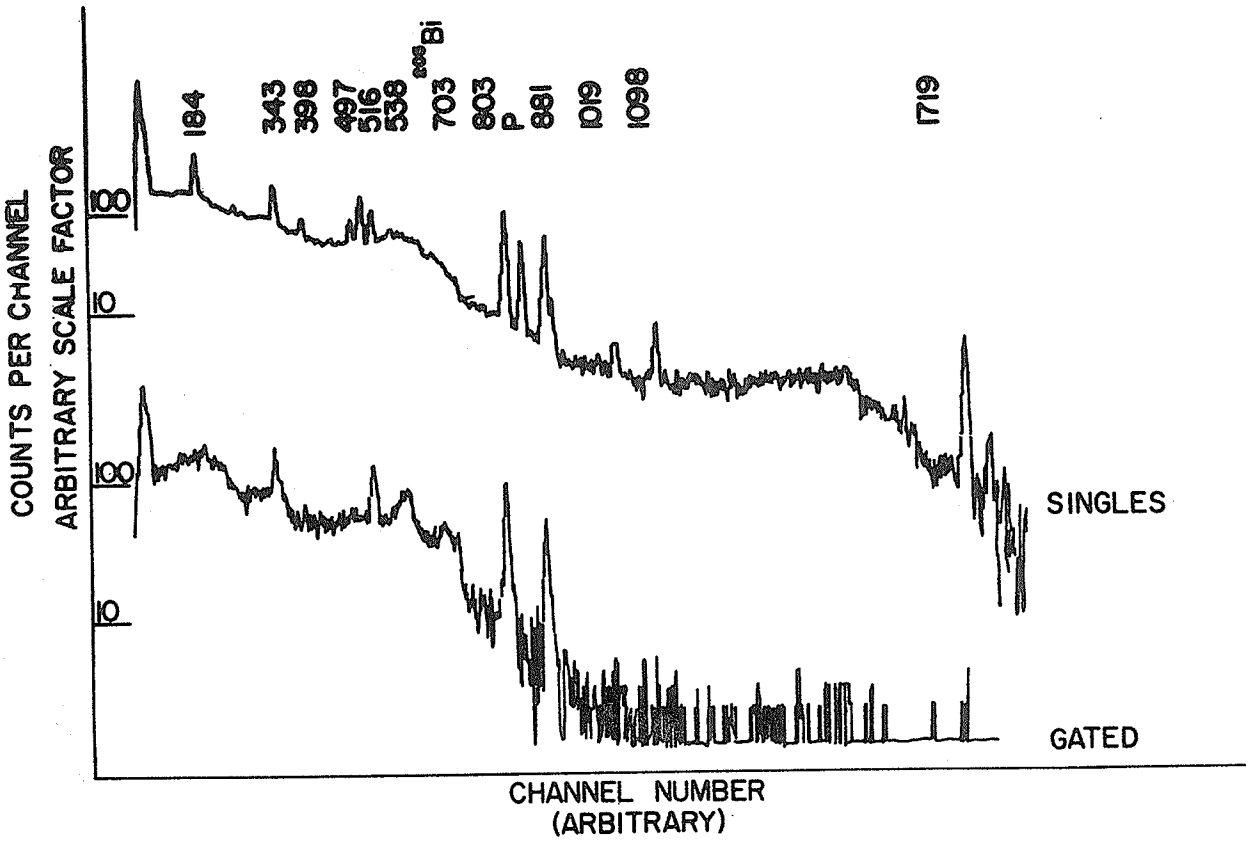
184
343
398
497
516
538
207Bi
703
803
P
881
1019
1098
1719
COUNTS PER CHANNEL
ARBITRARY SCALE FACTOR
10
10
10
SINGLES
GATED
CHANNEL NUMBER
(ARBITRARY)

proposed 3587 keV level is 3^-, 4^-, or 5^-.

(e) The 1844 keV Transition

The coincidence spectrum obtained by gating on the 1844 keV transition is shown in Fig. 6-13. It is somewhat more complicated than the previous two cases. In this spectrum we observe the 343, 538, 755, 803 and 881 keV γ-rays. We have concluded that the 1844 keV transition feeds the 803 keV level of ^{206}Pb from a level which is in turn fed by the 755 keV transition. The presence of the 343, 538, and 881 keV lines in the spectrum is readily explainable. To gate on the 1844 keV γ-ray the window of the ΔE S.C.A. is set on the 1844 keV peak. However, this peak sits on a background which includes contributions from compton scattered γ-rays from the 1878 and 1903 keV transitions. These transitions are in coincidence with the 343, 538, 803 and 881 keV γ-rays and therefore these lines appear in the coincidence spectrum. However, the intensity of the 803 keV line, relative to the 343, 538, and 881 keV lines was found to be ~40% higher than the value obtained when gating on the 1878 and 1903 keV transitions and this increased intensity is attributed to a true coincidence between the 1844 keV transition and the 803 keV γ-ray. It should be pointed out that this 40% increase is consistent with the ratio of the 1844 keV peak area to the background.

Thus the 1844 keV transition is in coincidence with the 803 and 755 keV transitions. If we assume that the 1844 keV transition

FIG. 6-13

The coincidence spectrum obtained by gating on the 1844 keV γ-ray. Also shown is an ungated singles spectrum. The peak labelled P is from a pulser.

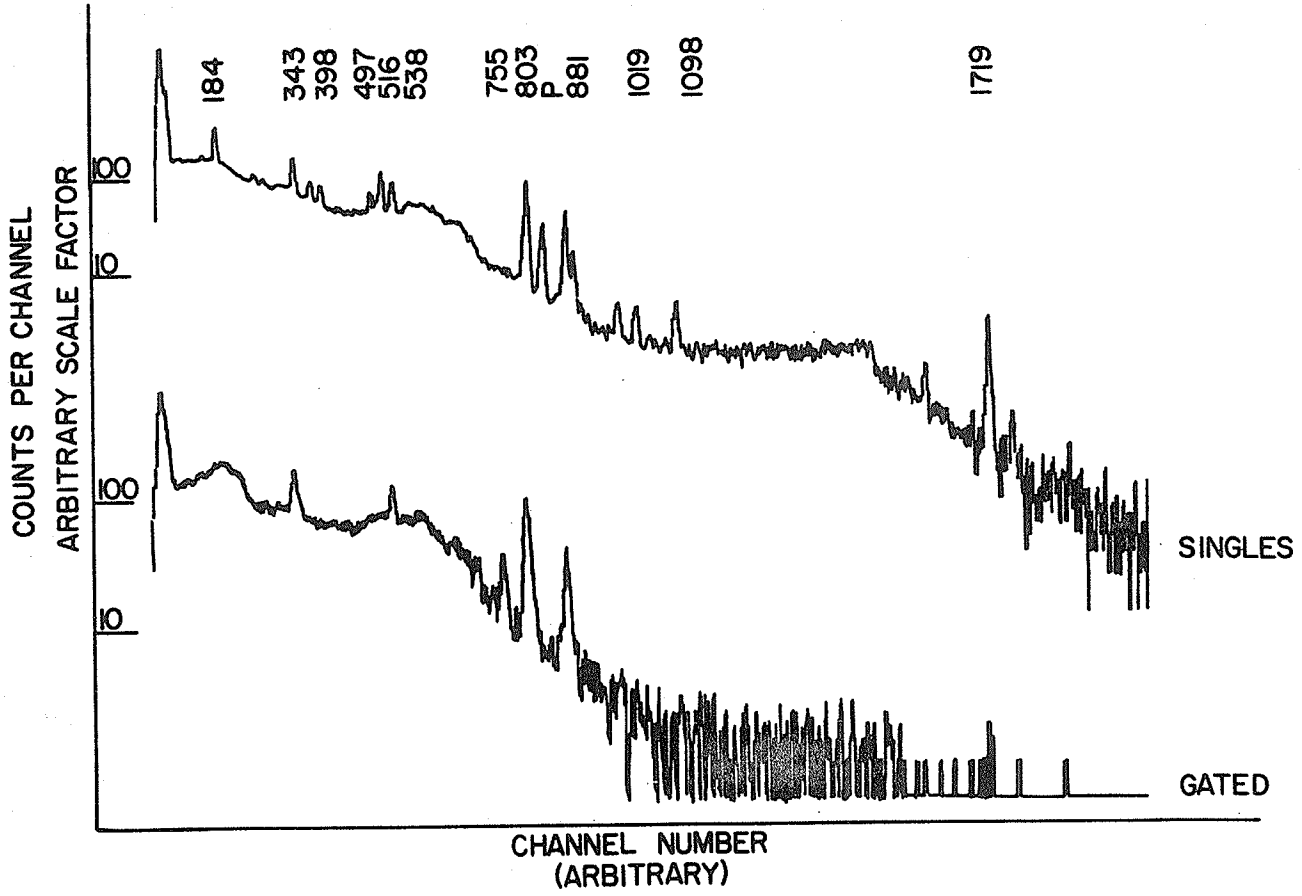
184
343
398
497
516
538
755
803
P
881
1019
1098
1719
100
10
100
10
COUNTS PER CHANNEL
ARBITRARY SCALE FACTOR
SINGLES
GATED
CHANNEL NUMBER
(ARBITRARY)

takes place to the 803 keV level then there is an excited state in ^{206}Pb at an energy E = 803.0 + 1844.1 = 2647.1 ± .7 keV. Vallois et al[19] has observed an excited state at E = 2648 ± 10 keV by inelastic proton scattering and Zeigler and Peterson [21] have assigned this level a spin and parity of 3^- on the basis of inelastic electron scattering. On the basis of the K-conversion coefficient the 1844 keV transition is E1 which agrees with the proposal that this transition feeds the 2^+ level at 803 keV from a 3^- level at 2647 keV.

Now let us consider the 755 keV transition. This γ-ray is in coincidence with the 1844 keV transition which is interpreted as implying that the 755 keV transition feeds the 2647 keV 3^- level which is then de-excited by the 1844 keV transition. This contention is supported by the fact that the measured intensities of the 1844 and 755 keV γ-rays are equal. (See table 6-4). It is proposed that the 755 keV γ-ray feeds the 2647 keV level directly from the 5^- level which Lederer et al [14] list as occurring at 3404 keV. (See Fig. 6-1). From the energy measurements previously discussed we obtain the following energies for the levels involved:

(a) 2647.1 ± .7 keV = 803.0 + 1844.1

and (b) 3402.6 ± .7 keV = 1718.6 + 803.0 + 881.0

Then the predicted transition energy is 755.5 ± 1.0 keV which agrees, within error, with the measured value of 754.9 ± .5 keV. Furthermore, the K-conversion coefficient for the 755 keV transition indicates an E2 multipolarity which agrees with the suggestion that this transition is occurring between the 5^-, 3403 keV, level and the 3^-, 2647 keV level.

It should be pointed out that Lederer et al [14] have the 755 keV transition feeding the 2526 keV level which then de-excites by an 842 keV transition. On the basis of the preceding discussion the 2526 keV level is not fed in this manner and it is possible that the 2526 keV level is not populated in any other fashion which would mean the 842 keV transition is incorrectly placed in the published level scheme.

(f) Summary of the γ-γ Coincidence Study

On the basis of the γ-γ coincidence work it is proposed that three levels are populated in the decay of ^{206}Bi which have not been observed in this decay before. These occur at 2647.1 ± .7, 3562.1 ± .7, and 3586.8 ± .7 keV. It is also proposed that the 755 keV transition takes place between the level at 3403 keV and the level at 2647 keV.

NEW TRANSITIONS

As seems customary when studying complicated nuclides with Ge(Li) detectors several new transitions were observed. These transitions were identified as belonging to ^{206}Pb by observing that they decay with the same half-life as ^{206}Bi. Table 6-6 shows the energies and γ-ray counting rate of these transitions relative to the 1719 keV counting rate for three different runs. The time between the first run and the last was 15 days, ~2.4 half-lives. Also shown, for the purposes of comparison, are several low intensity peaks which have been identified as "sum peaks" of two cascading γ-rays. These are labelled

TABLE 6-6

Relative γ-ray counting rates of several weak γ-peaks in ^{206}Bi which have been identified as new transitions. Those lines labelled with an asterisk have been identified as sum peaks.

TABLE 6-6

Energy:	Relative Counting Rate			
	Day 1	Day 10	Day 15	Average
147.5±1	.15	.11	.10	.12
157.8±1	.14	.14	.13	.14
157.8+147.5 =	.29	.25	.23	
582.0	.050	.051	.063	.055
696.6	.045	.047	.051	.048
784.5	.032	.037	.030	.033
858±1	.011	.013	.005	.010
955.5±1	.012	.010	.012	.011
966.6±1	.013	.0095	.012	.012
1141.4 1146.2* }	.0091	.0098	.0070	.0089
1195.5±1	.0085	.0130	.013	.011
1208.5±1	.032	.033	.035	.033
1239	.0037	.0050	.0043	.0043
1246±1	.0031	.0042	.0042	.0038
1319.5±1*	.0050	.0051	.0044	.0048
1333.7 1340.8* }	.0140	.016	.015	.015
1560.4 1564.5 }	.0190	.021	.018	.019
1791.2	.0046	.0039	.0035	.040

with an asterisk. It should be noted that several weak lines belonging to the decay of ^{205}Bi were observed in the singles spectra. These were readily identifiable and in fact, it was possible to observe that they did not decay with the ^{206}Bi half-life simply by observing, on a graphical display, the change with time of their intensity relative to that of neighbouring ^{206}Bi lines.

Since the relative γ-ray intensities of these new transitions are very small one must be careful that they are not "sum peaks" of two cascade γ-rays. Table 6-7 shows a comparison between the counting rates of these weak transitions, relative to the 1719 keV counting rate, and the calculated sum counting rates of various pairs of cascade γ-rays which might be causing these weak γ-ray peaks. Again, for the purposes of comparison, we have shown a few cases for which the peak has been identified as a sum peak. The calculations of the sum counting rates are based on the measured relative γ-ray intensity of the strong transitions, measured in the present work, and the decay scheme of Lederer et al [14]. As can be seen from the numbers involved, only the strong γ-rays need be taken into account and the case of a triple sum peak can be rejected. Finally the intensities of new γ-rays, relative to that of the 803 keV γ-ray, are shown in table 6-4.

On the basis of energetics we have been able to tentatively assign several of these transitions to the decay scheme. These assignments are shown in Fig. 6-14. Here, two types of levels have been used, (1) those levels which have previously been observed in ^{206}Pb following the decay of ^{206}Bi including the levels at 3587, 3562 and 2647 keV proposed in the present work, and (2) levels at 2931 and 1791 keV which

TABLE 6-7

Relative intensity of the weak γ-ray peaks of ^{206}Bi compared to that of possible sum peaks.

TABLE 6-7

Energy	Sum Peak	Sum Intensity	Measured Intensity	New
147.5	-			yes
157.8	-			yes
582.0	397.8+184.0	.014	.055	yes
696.6			.048	yes
784.5			.033	yes
858±1	343.4+516.1	.005	.010	?
1141.4			} .009	yes
1146.2	803.0+343.4	.0072		no
1195.5	314.5+881.0	very small	.011	yes
1208.5±1	-	-	.0334	yes
1239±1	894.9+343.4	.001	.0043	yes
1246±1	-	-	.0038	yes
1319.5±1	803.0+516.1	.005	.005	no
1333.7	-	-	.0122 } .0152	yes
1340.8	803.0+537.6	.005	.0030	no
1560.4			.010	yes
1564.5			.010	yes
955			.011	yes
966.6			.012	yes
1791			.040	yes

FIG. 6-14

Partial decay scheme of ^{206}Bi indicating the assignment of γ-rays suggested in the present work.

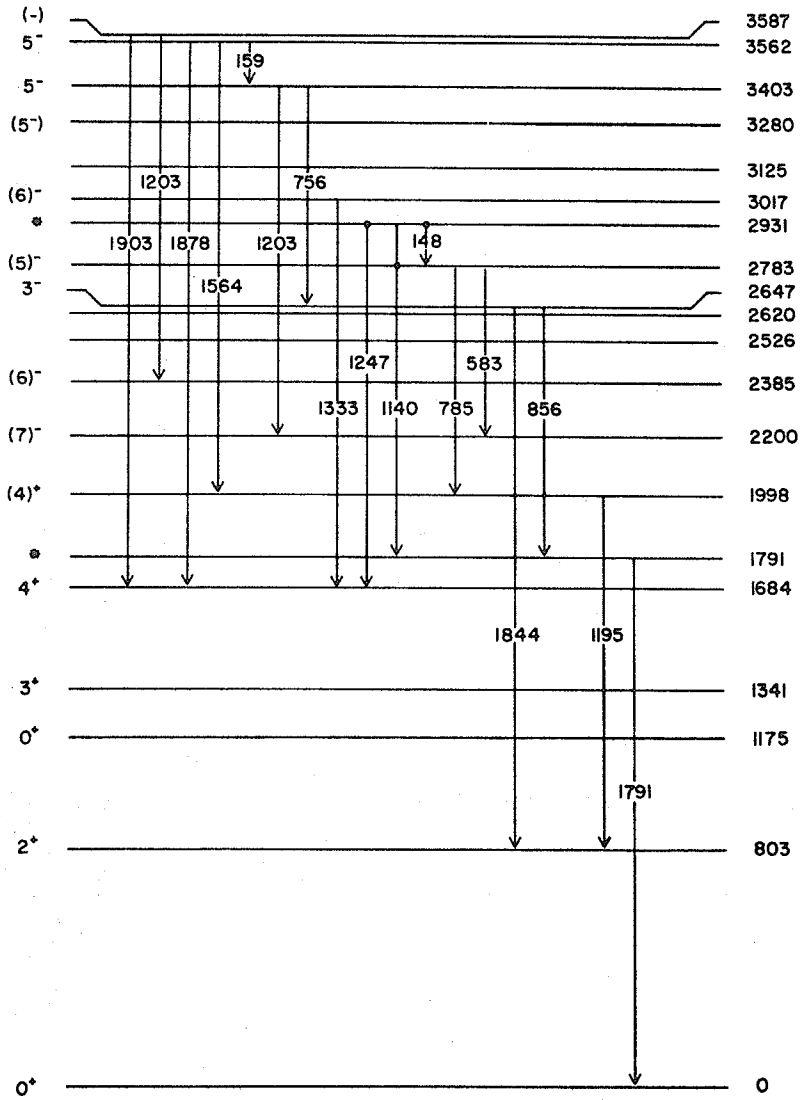
(-)
5⁻
5⁻
(5⁻)
(6)⁻
*
(5)⁻
3⁻
(6)⁻
(7)⁻
(4)⁺
*
4⁺
3⁺
0⁺
2⁺
0⁺
3587
3562
3403
3280
3125
3017
2931
2783
2647
2620
2526
2385
2200
1998
1791
1684
1341
1175
803
0
159
1203
756
1903
1878
1203
148
1564
1247
583
1333
1140
785
856
1844
1195
1791

^{206}Pb

have been identified, for example, by Vallois et al[19] by inelastic proton scattering and which have been labelled with an asterisk. It should be noted that the 1560.4 and 1565.4 keV transitions might be in cascade to the ground state from the 3125 keV level. This idea is supported by the fact that the γ-ray intensity of these transitions are roughly equal. However, the author is unaware of any strong evidence to suggest the existence of the necessary intermediate level at 1560 or 1565 keV and for this reason we have not included this possibility in Fig. 6-14.

INTERNAL PAIR PRODUCTION IN ^{206}Pb

As discussed in Chapter 5 the trochoidal β-ray spectrometer is well suited to the study of internal pair production. As a first attempt at using the present instrument as a pair spectrometer the total pair formation coefficient, α_π, was measured for the 1719 keV transition in ^{206}Pb. We shall discuss this measurement in some detail since the techniques used are of general application.

As will be recalled from Chapter 5 nuclear transitions with $E_\gamma > 2m_o c^2$ may de-excite by the creation of an electron-positron pair. The total kinetic energy available to the pair, $T = E_\gamma - 2m_o C^2$, is shared between the two particles, so that the energy distribution of each is a continuum. If, however, the outputs of the two sides of the spectrometer are added then the summed output will be a mono-energetic peak corresponding to the total pair kinetic energy T. Figure 6-15 shows such a sum spectrum for ^{206}Bi in which the pair sum peaks corresponding to the

FIG. 6-15

Pair sum spectrum obtained with ^{206}Bi.

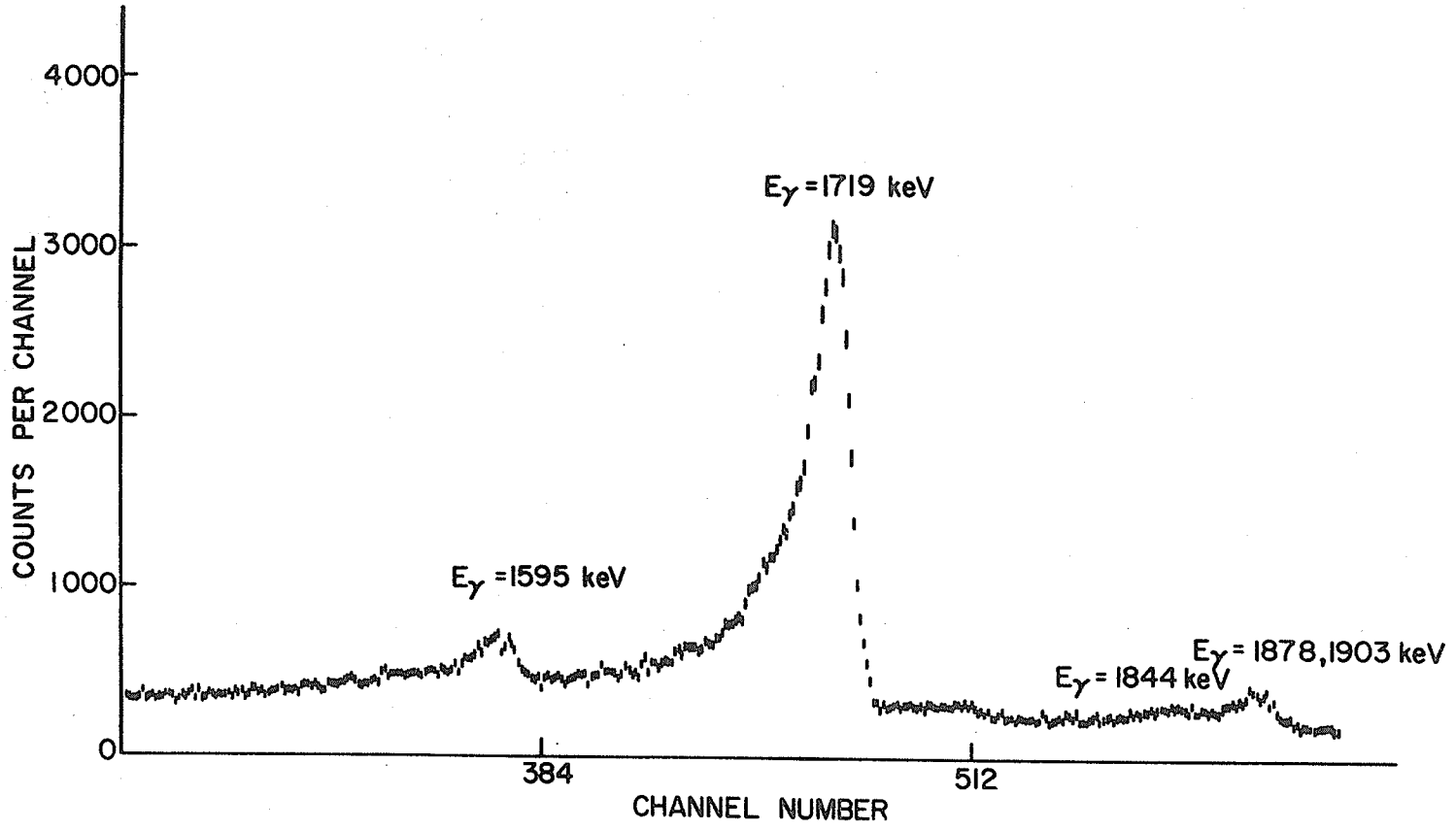
4000
3000
2000
1000
0
COUNTS PER CHANNEL
E_γ = 1719 keV
E_γ = 1595 keV
E_γ = 1878, 1903 keV
E_γ = 1844 keV
384
512
CHANNEL NUMBER

1595, 1719, 1845 and 1880 keV transitions can be seen. In the present work we have measured the ratio of pairs emitted per unit time to K-conversion electrons, $e^{\pm}/e_K$-, for the 1595 and 1719 keV transitions, as well as the total pair formation coefficients, α_π. The 1845 and 1880 keV sum peaks were not well separated and no attempt was made to obtain this ratio for these transitions. Here, the number of K-conversion electrons was obtained directly from the conversion spectrum. Thus the ratio $e^{\pm}/e_K$- does not depend on the absolute values of the efficiency curves but only on the relative efficiency.

By gating on the 1719 keV sum peak we have also obtained the positron continuum for this transition. Fig. 6-16 shows this spectrum, uncorrected for efficiency. This spectrum may be compared to the ungated positron singles spectrum shown in Fig. 6-17. In Fig. 6-17 it will be noted that the number of counts per channel abruptly drops at several locations. These drops occur at the end-point of the various positron continua, associated with the different transitions of ^{206}Pb which produce internal pairs. In Fig. 6-18 the theoretical shape of the positron continuum for the 1719 keV transition is compared to the experimental spectrum, (corrected for efficiency). The theoretical shape is calculated in the Born approximation and corrected for the effects of nuclear charge using the correction of Horton and Phibbs[13]. (See Chapter 5.) The experimental energy distribution shows a high energy cut-off at approximately 600 keV. The origin of this cut-off is to be found in the electronics and will be discussed shortly.

The block diagram of the electronics used in the pair production work is shown in Fig. 6-19. The system is relatively straight for-

FIG. 6-16

Positron spectrum obtained by gating on the 1719 pair sum peak.

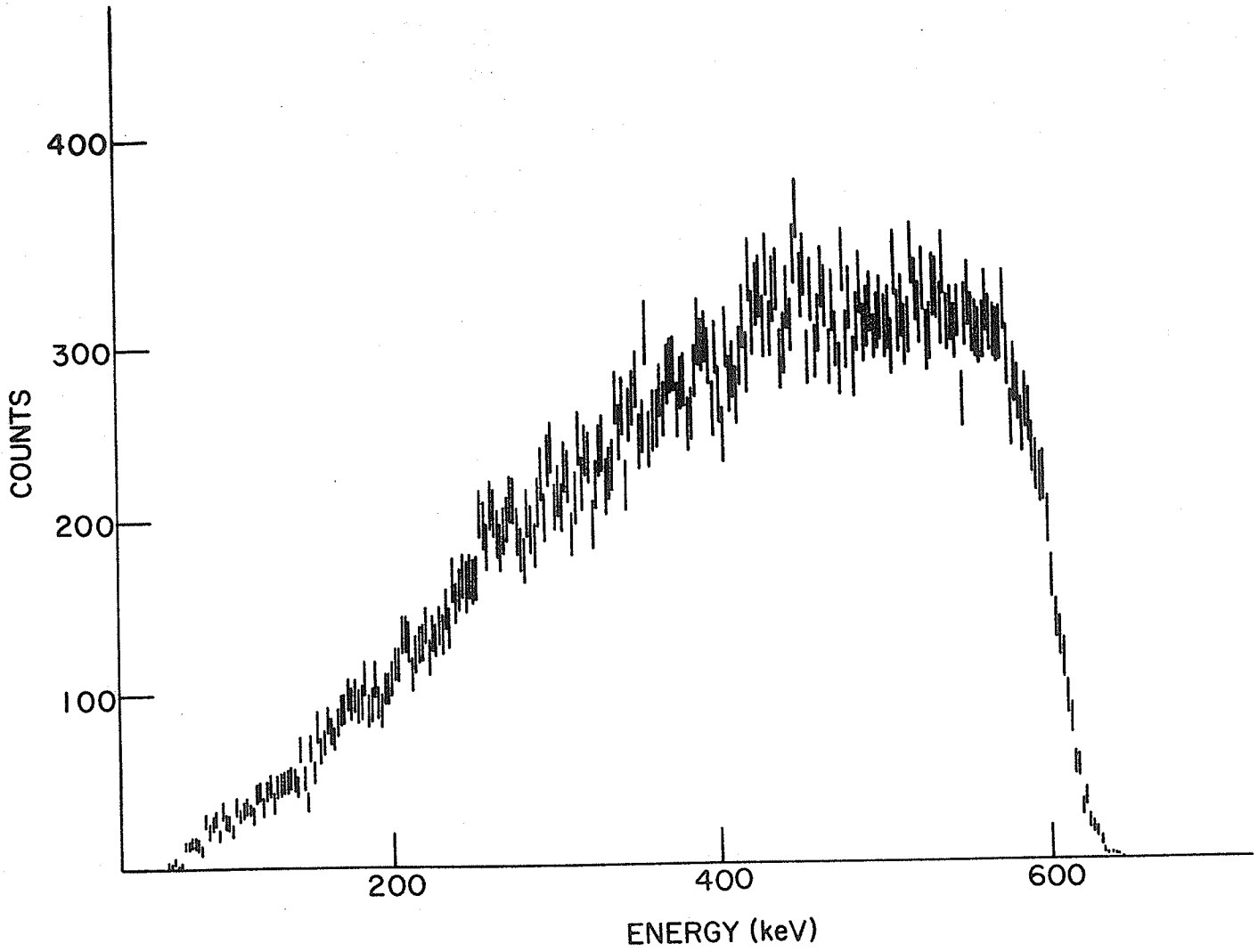
400
300
200
100
COUNTS
200
400
600
ENERGY (keV)

FIG. 6-17

Ungated positron spectrum.

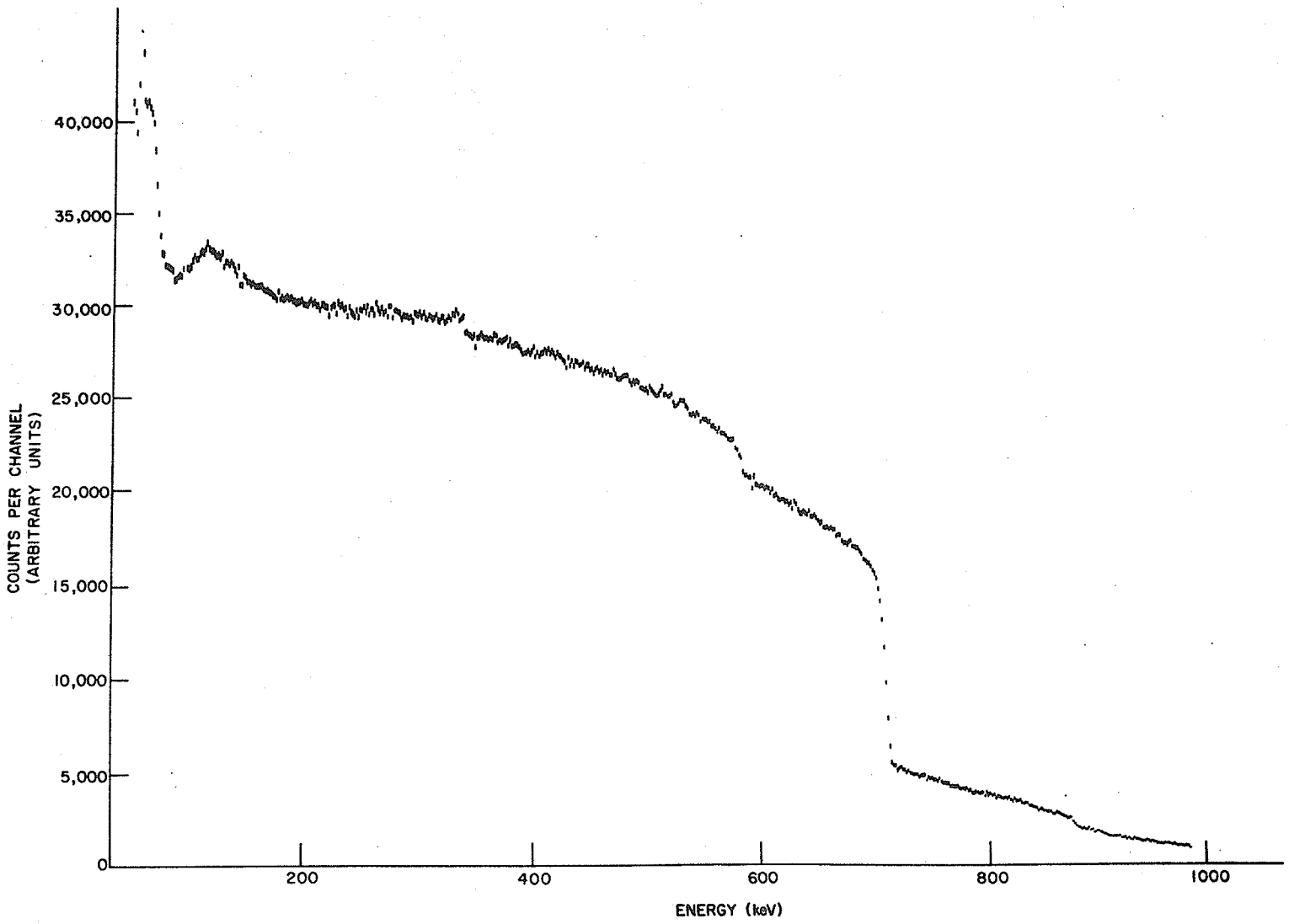
COUNTS PER CHANNEL
(ARBITRARY UNITS)
40,000
35,000
30,000
25,000
20,000
15,000
10,000
5,000
0
200
400
600
800
1000
ENERGY (keV)

FIG. 6-18

The 1719-pair positron spectrum compared with theoretical calculations described in Chapter 5.

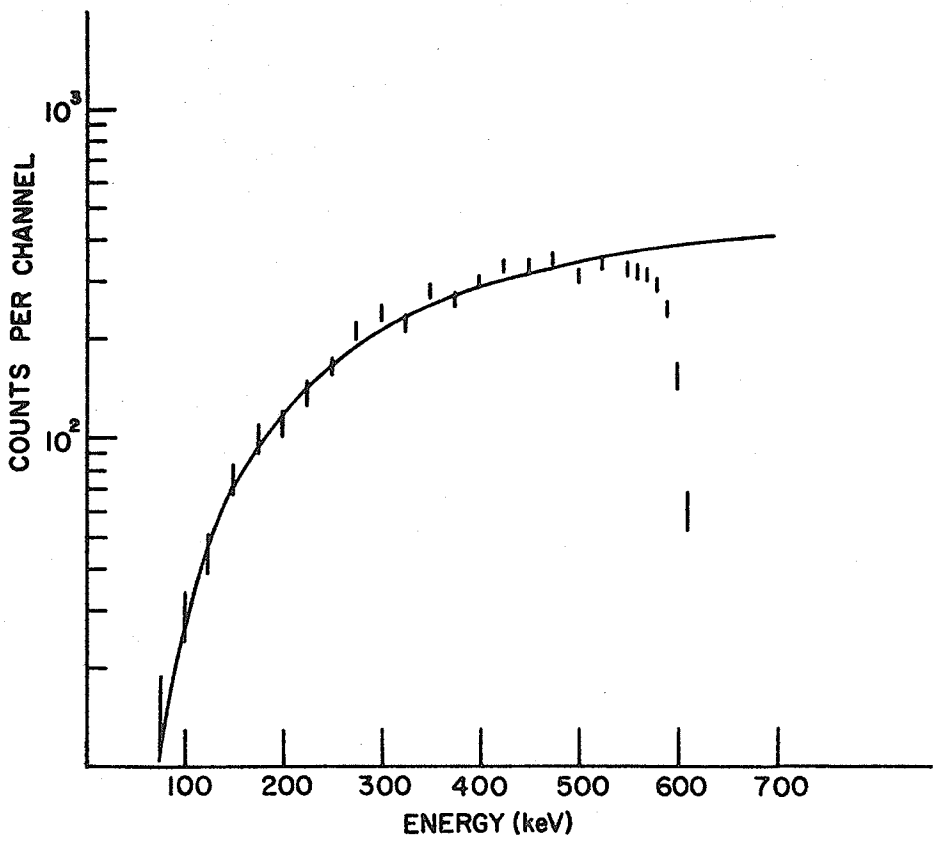
COUNTS PER CHANNEL
10^3
10^2
100
200
300
400
500
600
700
ENERGY (keV)

FIG. 6-19

Block diagram of the electronics used in the pair production study.

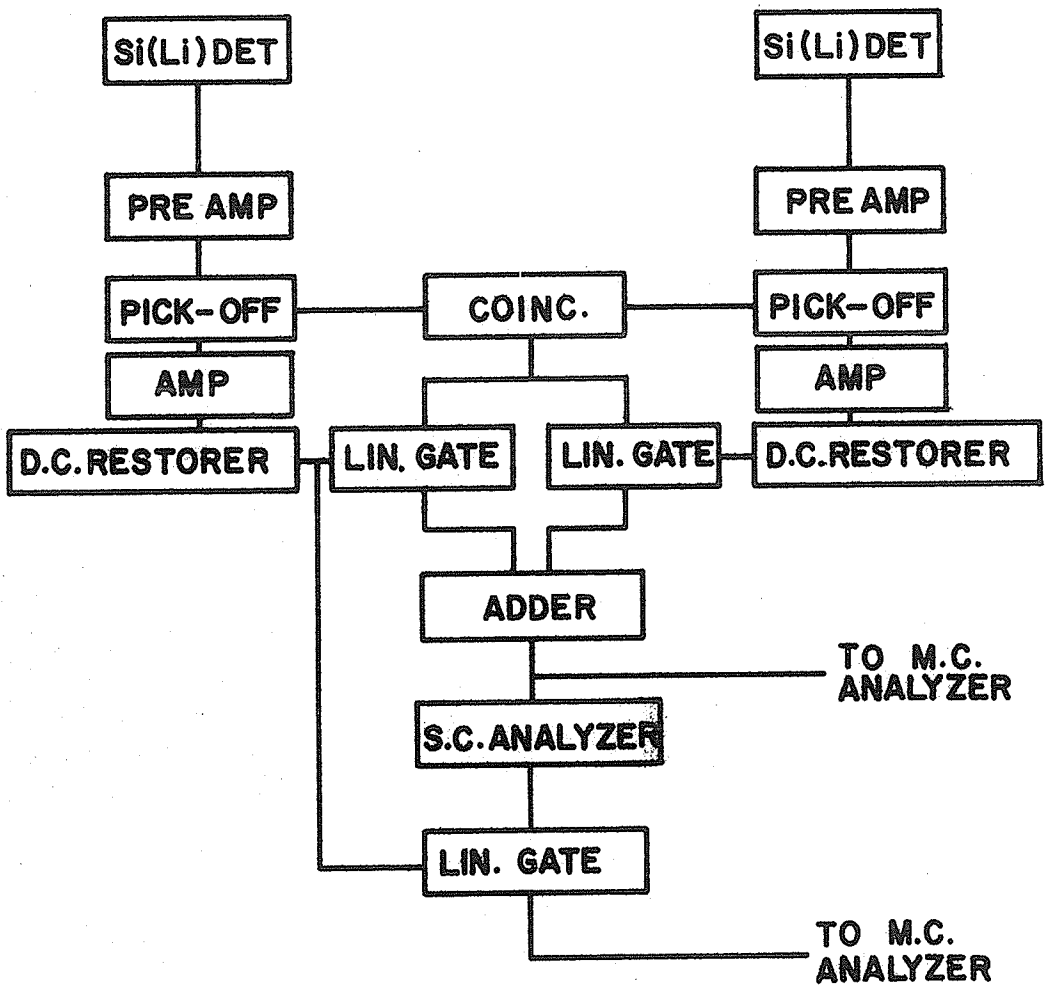
Si(Li) DET
Si(Li) DET
PRE AMP
PRE AMP
PICK-OFF
COINC.
PICK-OFF
AMP
AMP
D.C. RESTORER
LIN. GATE
LIN. GATE
D.C. RESTORER
ADDER
TO M.C. ANALYZER
S.C. ANALYZER
LIN. GATE
TO M.C. ANALYZER

ward. If a coincidence occurs between the two sides, the linear gates are triggered allowing the amplified outputs to enter the adder-amplifier. The summed output is then fed to a multi-channel analyzer and/or to a single channel analyzer, S.C.A. By setting a ΔE S.C.A. window on the appropriate sum peak the S.C.A. may be used to gate the positron side to collect the positron spectrum corresponding to a given transition. To collect the corresponding electron spectrum one simply reverses the magnet current which switches the response of side number 1 from positrons to electrons.

To obtain a monoenergetic pair sum peak the gains of the two sides must be matched. Rough gain adjustments are made using the main amplifiers and fine adjustments are made at the inputs to the adder amplifier. The gains are matched using the conversion electron spectrum. The resolution of the pair sum spectrum depends on this matching as well as on the resolution of each side. The 1719 keV sum peak shown in Fig. 6-15 is ~20 keV F.W.H.M. This somewhat poor resolution has been attributed to difficulties in matching the gains of the two sides. In subsequent experiments the situation has improved considerably. This improvement was achieved simply by switching the D.C. restorers, shown in Figure 6-19, from the passive mode to the active mode.

As discussed in Chapter 5, the coincidence resolving time is set at 400 nano-seconds. This means, in all cases of interest, that pair events, for which the positron or electron energy is $\lesssim$ 25 keV, will not contribute to the full energy pair sum peak since there will be no coincidence signals to trigger the gates. The time pick-off units, T.P.O., are biased so that they do not trigger unless the pre-amplifier output

pulses are sufficiently large. In this way the coincidence circuit is not triggered by electronic noise. In most experimental situations, it has turned out that the noise level corresponds to electrons (positrons) with an energy ~30-50 keV. Since the triggering level of the T.P.O. is set above the noise level those pair events for which $T \pm \lesssim 50$ keV then do not contribute to the sum peak. The main contribution to the electronic noise was found to be high frequency ripple, (~10MHz), on the magnet current. In the ^{206}Bi work the electron side of the system was particularly sensitive to this oscillation, because of the inadequate grounding, and the T.P.O. triggering level, for the electron side, had to be set at a level corresponding to an energy ~100 keV. Thus pair events for which $T - \lesssim 100$ keV do not contribute to the pair sum peak. This explains the cut-off at 600 keV in the positron spectrum of the 1719 keV transition.

The amplifier time constants used on the pair production work warrant a brief discussion. Consider a situation for which the total kinetic energy available to the pair is T = 1000 keV. In some given pair event let T_+ =900 keV and T- = 100 keV. Then the positron is detected about 100 nano-seconds before the electron. See Fig. 3-15. Therefore the amplified pulse from the positron side will reach full pulse height about 100 nano-seconds before that of the electron side. For some other pair event, however, for which $T_+ \sim T_-$ the amplified pulses from the two sides will reach full height at about the same time. Since the outputs of the two sides are to be added to give a unique sum

pulse, regardless of the energy sharing between the two particles, this variation in the time at which the pulses reach full height is potentially troublesome. The problem was very easily circumvented by using long amplifier time constants. The differentiation and integration time constants were both set at 4 μs. The resulting peak shape has a relatively "flat" top over a length of approximately 1 μs. The linear gates through which these pulses pass are held open for only 500 nano-seconds. The output of the coincidence circuit is delayed so that the gates are open when the amplified pulses reach full heighth. The adder amplifier therefore sees a pair of pulses which are essentially square wave pulses of length 500 nano-seconds. The variation in the times at which the outputs of the two sides reach full heighth is then effectively cancelled. This has been checked using a pulse generator. A pair of pulses of equal height are fed into the two sides of the system. If one pulse is delayed by 400 nano-seconds with respect to the other the change in the summed pulse height was found to be negligible.

Let us now turn to the anlysis of the data. The experimental data with which we have to work is essentially the full energy pair sum peak counting rate C_π. If C_K- is the full energy peak counting rate of the corresponding K-conversion line then

$\frac{e^{\pm}}{e_{K^-}} = \frac{C_\pi}{\epsilon_\pi} \times \frac{\epsilon_{K^-}}{C_{K^-}}$ where ϵ_π and ϵ_{K^-} are the appropriate peak detection efficiencies. If, for the moment, we assume that the pair sum peak contains contributions from all pair events, regardless of the value of T+, then ϵ_π =

$$\frac{\int_0^{T_+} \epsilon_1(T_+)\epsilon_2(T-T_+)N(T_+)dT_+}{\int_0^{T_+} N(T_+)dT_+}$$

where $\epsilon_{1,2}$ are the measured full energy peak detection efficiencies of sides 1 and 2 and N(T+) is the number of pairs per unit time with positron energy T_+. See Chapter 5.

The general method of evaluating ϵ_π was outlined in Chapter 5. Let us now consider the specific example of the 1719 keV transition in ^{206}Pb. In Fig. 6-20 we have plotted the product $\epsilon_1(T_+)\epsilon_2(T-T_+)$ against T_+ for this transition. Here we have assumed that $\epsilon_{1,2}(T) \equiv \epsilon_{1,2}(100)$ for all T $\lesssim$100 keV. Although the full energy peak detection efficiencies $\epsilon_{1,2}$ have not been measured for T <100 keV this assumption is reasonable. In practise, as explained earlier, the present instrument does not generally detect pair events for which T± $\lesssim$50 keV so that the behaviour of the efficiency curves, ϵ_1 and ϵ_2 below 50 keV is unimportant. The full energy peak detection efficiency curves for both sides of the spectrometer are constant from 500 keV to 100 keV. At some energy below 100 keV an appreciable fraction of the particles striking the detector will lose sufficient energy in the detector dead layer to reduce the full energy detection efficiency. In the early development of the instrument the line shape of 60 keV conversion electrons from ^{109}Cd

was found to be reasonably "sharp" which indicates that the efficiency curves are essentially constant to energies ~60 keV. Therefore no serious error is introduced by the above assumption.

The curve obtained by plotting $\epsilon_1(T_+)\epsilon_2(T-T_+)$ against T_+, Fig. 6-20, is characterized by a broad region over which the product $\epsilon_1 \times \epsilon_2$ = a constant = 3.11×10^{-2}. Therefore we set $\epsilon_\pi = \frac{(3.11 \times 10^{-2})}{C}$ where C is a correction factor to account for the fact that the product $\epsilon_1 \times \epsilon_2$ is not constant over the entire range of positron energy. To calculate the correction factor C we gate on the 1719 keV pair sum peak to obtain the positron spectrum shown in Fig. 6-16. If $C_x(T_+)$ is the observed number of counts in channel x corresponding to a positron energy T_+ then the correction is given by

$$C = \frac{\sum_x C_x(T_+)/\{\epsilon_1(T_+)\epsilon_2(T_+)\}}{\sum_x C_x(T_+)/(3.11 \times 10^{-2})} \qquad \text{where}$$

the summation is carried over all occupied channels. For the 1719 keV transition we obtain C = 1.02. Then the apparent ratio $\frac{e^\pm}{e_{K^-}}$ is given by

$$\frac{e^\pm}{e_{K^-}} = \frac{C_\pi \times 1.02}{3.11 \times 10^{-2}} \times \frac{\epsilon_{K^-}}{C_{K^-}}.$$

Although the correction factor, C, is small in the present example, in general, for higher energy transitions, it is considerably larger and must be taken into account in analyzing the data.

Since the pair sum peak contains no contributions from pairs for which $T_+ \geq 600$ keV the apparent ratio calculated above is low. We must,

FIG. 6-20

The product $\epsilon_1(T_+)\epsilon_2(T-T_+)$ versus T_+ for E_γ = 1719 keV.

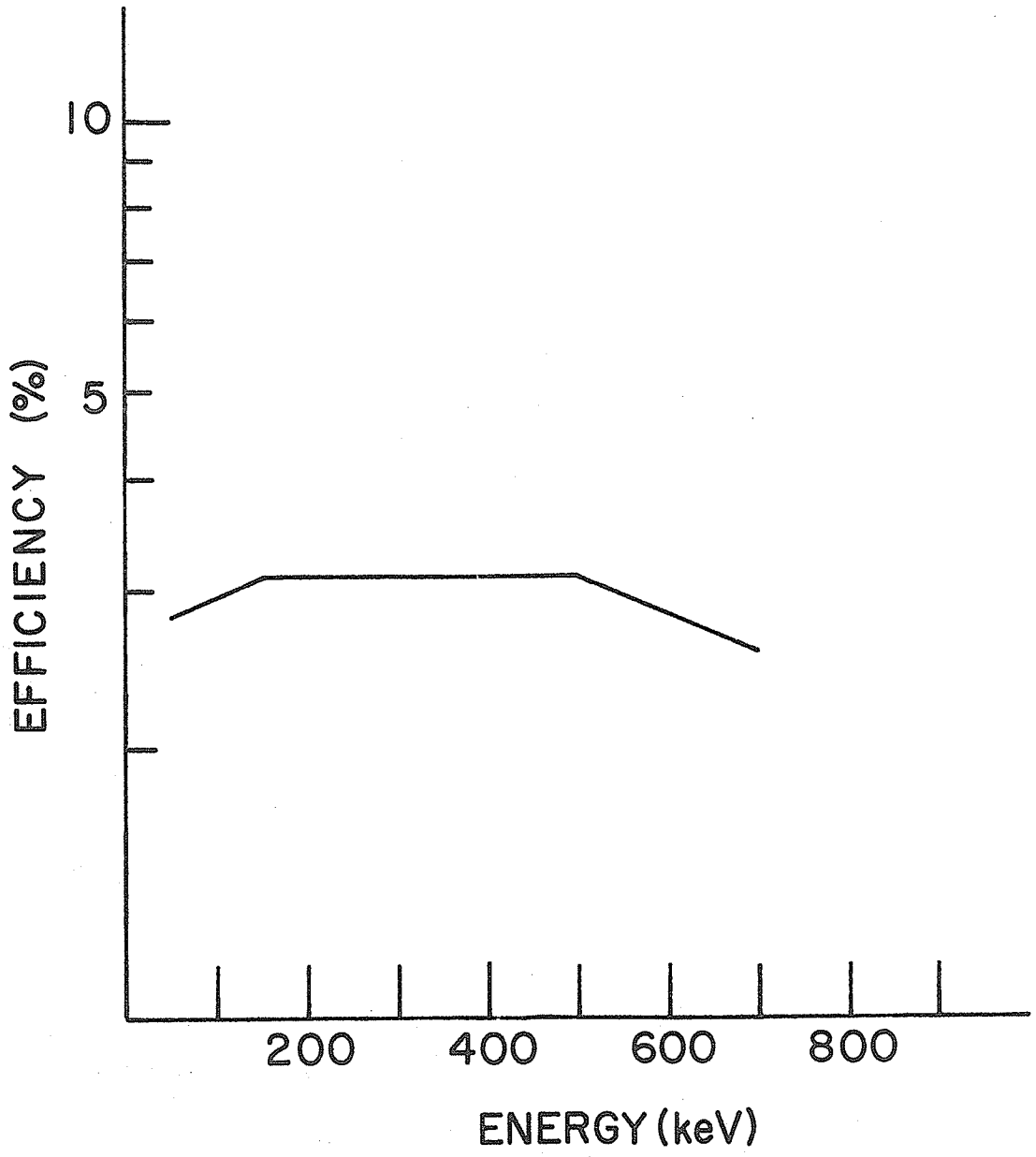
10
5
EFFICIENCY (%)
200
400
600
800
ENERGY (keV)

now, introduce a second correction term. Since the theoretical shape of the positron continuum fits the experimental data for $T_+ \lesssim 600$ keV we have used the theoretical positron energy distribution to correct for the high energy cut-off. The correction is then given by C_1=(Area under theoretical curve from 0 to 700 keV)÷(Area under the theoretical curve from 0 to 600 keV). Then C_1=1.25. ie. 25% of the pair events have positron energies with $T_+ \gtrsim 600$ keV. We have ignored the fact that there is also a low energy cut-off which means that the pair sum peak also contains no contributions from pair events for which $T_+ \lesssim T_o$, where T_o is low energy cut-off. In the present experiment the positron continuum obtained by gating on the 1719 keV sum peak, (Fig. 6-16) has no counts for $T_+ \lesssim 70$ keV. Thus the low energy cut-off, in the present experiment, occurs at about 70 keV. Because of the Coulomb repulsion of the positrons the number of pair events for which $T_+ < 70$ keV is negligible and no error is introduced by ignoring the low energy cut-off.

In summary, then, to obtain the ratio $\frac{e^{\pm}}{e_{K^-}}$ for the 1719 keV transition it was necessary to introduce two types of corrections to the pair sum peak counting rate. The first correction, which in the present case was small, accounts for the fact that the pair detection efficiency for different pair events varies with the positron energy T_+. The second correction accounts for the fact that the pair sum peak contains no contributions from pair events for which the positron energy, T_+, is greater than some cut-off energy.

In the present work we have also obtained the ratio $\frac{e^{\pm}}{e_{K^-}}$ for the 1595 keV transition. For this transition it was impossible to obtain, experimentally, the shape of the positron continuum because of the low intensity of the 1595 pair sum peak. However, it is not really necessary to do so. For this transition the kinetic energy available to the pair is 573 keV and the product $\epsilon_1(T_+)\epsilon_2(T_-T_+)$ is essentially constant for $T_+ \leq 573$ keV. Therefore the only correction which must be applied to the pair sum peak counting rate is that associated with the high-energy cut-off. As discussed previously this cut-off arises because electrons with $T_- \leq 100$ keV do not trigger the coincidence circuit. For the 1595 keV transition the pair sum peak then contains no contributions from pair events for which $T_+ \geq 473$ keV. We have calculated a correction for this effect using the corresponding correction obtained for the 1719keV transition. For the 1595 keV transition the positron energy region for which the pair sum peak contains no contributions is a larger fraction of the energy region open to the positron than for the 1719 keV transition. Therefore the correction term is corresponding by larger. For the 1595 keV transition we have calculated the correction term to be

$$C_1 = 1.25 \times \frac{(573/473)}{(700/600)} = 1.30$$

The results of the present measurements are summarized in Table 6-8. Here we have shown the measured pair formation coefficients, the measured ratios $e^{\pm}/e_{K^-}$ and the measured K-conversion coefficients for the 1595 and 1719 keV transitions. Also shown, for comparison,

TABLE 6-8

Summary of ^{206}Bi pair formation study.

TABLE 6-8

Transition	Quantity	Experimental	E1	E2	M1
	α_π	$2.5\pm.5\times10^{-4}$	2.2×10^{-4}	9.5×10^{-5}	1.6×10^{-4}
1595	α_K	$9.8\pm1.0\times10^{-4}$	9.5×10^{-4}	2.3×10^{-3}	4.7×10^{-3}
	$e^\pm/e_K$	$.25\pm.05$	.23	.042	.034
	α_π	$3.7\pm.6\times10^{-4}$	3.0×10^{-4}	1.45×10^{-4}	2.4×10^{-4}
1719	α_K	$8.9\pm.9\times10^{-4}$	8.5×10^{-4}	1.95×10^{-3}	3.9×10^{-3}
	$e^\pm/e_K$	$.42\pm.06$	.36	.074	.061

are the corresponding theoretical values for E1, E2 and M1 transitions based on the calculations of Lombard et al [10] and Hager and Seltzer[22]. The agreement between the theoretical values for an E1 multipolarity and the experimental data is excellent.

SUMMARY

In summary the study of ^{206}Pb following the decay of ^{206}Bi was very fruitful. The relative γ-ray intensities of the various transitions have been measured and the corresponding conversion coefficients have been deduced on the basis of these measurements and previous measurements of the relative K-shell conversion electron intensity. These conversion coefficients generally confirm the decay scheme of Lederer,Hollander and Perlman [14]. The calibration curves for the spectrometer have been verified. The positions of 1844, 1878 and 1903 keV transitions have been established and the position of the 755 keV transition has been changed from that suggested by Lederer et al. Several new transitions have been established and some of these transitions have been tentatively assigned to the decay scheme. Finally the spectrometer has been used for the first time as a pair spectrometer and several important aspects of its operation as such have been revealed.

CHAPTER 7

INTERNAL PAIR PRODUCTION AND INTERNAL CONVERSION IN ^{88}Sr FOLLOWING THE DECAY OF ^{88}Y.

"Observe how system into system runs,
What other planets circle other suns."

..... Alexander Pope

INTRODUCTION

^{88}Y decays to ^{88}Sr by approximately 100% E.C. capture. The decay scheme, according to Lederer et al [23] is shown in Fig. 7-1. The 2734 keV level of ^{88}Sr de-excites to the ground-state by two cascade transitions of 898 keV and 1836 keV and by a cross-over transition of 2734 keV. The 1836 keV level of ^{88}Sr is also weakly feed via positron decay of ^{88}Y. Previous workers have measured the K-conversion coefficients for the 898 and 1836 keVtransitions. For both the 1836 and 2734 keV transitions internal pair formation is one mode of de-excitation. The pair formation coefficients for these transitions had not been previously determined, so their measurement was undertaken. For completeness the K-conversion coefficients, α_K, and the ratios $\alpha_K|\alpha_L+\alpha_M+ \ldots$ were also measured for the 898 and 1836 keV transitions.

INTERNAL CONVERSION MEASUREMENTS

For the internal conversion coefficient work (and for the pair production studies) two independently prepared drop sources were used. For each source, electron runs were made, in succession, on

FIG. 7-1

Decay scheme of ^{88}Y.

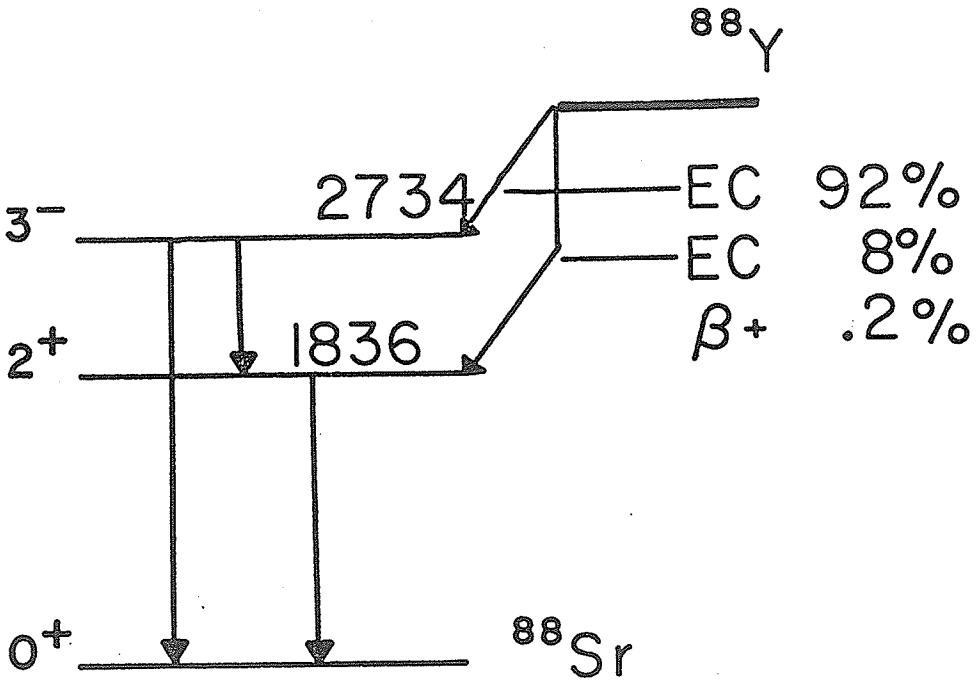
88Y
2734
EC 92%
EC 8%
β+ .2%
3−
2+
1836
0+
88Sr

either side of the spectrometer. A typical electron spectrum, using a logarithmic scale for the counts per channel, is shown in Fig. 7-2. In Fig. 7-3 the spectrum, in the vicinity of the conversion electron peaks, is shown in detail, on a linear scale. As can be seen the K and the L+M+... conversion peaks, for both the 898 and 1836 kev transitions, are not completely separated. Therefore it was necessary to do some very simple peak fitting. This was done graphically and the technique is illustrated in Fig. 7-4. The points represent the 898 K and L+M+... conversion electron peaks following a straight line background subtraction. The dashed curve represents the estimated contribution to the doublet from the higher energy peak. The shape of the fitting curve is the same as that of the lower energy peak. This is a reasonable shape to use. The "size" of the L+M+... conversion peak is roughly 15% of that of the K-conversion peak. Further, the two peaks are reasonably well separated so that the contribution to the lower energy peak from L+M+... conversion electrons is small. The lower energy peak is then relatively clean and the peak shape should be a good approximation to the "true" shape. It was found, using this technique, that the unresolved contribution to the L+M+... conversion peak was generally ~10% of the total contribution, for both the 898 and 1836 keV transitions. The number of counts in the K-conversion peak was obtained by subtracting the number of counts in the L+M+... peak, obtained in the above manner, from the total number of counts in both peaks. The absolute γ-ray strength of these transitions was found using an external Ge(Li) detector.

FIG. 7-2

Typical electron spectrum of ^{88}Y.

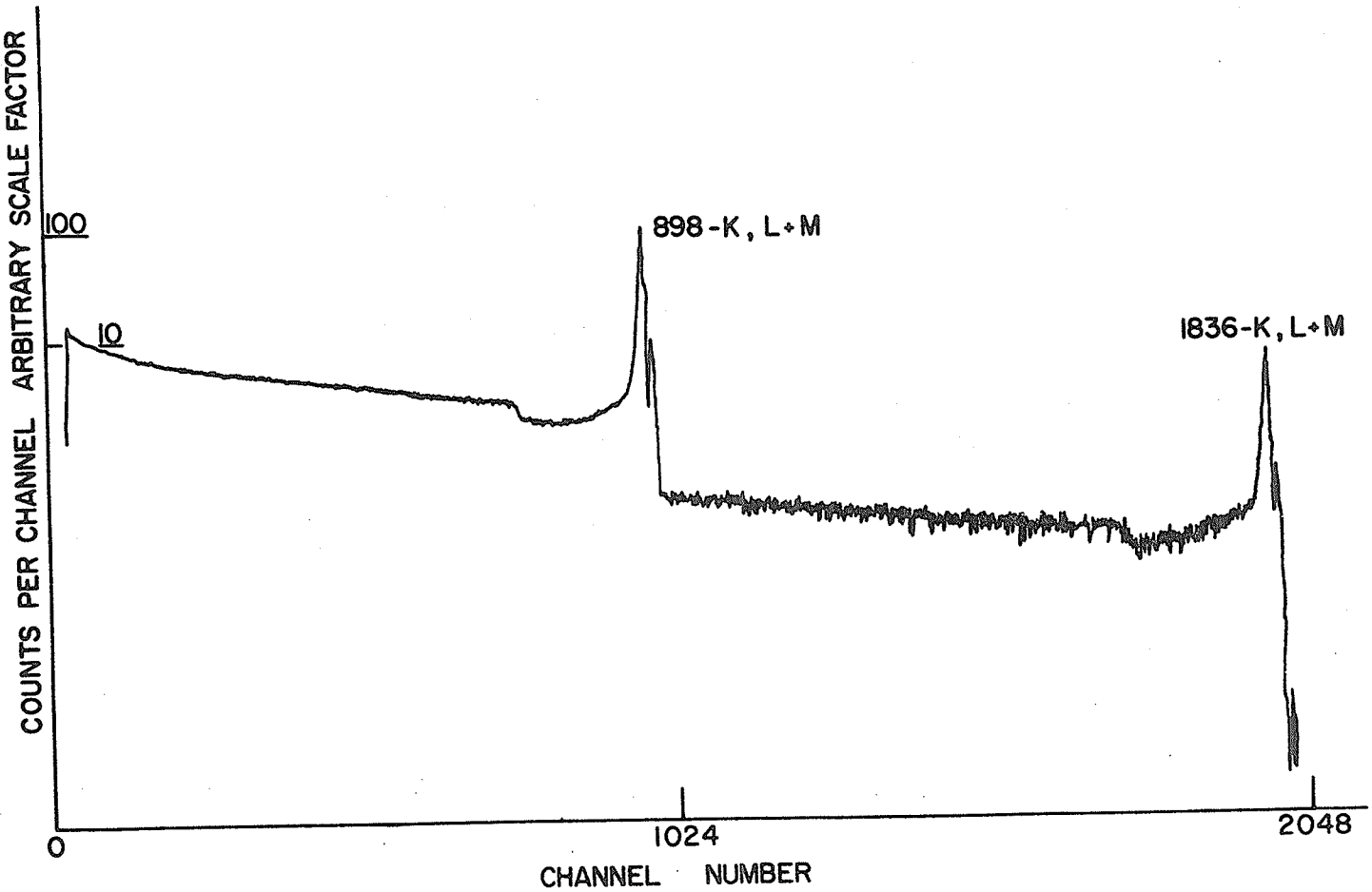
COUNTS PER CHANNEL ARBITRARY SCALE FACTOR
100
10
898-K, L+M
1836-K, L+M
0
1024
2048
CHANNEL NUMBER

FIG. 7-3

The ^{88}Y electron spectrum in the vicinity of the conversion peaks.

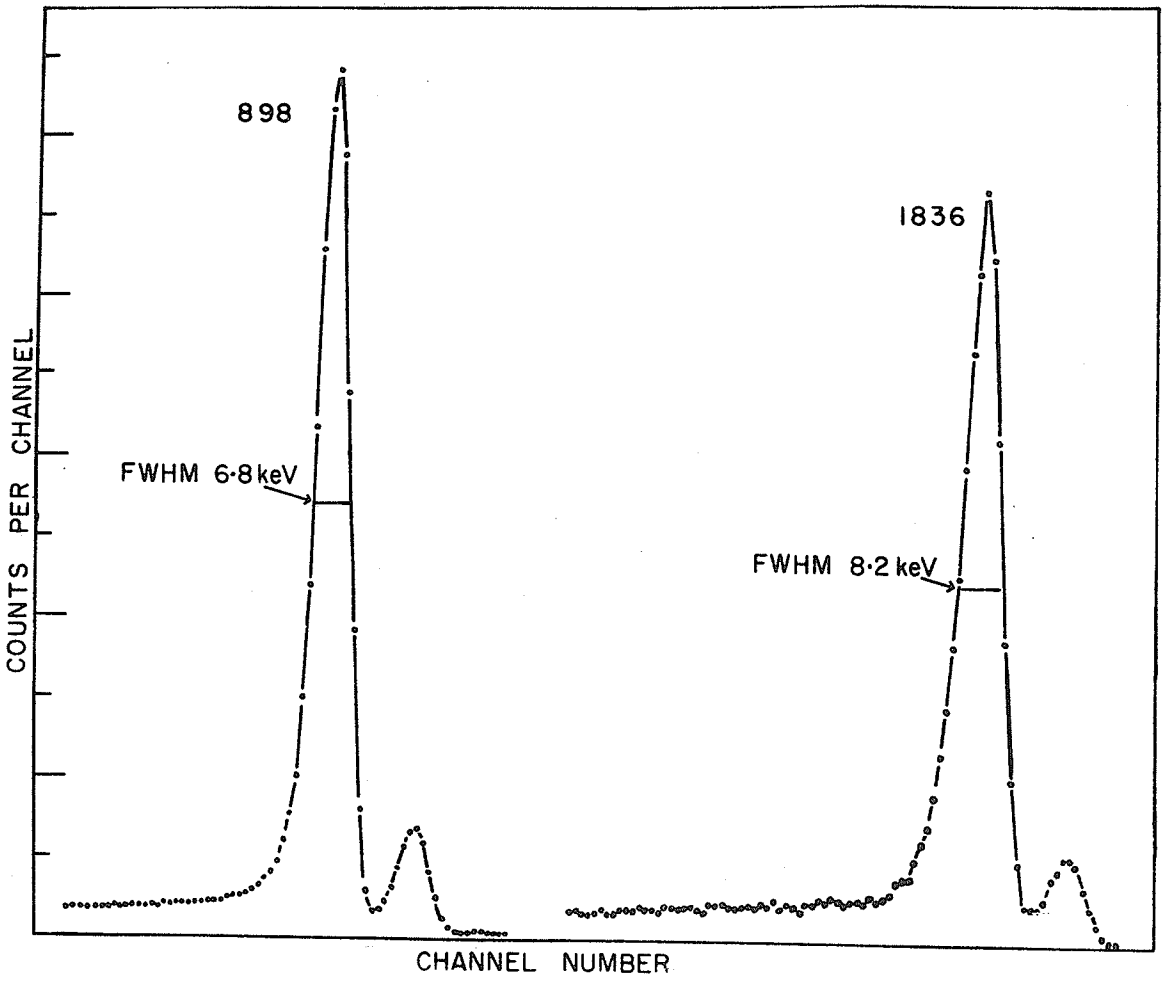
898
1836
FWHM 6·8 keV
FWHM 8·2 keV
COUNTS PER CHANNEL
CHANNEL NUMBER

FIG. 7-4

The separation of the K and the L+M conversion peaks for the 1836 keV transition of ^{88}Sr.

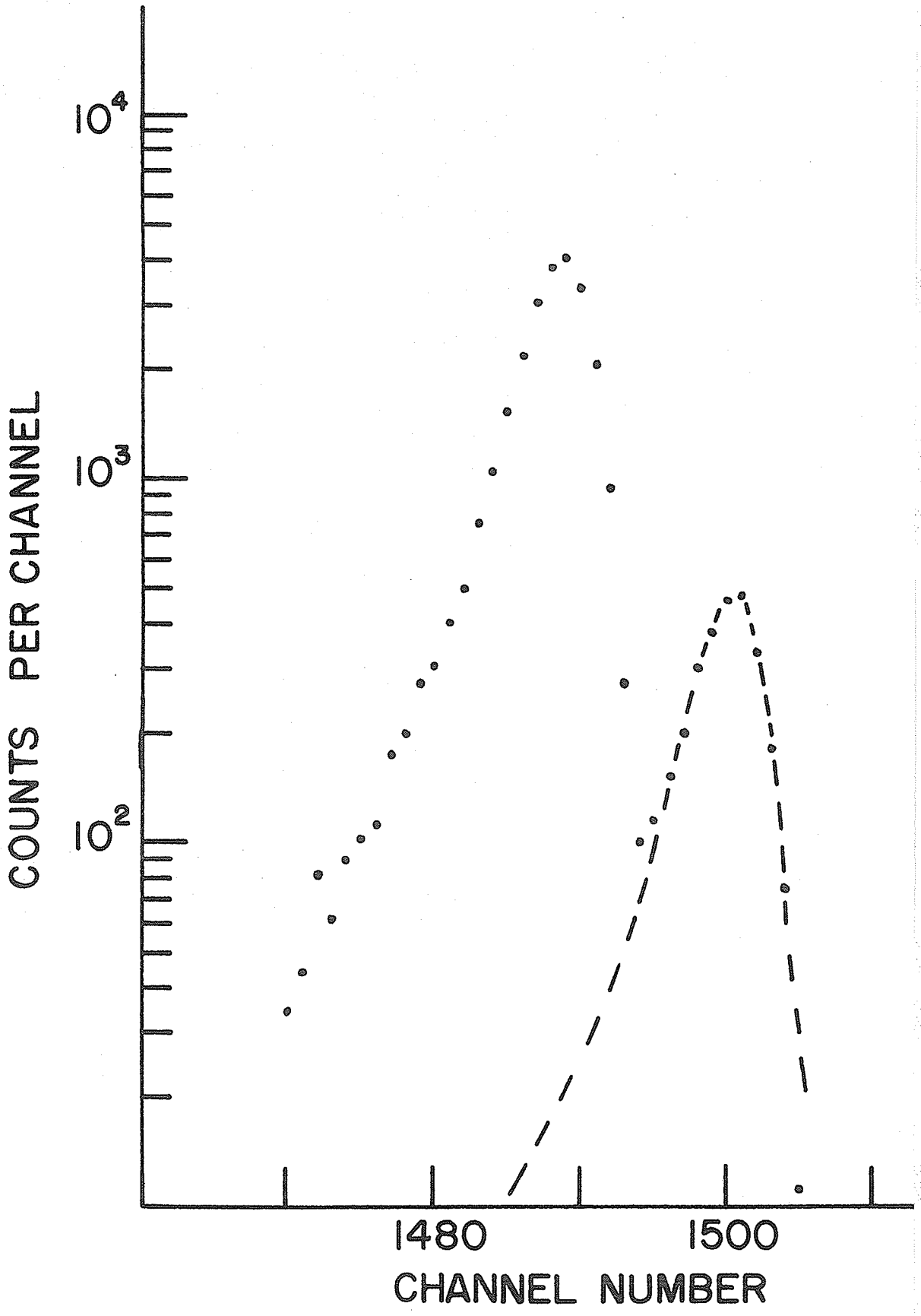
COUNTS PER CHANNEL
10^4
10^3
10^2
1480
1500
CHANNEL NUMBER

TABLE 7-1

The results of the internal conversion work on ^{88}Sr following the decay of ^{88}Y, compared to theory and to the results of previous workers.

TABLE 7-1

Quantity	Present Work	Theoretical[22]	Hamilton et al[24]	Metzger et al[25]	Peacock & Jones[26]
$\alpha_K(898)$	$2.5\pm.3\times10^{-4}$	2.7×10^{-4} (E1)	$3.0\pm.2\times10^{-4}$	------	------
K/L+M+...,898	8.0±.2	7.8	7.0±.5	------	------
$\alpha_T(898)$	$2.8\pm.3\times10^{-4}$	3.0×10^{-4}	3.45×10^{-4}	$3.4\pm.7\times10^{-4}$	2.7×10^{-4}
$\alpha_K(1836)$	$1.20\pm.16\times10^{-4}$	1.4×10^{-4} (E2)	------	------	------
K/L+M+...(1836)	7.8±.3	------	------	------	------
α_T (1836)	$1.34\pm.16\times10^{-4}$	------	------	$1.7\pm.4\times10^{-4}$	1.3×10^{-4}

The results of the internal conversion work are summarized in table 7-1 and compared to those of previous workers [24,25,26] and to the theoretical calculations.[22] The agreement is fairly good.

INTERNAL PAIR PRODUCTION MEASUREMENTS

Both 2734 keV level and the 1836 keV level may de-excite by the creation of an electron-positron pair. In the present work we have measured the pair formation coefficient, α_π, for both these transitions. Runs were made with two independently prepared drop sources. Fig. 7-5 shows a typical electron-positron sum spectrum in which the sum peaks corresponding to the 1836 and 2734 keV transitions can be seen. Here the number of counts per channel is plotted on a logarithmic scale. Fig. 7-6 shows typical sum peaks for the 1836 and 2734 keV transitions in more detail on a linear scale. The 1836 sum peak is ~15 keV F.W.H.M. Part of this resolution is surely attributable to difficulties in matching the gains of the two sides of the spectrometer. This gain matching was done using the ^{88}Y conversion electron spectrum and therefore we could check the matching at only two energies, the energies of the conversion electrons from the 898 and 1836 keV transitions.

Let us consider the 1836 keV transition first. By gating on the corresponding sum peak we have obtained both the positron continuum and the electron continuum. These spectra, uncorrected for efficiency, are shown in Fig. 7-7. The low energy cut-off in these spectra occurs at about 30 keV. In Fig. 7-8 the positron spectrum is compared to the theoretical calculations of Chapter 5. The symmetric curve of Fig. 7-8 is the calculated shape, for an E2 transition, using

FIG. 7-5

Typical pair sum spectrum of ^{88}Y.

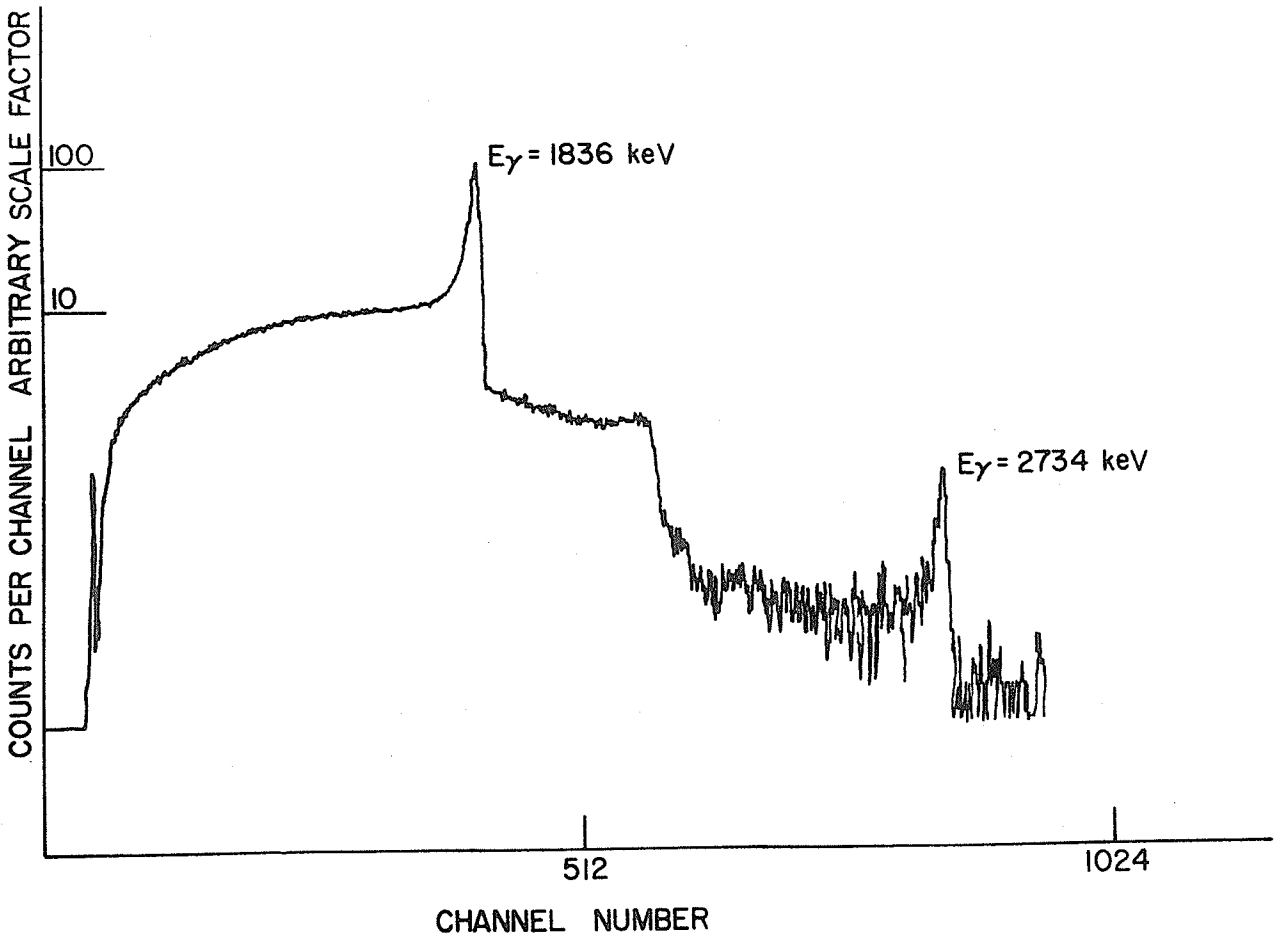
COUNTS PER CHANNEL ARBITRARY SCALE FACTOR
100
10
Eγ = 1836 keV
Eγ = 2734 keV
512
1024
CHANNEL NUMBER

FIG. 7-6

Typical pair sum peaks for the 1836 and 2734 keV transitions of ^{88}Sr.

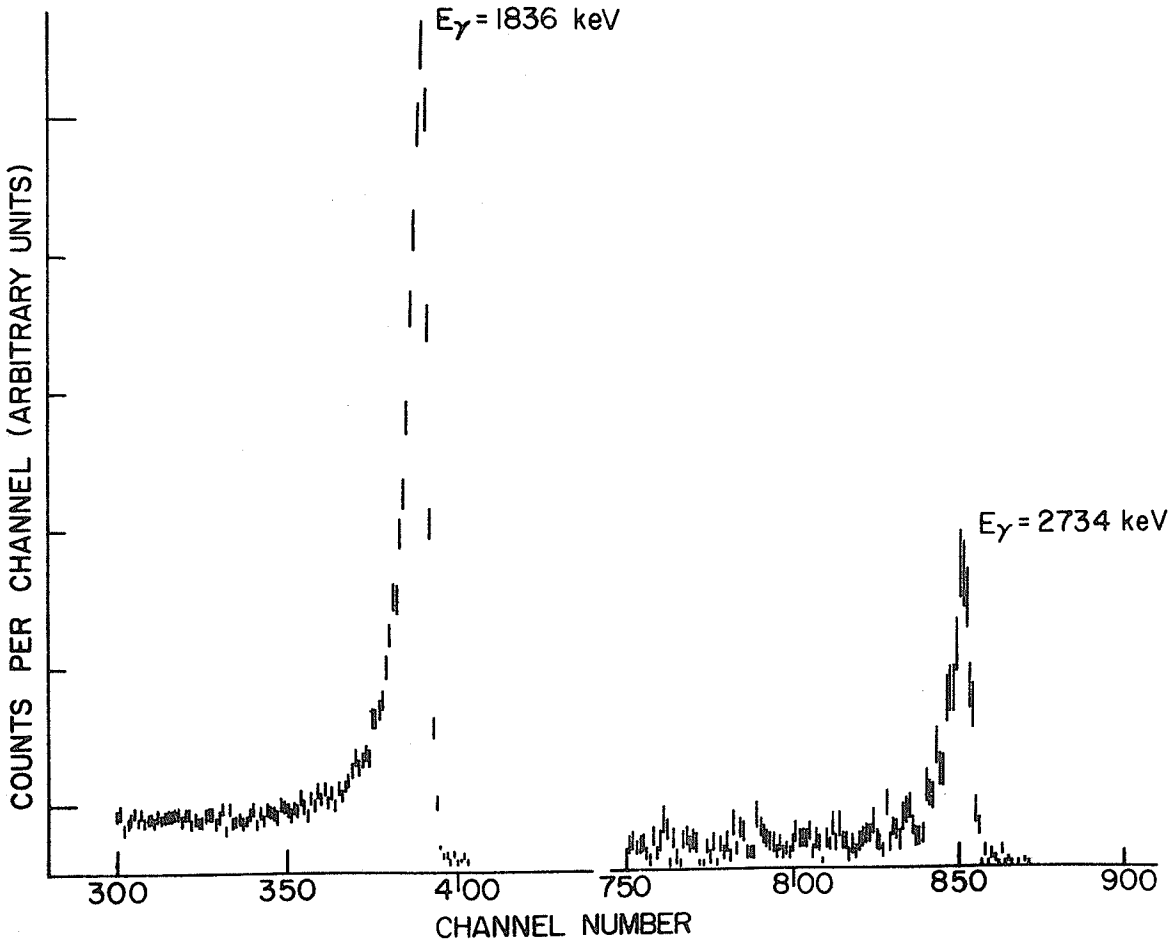
E_γ = 1836 keV
E_γ = 2734 keV
COUNTS PER CHANNEL (ARBITRARY UNITS)
300
350
400
750
800
850
900
CHANNEL NUMBER

the Born approximation and the second curve is the Born approximation calculation corrected for nuclear charge. Here the charge correction is that of Horton and Phibbs[13]. The Fermi correction gives essentially the same shape. Both the theoretical curves have been normalized to the experimental data at T_+=400 keV.

To calculate the pair formation coefficient for the 1836 keV transition we must correct the pair sum peak counting rate for the variation in pair detection efficiency with energy and for the lack of contributions to the sum peak from positrons with $T_+ \geq$ 784 keV. In Fig. 7-9 the product $\epsilon_1(T_+)\epsilon_2(T-T_+)$ is plotted against T_+ for the 1836 keV transition. Ignoring, for the moment, the high-energy cut-off, we set the pair detection efficiency, ϵ_π, = $\frac{3.05 \times 10^{-2}}{C}$ where C is the correction which accounts for the variation of pair detection efficiency with energy. C is calculated as for the case of the 1719 keV transition of ^{206}Pb, (see Chapter 6), using the experimental positron continuum obtained by gating on the 1836 keV pair sum peak. For this transition C = 1.09. The correction for the high energy cut-off was calculated by comparing the area under the theoretical positron continuum, corrected for nuclear charge, from 0 to 784 keV to the area under the curve from 0 to 814 keV. This method of calculation is justified by the good agreement between the theoretical shape of the positron continuum and the experimental shape. See Fig. 7-8. The correction was found to be 1.05 ie. The pair sum peak does not contain any contributions from 5% of the pair events.

FIG. 7-7

Comparison of the electron and positron continua from internal pairs from the 1836 keV transition of ^{88}Sr.

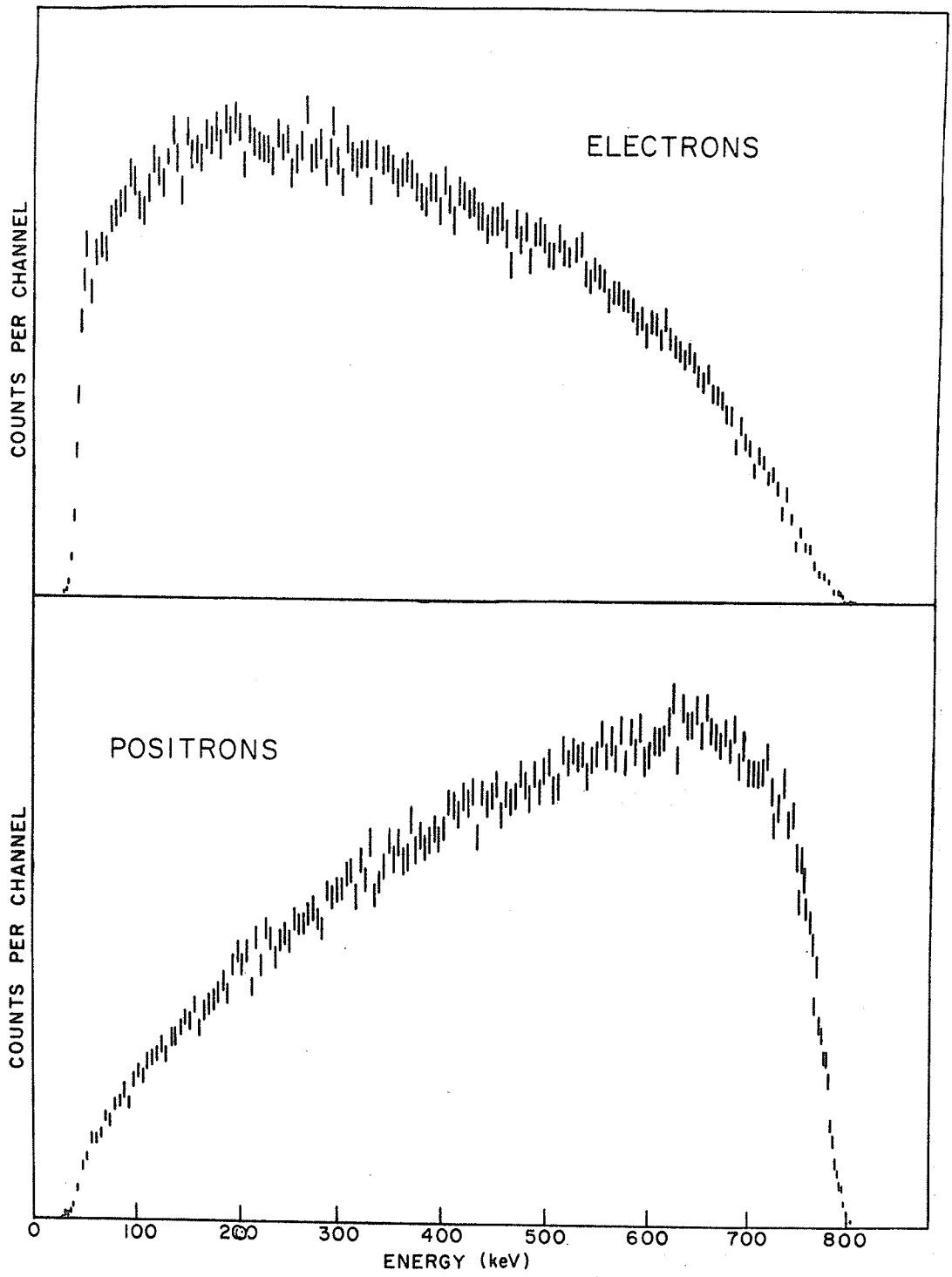
ELECTRONS
COUNTS PER CHANNEL
POSITRONS
COUNTS PER CHANNEL
0
100
200
300
400
500
600
700
800
ENERGY (keV)

FIG. 7-8

Comparison of experimental shape of the positron continuum of internal pairs from the 1836 keV transition of ^{88}Sr with theoretical calculations. The symmetric is the Born approximation for an E2 transition while the second curve is the same calculation multiplied by the charge correction factor of Horton and Phibbs (13). Both curves have been normalized to the data at 400 keV.

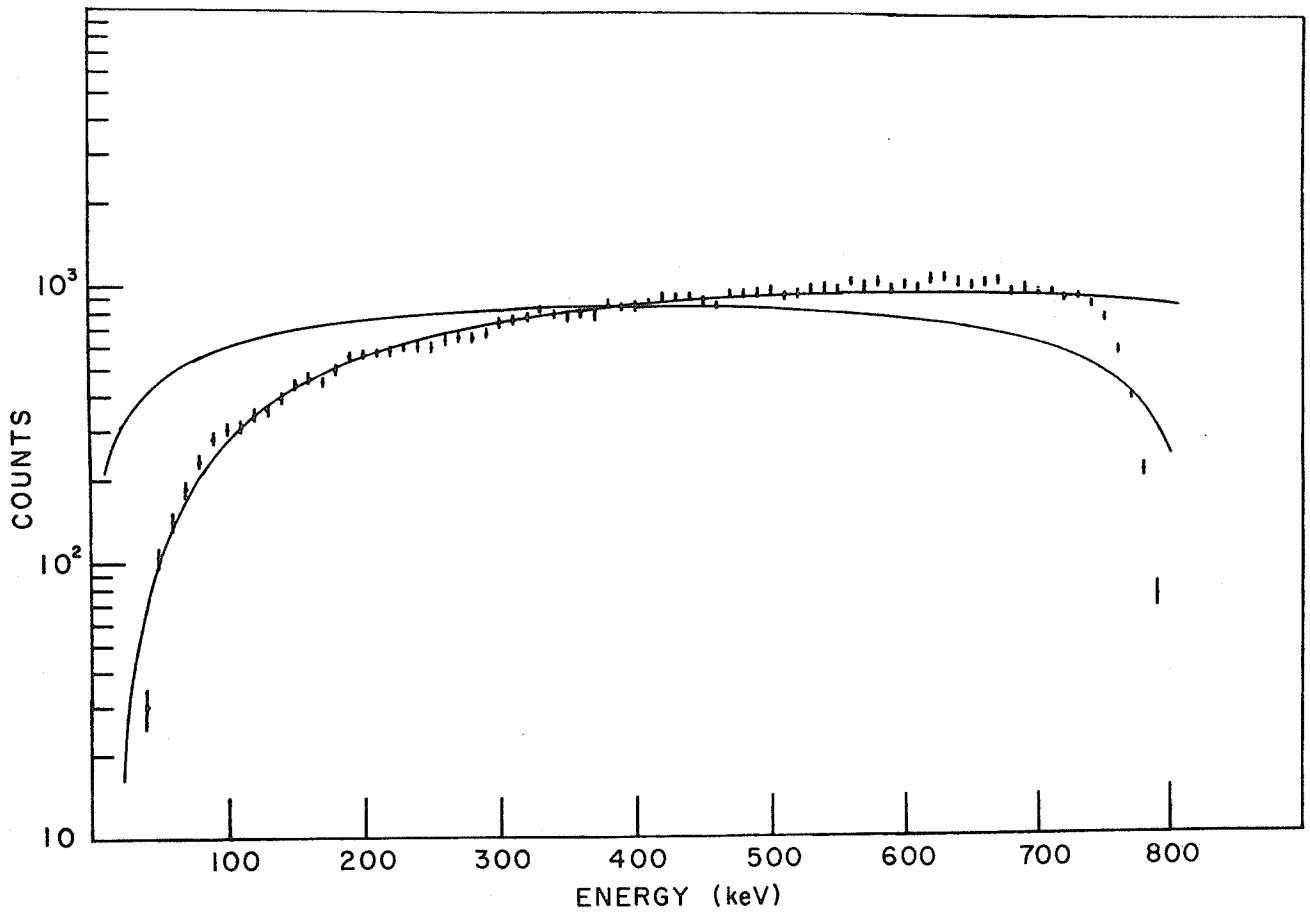
COUNTS
10^3
10^2
10
100
200
300
400
500
600
700
800
ENERGY (keV)

FIG. 7-9

The product $\epsilon_1(T_+)\epsilon_2(T-T_+)$ versus T_+ for E_γ = 1836 keV.

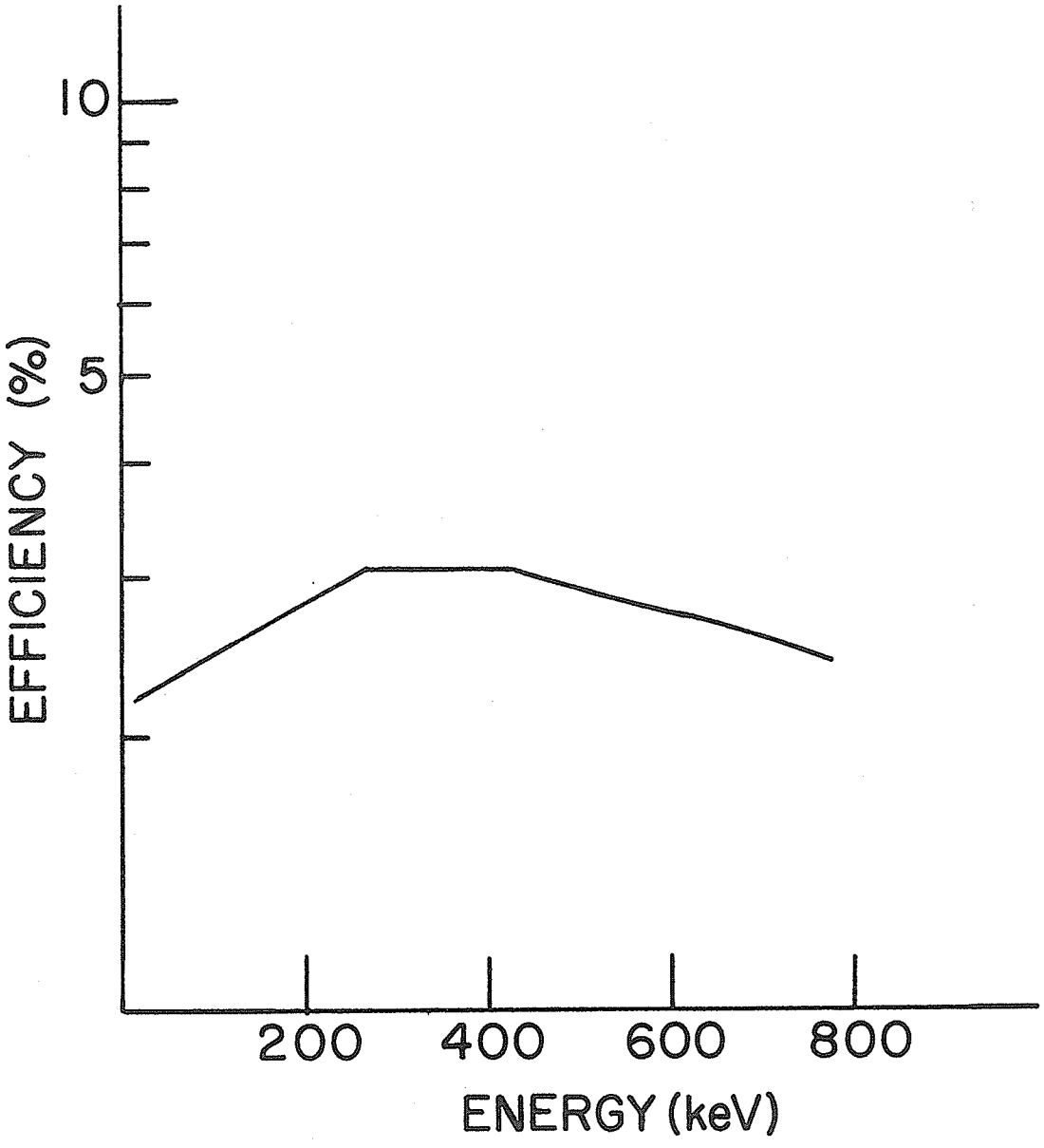
10
5
EFFICIENCY (%)
200
400
600
800
ENERGY (keV)

FIG. 7-10

The product $\epsilon_1(T_+)\epsilon_2(T-T_+)$ versus T_+ for E_γ = 2734 keV.

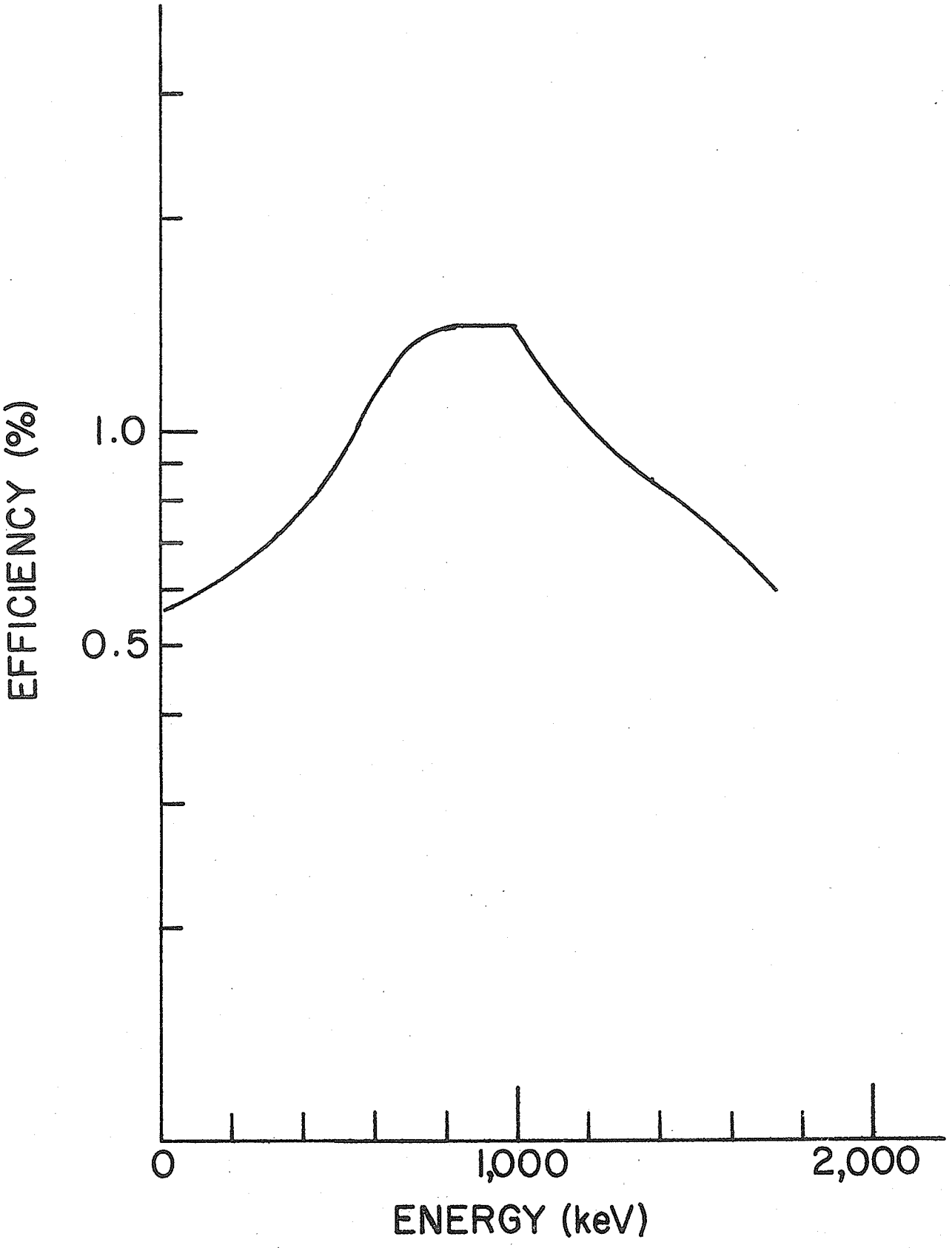
EFFICIENCY (%)
1.0
0.5
0
1,000
2,000
ENERGY (keV)

Now let us turn our attention to the 2734 keV transition. Because the pair sum peak corresponding to this transition is very weak it was impossible to obtain the shape of the positron continuum experimentally. Because of the high energy of the transition the variation in pair detection efficiency, with positron energy, is expected to be large and must be taken into account. This variation is shown in Fig. 7-10.For this transition we set $\epsilon_\pi = \frac{1.43}{C} \times 10^{-2}$ where C is the usual correction factor. We have calculated C using the theoretical shape of the positron continuum, corrected for the effects of nuclear charge, calculated as discussed in Chapter 5. Since the correction obtained in this way may depend on the multipolarity of the transition calculations were carried out for E1, E2, E3, M1, M2 and M3 transitions. The correction factor was found to vary from 1.37 to 1.42 for the different multipoles. To calculate the pair formation coefficient the value C = 1.40 was adopted. The pair formation coefficient obtained using this correction is expected to be valid for two reasons. (1) Although we have no direct confirmation of the theoretical shape of the positron continuum for the 2734 keV transition the theoretical shape obtained for the 1836 keVtransition is in excellent agreement with the experiment which gives us confidence in the theoretical formulae. (2) The correction factor represents a correction of 40% and, therefore an error in the correction of say 20% contributes an error of only 8% to the pair formation coefficient. Thus this procedure for accounting for the variation of pair detection efficiency with positron energy is justified. The correction to the pair sum peak counting rate arising from the high-energy positron cut-off is ≈1.02 for the 2734 keV

TABLE 7-2

Summary of pair formation study of ^{88}Sr following decay of ^{88}Y.

TABLE 7-2

E_γ	α_π	E1	E2	E3	M1	M2	M3
1836	$2.3\pm.3\times10^{-4}$	4.9×10^{-4}	2.3×10^{-4}	1.2×10^{-4}	1.6×10^{-4}	8.7×10^{-5}	4.6×10^{-5}
2734	$3.3\pm.5\times10^{-4}$	10.3×10^{-4}	6.4×10^{-4}	4.4×10^{-4}	4.4×10^{-4}	3.6×10^{-4}	2.5×10^{-4}

transition. (The percentage energy region for which the sum peak contains no contributions is ~30/1712≃2%).

The results of the pair production work are summarized and compared to theory in Table 7-2. For the E1, E2 and M1 transitions the theoretical pair formation coefficients are taken from the work of Lombard et al [10] while the E3 and M2 values are calculated using the Born approximation as discussed in Chapter 5. For the 1836 keV transition the multipolarity based on the pair formation coefficient is definitely E2. For the 2734 keV transition the best agreement between theory and experiment is for an M2 transition. However, from γ_{898} -γ_{1836} angular correlation [27] the transition must be E3. The lack of agreement between the calculated pair formation coefficient and experiment is believed to be a reflection of the inadequacy of the Born approximation.

CHAPTER 8

STUDY OF ^{205}Pb FOLLOWING THE DECAY OF ^{205}Bi

" 'Curiouser and curiouser!' cried Alice. "

..... Lewis Carroll

INTRODUCTION

^{205}Bi decays to ^{205}Pb by almost 100% electron capture. The subsequent transitions in ^{205}Pb are numerous and complicated. The decay scheme has been studied by numerous workers (16,28,29,30) and recently Kosanke et al (31) have reported on a study of ^{205}Bi using Ge(Li) detectors in which they were able to identify ~100 γ-rays. On the basis of γ-γ coincidence work Kosanke et al have proposed a partial decay scheme which is shown in Fig. 8-1. In the present work we have used the trochoidal β-ray spectrometer to measure several internal conversion coefficients and several internal pair formation coefficients.

It will be recalled that two transitions of ^{205}Bi were used in calibrating the spectrometer. (See Chapter 4.) These are the 703 and 1903 keV transitions and they are listed by Hamilton et al (6) as transitions for which the K-conversion coefficient is known to better than 10%. Since these transitions were used in calibrating the spectrometer the present work does not provide any information concerning them. It is well to point out though , that, historically, these transitions were used in calibrating the spectrometer but that there is independent evidence to support the calibrations. In particular,

FIG. 8-1

Decay scheme of ^{205}Bi.

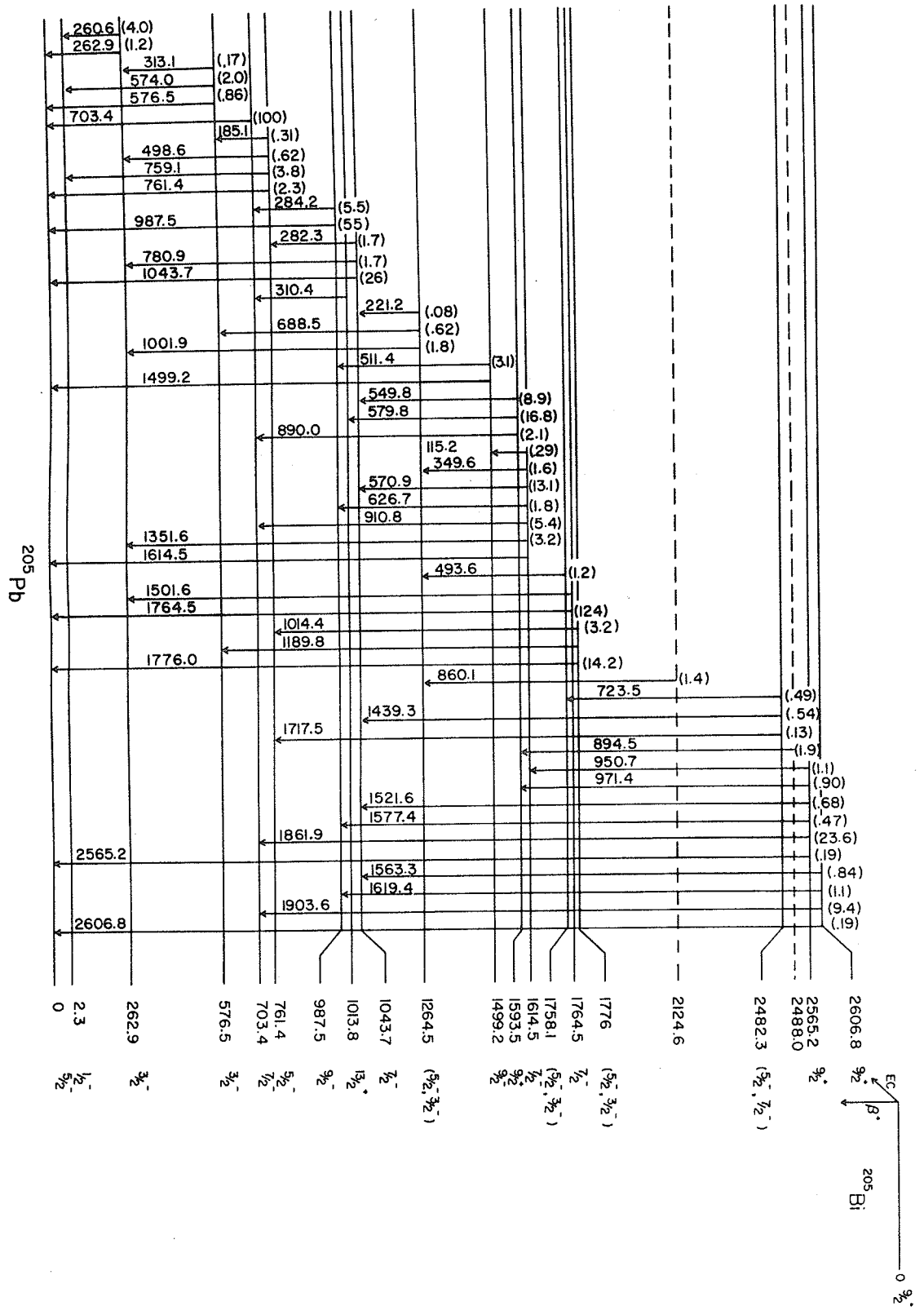
205 Pb
260.6 (4.0)
262.9 (1.2)
313.1 (.17)
574.0 (2.0)
576.5 (.86)
703.4 (100)
185.1 (.31)
498.6 (.62)
759.1 (3.8)
761.4 (2.3)
284.2 (5.5)
987.5 (55)
282.3 (1.7)
780.9 (1.7)
1043.7 (26)
310.4
221.2 (.08)
688.5 (.62)
1001.9 (1.8)
511.4 (3.1)
1499.2
549.8 (8.9)
579.8 (16.8)
890.0 (2.1)
115.2 (.29)
349.6 (1.6)
570.9 (13.1)
626.7 (1.8)
910.8 (5.4)
1351.6 (3.2)
1614.5
493.6 (1.2)
1501.6
1764.5 (124)
1014.4 (3.2)
1189.8
1776.0 (14.2)
860.1 (1.4)
723.5 (.49)
1439.3 (.54)
1717.5 (.13)
894.5 (1.9)
950.7 (1.1)
971.4 (.90)
1521.6 (.68)
1577.4 (.47)
1861.9 (23.6)
2565.2 (.19)
1563.3 (.84)
1619.4 (1.1)
1903.6 (9.4)
2606.8 (.19)
0
2.3
262.9
576.5
703.4
761.4
987.5
1013.8
1043.7
1264.5
1499.2
1593.5
1614.5
1758.1
1764.5
1776
2124.6
2482.3
2488.0
2565.2
2606.8
1/2- 5/2-
3/2-
3/2-
5/2- 1/2-
9/2-
13/2+
1/2-
(5/2-, 3/2-)
9/2+ 7/2+
(5/2-, 3/2-)
7/2-
(5/2-, 3/2-)
(5/2-, 7/2-)
9/2+
9/2+
EC
β+
205 Bi
0 9/2+

the values of the K-conversion coefficients for the 803, 1719, and 1878 keV transitions of ^{206}Bi and the 1836 keV transition of ^{88}Y, obtained using the spectrometer, are in good agreement with the values reported by previous workers. (See Chapters 6 & 7).

The conversion coefficients and internal pair formation coefficients were obtained by first measuring the relative γ-ray intensities of the various transitions and then the relative electron, or pair, strengths. The coefficients were then calculated from this data assuming that $\alpha_K = 1.05 \times 10^{-2}$ for the 703 keV transition.

GAMMA AND ELECTRON WORK

Gamma ray singles spectra were acquired using the Ortec $35cm^3$ co-axial Ge(Li) detector referred to in Chapter 6. A typical γ-spectrum is shown in Fig. 8-2. Besides being used to determine the relative γ-ray intensities the singles work was used to determine the energies of the stronger transitions. The energy determination was carried out in the same manner as for ^{206}Bi, (See Chapter 6), using a mixed ^{205}Bi plus standard sources spectrum. The results of this energy calibration are summarized in Table 8-1. The values obtained are compared to those of Vegors et al [30], Schmorak et al [29], and Kosanke et al [31]. There is excellent agreement between the results of Kosanke et al and those of the present work for all energies but above about 1600 keV there are small but significant discrepancies between the present values and those of Vegors et al and Schmorak et al.

FIG. 8-2

Typical ^{205}Bi γ-spectrum.

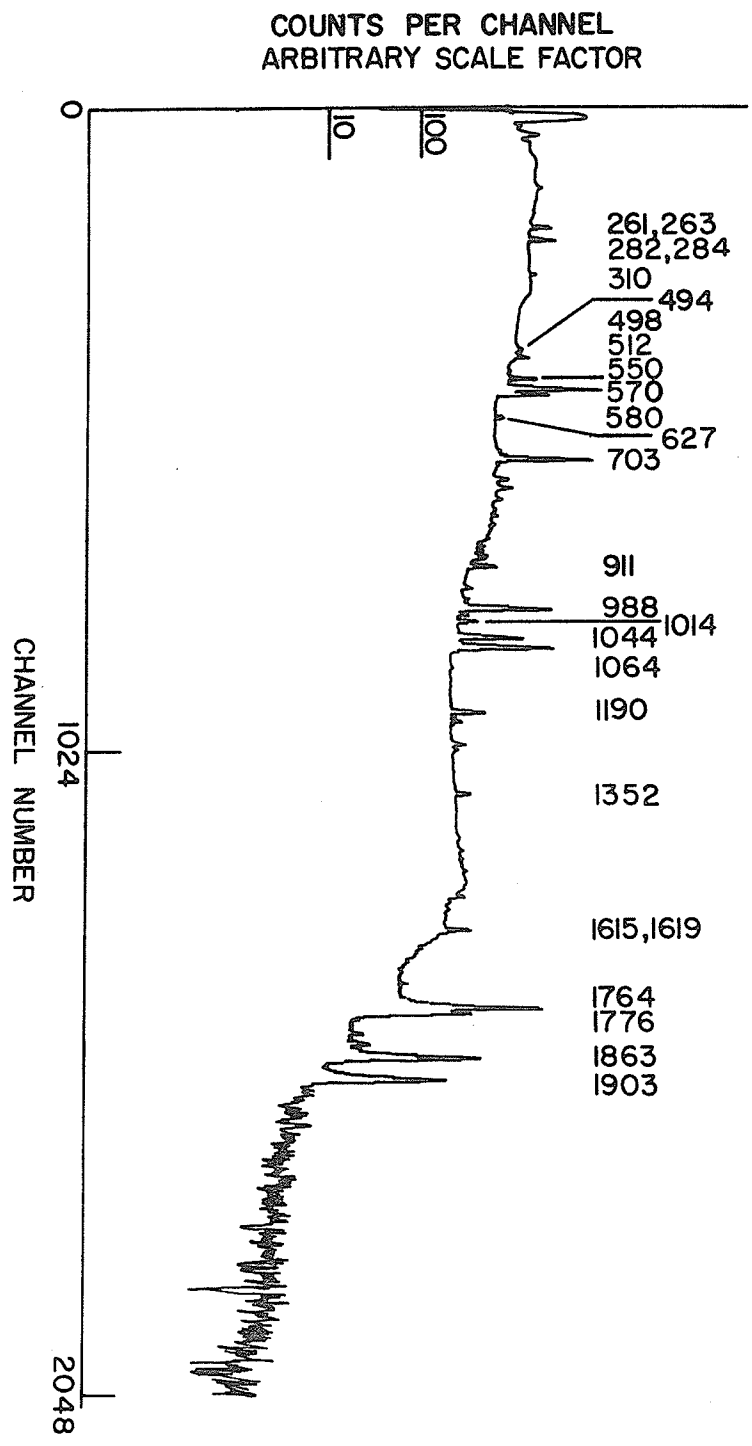
COUNTS PER CHANNEL
ARBITRARY SCALE FACTOR
0
10
100
261,263
282,284
310
494
498
512
550
570
580
627
703
911
988
1014
1044
1064
1190
1352
1615,1619
1764
1776
1863
1903
1024
2048
CHANNEL NUMBER

TABLE 8-1

Summary of the transition energies of the strong line in ^{205}Bi.

TABLE 8-1

TRANSITION ENERGY.

This Work	Vegors et al[30]	Schmorak et al[29]	Kosanke et al[31]
260.9±.5	260.5 262.9	260.5±.13	260.6 262.9
549.9±.3	550.1	550.0±.28	549.8
579.9±.3	580.0	580.0±.29	579.8
703.5±.3	703.4	703.3±.35	703.4
987.6±.3	987.8	987.8±.5	987.9
1043.5±.3	1043.7	1043.7±.5	1043.7
1189.8±.3	1190.0	1190.3±.6	1190.0
1614.0±.4	1615.4	1614.6±.8	1614.5
1764.2±.4	1766.1	1766.4±.9	1764.5
1775.8±.4	1777.7	1777.4±.9	1776.0
1861.8±.4	1863.9	1863.3±.9	1861.9
1903.4±.4	1905.9	1906.5±1.0	1903.6

TABLE 8-2

Summary of the relative γ-ray intensities obtained in the present study of ^{205}Bi.

TABLE 8-2

Transition Energy	Relative γ-ray Intensity	
	Present Work	Kosanke et al[31]
282.3	} 7.67	1.7
284.2		5.5
310.4	} .53	.34
313.1		.17
349.6	1.9	1.6
493.7	1.23	1.2
498.6	.64	.62
511.4	4.6	3.1
549.8	8.95	8.9
570.9	16.1	13.1
574.0	-	2.0
576.4	-	.86
579.8	17.6	16.8
626.7	1.67	1.8
703	100	100
745	-	1.8
759	4.5	3.8
761	1.5	2.3
911	4.9	5.4
988	49.3	55.3
1014	3.1	3.2
1044	23.8	25.8
1190	7.15	8.1
1352	3.55	3.25
1764	100	124

..... cont.

.....con't.

TABLE 8-2

Transition Energy	Present Work	Kosanke et al[31]
1776	12.1	14.2
1863	18.4	23.6
1903	7.3	9.4

In Table 8-2 we have compared the relative γ-ray intensities of those transitions for which we have obtained conversion coefficients to the results of Kosanke et al [31]. A great many additional γ peaks were observed in the spectra but the emphasis of the present study was on the electron and pair spectra and hence we have not included these in the present report. As can be seen from Table 8-2 there is general agreement between the present results and those of Kosanke et al. For the higher energies, however, the relative γ-ray intensities obtained by Kosanke et al tend to be about 20% higher than those of the present work.

It should be noted that the ^{205}Bi had, as a contaminant, 30y ^{207}Bi which contributes γ-peaks at 570, 1064 and 1770 keV. To obtain the relative γ-intensity of the 570keV ^{205}Bi transition the contribution from ^{207}Bi must be subtracted. This was done by predicting the number of ^{207}Bi 570 keV γ's from the observed number of 1064 ^{207}Bi γ's, using the relative γ-ray intensities of Lederer et al[32]. Here we have assumed that the 1064 keV peak was entirely attributable to ^{207}Bi. The measured intensity of the 1770 ^{207}Bi γ-ray relative to the 1064 keV transition supports this assumption. At the time the γ-spectra were acquired it turned out that approximately 33% of the 570 keV γ-ray peak was contributed by ^{207}Bi.

The conversion spectrum of ^{205}Bi is very complicated since for every γ-transition we observe the K, L and M conversion lines. However, we were successful in extracting the relative electron intensities of a number of conversion peaks. Two electron sources were used

and for each source independent runs were made on each side of the spectrometer. A typical electron spectrum is shown in Fig. 8-3. A number of the conversion peaks are multiplets and it was necessary to do some simple peak fitting to extract the contributions from the different transitions. The procedure followed was the same as that described in Chapter 6. The peak shapes adopted for the fitting curves were those of the 615 keV peak, (703-K conversion line), and the 1102 keV peak, (the 1190-K conversion line).

The results of the electron work are summarized in Tables 8-3 and 8-4. In Table 8-3 we have compared the relative electron intensities to the values obtained by Schmorak et al [29] and by Stockendal and Hultberg [16]. This comparison is interesting because Lederer et al [5] list the relative intensities of the 282-K plus 284-K, 550-K, 703-K, 911-K,1044-K, 1190-K and 1766-K conversion lines, as measured by Schmorak et al, as efficiency calibration standards. For the majority of the transitions there is reasonable agreement between the values obtained in the present work and those of Schmorak et al but for the 282-K plus 284-K, and the 1765-K peaks there is a serious discrepancy between the two values. In both these cases the present values are closer to those of Stockendal. It is doubtful, then, if these two electron peaks can be used as efficiency calibration standards.

In Table 8-4 we have calculated the conversion coefficients for the various transitions, based on the relative γ-ray and electron intensities, assuming that $\alpha_K = 1.05 \times 10^{-2}$ for the 703 keV transition.

FIG. 8-3

Typical ^{205}Bi electron spectrum.

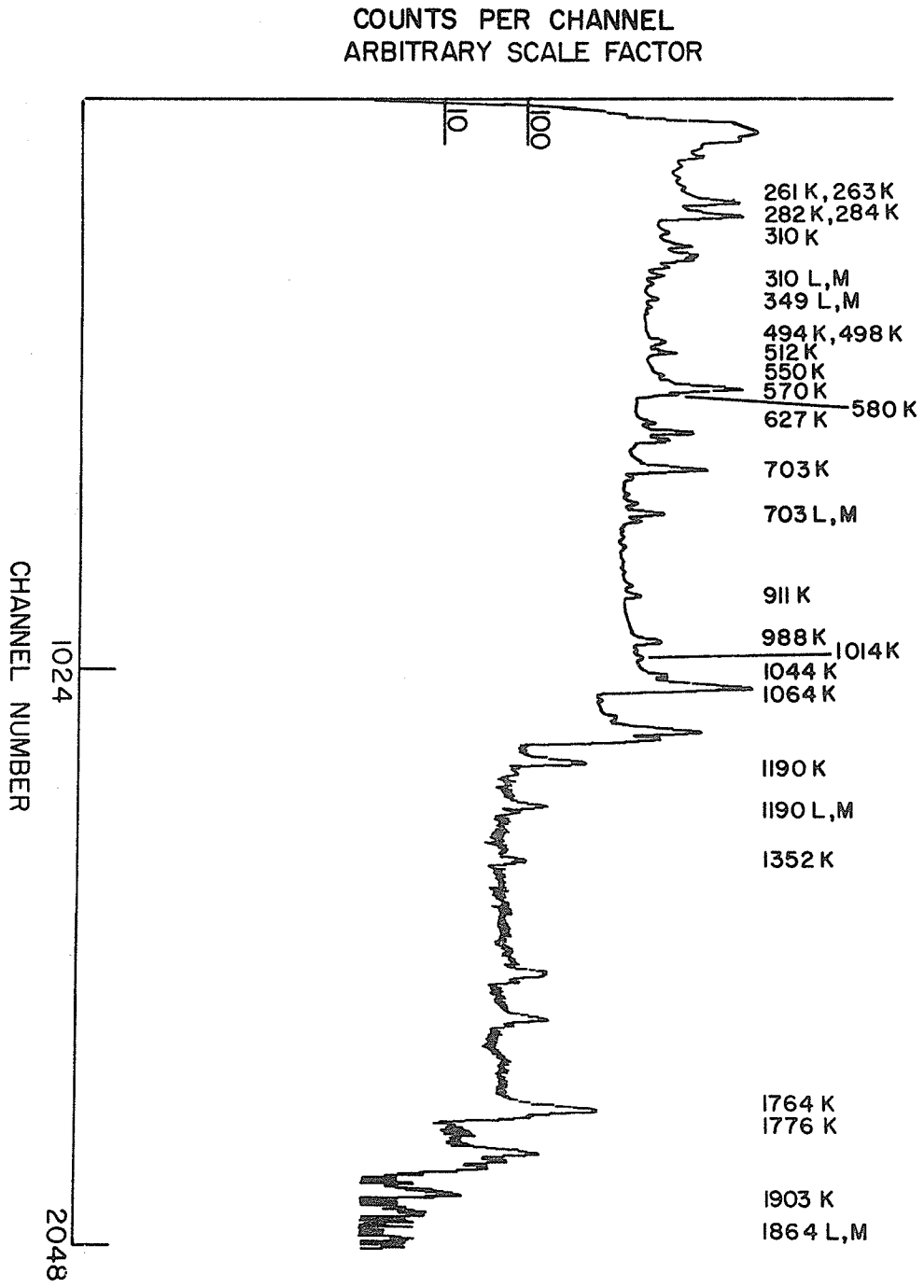
COUNTS PER CHANNEL
ARBITRARY SCALE FACTOR
10
100
261 K, 263 K
282 K, 284 K
310 K
310 L, M
349 L, M
494 K, 498 K
512 K
550 K
570 K
580 K
627 K
703 K
703 L, M
911 K
988 K
1014 K
1044 K
1064 K
1190 K
1190 L, M
1352 K
1764 K
1776 K
1903 K
1864 L, M
CHANNEL NUMBER
1024
2048

TABLE 8-3

Summary of the relative electron intensities obtained in the present study of ^{205}Bi.

TABLE 8-3

Conversion Line	Relative Electron Intensity		
	Present Work	Schmorak et al[29]	Stockendal and Hultberg[16]
282-K+284-K	290±40	200	240
310-K+313-K	9.3±3		
310-L+313-L	6.7±1		
310-L+M+313-L+M	9.8±2		
349.5-K	43 ±5	28	30
349-L	6.6±.5		
349-L+M	8.2±1		
494-K	9.7±1	11	
498-K	4.7±.4		
512-K	19.0±2	22	
550-K	7.9±1	6.3	6.3
570-K	90±10	74	89
580-K	24.3±3	24	24
627-K	8.4±.9	6.7	
703-K	100	100	100
703-L	22.7±1.5		
703-L+M	30.5±2		
745-K	1.5±.2		
759-K+761-K	5.1±.5		
911-K	8.1±.8	9.8	8.4
988-K	24.7±2.5	27.5	27
1014-K	5.1±.6	4.9	
1044-K	34.1±4	32.5	28
1190-K	6.4±.6	7.6	
1190-L	1.47±.15		
1190-L+M	2.0±.2		
1352-K	.90±.09	1.1	
1352-L	.16±.03		

..... con't.

con't.

TABLE 8-3

Conversion Line	Relative Electron Intensity Present Work	Schmorak et al[29]	Stockendal and Hultberg[16]
1499-K+1503-K	.29±.07		
1552-K	.65±.15		
1764-K	27±3	43.6	.34
1776-K	2.9±.3	5.2	4.0
1863-L	.15±.03		
1863-L+M	.20±.03		
1903-K		.60	.40

TABLE 8-4

Summary of the conversion coefficients obtained in the present study of ^{205}Bi.

TABLE 8-4

Conversion Line	Relative γ-ray Intensity	Relative Electron Intensity	Conversion Coefficient Experimental	Conversion Coefficient Theoretical	Suggested Multipolarity
282.3-K	} 7.57	} 290±40	}$4.0\pm.5\times10^{-1}$	} 4.2×10^{-1}	M1
284.2-K				both M1	M1
310-K	.34	} 9.3±3	}$1.9\pm.5\times10^{-1}$	} 2.2×10^{-1}	E3
313-K	.17				M1
310-L+M	.34	} 9.8±2	}$2.0\pm.4\times10^{-1}$	} 2.7×10^{-1}	E3
313-L+M	.17				M1
350-K	1.91	43±5	$2.4\pm.3\times10^{-1}$	2.4×10^{-1}	M1
350-L	1.91	6.6±.5	$3.6\pm.5\times10^{-2}$	4.0×10^{-2}	M1
350-M	1.91	2.1±.3	$1.2\pm.3\times10^{-2}$	1.0×10^{-2}	M1
494-K	1.23	9.7±1.0	$8.3\pm1.0\times10^{-2}$	9.5×10^{-2}	M1
498-K	.64	4.7±.5	$7.7\pm1.0\times10^{-2}$	9.3×10^{-2}	M1
512-K	4.55	19.0±2.0	$4.4\pm.4\times10^{-2}$	8.7×10^{-2} or 2.0×10^{-2}	M1 or E2
550-K	8.95	7.9±2.0	$9.2\pm2.0\times10^{-3}$	6.5×10^{-3}	E1
570-K	16.1	90±10	$5.9\pm.6\times10^{-2}$	6.5×10^{-2}	M1
580-K	17.6	24.3±3.0	$1.5\pm.2\times10^{-2}$	1.5×10^{-2}	E2
627-K	1.67	8.4±.9	$5.3\pm.6\times10^{-2}$	5.0×10^{-2}	M1
703-K	100	100	1.05×10^{-2}*	1.05×10^{-2}*	
703-L	100	22.7±1.5	$2.4\pm.2\times10^{-3}$	2.4×10^{-3}	E2
703-M	100	7.8±1	$8.2\pm1.0\times10^{-4}$	6.0×10^{-3}	

....con't.

Conversion Line	Relative γ-ray Intensity	Relative Electron Intensity	Conversion Coefficient: Experimental	Conversion Coefficient: Theoretical	Suggested Multipolarity
745-K	1.8	1.5±.2	$8.8\pm2.\times10^{-3}$	9.3×10^{-3}	E2
759-K	4.5	} 5.1±.6	} 8.9×10^{-3}	} 8.8×10^{-3}	E2
761-K	1.5				E2
911-K	4.9	8.1±.8	$1.7\pm.2\times10^{-2}$	1.95×10^{-2}	M1
988-K	49.3	24.7±.2	$5.3\pm.6\times10^{-3}$	5.5×10^{-3}	E2
1014-K	3.1	5.1±.5	$1.7\pm.3\times10^{-2}$	1.5×10^{-2}	M1
1044-K	23.8	3.4±.3	$1.5\pm.2\times10^{-2}$	1.4×10^{-2}	M1
1190-K	7.15	6.4±.6	$9.4\pm.9\times10^{-3}$	9.7×10^{-3}	
1190-L	7.15	1.5±.2	$2.2\pm.3\times10^{-3}$	1.8×10^{-3}	M1
1190-M	7.15	.30±.06	$4.4\pm.9\times10^{-4}$	3.3×10^{-4}	
1352-K	3.55	.9±.1	$2.7\pm.3\times10^{-3}$	3.1×10^{-3}	
1352-L	3.55	.16±.03	$4.7\pm1.0\times10^{-4}$	5.4×10^{-4}	E2
1499-K	.94	} .3±.1	} $2.0\pm.6\times10^{-3}$	} 2.5×10^{-3}	E2
1503-K	.66				E2
1552-K	3.2	.65±.1	$2.2\pm.3\times10^{-3}$	2.3×10^{-3}	E2
1764-K	100	27±3	$2.8\pm.3\times10^{-3}$	3.5×10^{-3} or 1.7×10^{-3}	M1 or E2
1776-K	12.1	2.9±.3	$2.5\pm.3\times10^{-3}$	3.5×10^{-3} or 1.7×10^{-3}	M1 or E2

.....con't

Conversion Line	Relative γ-ray Intensity	Relative Electron Intensity	Conversion Coefficient		Suggested Multipolarity
			Experimental	Theoretical	
1863-L	18.4	.15±.03	$8.6\pm1.6\times10^{-5}$	1.05×10^{-4}	E1
1863-L+M	18.4	.20±.02	$1.2\pm.2\times10^{-4}$	1.2×10^{-4}	
1903-K	7.3	.50±.05	6.7×10^{-4}*	7.2×10^{-4}	E1

* Assumed in calibrating the spectrometer.

We have also included in Table 8-4 the theoretical conversion coefficients [22], which lie closest to the experimental values and the suggested multipolarity of the transitions.

The analysis of the data in many cases is not straight forward and it is necessary to consider these cases in some detail. Let us begin by considering the 570 and 580 keV transitions. The energies of the K-conversion electrons from these transitions are 482 and 492 keV respectively. In this energy region there are several conversion lines besides the 570 and 580 K-lines. There are (1) lines at 478 and 483 keV attributable to the L-conversion electrons of the 494 and 499 keV transitions, (2) lines at 490 and 495 keV attributable to the M-conversion electrons of the 494 and 499 keV transitions and (3) a line at 496 keV attributable to the L-conversion electrons of the 512 keV transition. An added difficulty is the presence of ^{207}Bi as a contaminant which has a conversion line at 482 keV corresponding to the K-electrons of the 570 keV ^{207}Pb transition. By peak shape analysis we were able to obtain the number of counts in two peaks centered at 482 keV and 492 keV respectively. Let us consider the 482 keV peak first. We have assumed that this peak consists of the K-conversion electrons from the 570 keV transitions of ^{205}Bi and ^{207}Bi and the L-conversion electrons from the 494 and 499 keV. transitions of ^{205}Bi. Since ^{207}Bi was used in calibrating the spectrometer the relative counting rates of the 570-K and the 1064-K conversion peaks of ^{207}Bi are known and from the observed number of 1064-K electrons we calculated the number of ^{207}Bi 570-K electrons. Here we assumed that there is no 1064 keV transition in ^{205}Bi.

It was found that approximately 60% of the 482 keV electron peak was attributable to ^{207}Bi. It was also possible to estimate the contributions to the 482 keV peak from the 494-L and 499-L conversion lines. The K-conversion coefficients for these transitions imply that they are both M1. (See Table 8-4). Using the theoretical K/L ratios for M1 transitions and the observed number of K-conversion electrons we calculated the number of L-conversion electrons and found that, having already subtracted the contribution from ^{207}Bi, the 482 keV peak contained a total contribution of approximately 2% from the 494 and 499-L conversion electrons. By subtracting out these contributions we were finally able to obtain the number of ^{205}Bi 570-K electrons in the 482 keV peak, and, from this value, the relative K-electron intensity and the K-conversion coefficient shown in tables 8-3 and 8-4.

Next let us consider the 492 keV electron peak, which we assume consists of the 580-K conversion line, the 512-L conversion line and the 494 and 499-M conversion lines. The number of 494-M and 499-M conversion electrons in this peak was estimated from the theoretical K/M ratios for these transitions assuming they are both M1, and were found to account for approximately 2% of the total number of counts in the peak. An estimate of the contribution from the 512-L electrons was also obtained. In discussing this value it is necessary to consider the 512 keV transition in some detail since the multipolarity of this transition is in doubt. We have obtained $\alpha_K = 4.4 \times 10^{-2}$ for the 512 keV transition. (See Table 8-4). This value lies between the conversion coefficients for an E2, ($\alpha_K = 2.0 \times 10^{-2}$), and an M1, ($\alpha_K = 8.7 \times 10^{-2}$), transition.

Thus the transition may be E2, M1 or an admixture of E2 and M1. In this respect it is worth noting that the relative γ-ray intensity obtained by Kosanke et al [31] differs appreciably from the value obtained in the present work and leads to a conversion coefficient of $\alpha_K = 6.4 \times 10^{-2}$. (See Table 8-2) This latter value leads to a E2, M1 mixing of 66% M1 plus 34% E2 while our value of 4.4×10^{-2}, suggests a mixing of 67% E2 plus 33% M1. Because of the uncertainty in the nature of the 512 keV transition we have calculated two estimates of the 512-L contribution to the 492 keVpeak, assuming firstly that the transision is "pure" E2 for which K/L = 3.2/1 and then that it is "pure" M1 for which K/L = 6.0/1. We have then used the average of these two estimates. In this manner we have estimated that the 512-L conversion line accounts for about 14% of the 492 keV peak.

So far in our discussion of the 570 and 580 keV transitions we have ignored the 574 and 576 keV transitions observed by Kosanke et al (see Table 8-2). The data has been analysed so that the contributions from these transitions have been included in the contributions from the 570 and 580 keV transitions. Although the exact division of the contributions of the 574 and 576 keV transitions between the 570 and 580 peaks, (γ-peaks and electron lines), is not known we know that the conversion coefficients for the 570 and 580 keV transitions, shown in Table 8-4, represent some kind of "average". Since the 570 and 580 keV transitions are much stronger than the 574 and 576 keV transitions, (see Table 8-2), these "average" coefficients will be dominated by them so that the suggested multipolarities shown in Table 8-4 are valid.

Several other conversion electron lines were corrected for contributions from other transitions. The K-conversion peak of the 627 keV transitions was corrected for contributions from the 550-L conversion electrons. This contribution was estimated from the observed 550-K electron strength assuming that the 550 keV transition is E1, for which K/L = 6.2/1. In this case the correction was ~14% of the peak intensity. Similarily the 703-K line was corrected for contributions from the 627-L and 627-M conversion electrons, assuming K/L+M = 5/1, (M1) and the 988-K line was corrected for contributions from 911-L and 911-M conversion electrons assuming K/L+M =5/1, (M1). These corrections accounted for 2% and 6% of the respective peak intensities.

It is well to point out that the presence of ^{207}Bi as a contaminant complicated, somewhat, the analysis of the 1764-K and 1776-K conversion lines since the 1770-K line of ^{207}Bi lies between these two peaks. However, we were able, by peak shape analysis, to extract the contributions of these three peaks. Since ^{207}Bi was used as a calibration source the counting rate of the 1770-K line relative to the 1064-K line was known. By comparing the number of 1770-K counts obtained in the peak shape analysis with the number predicted from the observed number of 1064-K counts we were able to check the validity of the analysis. In all cases the two values agreed to within ±10%.

The conversion coefficients obtained in the present study suggest a multipole assignment for the various transitions. It is interesting to compare these assignments with those of other workers and this comparison will be made following the discussion of the internal pair formation study.

INTERNAL PAIR FORMATION

Several pair sum spectra were acquired. A typical sum spectrum is shown in Fig. 8-4 where the pair sum peaks corresponding to the 1903, 1863, 1776 plus 1764 (unresolved), and the 1619 plus 1615 keV (unresolved) transitions can be seen. Although the 1764 and 1776 sum peaks are not resolved we were able, by peak shape analysis, to extract the relative contributions from these two transitions. However, we were unable to separate the 1619 and 1615 sum peaks from one another. The pair sum peak resolution obtained in the present experiment was ~12-13 keV F.W.H.M. This good resolution was achieved because the large number of conversion electron lines facilitated the gain matching of the two sides of the spectrometer.

From the pair sum spectra we were able to obtain the total internal pair formation coefficients for the 1615 plus 1619, 1765, 1776, 1863 and 1903 keV transitions. The analysis of the data was similar to that for the ^{206}Bi and ^{88}Y cases. (See Chapters 6 and 7) However, it is necessary to consider several points in some detail. By gating on the 1765 plus 1776 pair sum peak we obtained the corresponding positron and electron spectra, uncorrected for efficiency, which are shown in Fig. 8-5. (The reader will immediately note the presence of the 703-K and 703-L+M conversion lines in the electron continuum. The presence of these lines is readily explainable but for the moment let us pass over this point and continue with a discussion of the data analysis.) Using the shape of the positron continuum we were able to obtain for the 1764 plus 1776 pair sum peak, in the manner described in Chapter 6, an effective pair detection efficiency, $\epsilon_\pi = \frac{3.11}{1.05} \times 10^{-2}$.

FIG. 8-4

Typical ^{205}Bi pair sum spectrum.

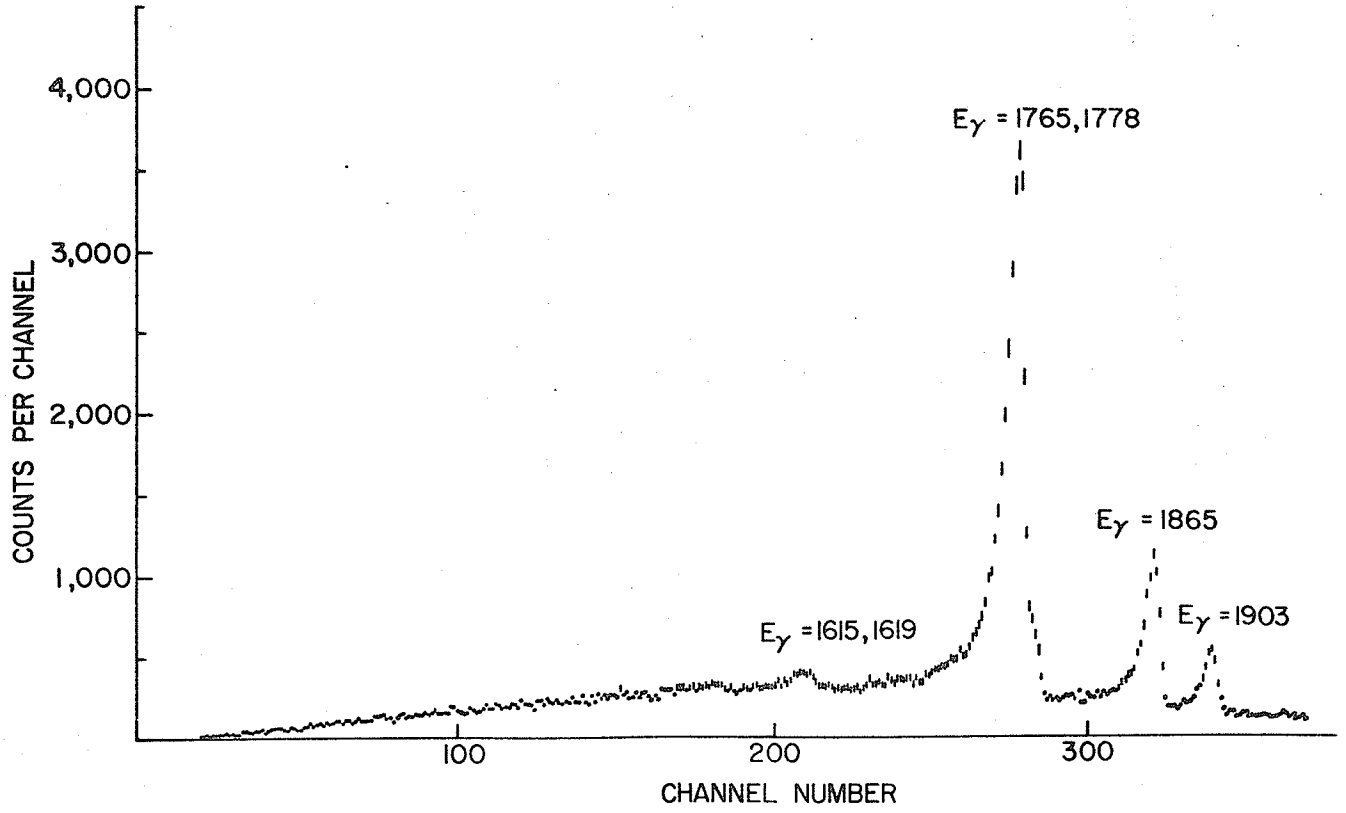
4,000
3,000
2,000
1,000
COUNTS PER CHANNEL
Eγ = 1765, 1778
Eγ = 1865
Eγ = 1903
Eγ = 1615, 1619
100
200
300
CHANNEL NUMBER

FIG. 8-5

The electron and positron continua obtained by gating on the 1764 plus 1776 pair sum peak.

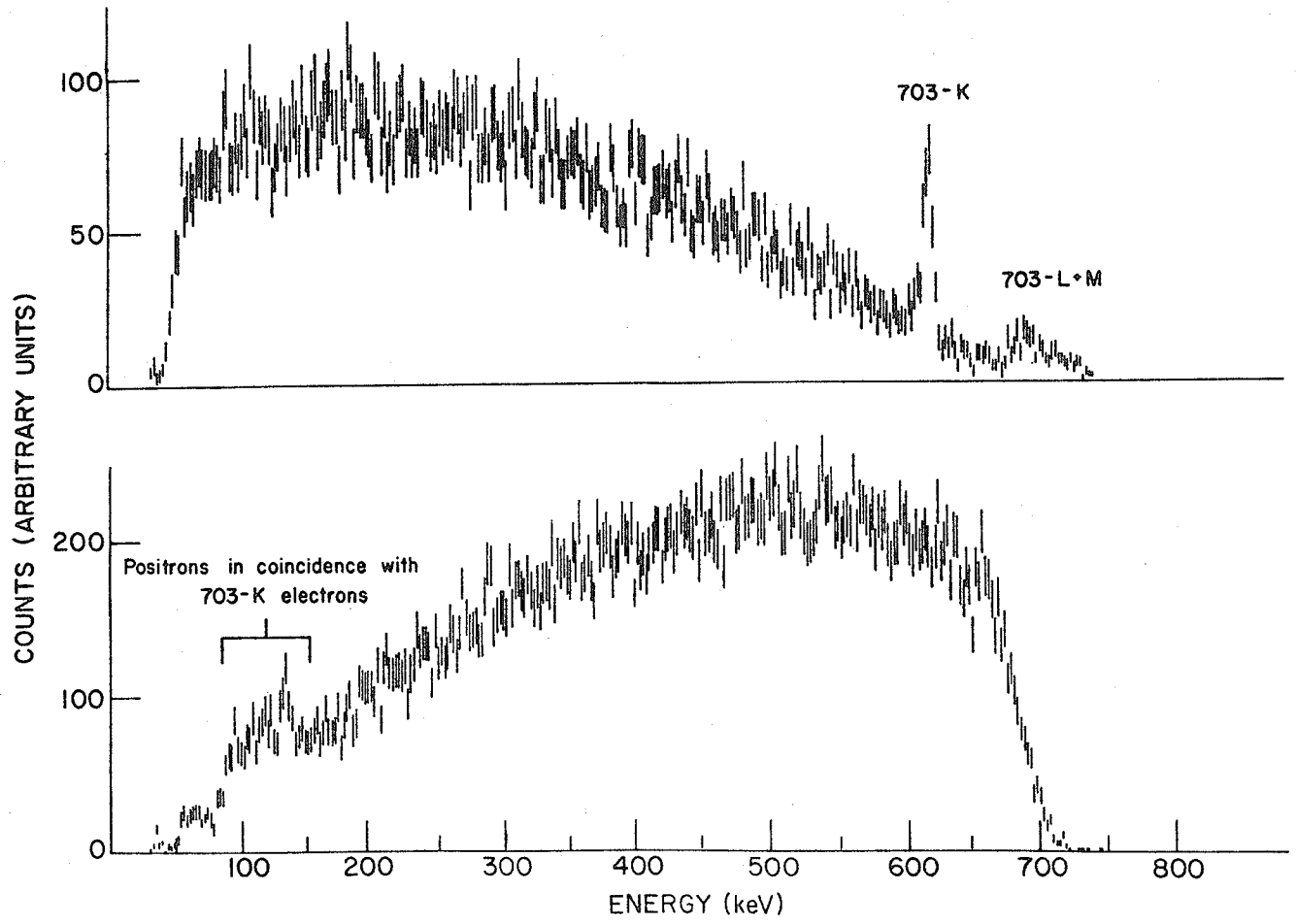
703-K
703-L+M
100
50
0
200
100
0
Positrons in coincidence with
703-K electrons
COUNTS (ARBITRARY UNITS)
100
200
300
400
500
600
700
800
ENERGY (keV)

This effective efficiency includes the effects of the variation of pair detection efficiency with positron energy. Because of the reduced intensity of the other pair sum peaks we did not "gate" on them to obtain the corresponding positron continua. Thus we could not determine, directly, the effective pair detection efficiencies for these peaks. However, we were able to estimate the effective efficiencies. For electron (positron) energies $\lesssim$530 keV the measured full energy peak detection efficiencies of both sides of the spectrometer are constant. (See Fig. 4-9). Thus the pair detection efficiency, for $E_\gamma \lesssim 1550$ keV, does not vary with the energy of the positron, and is given by $\epsilon_\pi = 3.11 \times 10^{-2}$. To estimate the effective pair detection efficiencies for the 1615 plus 1619, 1863 and 1903 pair sum peaks we have assumed that ϵ_π varies linearly with E_γ, for $E_\gamma \gtrsim 1550$ keV, and we have used the effective efficiency for the 1765 plus 1776 sum peak to define the slope. The estimates obtained were $\frac{3.11}{1.02} \times 10^{-2}$, $\frac{3.11}{1.07} \times 10^{-2}$ and $\frac{3.11}{1.08} \times 10^{-2}$ respectively for E_γ = 1615, 1863 and 1903 keV.

From the positron and electron continua obtained by gating on the 1765 plus 1776 sum peak we were able to determine that this sum peak contained no contributions from pair events for which $T \pm \lesssim 50$ keV. Since the relative number of pair events for which $T_+ \lesssim 50$ keV is negligible only the high-energy cut-off in the positron continuum is important. For the 1764 keV transition the effect of this cut-off was estimated by extrapolating the experimental positron continuum to the end point energy, 743 keV, from the cut-off energy, 693 keV. In this way it was estimated that the 1764 pair sum peak

contained no contributions from 13% of the pair events and the 1764 data was corrected correspondingly.

For the 1764 keVtransition the positron energy region from which the sum peak contains no contributions represents 6.7% of the total "open" energy region. Because of the Coulomb repulsion of the positrons 13% of the total number of pair events occur in this region. Thus the effective size of the "closed" energy region is doubled. To estimate the correction which must be applied to the 1615 plus 1619, 1863 and 1903 pair sum peaks, occassioned by the high energy cut-off in the positron spectrum, we have calculated the percentage size of the closed energy region, assuming the cut-off occurs 50 keV from the end point energy, and have then doubled the result. Thus for the 1863 keV transition the "closed" region is 5.9% of the total availalbe energy region which leads us to estimate that the 1863 sum peak contains no contributions from 12% of the total number of pair events. The datum was corrected accordingly. For the 1615 plus 1619 and 1903 keV transitions the corresponding corrections were estimated to be 16% and 11% respectively.

As was mentioned previously the presence of the conversion lines of the 703 keV transition in the electron continuum, obtained by gating on the 1765 plus 1776 pair sum peak, is readily explained. The appearance of these lines results from a genuine coincidence. One mode by which ^{205}Bi decays, albeit a weak one, is the emission of a β^+ particle [31], populating the 703 keV level of ^{205}Pb. If this level then de-excites by the ejection of a conversion electron the electron will be in "true" coincidence with the positron. Since the positrons from the β^+ decay form a continuum, $T_{max} \sim 980$ keV, the summed output of the spectrometer

will also be a continuum for events of this type. The pair sum peaks lie on top of this continuum. To obtain the total number of counts in the full energy pair sum peak a straight line background subtraction was made. Therefore events of this type are subtracted out and do not lead to an incorrect estimate of the pair formation coefficient. However, the conversion lines do appear in the electron spectrum since the ΔE window setting of the S.C.A. used to gate the electron side of the spectrometer, does not discriminate between background events and pair events. Since the conversion electrons have a unique energy, the summed output of the system, for events of this nature, will lie within the ΔE window setting of the single channel analyser, S.C.A., only if the positron has an energy $E_{\beta^+} = (E_{S.C.A.} - E_{e^-}) \pm \Delta E/2$ where $E_{S.C.A.}$ is the energy level at which the S.C.A. is set and E_{e^-} is the energy of the conversion line. Thus one would expect to see a "mono-energetic" positron peak in the positron continuum and in fact this peak can be seen in Fig. 8-5.

As was stated at the beginning of this section we were able to extract the relative intensities of the 1764 and 1776 sum peaks by peak shape fitting. This process is illustrated in Fig. 8-6. The points are the experimental counts per channel, following a straight line background subtraction, and the dashed curve represents the estimated contribution from the 1776 keV transition. This curve has the same shape as the 1863 sum peak. Up until now we have ignored the presence of ^{207}Bi as a contaminant. This nuclide has a trans-

FIG. 8-6

Typical 1764 plus 1776 pair sum peak showing the separation of the contributions from the two transitions.

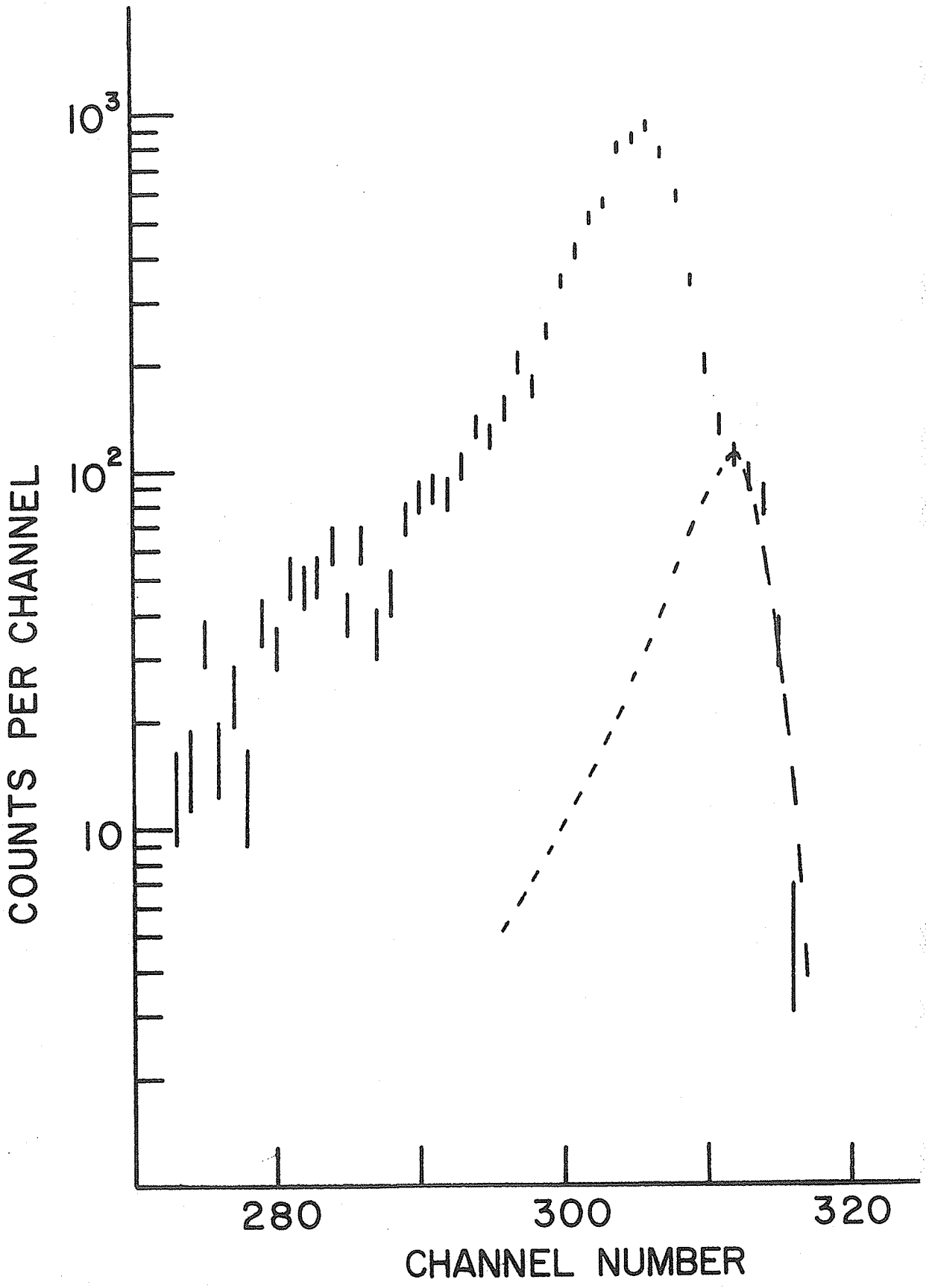
COUNTS PER CHANNEL
10^3
10^2
10
280
300
320
CHANNEL NUMBER

ition of 1770 keV which will contribute a peak to the pair sum spectrum which lies midway between the 1764 and 1776 sum peaks. As will be described below we were able to estimate the number of 1770 ^{207}Bi pair sum counts from the observed intensity of the 1064-K conversion line. It was found that this transition accounted for ~1-2% of the total number of counts in the 1764 plus 1776 sum peak. From the relative γ-ray intensities of the 1764 and 1776 keV transitions we expect the 1764 plus 1776 pair sum peak to contain about a 10% contribution from the 1776 keV transition. Thus the main contributions to the peak are from the 1765 and 1776 keV transitions of ^{205}Bi and the contribution from ^{207}Bi is much smaller than either of these. Therefore the extraction of the 1776 keV contribution by peak shape fitting is valid. Having effected the separation of the sum peak into two peaks, these individual peaks were then corrected for contributions from the 1770 keV transition of ^{207}Bi by assuming that the 1770 counts were equally divided between the two peaks. This correction was ~1% for the 1764 keV transition and ~5-10% for the 1776 keV transition.

To correct the ^{205}Bi data for contributions from the 1770 keV transition of ^{207}Pb an independent experiment was performed to obtain the observed ratio of the 1770 pair sum peak intensity to the 1064-K line intensity. Two ^{207}Bi sources, previously used in calibrating the spectrometer, were used to obtain this ratio. A sample sum spectrum is shown in Fig. 8-7. From this ratio the pair formation coefficient for this transition was extracted assuming the re-

FIG. 8-7

Typical ^{207}Bi pair sum spectrum in the vicinity of the 1770 pair sum peak.

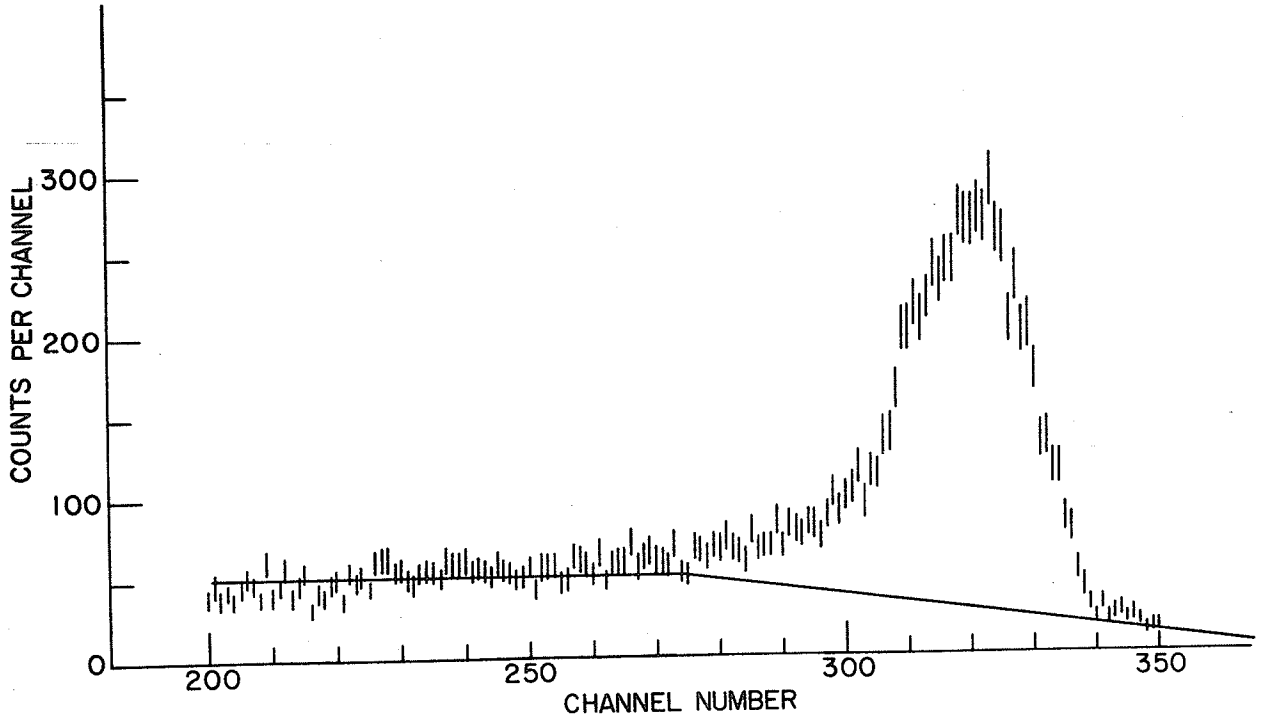
COUNTS PER CHANNEL
300
200
100
0
200
250
300
350
CHANNEL NUMBER

lative γ-ray intensities of Lederer et al [32] for ^{207}Bi. The results of this work are summarized in Table 8-5 where we have compared the measure pair formation coefficient to the theoretical calculations of Lombard et al [10]. The best agreement between theory and experiment is for an E2 multipolarity which agrees with the decay scheme given by Lederer et al [32].

The results of the ^{205}Bi pair production work are presented in Table 8-6. Again we have compared the results to the theoretical calculations of Lombard et al [10]. From the pair formation coefficient the 1764 and 1776 keV transitions are either M1 or E1 whereas the K-conversion data suggests an assignment of either M1 or E2. Combining the two sets of data we conclude that the 1764 and 1776 keV transitions are both M1. The pair data for the 1863 and 1903 keV transitions indicate that both these transitions are E1 in agreement with the conversion data. It is difficult to draw any firm conclusions concerning the 1615 and 1619 keV transitions from the combined pair formation coefficient. However, if we assume that the 1615 keV transition is E2 and the 1619 keV transition is E1 then the effective theoretical pair coefficient is $\alpha_\pi = 1.2 \times 10^{-4}$. This value is in reasonable agreement with the measured coefficient and therefore the present work tentatively suggests such a multipole assignment for these transitions.

TABLE 8-5

Summary of the pair formation study of the 1770 keV transition of ^{207}Pb.

TABLE 8-5

E_γ = 1770 keV

Quantity	Experimental Value	E1	E2	M1
α_π	$1.9\pm.6\times10^{-4}$	3.3×10^{-4}	1.65×10^{-4}	2.75×10^{-4}
$e^\pm/e_K$-	$.09\pm.02$	.41	.090	.073

TABLE 8-6

Summary of the pair formation study of ^{205}Bi.

TABLE 8-6

Transition	Quantity	Experiment	E1	E2	M1
1615 plus 1619	α_π	$1.5\pm.4\times10^{-4}$	2.3×10^{-4}	1.0×10^{-4}	1.75×10^{-4}
1764	α_π	$3.4\pm.6\times10^{-4}$	3.3×10^{-4}	1.6×10^{-4}	2.70×10^{-4}
	α_K	$2.8\pm.3\times10^{-4}$	8.2×10^{-4}	1.9×10^{-3}	3.8×10^{-3}
	$e^\pm/e_K$	$.12\pm.02$	.40	.087	.071
1776	α_π	$3.0\pm.6\times10^{-4}$	3.4×10^{-4}	1.7×10^{-4}	2.8×10^{-4}
	α_K	$2.5\pm.3\times10^{-4}$	8.2×10^{-4}	1.9×10^{-3}	3.7×10^{-3}
	$e^\pm/e_K$	$.12\pm.02$	.41	.092	.076
1863	α_π	$4.5\pm.8\times10^{-4}$	4.0×10^{-4}	2.1×10^{-4}	3.4×10^{-4}
	α_{L+M}	$1.2\pm.2\times10^{-4}$	1.2×10^{-4}	2.8×10^{-4}	5.2×10^{-4}
1903	α_π	$4.3\pm.8\times10^{-4}$	4.2×10^{-4}	2.2×10^{-4}	3.6×10^{-4}
	α_K	6.7×10^{-4}	7.3×10^{-4}	1.6×10^{-3}	3.1×10^{-3}
	$e^\pm/e_K$	$.64\pm.12$	.59	.14	.12

TABLE 8-7

Summary of the multipole assignments suggested by the present work. The present assignments are compared with those of Vegors Jr. et al (30) a, Stockendal et al (16), b, Schmorak et al (29), c, Stockendal (33), d, and Ahluwalia et al (34),e.

TABLE 8-7

Transition	Multipolarity Suggested in Present Work	Nature of Transition according to Kosanke et al (31)	Multipolarity Suggested by Previous Workers
282 keV	M1	$7/2^- \rightarrow 5/2^-$	M1 or M2[a], M1[b], M1[c]
284 keV	M1	$9/2^- \rightarrow 7/2^-$	M1 or M2[a], M1[b], M1[c]
310 keV	E3	---	E3[d]
313 keV	M1	$3/2^- \rightarrow 3/2^-$	------
349 keV	M1	$7/2^- \rightarrow (5/2^-, 3/2^-)$	M1 or E2[a], M1[c]
494 keV	M1	$? \rightarrow (5/2^-, 3/2^-)$	M1 or E2[a]
498 keV	M1	$5/2^- \rightarrow 3/2^-$	------
512 keV	M1 or E2	$9/2^- \rightarrow 9/2^-$	M1 or E2[a], M1[b], M1[c]
550 keV	E1	$9/2^+ \rightarrow 7/2^-$	E1 or E2[a], E1[b]
570 keV	M1	$7/2^- \rightarrow 7/2^-$	M1 or M2[a], M1[b], M1[c]
580 keV	E2	$9/2^+ \rightarrow 13/2^+$	E1 or E2[a], E2[b]
627 keV	M1	$7/2^- \rightarrow 9/2^-$	E2[a], E2[c]
703 keV	E2	$7/2^- \rightarrow 5/2^-$	E2[a], E2[b], E2+1%M1[e]

..... con't

Transition	Multipolarity Suggested in Present Work	Nature of Transition according to Kosanke et al (31)	Multipolarity Suggested by Previous Workers
745 keV	E2	----	------
759 keV	E2	$5/2^- \rightarrow 1/2^-$	------
761 keV	E2	$5/2^- \rightarrow 5/2^-$	------
911 keV	M1	$7/2^- \rightarrow 7/2^-$	E2[a], E2[b], E2[c], M1[e]
988 keV	E2	$9/2^- \rightarrow 5/2^-$	E2[a], E2[b]
1014 keV	M1	$(5/2^-,3/2^-) \rightarrow 5/2^-$	
1044 keV	M1	$7/2^- \rightarrow 5/2^-$	M1[a], M1[b], M1[c]
1190 keV	M1	$(5/2^-,3/2^-) \rightarrow 3/2^-$	M1[a], M4, M3 or E2[c]
1352 keV	E2	$7/2^- \rightarrow 3/2^-$	E2[a]
1499 keV	E2	$9/2^- \rightarrow 5/2^-$	------
1502 keV	E2	$7/2^- \rightarrow 3/2^-$	=-----
1552 keV	E2	$9/2^+ \rightarrow 13/2^+$	E2 or M1[a]
1615 keV	E2	$7/2^- \rightarrow 5/2^-$	M1[a]
1619 keV	E1	$9/2^+ \rightarrow 9/2^-$	------
1764 keV	M1	$7/2^- \rightarrow 5/2^-$	M1 or M2[a], M1[b], E2[c]
1776 keV	M1	$(5/2^-,3/2^-) \rightarrow 5/2^-$	M1[b], E1[c]
1863 keV	E1	$9/2^+ \rightarrow 7/2^-$	E1[a], E1[b], E1[c]

.....con't.

Transition	Multipolarity Suggested in Present Work	Nature of Transition according to Kosanke et al (31)	Multipolarity Suggested by Previous Workers
1903 keV	E1	$9/2^+ \rightarrow 7/2^-$	E1[b], E1[c]

SUMMARY

In Table 8-7 we have shown the multipolarities of the various transitions which are suggested by the present work. Also shown are the spins and parities of the levels involved according to the decay scheme of Kosanke et al [31] and the multipolarities suggested by previous workers. There is general agreement between the decay scheme and the present work and this agreement is very gratifying.

CHAPTER 9

DISCUSSION OF THE SPECTROMETER

" 'Begin at the beginning,' the King said gravely, 'and go on till you come to the end: then stop' "

..... Lewis Carroll

As a spectroscopic tool the trochoidal β-ray spectrometer can and has been used to measure internal pair formation coefficients and internal conversion coefficients. In these two areas how does the performance of the present spectrometer compare with that of other spectrometers? Let us consider first pair spectrometers. In the trochoidal β-ray spectrometer mono-energetic pair lines are obtained by adding the outputs of the two sides of the spectrometer. Such line spectra have been observed by previous workers [36], for both internally and externally converted γ-rays, using magnetic spectrometers. In particular Alburger [36] has used an intermediate image focusing β-ray spectrometer to observe internally converted pairs. The source is located on the magnetic axis of the spectrometer and the arrival of a positron-electron pair is recorded by means of a "statistical separation" technique. Here, the small circular detecting area into which the particles are focused is split into two halves using two semi-circular detectors and a pair event is defined by the "simultaneous" detection of particles in both detectors. Since for a given magnetic field setting the spectrometer transmits particles of a fixed energy the spectrometer responds only to pair events for which the positron and electron have

the same energy $T = \frac{1}{2}(E_\gamma - 2m_oC^2)$. At a maximum transmission setting Alburger [36] obtained a pair detection efficiency $\sim 10^{-4}$ counts per pair corresponding to a pair line width ~2.5% in momentum. By comparison the pair detection efficiency of the present instrument is $\sim 10^{-2}$ at a resolution of 12-14 keV F.W.H.M. The resolution of the two instruments is roughly the same, for E_γ ~1700 keV, but the detection efficiency of the trochoidal β-ray spectrometer is two orders of magnitude larger. The small pair detection efficiency obtained by Alburger is typical of magnetic pair spectrometers. As previously stated magnetic spectrometers, by their very nature, transmit electrons (positrons) of fixed energy and such instruments when used as pair spectrometers respond to only a small percentage of the pair events which occur. The trochoidal β-ray spectrometer, on the other hand, responds to "all" pair events regardless of how the available energy is shared between the positron and electron.

It should be pointed out that the present instrument has not been calibrated, for use as a pair spectrometer, for $E_\gamma > 3$MeV. Above 3 MeV the pair detection efficiency is expected to fall off with increasing energy because of the reduction in detection efficiency of both sides of the spectrometer with increasing energy. The efficiency of the magnetic pair spectrometers on the other hand do not change with energy.

In principle it should be possible to use the instrument as a pair spectrometer, with high detection efficiency for E_γ as high as 5 MeV. Si(Li) detectors with depletion depths of 5mm. and good resolu-

tion ($\lesssim$8keV F.W.H.M.) are commercially available. Five mm. of Si is sufficient to stop electrons with energies ~3MeV. Because of the curved paths which the particles follow in the trochoidal β-ray spectrometer the effective thickness of any detector is increased so that the full energy peak detection efficiency of a 5mm. Si(Li) detector is expected to fall of rather slowly with energy, for energies greater than 3 MeV. Hence the detection of high energy pair events (E_γ~5MeV), for which the positron or electron receives most of the available energy, is not limited by the detectors.

The critical difficulty to be overcome is the decrease with energy of the number of particles striking the detectors. One can think of a number of ways of overcoming this problem. Perhaps the most straight forward technique would be to use larger area detectors. Based on the calculations of Chapter 3 the number of electrons striking the detector area is linearly related to this area. Detectors with active areas of 500mm^2 and depletion depths of 5mm. can be obtained commercially and such a detector would increase the detection efficiency by about a factor of 2 for electrons with energies above 1 MeV. (See Fig. 3-10).

A second way of increasing the detection efficiency of the spectrometer would be to increase the strength of the magnetic field, without changing the actual field shape. In this way the radial and vertical distributions of the particles would be reduced. Alternately, by shaping the pole tips it might be possible to introduce "focussing". For example, if the gap space between the pole tips decreased with angular distance from the source, (See Fig. 9-1), the particles might be brought to some sort of broad focus at the detector locations re-

FIG. 9-1

Proposed field shaping to introduce a "focus" at the detector location.

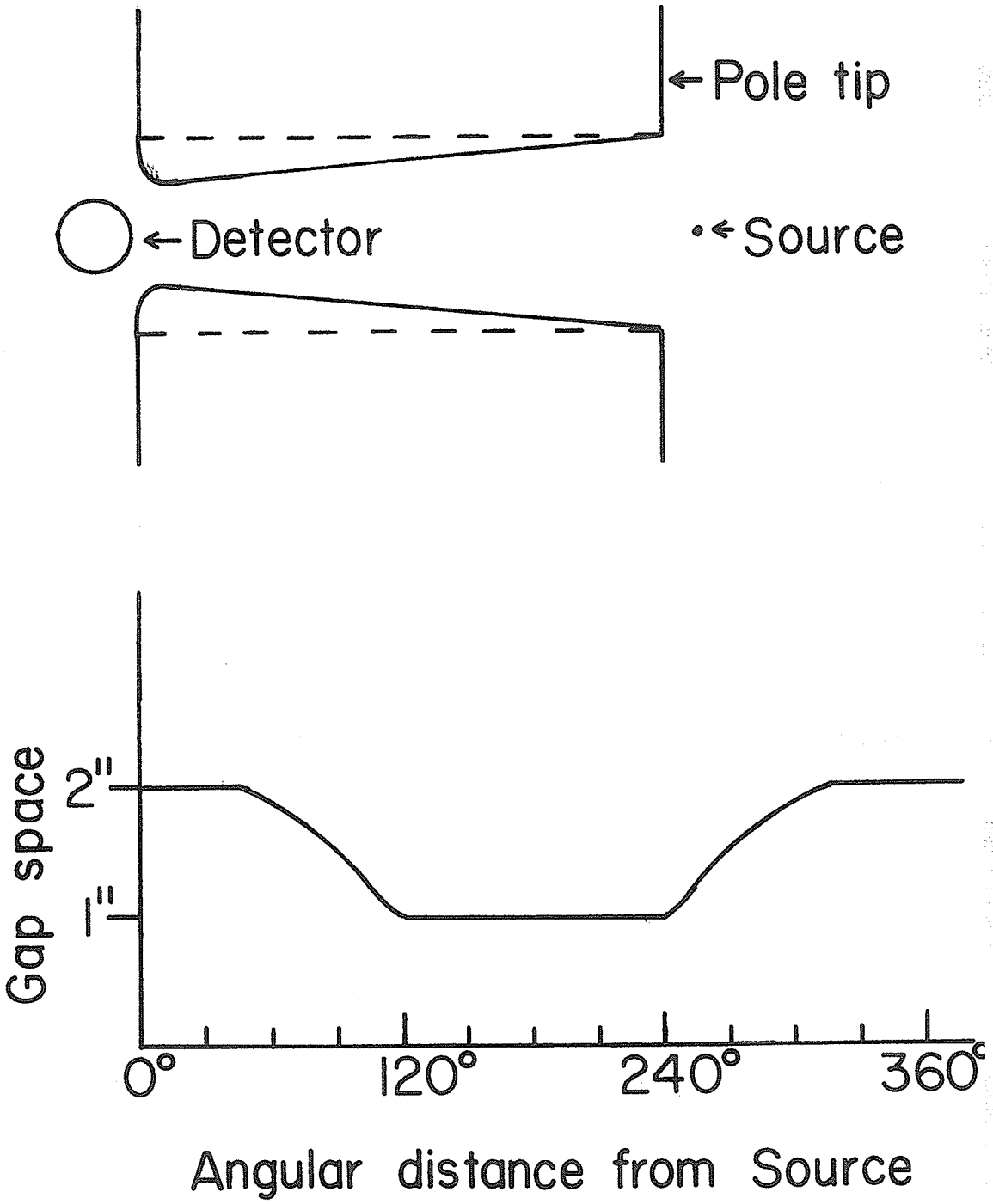
Pole tip
Detector
Source
Gap space
2"
1"
0°
120°
240°
360°
Angular distance from Source

sulting in an increased detection efficiency.

Whether or not such an improvement is possible in practise is a matter of conjecture. One major difficulty which would have to be overcome is the experimental fact that as the magnetic field strength is increased the electron line shape degenerates. This degeneration is believed caused by energy loss in the detector dead layer. The detectors now being used have a washable entry window. If the vacuum system could be improved sufficiently to reduce the problem of vapours condensing on the face of the detectors it would be possible to use detectors with a much thinner dead layer. An important point to take into account is that for high energy transitions both the positron and electron tend to be energetic. The problem of energy loss in the detector dead layer then becomes less pronounced and this improves the situation somewhat. It is felt therefore that there is a good possibility of extending the operating range of the spectrometer.

Now let us turn our attention to the measurement of internal conversion coefficients. In this area the present instrument is competing with high transmission magnetic spectrometers and with the "conventional" use of solid state detectors. In Table 9-1 the performance of the present spectrometer is compared to that of a high transmission spectrometer built by Freedman et al [37]. This instrument is representative of the best of the current high transmission spectrometers. The resolution of Freedman's spectrometer depends on the source size and transmission and we have included various values of these parameters. Usually the resolution of a magnetic spectro-

TABLE 9-1

Comparison of the present spectrometer with a high transmission magnetic spectrometer constructed by Freedman et al (37).

Performance of Present Instrument
Source diameter ~2mm.

Electron Energy	Efficiency	Resolution
100 keV	23%	5 keV
300 keV	23%	5 keV
500 keV	23%	5 keV
750 keV	17.5%	5 keV
1000 keV	11.5%	5 keV
1400 keV	7.2%	~5.5 keV
1800 keV	3.5%	~6-7 keV

Performance of Toroidal Magnetic Spectrometer

Source Diameter = 1/8"		Source Diameter = 1mm.	
Transmission	Resolution	Transmission	Resolution
19%	.12 keV (.9% mtm.)	13%	.03 keV
16%	.06 keV (.4% mtm.)		
19%	1.6 keV	13%	.36 keV
16%	.7 keV		
19%	3.4 keV	13%	.75 keV
16%	1.5 keV		
19%	5.6 keV	13%	1.3 keV
16%	2.5 keV		
19%	7.7 keV	13%	1.7 keV
16%	3.4 keV		
19%	11.8 keV	13%	2.6 keV
16%	5.2 keV		
19%	15.4 keV	13%	3.4 keV
16%	6.8 keV		

meter is expressed as a percentage of the particle's momentum but for purposes of comparison we have expressed the resolution here in terms of energy. The resolution of the present instrument depends on the detectors used and in Table 9-1 we have used the values obtained with the detectors which are now being used, when they were new. Si(Li) detectors with resolutions ~3-4 keV in the energy range 100 - 1000 keV are commercially available and therefore it should be possible to obtain such resolution without any loss in full energy peak detection efficiency.

At first glance the performance of Freedman's spectrometer would appear to be superior to that of the present instrument. However, the relative merits of the two instruments depends on the particular application. The transmission of Freedman's spectrometer and the full energy peak detection efficiency of the trochoidal β-ray spectrometer provide a rough comparison between the two instruments but one must also consider the time required to accumulate a given spectrum. Using the Freedman's spectrometer data is acquired point by point whereas the present instrument permits simultaneous broad energy range collection of data. In experimental situations for which the conversion spectra contain a large number of lines the effective efficiency of the trochoidal β-ray spectrometer is then many times higher than that of the other spectrometer.

Compared to conventional use of solid state detectors there is, in many situations, no advantage in using the present spectrometer. The detection efficiency, (for conventional use of Si(Li) detectors),

depends on geometrical parameters such as detector size and source location and the efficiency can be comparable to that of the trochoidal spectrometer. Furthermore, the line shape obtained tends to be better in such cases because the electrons enter the detector "normally" and the detector dead layer is not as important. However, in several applications the filtering aspect of the trochoidal β-ray spectrometer is an important consideration. For example, if one is trying to observe a weak conversion line in the presence of a high positron background, from β^+ decay, the present instrument is clearly very useful since the electron side of the spectrometer responds only to electrons and the positron background is eliminated. A second area in which the use of the present instrument is advantageous is the study of conversion spectra of high A nuclides fed by α-decay. The spectrometer does not transmit heavy particles and the detector is therefore "shielded" from the α-particles. The electron spectrum is then free of interfering α-lines. Further, the problem of radiation damage to the detectors, by the α's, is circumvented. W. Teoh [38] has employed the spectrometer in just such a situation, to study the conversion spectrum of ^{227}Ac following the α-decay of ^{231}Pa.

A similar application for which the spectrometer is potentially useful is the on-line study of the conversion spectra of short-lived nuclides produced by an accelerator beam, such as that of the University of Manitoba's cyclotron. The detector is then shielded from the beam. What sort of counting rates might be expected in such an application? For the sake of discussion let us assume that we have

a 1μA proton beam, (10^{13}/1.6 protons per second), incident on a target of thickness 100 μg/cm^2. If σ is the total reaction cross-section which populates the level of interest then the number of reaction events per unit time is given by

$$N = \frac{10^{13}}{1.6} \times \sigma \times n \times \frac{100\times10^{-6}}{P}$$ where n is the number of target atoms per unit volume and P is the density of the target material. But

$$n = \frac{P\times6\times10^{23}}{A}$$ where A is the gram-molecular weight of the target. Thus the number of reaction events per unit time is given by

$$N = \frac{10^{13}\times6\times10^{23}\times10^{-4}\times\sigma}{1.6\times A}$$

If we take σ=100mb and A=50 as typical sort of numbers then N~10^6/sec. Then the number of internal pairs that we observe per unit time is given by $N_\pi = 10^6 \times \alpha_\pi \times \epsilon_\pi$ where α_π is the pair formation coefficient and α_π is the pair detection efficiency. Taking as typical numbers $\alpha_\pi \sim 10^{-4}$ and $\epsilon_\pi \sim 10^{-2}$ we obtain N_π~1 per second. On the other hand if we are interested in the observed number of conversion electrons then $N_{e^-} = 10^6 \times \alpha_{e^-} \times \epsilon_{e^-}$. Again taking as typical numbers $\alpha_{e^-} \sim 10^{-3}$ and $\epsilon_{e^-} \sim 10^{-1}$ we obtain N_{e^-}~100/second. Thus the counting rates one might expect are reasonable.

Although the detectors are shielded from the accelerator beam there may still be serious background problems, in such an application, caused by knock-out electrons and/or neutrons. The neutron background can be particularly troublesome because of the possible radiation damage to the detectors which might seriously limit their life-time.

In conclusion then the trochoidal β-ray spectrometer is a useful spectroscopic tool in the study of internal conversion and internal pair formation.

REFERENCES

1. J. Thibaud, Physics Review 45 (1934) 781.
2. K. G. Malmfors, Ark. F. Fys. 13 (1958) 237; 13 (1958) 247.
3. J. D. Jackson, Classical Electrodynamics, (John Wiley and Sons, Inc., 1963) p. 60.
4. S. Gill, Proc. Cambridge Phil. Soc. 17 (1951) 96.
5. C. M.Lederer, J. M. Hollander, and I. Perlman, Table of Isotopes 6th Ed. (John Wiley and Sons, Inc.)
6. J. H. Hamilton et al, Nuclear Data Tables A1 (1966) 521 (No. 6).
7. M. J. Canty, University of Manitoba, private communication.
8. J. C. Jaeger and H. R. Hulme, Proc. Roy. Soc. 148 (1935) 708.
9. M. E. Rose and G. E. Uhlenbeck, Phys. Rev. 48 (1935) 211.
10. R. J. Lombard et al, Nucl. Phys. A110, (1968) 41.
11. M. E. Rose, Phys. Rev. 76 (1949) 678.
12. M. E. Rose, Phys. Rev. 78 (1950) 184.
13. G. K. Horton and E. Phibbs, Phys. Rev. 96 (1954) 1066.
14. C. M. Lederer et al, Ref. 5, p. 395.
15. D. E. Alburger and M. H. L. Pryce, Phys. Rev. 95 (1954) 1482.
16. R. Stockendal and S. Hultberg, Ark. F. Fys. 15, (1959) 33.
17. R. Wiener et al, Phys. Rev. 130 (1963) 1069.
18. C. F. Perdrisat et al, Helv. Phys. Acta 35 (1962) 175.
19. G. Vallois et al, Phys. Lett. 24B (1967) 512.
20. R. K. Jolly et al, Phys. Rev. 128 (1962) 2292.
21. J. F. Ziegler and G. A. Peterson, Phys. Rev. 165 (1968) 1337.
22. R. S. Hager and E. C. Seltzer, Nuclear Data A4 (1968) 1.

.....con't.

23. C. M. Lederer et al, Ref. 5. p 223.

24. J. H. Hamilton et al, Phys. Lett. 19, (1966) 682.

25. F. R. Metzger and H. C. Amacher, Phys. Rev. 88 (1952) 147.

26. W. C. Peacock and J. W. Jones, A.E.C. Report A.E.C.D. 1812 (unpublished).

27. E. D. Klema, Phys. Rev. 102 (1956) 449.

28. C. M. Lederer et al, Ref. 5. p. 394.

29. M. Schmorak et al, Nuclear Physics 2 (1956-7) 193.

30. S. H. Vegors Jr. et al, Nuclear Physics 48 (1963) 230.

31. K. Kosanke et al, Bull. Am. Phys. Soc. 15 (1970) 546.

32. C. M.Lederer et al, Ref. 5 p. 398.

33. R. Stockendal, Ark. F. Fys. 17, (1960) 553.

34. B. Ahluwalia and B. Chasan, Bull. Am. Phys. Soc. 15 (1970) 546.

35. R. Wilson, Alpha-beta-gamma-ray Spectroscopy (ed. Kai Siegbahn; North-Holland Publ. Co. Amsterdam, 1966) p. 1557.

36. D. E. Alburger, Ibid, p. 756.

37. M. S. Freedman et al, Nucl. Instr. and Methods 8 (1960) 225.

38. W. C. Teoh et al, Phys. in Canada 26 (1970) 77.